PNNL-31208

High-Resolution Regional Wave Hindcast for U.S. Pacific Island Territories

May 2021

G García-Medina
Z Yang
N Li
K F Cheung
H Wang
F Ticona Rollano

U.S. DEPARTMENT OF ENERGY

Prepared for the U.S. Department of Energy
under Contract DE-AC05-76RL01830

DISCLAIMER

PACIFIC NORTHWEST NATIONAL LABORATORY
operated by
BATTELLE
for the
UNITED STATES DEPARTMENT OF ENERGY
under Contract DE-AC05-76RL01830

Printed in the United States of America

Available to DOE and DOE contractors from the
Office of Scientific and Technical Information,
P.O. Box 62, Oak Ridge, TN 37831-0062;
ph: (865) 576-8401
fax: (865) 576-5728
email: reports@adonis.osti.gov

Available to the public from the National Technical Information Service
5301 Shawnee Rd., Alexandria, VA 22312
ph: (800) 553-NTIS (6847)
email: orders@ntis.gov <https://www.ntis.gov/about>
Online ordering: http://www.ntis.gov

PNNL-31208

High-Resolution Regional Wave Hindcast for U.S. Pacific Island Territories

May 2021

G García-Medina
Z Yang
N Li
K F Cheung
H Wang
F Ticona Rollano

Prepared for
the U.S. Department of Energy
under Contract DE-AC05-76RL01830

Pacific Northwest National Laboratory
Richland, Washington 99354

Summary

This report summarizes modeling efforts for hindcasting the wave climate within the Exclusive Economic Zone around American Samoa, Baker Island and Howland Island, Commonwealth of Northern Mariana Islands, Guam, Jarvis Island, Johnston Atoll, Palmyra Atoll and Kingman Reef, and Wake Island. The report describes the mesh development and data sources used in the process. In addition, it provides the results of a sensitivity analysis performed to determine the optimal model configuration, details the data used for model forcing, shows a detailed skill assessment, and depicts the output.

Acknowledgments

This study was funded by the U.S. Department of Energy, Office of Energy Efficiency & Renewable Energy, Water Power Technologies Office under Contract DE-AC05-76RL01830 to Pacific Northwest National Laboratory.

A steering committee, chaired by Dr. Bryson Robertson, provided external oversight for, input to, and review of this study.

The model computations were performed using resources available through Research Computing at Pacific Northwest National Laboratory (PNNL). PNNL is operated by Battelle for the U.S. Department of Energy under Contract DE-AC05-76RL01830.

Acronyms and Abbreviations

AS	American Samoa
BI	Baker and Howland Islands
CDIP	Coastal Data Information Program
CFL	Courant–Friedrichs–Lewy
CNMI	Commonwealth of Northern Mariana Islands
CFSR	Climate Forecast System Reanalysis
DEM	Digital Elevation Model
EEZ	Exclusive Economic Zone
EPRI	Electric Power Research Institute, Inc.
GSE	Garden Sprinkler Effect
Hz	Hertz
IEC	International Electrotechnical Commission
JI	Jarvis Island
JA	Johnston Atoll
km	kilometer(s)
kW/m	kilowatt(s) per meter
LiDAR	Light Detection and Ranging
m	meter(s)
MHK	marine and hydrokinetic
MI	Commonwealth of Northern Mariana Islands and Guam
NDBC	National Data Buoy Center
NCEP	National Centers for Environmental Prediction
NOAA	National Oceanic and Atmospheric Administration
NREL	National Renewable Energy Laboratory
PacIOOS	Pacific Islands Ocean Observing System
PA	Palmyra Atoll and Kingman Reef
PE	percentage error
R	correlation coefficient
RMSE	root-mean-square-error
s	second(s)
SHOALS	Scanning Hydrographic Operational Airborne
SI	scatter index
SOEST	School of Ocean and Earth Science and Technology
ST	source term
SWAN	Simulating WAves Nearshore
TB	terabyte(s)

TS	Technical Specification
UnSWAN	Unstructured-grid Simulating Waves Nearshore
USACE	U.S. Army Corps of Engineers
WI	Wake Island
WRF	Weather Research and Forecasting
WW3	WAVEWATCH III
yr	year(s)

Contents

Figures

Tables

1.0 Introduction

Ocean waves have the highest amount of energy of the U.S. marine and hydrokinetic energy resources, which also include tidal and ocean currents, ocean thermal gradients, and river streams. To characterize this large energy resource in the U.S. coastal regions, the Electric Power Research Institute, Inc. (EPRI) conducted the first U.S. nationwide wave resource assessment based on wave hindcast data generated by the National Oceanic and Atmospheric Administration (NOAA) using a nested WAVEWATCHIII® (WW3) model (Hagerman and Scott 2011). However, the WW3 hindcast data used in EPRI's study only covered a short 51-month period with a spatial resolution of 4 arc-minutes (approximately 7.2 km at latitude 13°N), which is insufficient to characterize and assess the wave resource accurately, especially for the nearshore regions where wave conditions rapidly change. The U.S. island territories in the Pacific Ocean were not included in the resource characterization in the EPRI study, which only covered the regions of the U.S. West Coast, East Coast, Alaskan Coast, Gulf of Mexico, Hawaii, Puerto Rico, and the U.S. Virgin Islands (Figure 1.1). Better understanding of the wave resource in the U.S. Pacific Island territories is of great interest to the nation because of their important geographic locations and values, especially in the context of Powering the Blue Economy (PBE). U.S. Department of Energy's (DOE's) PBE is an initiative to understand the power requirements of emerging coastal and maritime markets and advance technologies that could integrate marine renewable energy to relieve power constraints and promote economic growth. This is particularly relevant for remote island communities. Therefore, it is important to characterize the wave resources in all the U.S. Pacific Island territories based on long-term (e.g., multi-decades) and high-resolution (in the order of a couple of hundred meters) wave hindcast datasets.

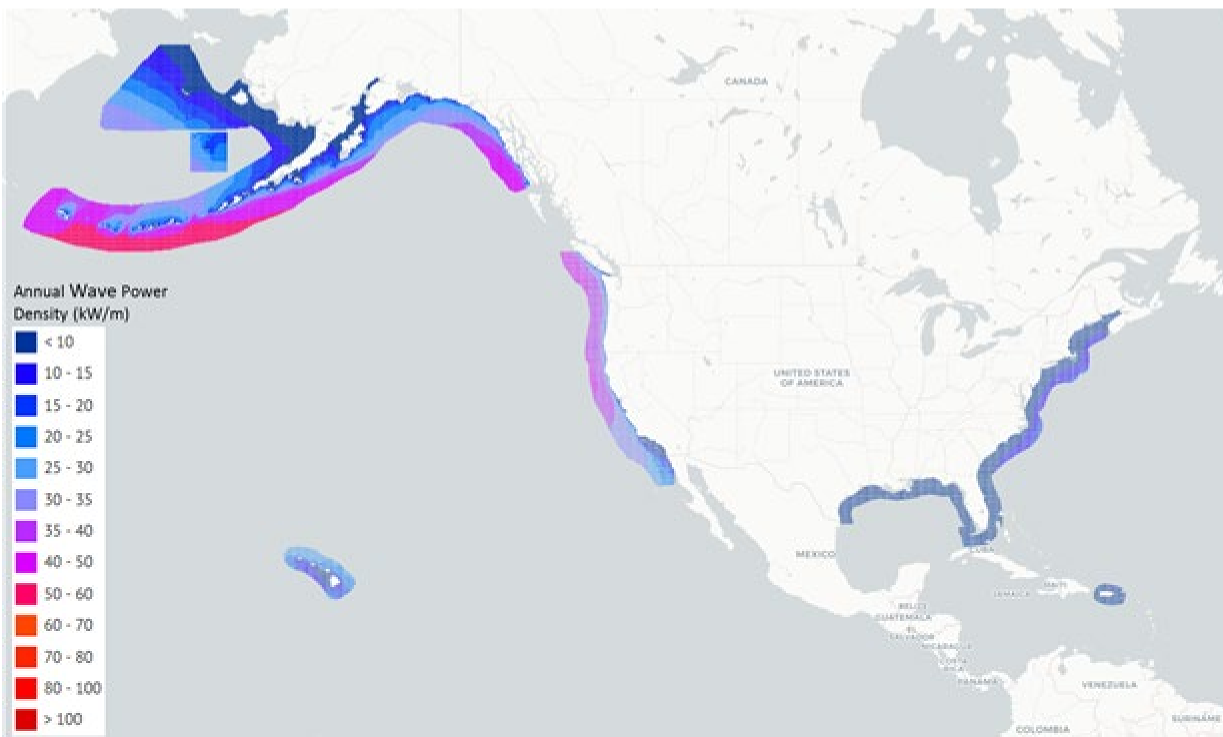

Figure 1.1. Annual wave power density distribution in U.S. coastal regions, based on NOAA's 4 arc-minute resolution WW3 hindcast. This image was obtained from https://maps.nrel.gov/mhk-atlas.

The DOE's Water Power Technologies Office contracted the Pacific Northwest National Laboratory to conduct a high-resolution wave hindcast and characterize the wave resource around the U.S. Pacific Island territories. This report describes the development and validation of a set of wave models and the resource characterization for eight U.S. Pacific Island territories, including American Samoa, Baker Island and Howland Island, Commonwealth of Northern Mariana Islands (CNMI), Guam, Jarvis Island, Johnston Atoll, Palmyra Atoll and Kingman Reef, and Wake Island. Together with the U.S. West Coast, Alaskan Coast, and Hawaiian Islands, the 32-year wave hindcast for U.S. Pacific Islands provides complete coverage for the United States' exclusive economic zones (EEZs) in the Pacific Ocean. This wave hindcast implemented a unified modeling approach as applied in other regions that involves third generational spectral models WW3 on nested grids and Simulating WAves Nearshore (SWAN) on an unstructured grid. International Electrotechnical Commission (IEC) wave resource characterization parameters, as well as conventional bulk wave parameters, were computed and validated against observations from satellite altimeters and measurements from a wave buoy, which is owned and maintained by the Pacific Islands Ocean Observing System (PacIOOS) . Model results will be disseminated and made available to interested stakeholders on the Amazon Web Services through the National Renewable Energy Laboratory.

Model configurations for both WW3 and SWAN, including computational grids, spectral and directional resolutions, time steps, and wind forcing, are provided in Section 2. Wave buoy data for model validation are also summarized in the same section. Model simulations and validation results are presented in Section 3. Spatial and temporal distributions of wave resource parameters are discussed in Section 4, followed by the conclusions of the study in Section 5. Monthly and yearly distributions of bulk wave parameters from the hindcast dataset are listed in Appendix A. Model sensitivity to time step is shown in Appendix B. Comparisons of the wave hindcast with buoy data in term of the bulk wave parameters are provided in Appendix C, and the model performance metrics in Appendix D.

2.0 Study Area and Data

This study focuses on the wave climate of the eight U.S. territories in the tropical Pacific Ocean, namely American Samoa, Baker Island and Howland Island, CNMI, Guam, Jarvis Island, Johnston Atoll, Palmyra Atoll and Kingman Reef, and Wake Island. These territories span a vast region of the Central Pacific Ocean for a combined EEZ area of 3,512,812 km^2 (Table 2.1). This is a large proportion of the total U.S. EEZ, which covers an aera of 11,351,000 km^2. Some territories are more than 6,000 km apart from east to west (Figure 2.1); thus, for practical purposes, seven models are developed for the hindcast. All territories lie in the low latitudes (between 30°S and 30°N) where the local climate is dominated by the trade winds. This wind pattern is expected to be reflected in the wave climate as it is in the case of the major Hawaiian Islands (Li et al. 2021) and atolls southeast of American Samoa (Dutheil et al. 2021). In addition to the persistent trade winds, the wave conditions around some islands are influenced by tropical and subtropical cyclones, monsoons, and extratropical storms. The complex wave conditions in the Pacific Ocean require a long-term and high-resolution wave hindcast for climate and energy resource analysis.

Table 2.1. Exclusive Economic Zone area of the Pacific Island Territories.

Model	EEZ Area (km^2)
American Samoa	404,391
Commonwealth of Northern Mariana Islands and Guam	1,153,659
Baker and Howland Islands	434,921
Jarvis Island	316,665
Johnston Atoll	442,635
Palmyra Atoll and Kingman Reef	353,300
Wake Island	407,241
Total Area	3,512,812

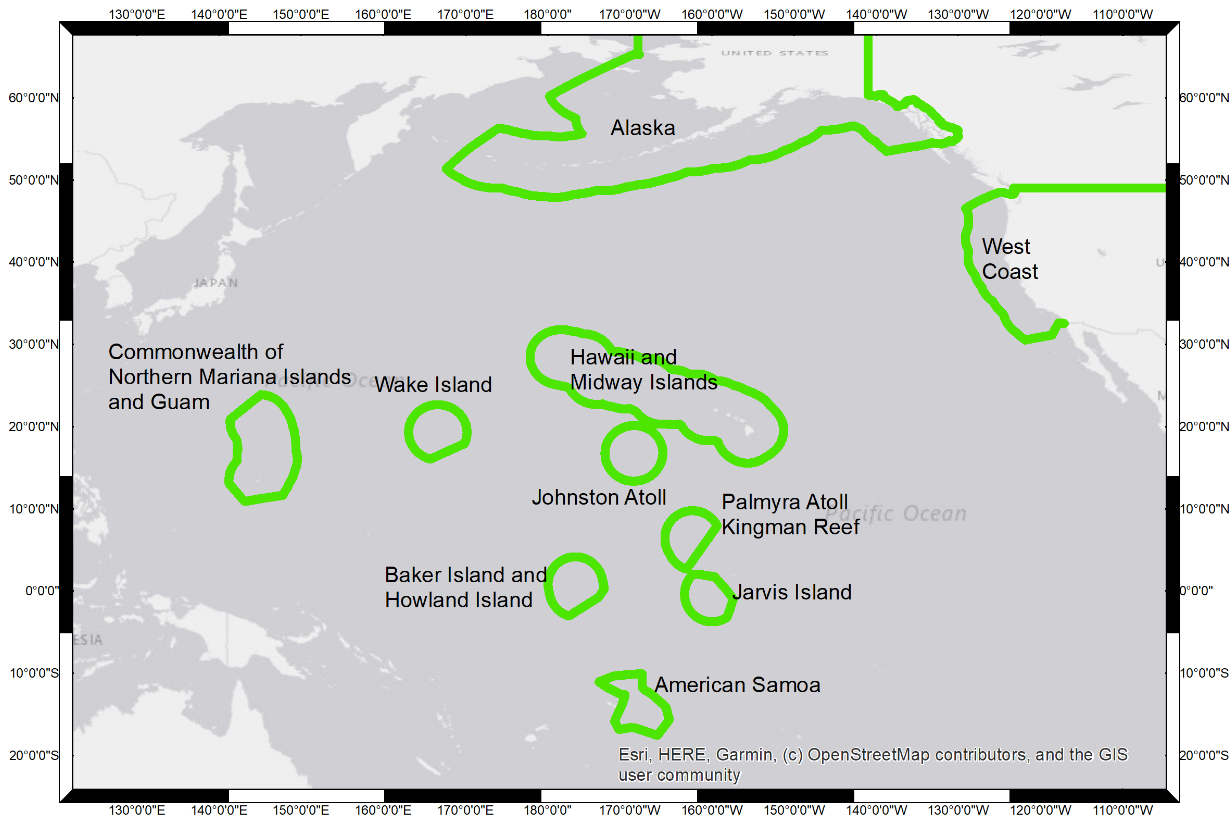

Figure 2.1. U.S. Exclusive Economic Zone in the Pacific Ocean.

2.1 Measured Data for Model Validation

Model validation was conducted using measurements from a buoy and observations from satellite-borne altimeters. During the hindcast period (1979–2010) only one buoy was deployed in the study sites; it was located approximately 1.6 km off Ipan, at 200 m water depth east of Guam as shown in Figure 2.2. This Ipan buoy (NDBC #52200; CDIP #121) has been deployed since July 2003 and is currently maintained by PacIOOS. This station provides bulk wave parameters and the 2D wave spectra every 30 minutes that allow for model-data comparisons in terms of six - wave energy resource parameters recommended by IEC-Technical Specification (TS). The detailed comparisons are shown in Section 4.2.

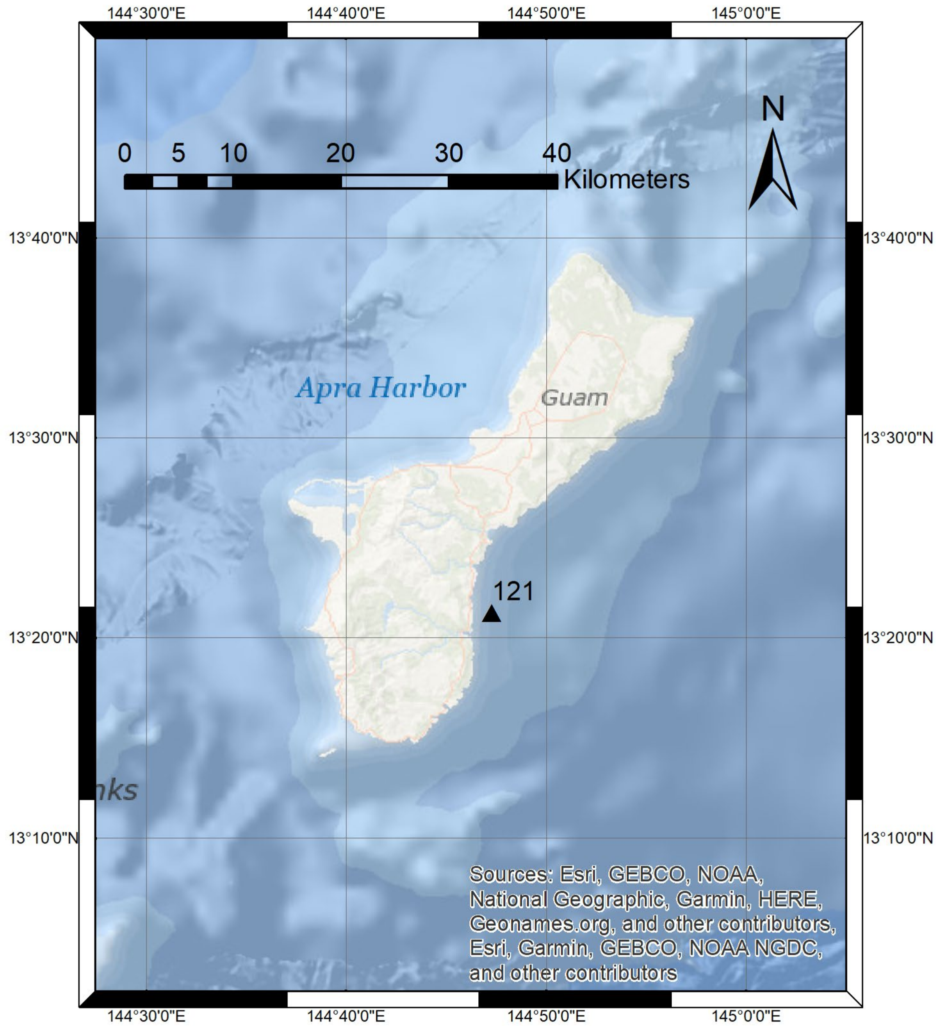

Figure 2.2. Location of the Ipan buoy (#121) off the east shore of Guam.

Data from one wave buoy are not enough to validate the suite of models that cover such a large region. Satellite-borne altimeters provide wave height measurements, starting with the GEOSAT mission in 1985. Since then, altimeters have provided nearly continuous measurements covering most of the ocean. There are a total of nine missions having wave height measurements during the hindcast period, and the mission timelines are shown in Figure 2.3. Although the altimetry dataset provides large spatial coverage, it has limitations. First, the orbital repeat cycle is generally long; for instance, 10 days for the JASON-1 and JASON-2 missions. Second, the on-board sensors only provide significant wave height estimates having a level of uncertainty comparing with buoy measurement. Nevertheless, this is still a very valuable source for model validation and has been used in previous wave resource assessments (e.g., Li et al. 2016). For model-data comparisons the data are binned over a 0.2° grid. These bins measure 22 km in the meridional direction and vary from 22 km at the equator to 20 km at 25°N in the zonal direction. The bins are selected for adequate description of the spatial variations as well as sufficient satellite data in each bin for a statistical analysis. The availability of the satellite measurements is shown in Figure 2.4. Measurements considered in this study are based on the Ku band (13–17 GHz). Data were downloaded from the Australian Ocean Data Network portal (https://portal.aodn.org.au/), technical details of the data curation can be found on Ribal and

Young (2019). More than five million observations are available during the hindcast period (Table 2.2) providing a robust data set for model performance evaluation.

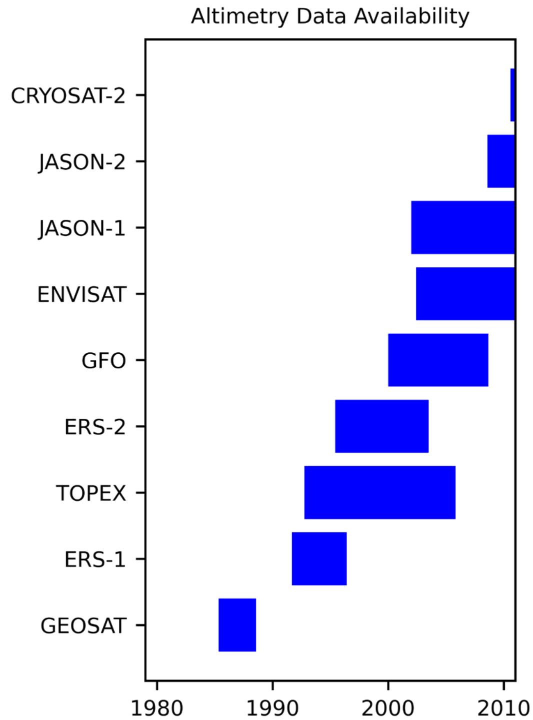

Figure 2.3. Satellite missions with altimeter data from 1979 to 2010.

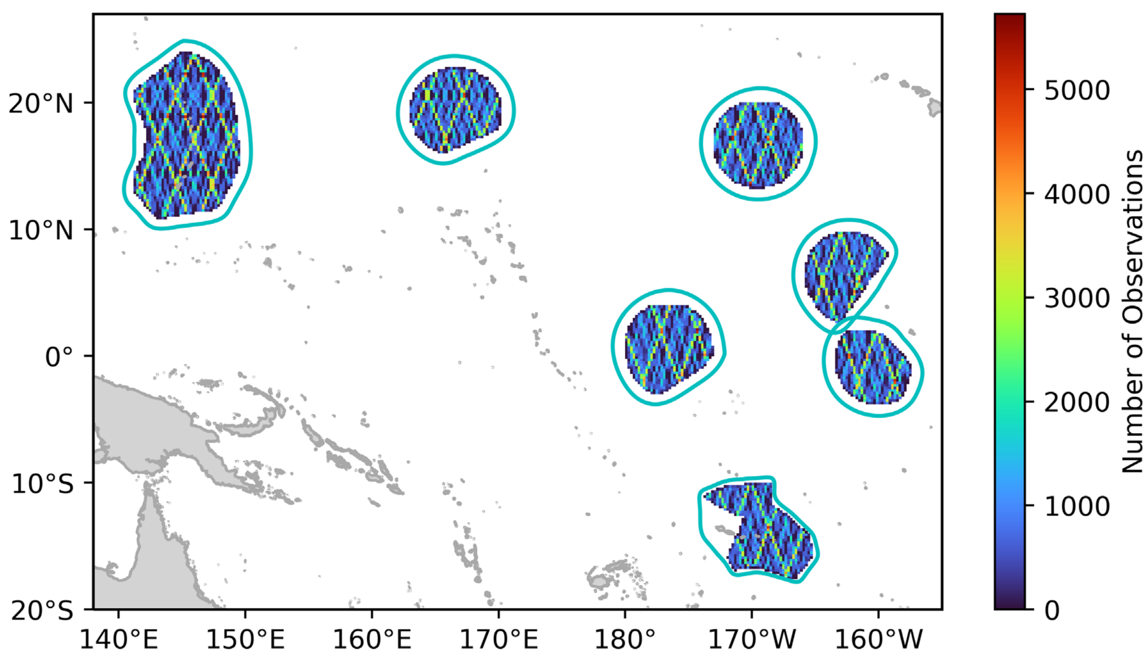

Figure 2.4. Satellite-borne significant wave height measurements from 1979 to 2010. The data were binned every 0.2°.

Table 2.2. Number of altimetry-derived measurements for validation.

Model	Number of Observations
American Samoa	767,834
Commonwealth of Northern Mariana Islands and Guam	1,980,674
Howland and Baker Islands	858,522
Jarvis Island	638,632
Johnston Atoll	911,771
Palmyra Atoll and Kingman Reef	689,716
Wake Island	853,620

2.2 Atmospheric Forcing

The wave hindcast in this study covers a period of 32 years from 1979 to 2010. This period corresponds to the available wind forcing (wind speed at 10 m height) from the Climate Forecast System Reanalysis (CFSR, Saha et al. [2010]), produced by the National Centers for Environmental Prediction (NCEP). This data set has a temporal resolution of 1 hour, which meets the IEC-TS requirements for Class 3 (design) assessments. The spatial resolution is 0.5 arc-degrees (55.6 km), which is close to the Class 1 (feasibility) requirement of 50 km. Figure 2.5 shows an example of global wind speed at 10 m elevation at 1:00 am UTC time, on 8 September 2009. The seven model regions are outlined in the global wind field. It also provides detailed local wind vectors, which are shown for the CNMI and Guam, and American Samoa regions, as examples. The CFSR data are bilinearly interpolated into the model grid at the model execution time.

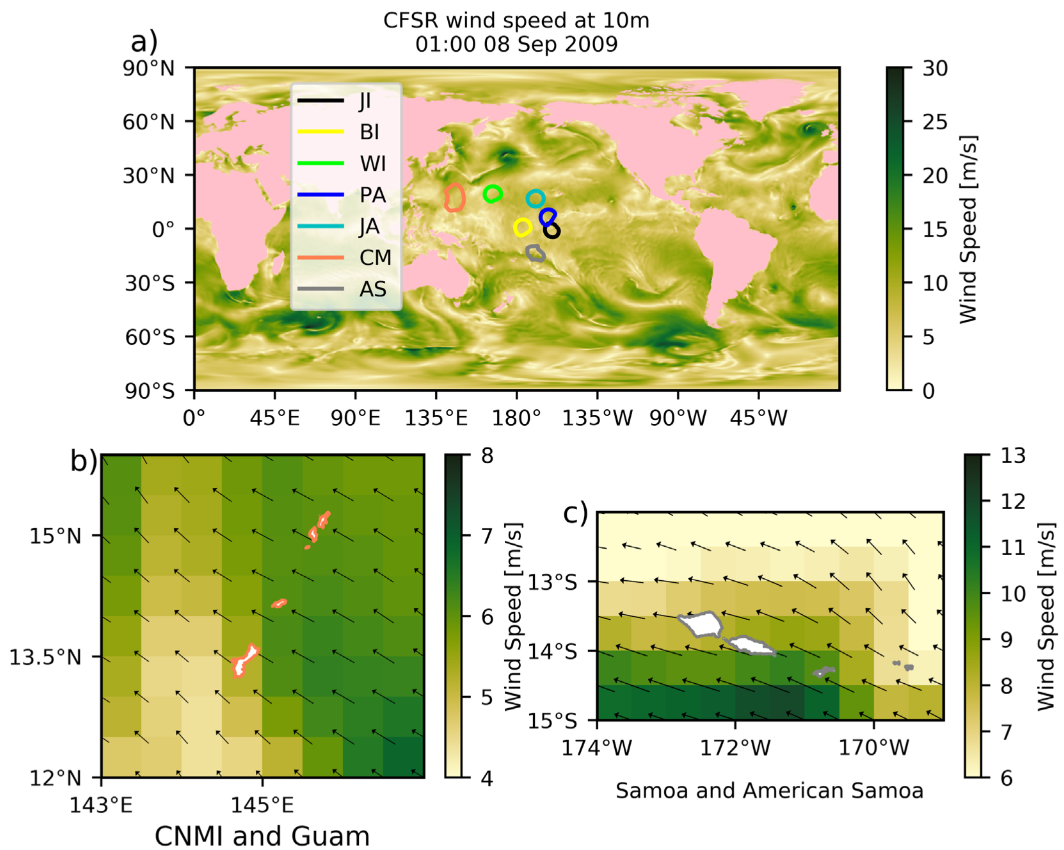

Figure 2.5. Example of CFSR data products. (a) Surface winds around the globe at 01:00 on 8 September 2010. The SWAN domains are outlined by colored lines. (b) Close-ups around Guam and CNMI, and (c) American Samoa with different color scales for wind speeds.

Comparison of CFSR wind speeds with observed data at four shore-based stations show general overprediction due to the lack of resolution of the islands and subsequently the orographic effect in the atmospheric model. This is particularly evident in the stations around Guam (Figure 2.6, Figure 2.7) and Tutuila, American Samoa (Figure 2.8) which have a steep nearshore terrain. However, the CFSR winds are better resolved over the ocean for wave hindcasting (Stopa and Cheung 2014). This is shown in the improved wind speed comparison at Wake Island (Figure 2.8), a small atoll that has no terrain features. The overestimation of wind speed near the shore and over the land will have a minimal effect on the wave hindcasting because of the limited fetch for wave generation. The wind product is implemented in parallel studies for other U.S. regions and proven accurate in wave hindcasting (Allahdadi et al. 2019; Ahn et al. 2020; García-Medina et al. 2019, 2021; Yang et al. 2017, 2018, 2019, 2020; Wu et al. 2020).

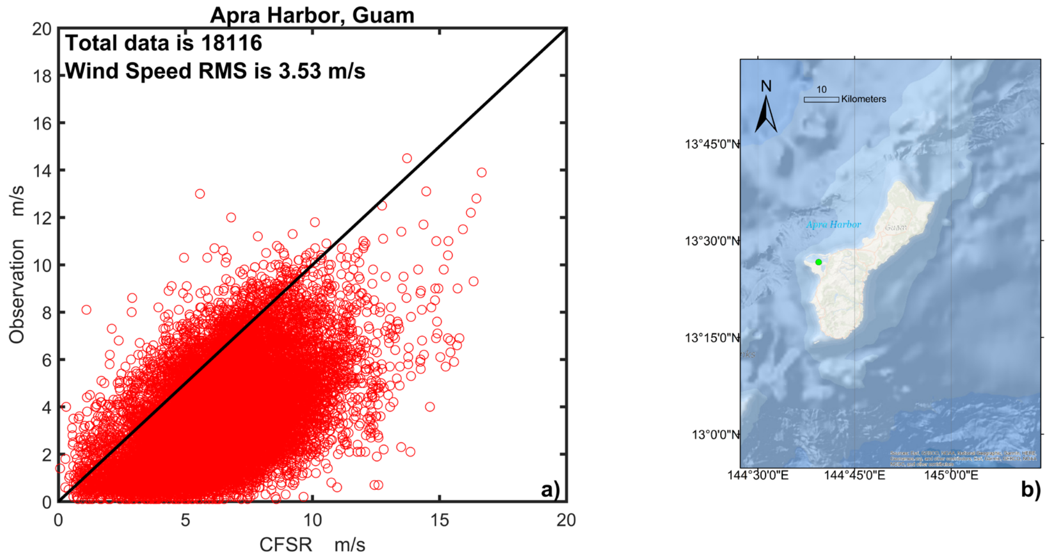

Figure 2.6. (a) Wind velocity comparison of buoy observation and the CFSR model. (b) Buoy location at Apra Harbor, Guam (green circle).

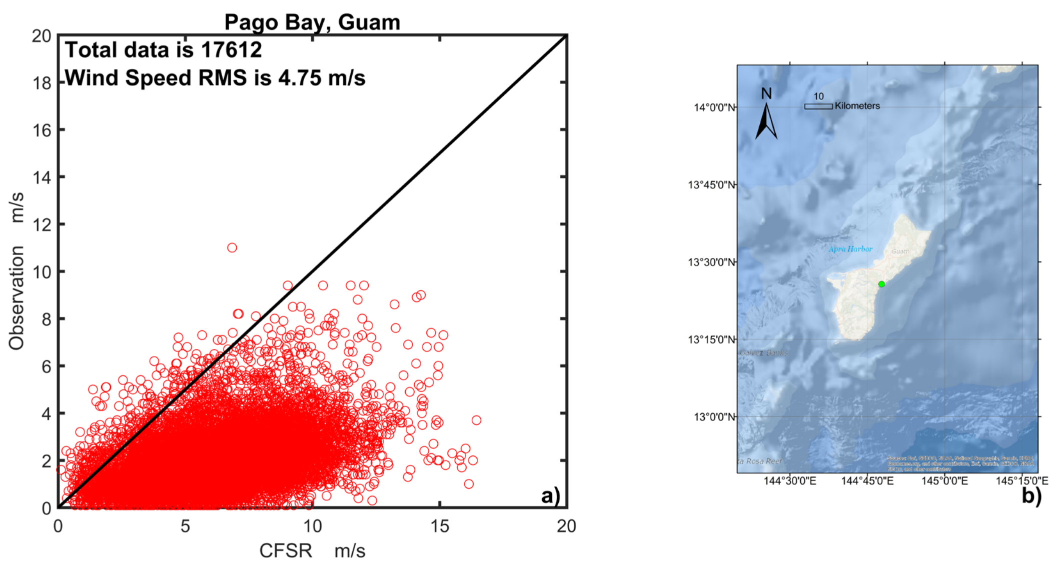

Figure 2.7. (a) Wind velocity comparison of buoy observation and the CFSR model. (b) Buoy location at Pago Bay, Guam (green circle).

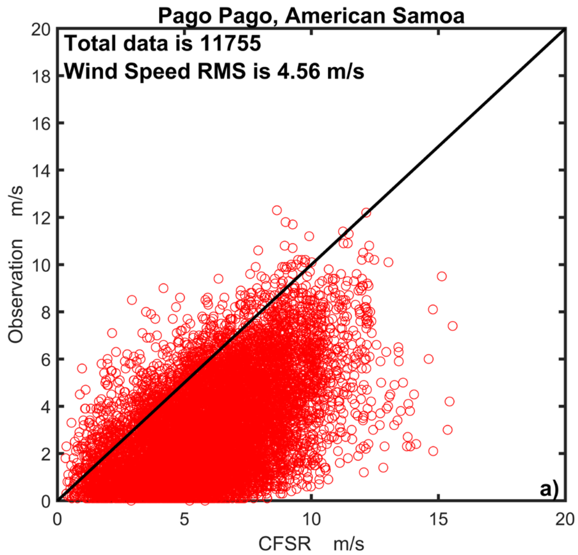

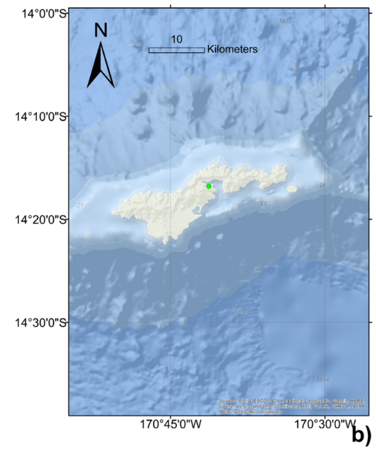

Figure 2.8. (a) Wind velocity comparison of buoy observation and the CFSR model. (b) Buoy location at Pago Pago, American Samoa (green circle).

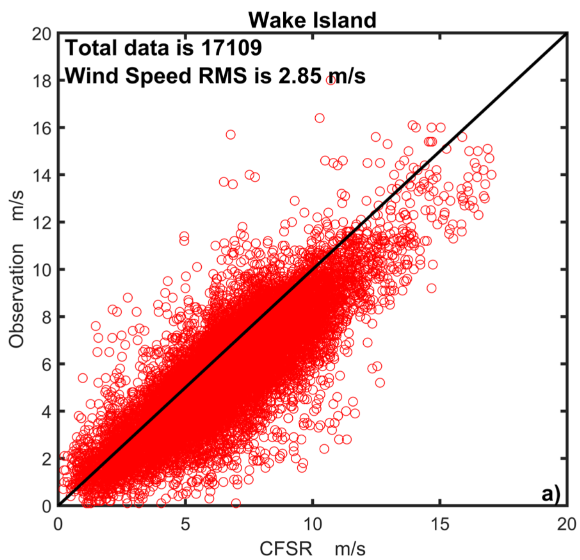

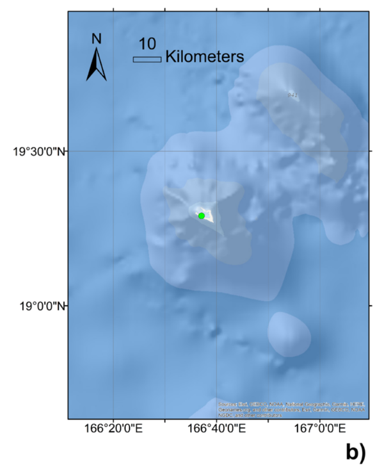

Figure 2.9. (a) Wind velocity comparison of buoy observation and the CFSR model. (b) Buoy location at Wake Island (green circle).

3.0 Methods

A telescopic nested-grid modeling approach that combines structured WW3 (v5.16) and unstructured-grid SWAN (v41.10) models was used in this study. Three levels of WW3 grids were configured to resolve the global and regional wave climate and dynamically downscale waves near the boundaries of study areas. This multi-grid WW3 model also provides boundary conditions for the seven high-resolution SWAN models around the Pacific Island territories. This combined WW3 and SWAN model approach becomes a standard tool in wave modeling and has been used in similar applications (e.g., García-Medina et al. 2021; Li et al. 2016; Stopa et al. 2011; Wu et al. 2018, 2020).

3.1 WW3 Model Configuration

The Level 1 (L1) grid for global WW3 was adapted from NOAA NCEP's operational model. It has a resolution of 0.5 arc-degree, which is equivalent to 55.6 km at the equator. The second level (L2) was configured to dynamically downscale the waves in the central Pacific Ocean covering all U.S. EEZs and surrounding waters, as shown in Figure 3.1. This model has a resolution of 10 arc-minutes, which is a threefold increase from the global model. Finally, a third level (L3) of modeling was configured with 4 arc-minute resolution and extends from the islands to a distance equivalent to about 1 arc-degree beyond the EEZ. The bathymetry for L2 and L3 was obtained from ETOPO1 (Amante and Eakins 2009), which has a global coverage at 1 arc-minute resolution. The L3 model provides the boundary conditions for the SWAN models. Further details of the WW3 domains are shown in Table 3.1.

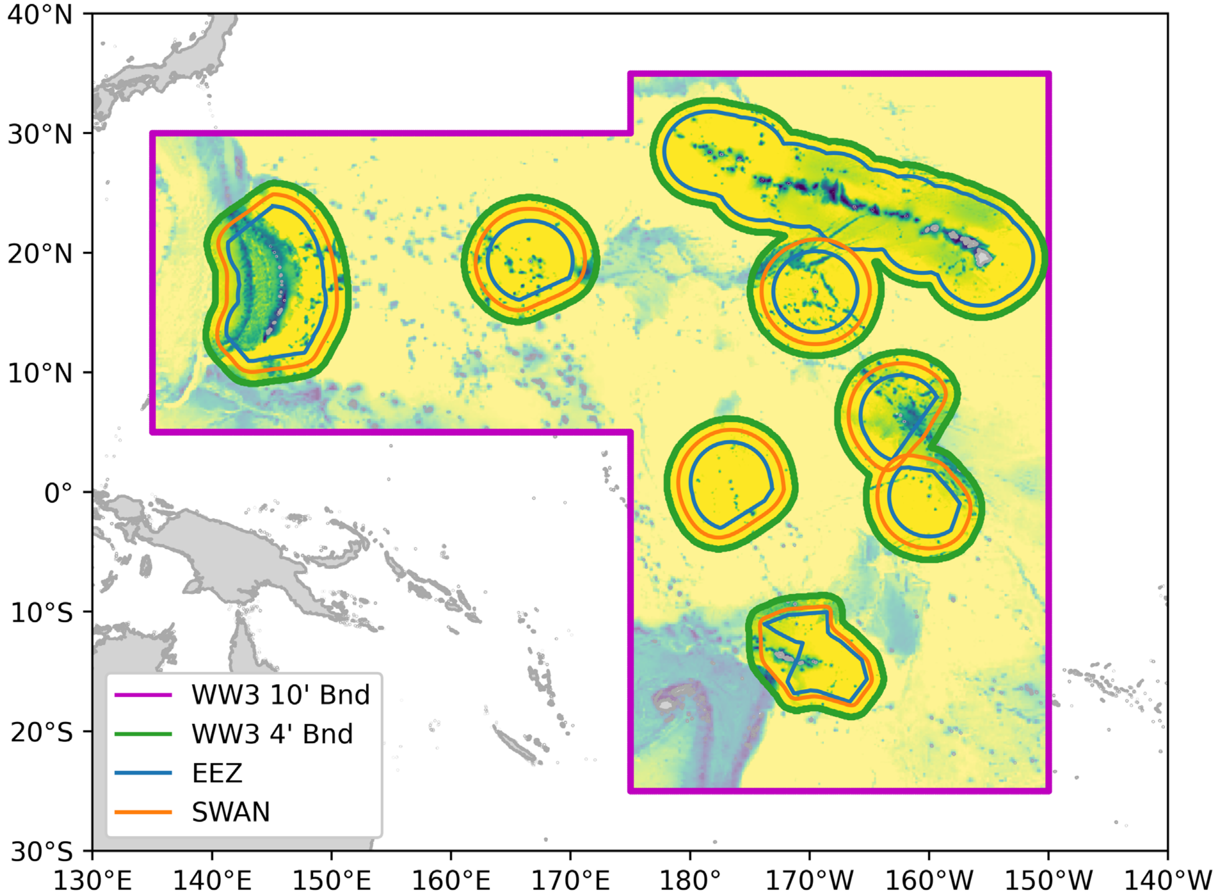

Figure 3.1. Model domains for the Pacific Islands. The global WW3 domain is not shown.

Table 3.1. Summary of nested WW3 model grids.

Grid Name	Coverage	Resolution (long x lat)	Resolution [km] (zonal x meridional) at 20°N	Active Grid Points	Agency
Global Grid L1	77.5°S – 77.5°N 0 – 360°W	0.5° × 0.5°	52.2 × 55.6	191,352	NOAA
Nested Grid L2	25.0°S – 35.0°N 135.0°E – 150.0°W	10' × 10'	17.4 × 18.5	213,686	PNNL
Nested Grid L3	1° beyond the EEZ	4' × 4'	7.0 × 7.4	112,284	PNNL

WW3 is configured using the ST4 source term package (Ardhuin et al. 2010) to simulate wind input and dissipation due to whitecapping. This parameterization has been shown to provide good results in previous model hindcasting in the Pacific Ocean (Yang et al. 2017; Wu et al. 2020). Depth-induced wave breaking is simulated with the Battjes and Janssen (1978) formulation and the dissipation due to bottom friction uses the JONSWAP parameterization (K. Hasselmann et al. 1973).

The time steps used in the WW3 model are summarized in Table 3.2. Each model grid requires four time steps: (1) the global time step Δt_g, (2) the spatial propagation time step Δt_{xy}, (3) the intra-spectral propagation time step Δt_k, and (4) the source term time step Δt_s (WW3DG 2016). The spatial propagation time step Δt_{xy} must conform with the Courant–Friedrichs–Lewy (CFL) limit to ensure model stability.

Table 3.2. Time steps for WW3.

Nested Grid	Δt_g (s)	Δt_{xy} (s)	Δt_k (s)	Δt_s (s)
L1	1,800	600	900	30
L2	300	300	150	10
L3	300	150	150	10

All WW3 simulations used 24 direction bins and 32 frequency bins with a logarithmic increment factor of 1.1 starting from 0.035 Hz to 0.672 Hz. This configuration in spectral space meets the minimum requirements specified in the IEC-TS (i.e., a minimum of 25 frequency components covering at least 0.04 to 0.5 Hz and 24 to 48 directional components).

3.2 Unstructured-grid SWAN Model Configuration

Seven unstructured-grid SWAN models were developed to cover the EEZ (see Figure 3.1). An unstructured-grid model provides the flexibility to increase resolution in shallow and nearshore areas for depth-induced wave transformation processes while reducing the resolution in deep waters. This approach has been used on hindcasts for wave resource assessments on the U.S. East Coast (Allahdadi et al. 2019), West Coast (Yang et al. 2017; Wu et al. 2020; Yang et al. 2020), Alaska (Yang et al. 2019; García-Medina et al. 2021), and in Hawaii (García-Medina et al. 2019, Li et al. 2021), as well as in locations around the world (e.g., Robertson et al. 2014, Lokuliyana et al. 2020).

3.2.1 Model Development

Model meshes were developed starting from the coastlines and expanding toward the EEZ boundaries to cover the entire domain. Shoreline data for Sarigan and Aguijan (CNMI) were obtained from NOAA's National Center for Coastal Ocean Science.[1] The shoreline for Kingman Reef was manually delineated based on a PacIOOS survey of its coral distribution and satellite imagery. The coastlines for the rest of the islands were obtained from PacIOOS[2]. The mesh resolution at the shoreline was specified at 100 m by subsampling the coastline data to accurately resolve the islands.

The mesh size resolution transitions from 100 m at the shore to 300 m at 30 km offshore. The model mesh meets the IEC-TS Class 2 requirement for spatial resolution. Beyond 30 km offshore, the mesh density is gradually reduced reaching a resolution of 5,000 m at the model boundary for the CNMI-Guam and American Samoa. In addition, the mesh is configured to be depth dependent. The resolution increases with water depth shallower than 1,000 m where waves 30 s or shorter are affected by bottom topography. The resolution reaches 100 m for

[1] https://products.coastalscience.noaa.gov/collections/benthic/e99us_pac/data_cnmi.aspx Last accessed 11 March 2020.
[2] https://www.pacioos.hawaii.edu/metadata/pac_comp_all_shore.html Last accessed 11 March 2020.

water depths of 250 m or shallower. The rest of the models has a mesh resolution specified by the topography and constrained to be 100 m at the coastline and 5,000 m at the open boundary, (i.e., the resolution is not constrained to 300 m in the inner 30 km region). The objective of this approach is to assure that the model has enough resolution to capture the effect of underwater volcanoes and small islands in wave propagation. This effect has been shown to be important in other regions featured with similar characteristics (Sosa et al. 2017). Smooth transitions were specified during mesh development by restricting the area change between neighboring elements to a maximum of 10%. The model resolution for the different models is shown in Figure 3.2.

All models were configured using the World Geodetic System 84 spheroid and the mean sea level as the vertical datum. ETOPO1 provides the background bathymetry for the Central Pacific. The datasets for the nearshore bathymetry are outlined below in order of precedence.

Commonwealth of Northern Mariana Islands and Guam:

1. 2001 USACE Scanning Hydrographic Operational Airborne (SHOALS) LiDAR bathymetry to 40 m depth at 4 m resolution.
2. 2003 University of Hawaii School of Ocean and Earth Science and Technology (SOEST) multibeam bathymetry to 3.5 km depth at 60 m resolution.
3. 2007 University of Hawaii SOEST multibeam bathymetry to 400 m depth at 5 m resolution.
4. 2007 USACE LiDAR topography at 0.5 m resolution for the entire island of Guam.
5. 2007 USACE LiDAR bathymetry at 4 m resolution (limited coverage).
6. 2008 US Navy & NOAA multibeam bathymetry of Apra Harbor at 1 m resolution.
7. 2011 University of Hawaii SOEST multibeam bathymetry to 3.5 km depth at 60 m resolution.

American Samoa

1. 40 m DEM of Rose Atoll originated by PIBHMC, Coral Reef Ecosystem Division, Pacific Islands Fisheries Science Center, National Marine Fisheries Service (NMFS), NOAA[3].
2. 40 m DEM of Swains Island originated by PIBHMC and distributed by PacIOOS[4].
3. NOAA National Geophysical Data Center (now National Centers for Environmental Information [NCEI]) 90 m Bathymetry: American Samoa (Lim et al. 2010).

The Pago Pago tide gauge (NOAA ID 1770000) was used to transform vertical datum to mean sea level.

Howland and Baker Islands, Jarvis Island, Johnston Atoll, Palmyra Atoll, and Kingman Reef

1. Gridded bathymetry by the (PIBHMC) provided with Mean Lower Low Water (MLLW) as vertical datum:
   a. Howland Island: 2 m, 5 m, and 40 m DEM
   b. Baker Island: 5 m and 40 m DEM

[3] https://www.coris.noaa.gov/metadata/records/html/rose_40m_hardsoft.html
[4] http://pacioos.org/metadata/pibhmc_bathy_40m_swains.html

   c. Jarvis Island: 5 m and 20 m DEM
   d. Johnston Atoll: 5 m and 20 m DEM
   e. Palmyra Atoll: 5 m and 40 m DEM
   f. Kingman Reef: 5 m and 20 m DEM
2. 3 arc-second gridded multibeam bathymetric data by NOAA’s NCEI sampled at Winslow Reef, which is located within the Howland and Baker Islands domain (NOAA National Centers for Environmental Information 2004).

Howland and Baker Islands are part of the Phoenix Islands. Without tide gauges located in that region, we use mean values between the Johnston Atoll gauge (NOAA 161900) and the Pago Pago gauge (NOAA ID 1770000) to convert the MLLW to the mean sea level. The remaining sites (i.e., Jarvis Island, Johnston Atoll, Palmyra Atoll, and Kingman Reef) are all part of the Line Islands, so the datum conversions reference the Johnston Atoll gauge.

Wake Island

1. 1/3 arc-second NCEI DEM bathymetry (Mean High Water vertical datum, [NOAA National Geophysical Data Center 2009a]).
2. 3 arc-second NCEI DEM bathymetry (Mean High Water vertical datum, [(NOAA National Geophysical Data Center 2009b]).
3. 3 arc-second gridded multibeam bathymetry sampled at the location of five seamounts within the domain (NOAA National Centers for Environmental Information 2004).

The Wake Island tide gauge (NOAA ID 1890000) was used to convert elevations to mean sea level vertical datum.

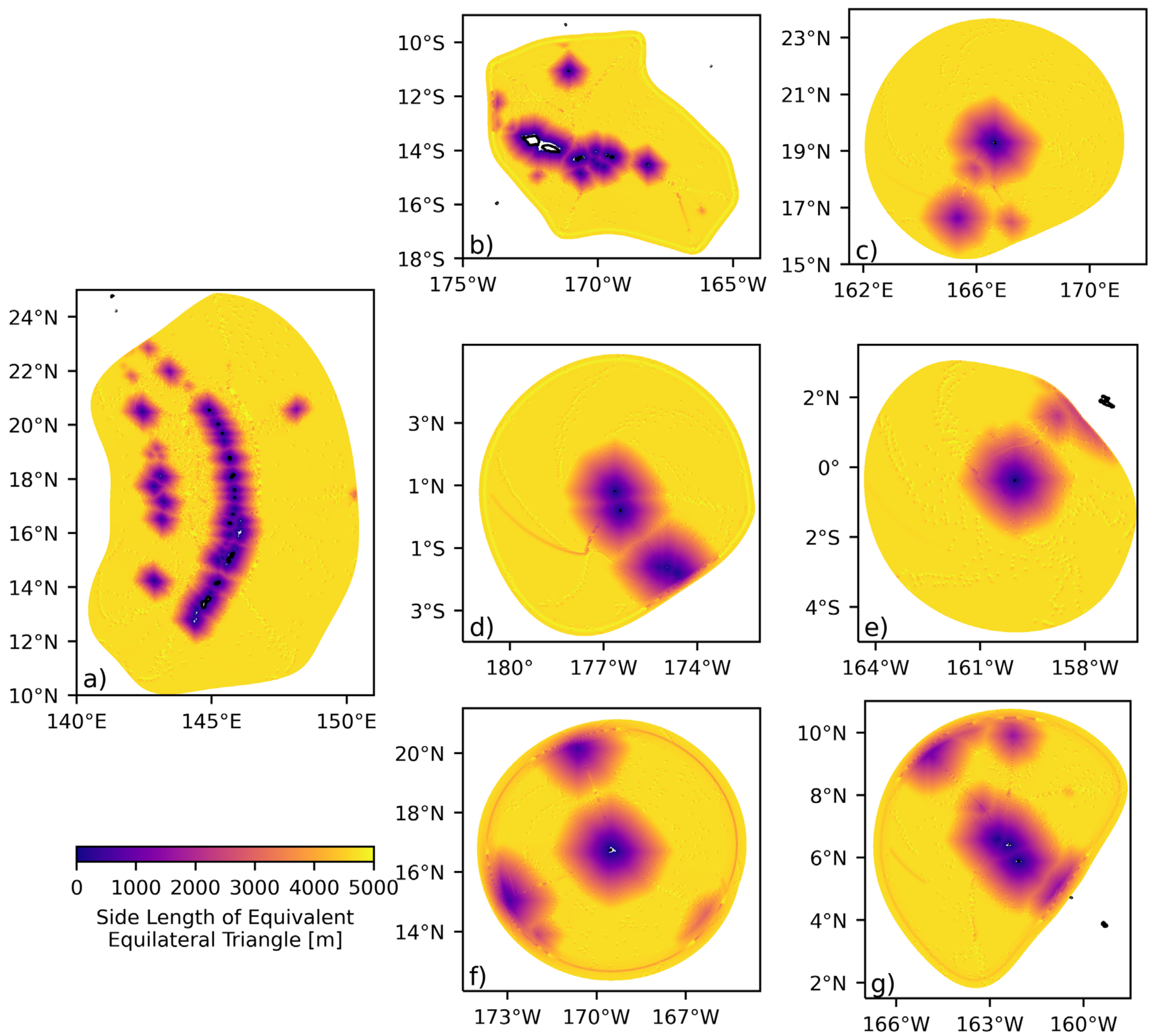

Figure 3.2. Model resolution expressed as the side length of an equilateral triangle of equal area to that of each element: (a) Commonwealth Northern Mariana Islands and Guam; (b) American Samoa; (c) Wake Island; (d) Baker and Howland Islands; (e) Jarvis Island; (f) Johnston Atoll; and (g) Palmyra Atoll and Kingman Reef.

3.2.2 Model Convergence

Model convergence tests were performed to find an optimal balance between model accuracy and efficiency. Seven days were used to spin up the wave models, as was used for other regions (e.g. García-Medina et al. 2019). To solve the interactions between directional quadrants, SWAN employs a Gauss-Seidel technique that operates independently on the quadrants of the spectral computational grid. Numerical convergence might require multiple iterations. The number of iterations is directly proportional to the runtime, and because of practical considerations regarding the computing time it is desirable to evaluate the model's sensitivity to this parameter. Figure 3.3 shows the number of iterations required to achieve convergence for a model configuration. Six models consistently achieve convergence in two iterations. The Wake Island model converges in four iterations most of the time. During the first 6 months of 2000, 49 out of 54,420 (0.09%) time steps did not converge in four iterations for this model. No consecutive time steps requiring five iterations were found. Good convergence with few iterations has been found in previous studies (García-Medina et al. 2019; Allahdadi et al. 2019; Yang et al. 2019). Based on the convergence test, a maximum of 5 iterations was selected for all seven models.

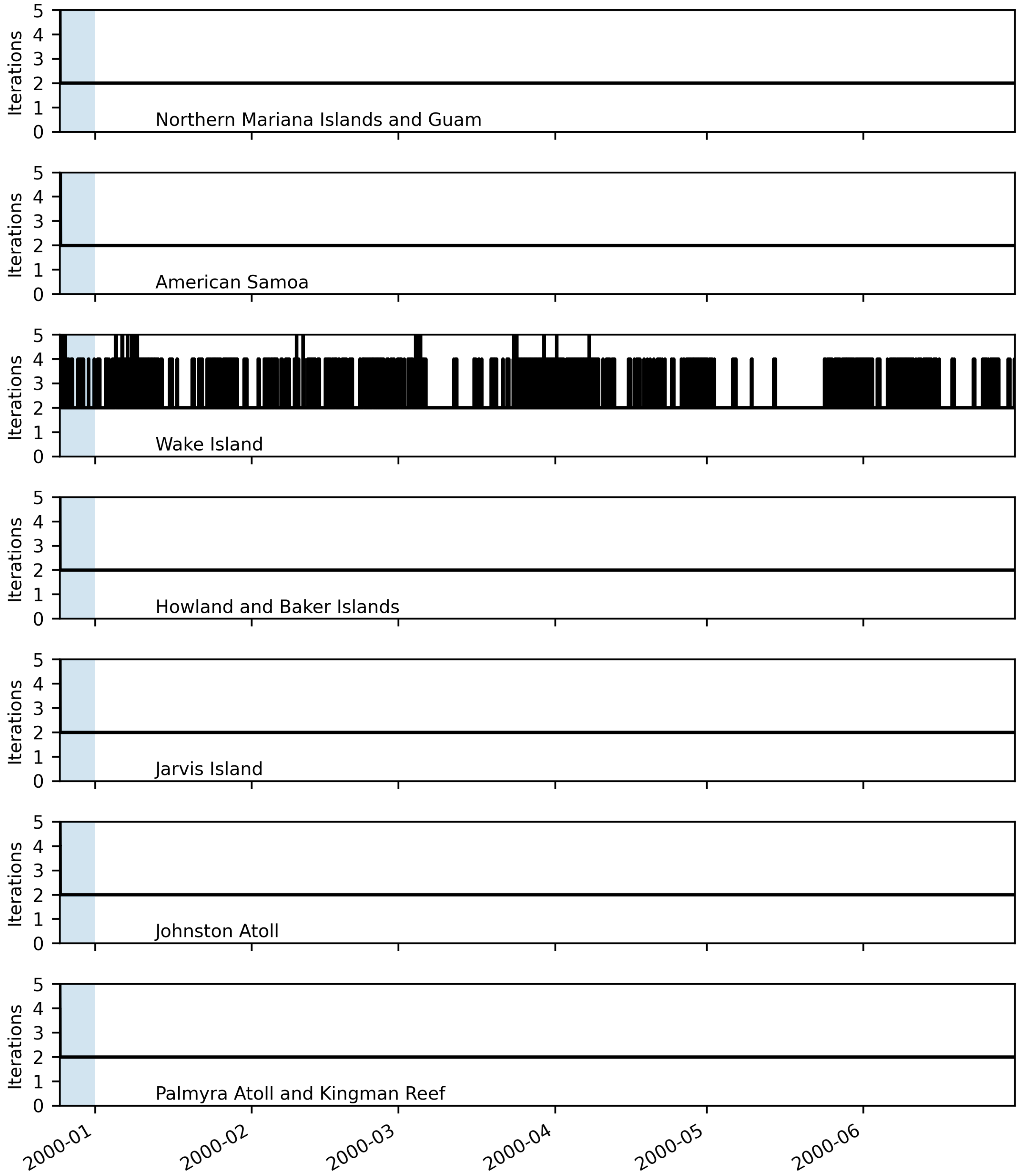

Figure 3.3. Convergence time series for a 6-month simulation with maximum number of iterations set at 5.

SWAN implements a first-order implicit Euler scheme that is not constrained by the CFL condition (Zijlema 2010) when using the unstructured mesh solver. This results in an unconditionally stable model. However, the accuracy can be affected by the solution time step (e.g., García-Medina et al. 2019; Yang et al. 2019). Therefore, an optimal time step must be chosen based on convergence analysis. Large time steps are desirable for computational efficiency. Based on previous experience, a time step of 5 minutes is sufficient to achieve numerical convergence. To test this hypothesis, additional 2-month simulations were conducted with a time step of 3 minutes for all the models. Significant wave height and energy period are computed and compared between simulations. For example, time series of wave conditions near Wake Island are shown in Figure 3.4. Results for other domains are shown in Appendix B. The differences between the 5- and 3-minute integration time steps were found to be virtually indistinguishable, except for Palmyra Atoll and Kingman Reef, and Johnston Atoll where slight phase differences were seen in the arrival of swells. Another simulation with a 2-minute time step were performed in those domains, and the results shows model convergence with the 3-minute time step.

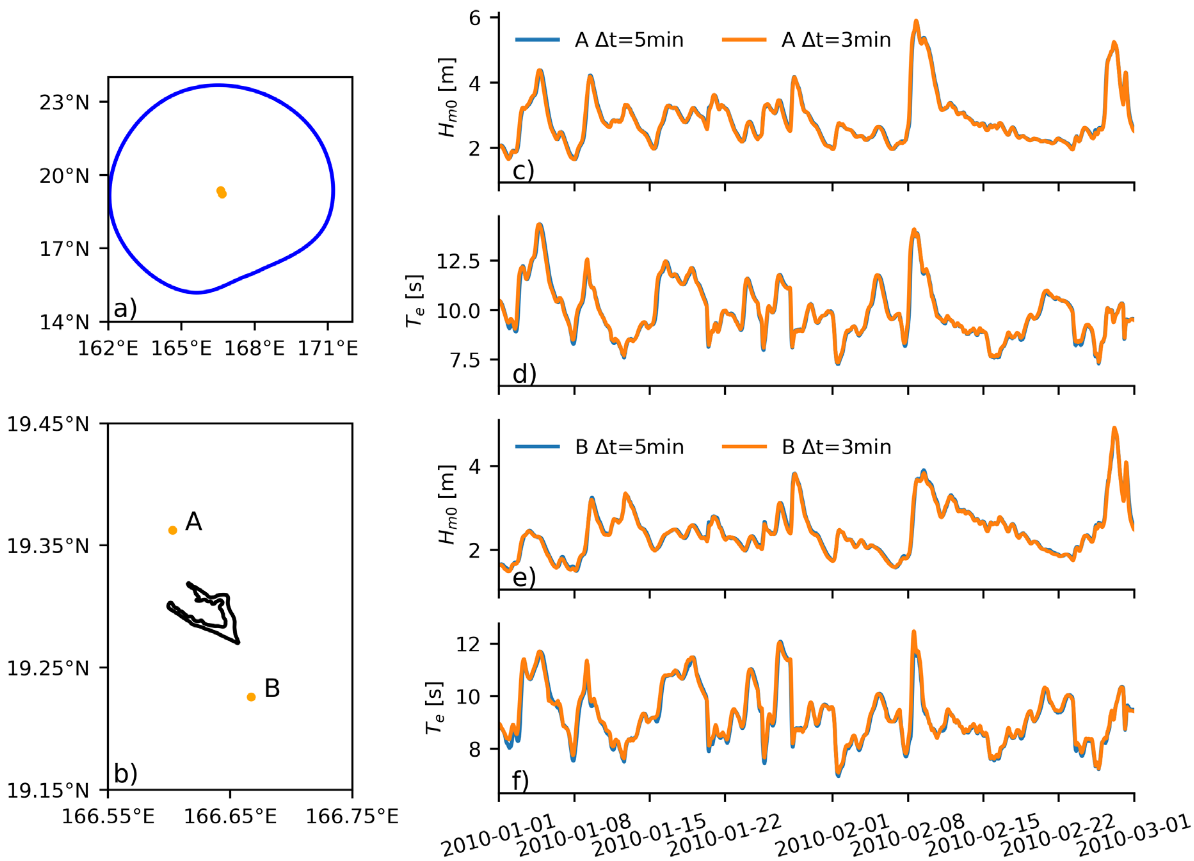

Figure 3.4. Wake Island domain (a and b). Sensitivity run for significant wave height (c) and peak wave period (d) for different integration time steps at site A, same for (e) and (f) at site B.

3.2.3 Practical Aspects

All seven SWAN models were executed using the high-performance computing cluster at PNNL. To optimize the computing resources, the 32-year hindcast was divided into 64 segments. Each segment was started 7 days in advance to ensure adequate time for propagation of the boundary conditions to the interior of the model domain. An initial condition was estimated using the stationary solution for the initial time. It took less than 7 days to complete the computation of each individual segment.

The wave spectrum was discretized with 5° directional resolution to accurately account for wave propagation and transformation processes. In frequency space, 31 logarithmically spaced bins from 0.035 to 0.505 Hz were used for the American Samoa and the Commonwealth Northern Mariana Islands and Guam models. For the other domains, 34 logarithmically spaced bins from 0.030 to 0.697 Hz were implemented. Table 3.3 shows the IEC-TS homologation based on the computational model setup. A detailed model output inventory is presented in Section 4.3.

Table 3.3. IEC-TS homologation table for a Class 2 (Feasibility) study for the model setup.

Criterion	IEC-TS Requirement	This Study
Coarsest spatial resolution	Maximum of 500 m	Maximum of 300 m within 30 km from shore and 100 m resolution at shoreline
Minimum output intervals	3 h	3 h
Minimum number of wave frequency bins	25	31 – 34
Minimum number of directional bins	36	72
Wind-wave growth	Required	Komen et al.1984
Whitecapping	Required	Komen et al. 1984)
Quadruplet interactions	Required	Hasselmann et al. 1985
Wave breaking	Required	Battjes and Janssen 1978
Bottom friction	Required	Hasselmann et al. 1973
Triad interactions	Required	Eldeberky 1996
Diffraction	Required	Considered
Refraction	Required	Considered
Sea-ice	Required	No ice present in the region
Water level variations	Required	Not considered
Wave reflections	Required	Not considered
Wave-current interactions	Required	Not considered

4.0 Model Hindcast and Validation

This section presents the model results, including the relevant parameters for wave resource assessment following IEC-TS, the model validation, and a catalog of the model output.

4.1 IEC Resource Parameters

Six integrated parameters are recommended by the IEC-TS to characterize the wave resource. They were calculated internally within the model at every grid point. These parameters include the omnidirectional wave power, significant wave height, energy period, spectral width, direction of maximum directionally resolved wave power, and directionality coefficient defined below.

4.1.1 Parameter Definitions

The omnidirectional wave power, J, is the sum of the contributions to energy flux from each spectral component S_{ij} across a cylinder of unit cross-sectional area over the water column,

$$J = \rho g \sum_{i,j} c_{g,i} S_{ij} \Delta f_i \, \Delta\theta_j \tag{1}$$

where ρ = the density of sea water;
g = the acceleration due to gravity;
$c_{g,i}$ = the group velocity, which is a function of frequency and depth;
Δf_i = the frequency bin width at each discrete frequency index i; and
$\Delta\theta_j$ = the direction bin width at each discrete direction index j.

Directionally integrated parameters are calculated from one-dimensional (directionally unresolved) frequency variance density obtained by summing over direction

$$S_i = \sum_j S_{ij} \Delta\theta_j. \tag{2}$$

The significant wave height is defined from the zeroth spectral moment

$$H_s \sim H_{m0} = 4\sqrt{m_0}\,, \tag{3}$$

where the moments of a variance spectrum are defined as

$$m_n = \sum_i f_i^n S_i \Delta f_i. \tag{4}$$

The energy period, T_e, is defined as

$$T_e = \frac{m_{-1}}{m_0}. \tag{5}$$

The combination of T_e and H_{m0} is used to define a sea state. The energy period is the variance-weighted mean period of the directionally integrated variance density spectrum. It is preferred over the peak period, because it has lower sensitivity to spectral shape. Particularly for multi-modal spectra.

The spectral width, ϵ_0

$$\epsilon_0 = \sqrt{\frac{m_0 m_{-2}}{(m_{-1})^2} - 1}, \tag{6}$$

is a measure of the spreading of energy in frequency space. The smaller the spectral width the more homogeneous the sea state.

The directionally resolved wave power, J_θ, is the sum of the wave power crossing a plane perpendicular to a direction, θ:

$$J_\theta = \rho g \sum_{i,j} c_{g,i} S_{ij} \Delta f_i \, \Delta\theta_j cos(\theta - \theta_j)\delta$$
$$\begin{cases} \delta = 1, & cos(\theta - \theta_j) \geq 0 \\ \delta = 0, & cos(\theta - \theta_j) < 0 \end{cases} \tag{7}$$

The maximum time-averaged wave power propagating in a single direction, $J_{\theta_{J_{max}}}$, is the maximum value of J_θ. The corresponding direction, θ_{Jmax}, describes the direction of maximum energy flux.

The directionality coefficient, d, is a characteristic measure of the directional spreading of the wave power. It is defined as the ratio of the maximum directionally resolved wave power to the omnidirectional wave power,

$$\mathrm{d} = \frac{J_{\theta_{jmax}}}{J}, \tag{8}$$

where a value of 1 describes a sea state where all energy is aligned in one direction. Low values indicate the wave energy flux at a point is directionally heterogeneous.

4.1.2 Distribution across the Study Area

Figure 4.1 through Figure 4.7 show the distributions of the six IEC wave resource characterization parameters averaged over the 32-year hindcast. These maps show the spatial distribution of the resource. Seasonal variability can be seen in the monthly averages shown in Appendix A.

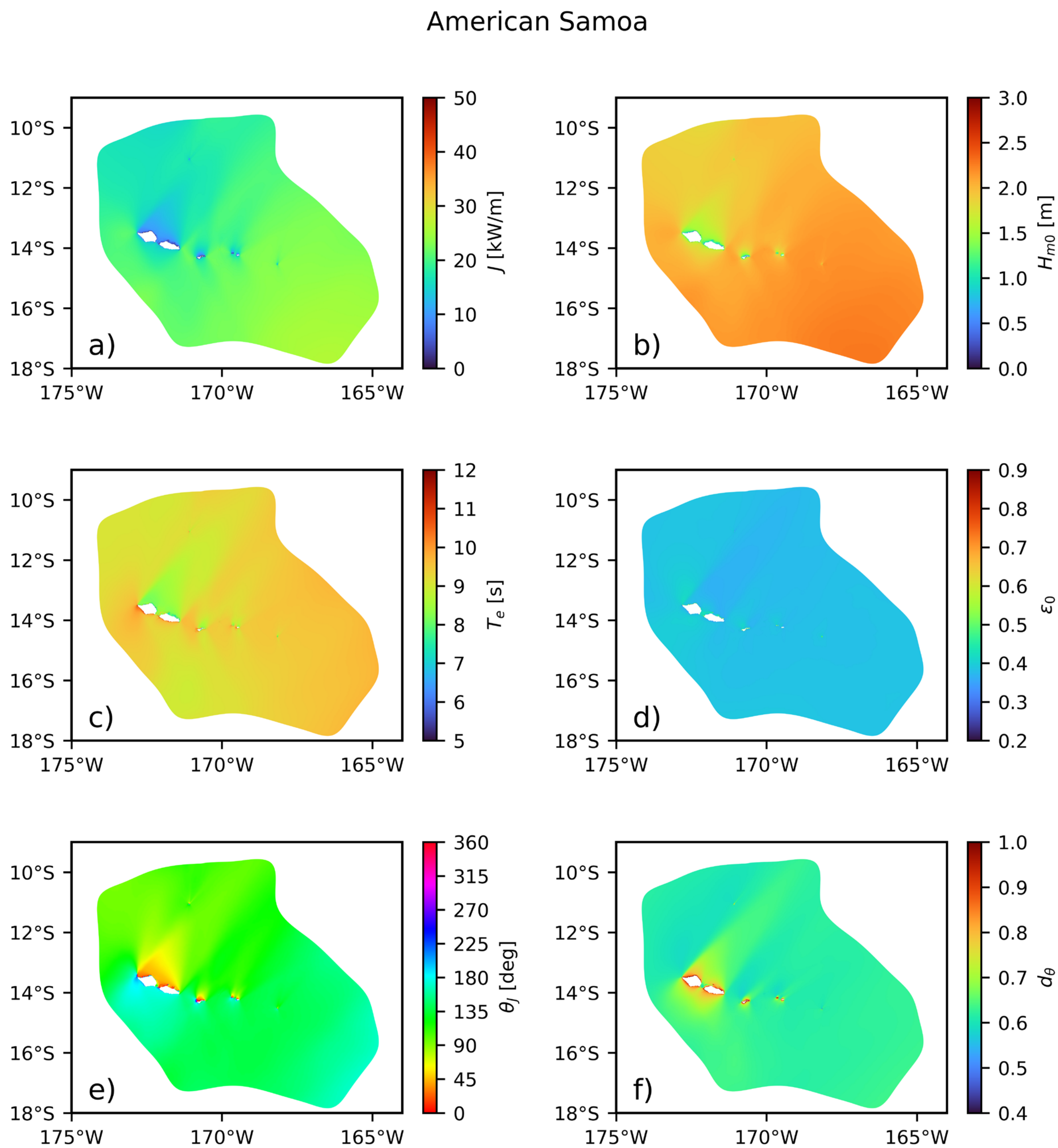

Figure 4.1. Simulated 32-year annual distribution of six IEC wave resource characterization parameters: (a) omnidirectional wave power, (b) significant wave height, (c) energy period, (d) spectral width, (e) direction of maximum directionally resolved wave power, and (f) directionality coefficient around American Samoa.

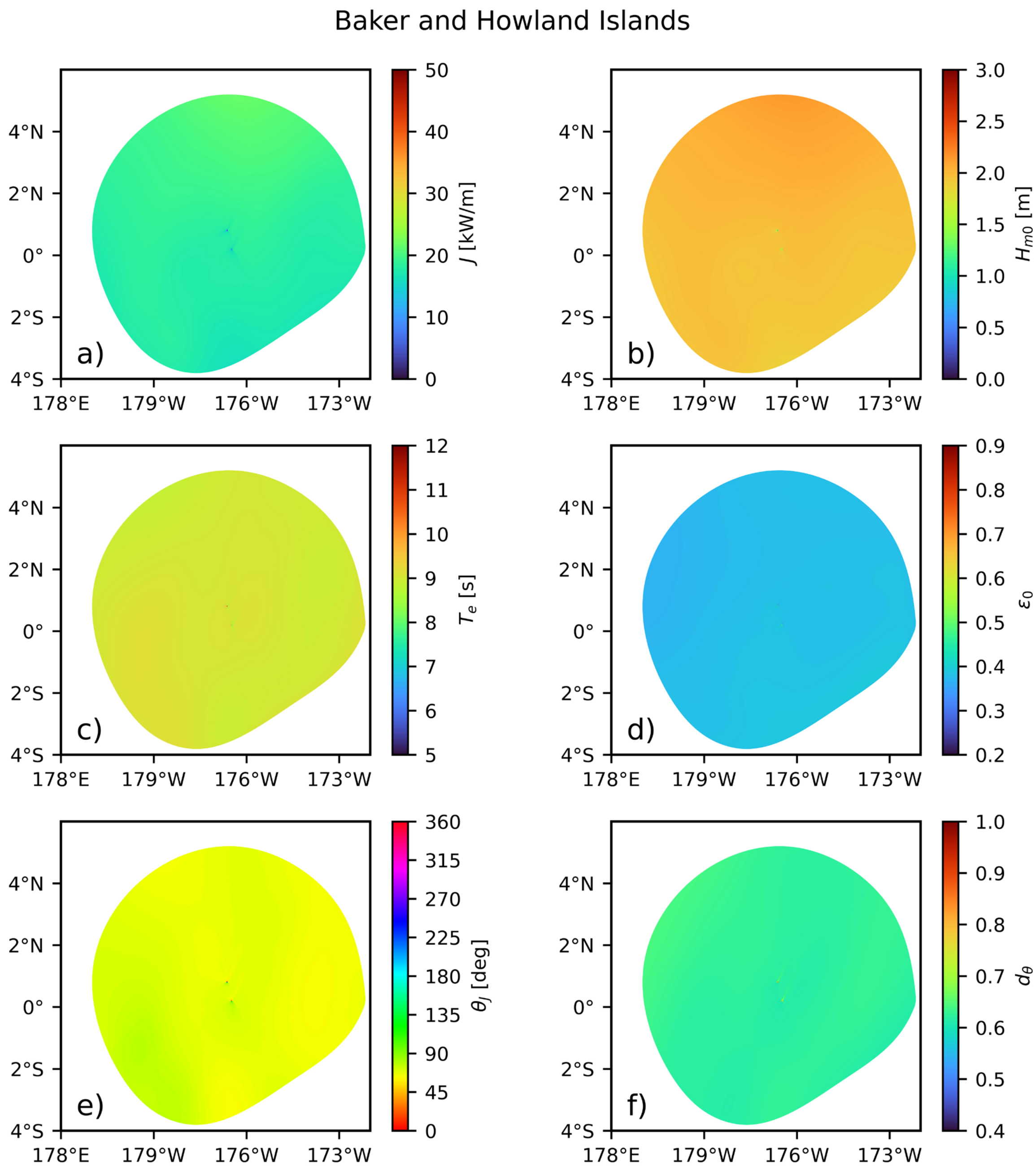

Figure 4.2. Simulated 32-year annual distribution of six IEC wave resource characterization parameters: (a) omnidirectional wave power, (b) significant wave height, (c) energy period, (d) spectral width, (e) direction of maximum directionally resolved wave power, and (f) directionality coefficient around Baker and Howland Islands.

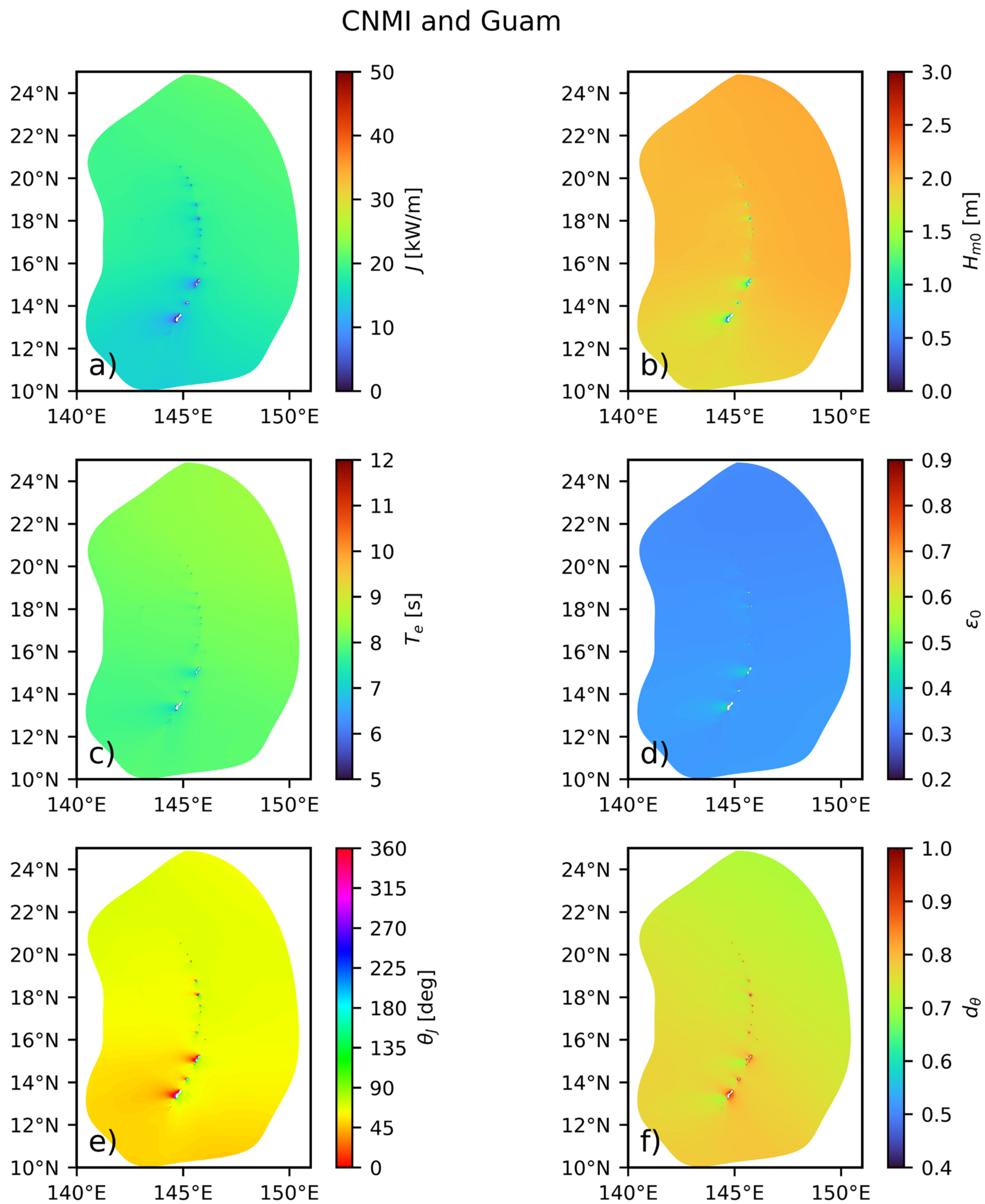

Figure 4.3. Simulated 32-year annual distribution of six IEC wave resource characterization parameters: (a) omnidirectional wave power, (b) significant wave height, (c) energy period, (d) spectral width, (e) direction of maximum directionally resolved wave power, and (f) directionality coefficient around Commonwealth of Northern Mariana Islands and Guam.

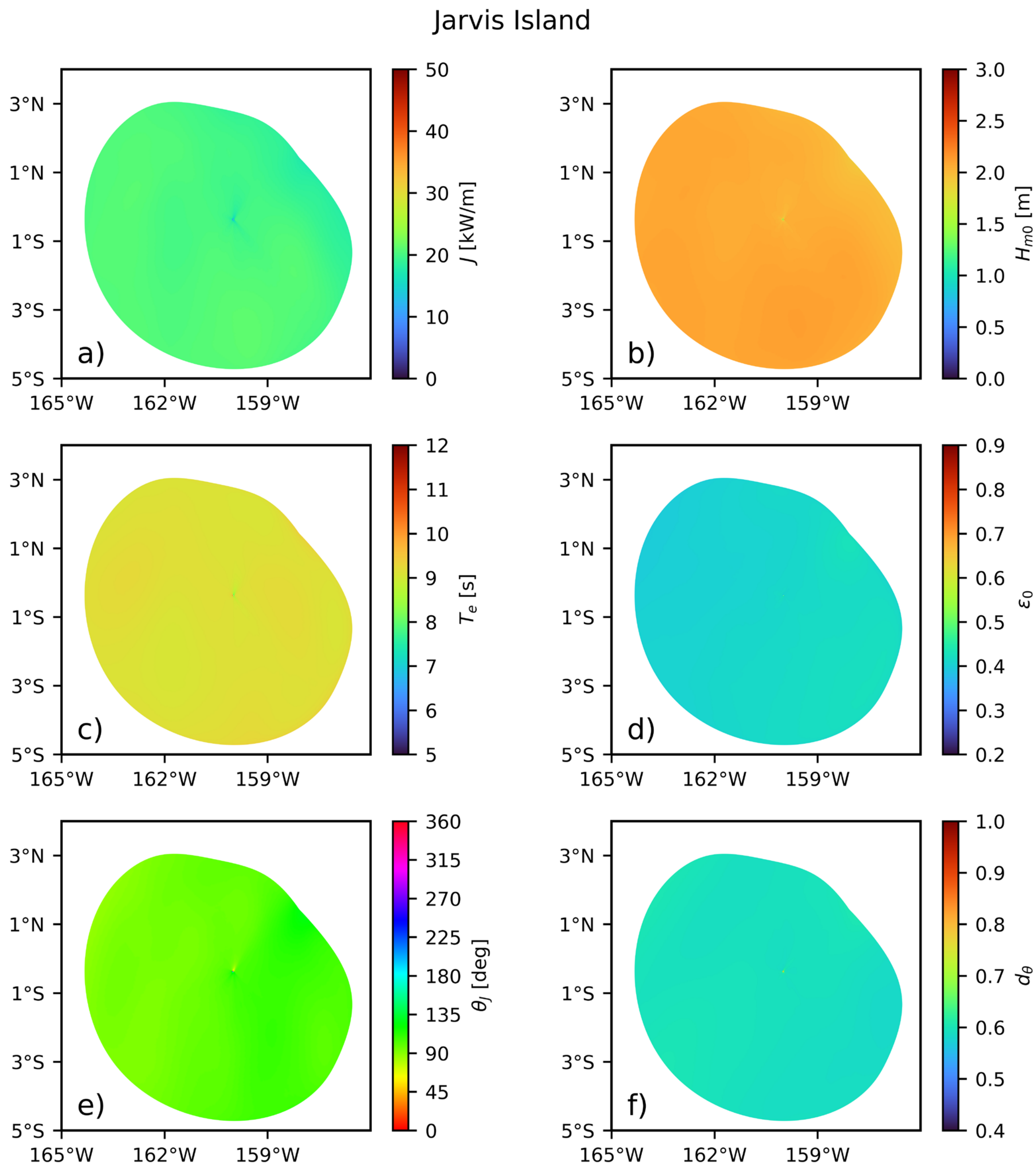

Figure 4.4. Simulated 32-year annual distribution of six IEC wave resource characterization parameters: (a) omnidirectional wave power, (b) significant wave height, (c) energy period, (d) spectral width, (e) direction of maximum directionally resolved wave power, and (f) directionality coefficient around Jarvis Island.

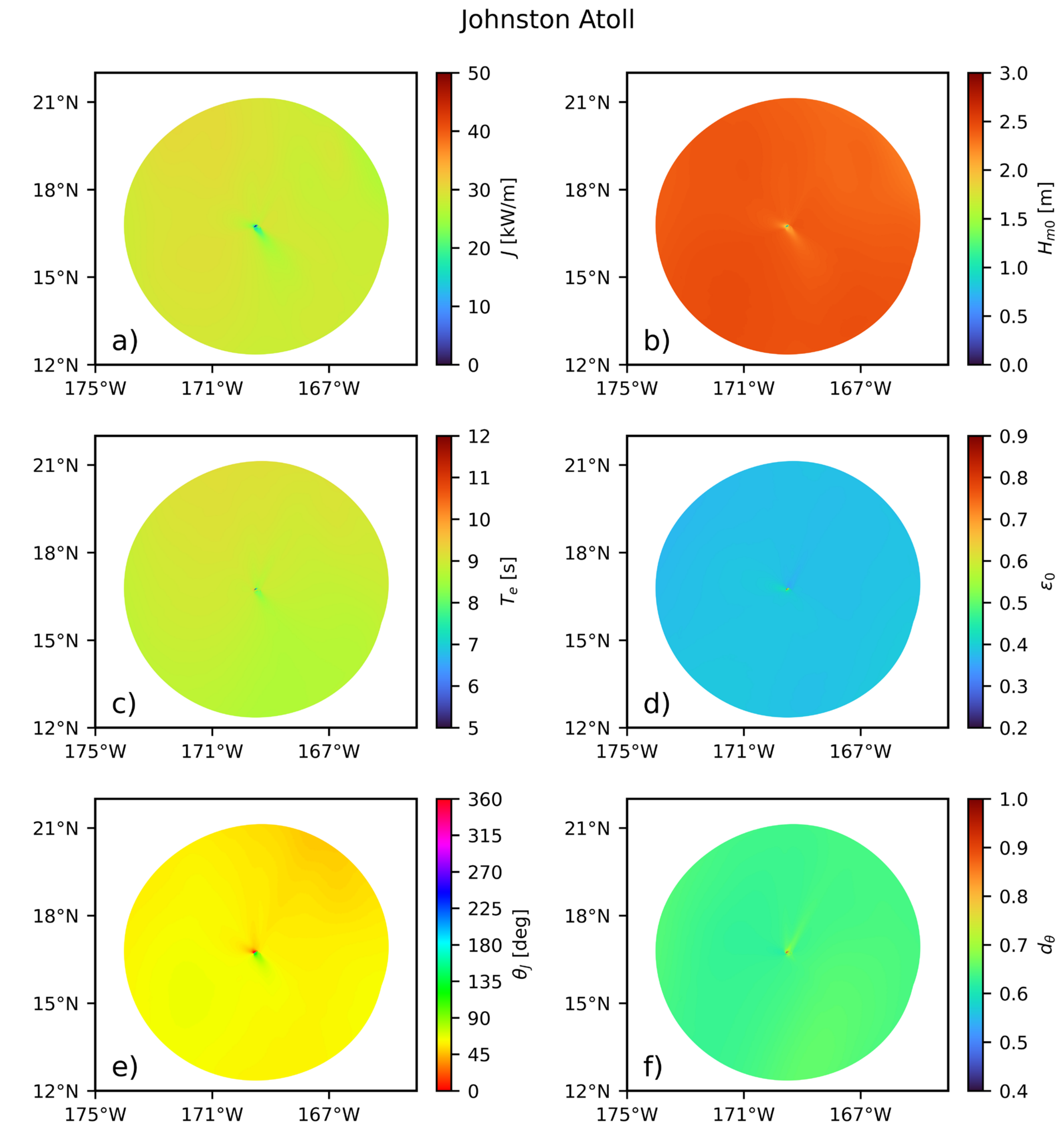

Figure 4.5. Simulated 32-year annual distribution of six IEC wave resource characterization parameters: (a) omnidirectional wave power, (b) significant wave height, (c) energy period, (d) spectral width, (e) direction of maximum directionally resolved wave power, and (f) directionality coefficient around Johnston Atoll.

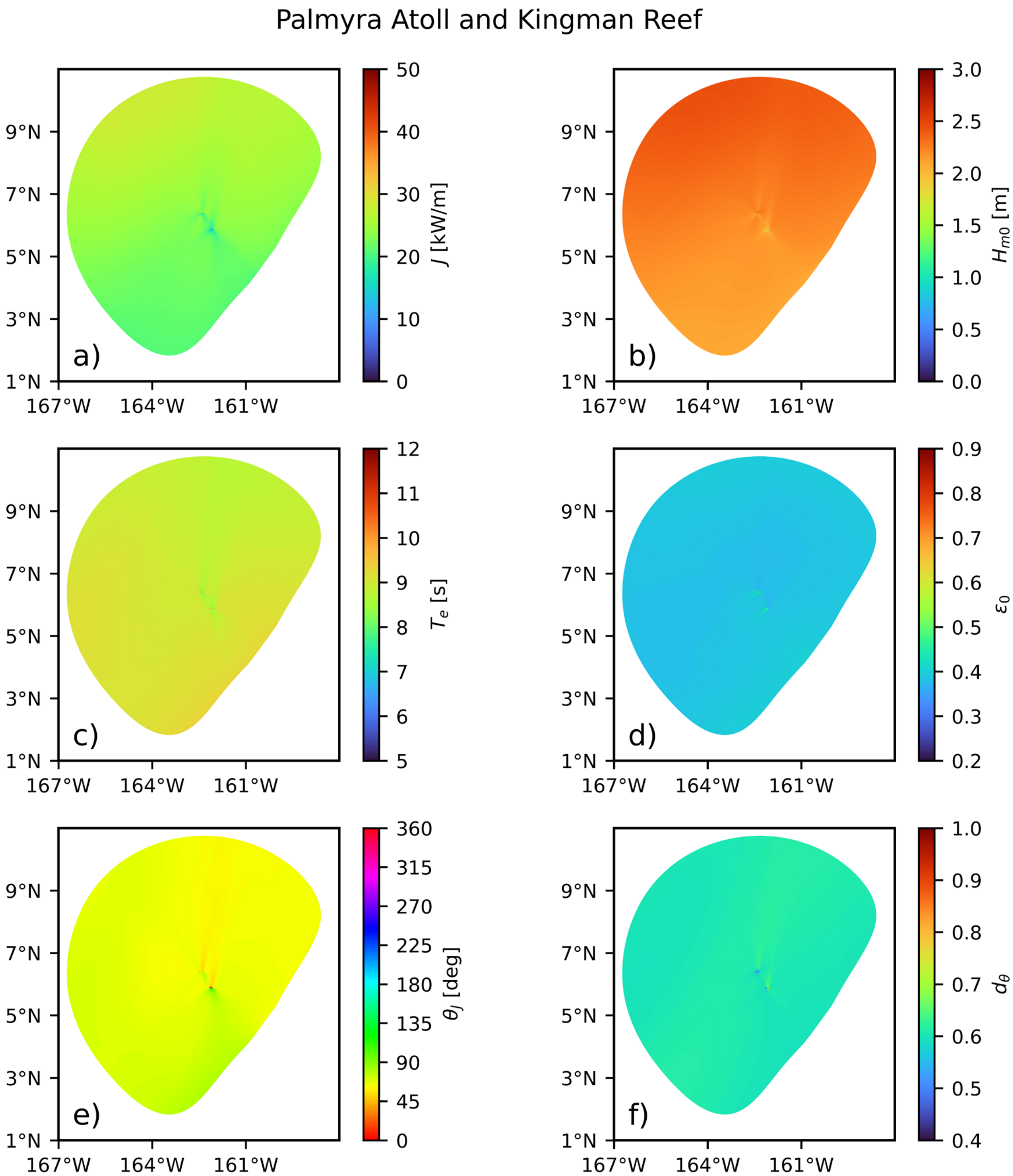

Figure 4.6. Simulated 32-year annual distribution of six IEC wave resource characterization parameters: (a) omnidirectional wave power, (b) significant wave height, (c) energy period, (d) spectral width, (e) direction of maximum directionally resolved wave power, and (f) directionality coefficient around Palmyra Atoll.

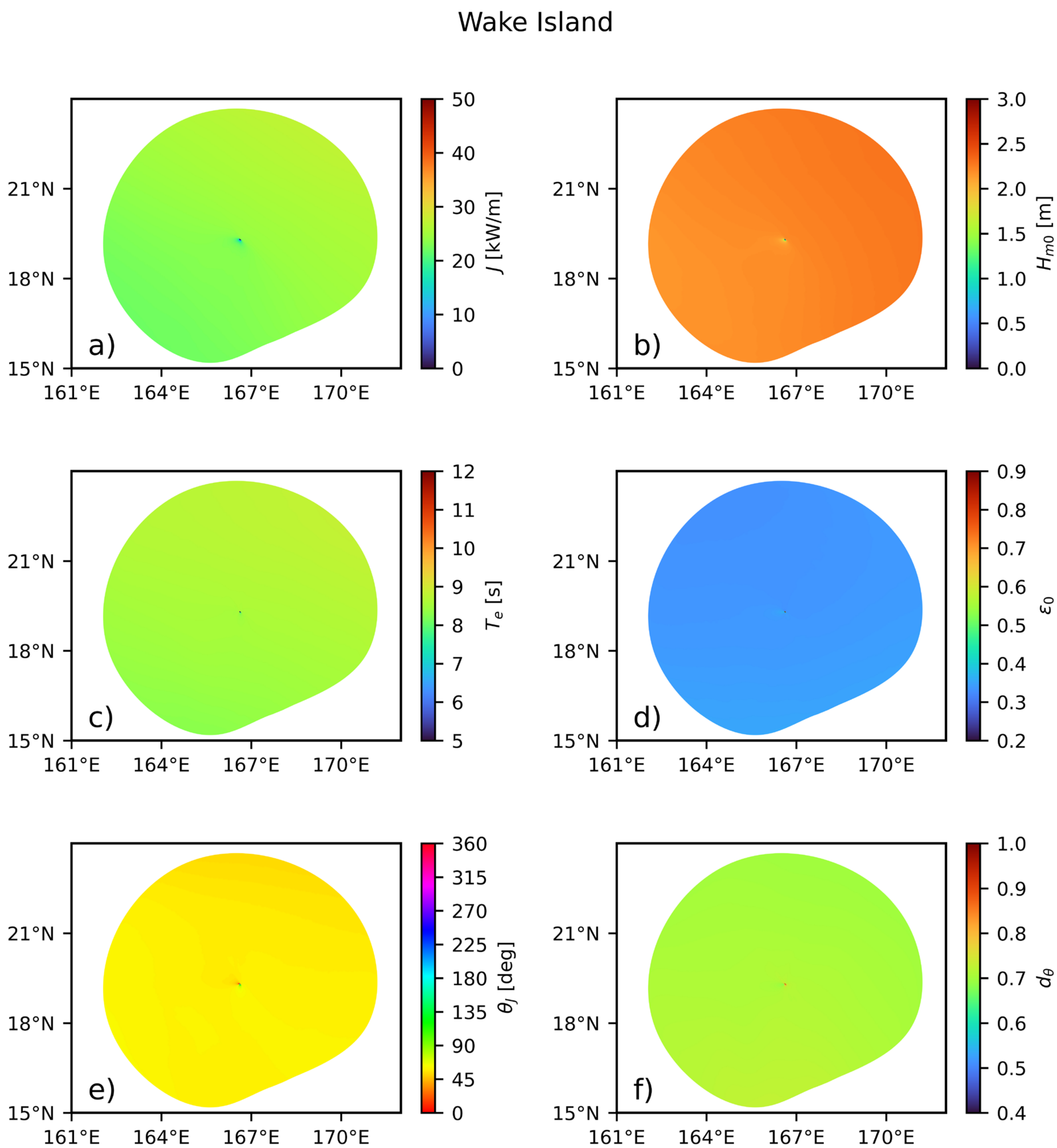

Figure 4.7. Simulated 32-year annual distribution of six IEC wave resource characterization parameters: (a) omnidirectional wave power, (b) significant wave height, (c) energy period, (d) spectral width, (e) direction of maximum directionally resolved wave power, and (f) directionality coefficient around Wake Island.

4.2 Model Validation

Model validation was conducted by comparing the six simulated and measured IEC parameters at the Ipan, Guam buoy station. The time history and scatter plots from the two data sets were generated and model performance metrics were calculated to evaluate the model skills when predicting the six IEC parameters. The following performance metrics, widely used in the industry, were adopted here for model validation.

The root-mean-square-error (*RMSE*) is defined as

$$RMSE = \sqrt{\frac{\sum_{i=1}^{N}(P_i - M_i)^2}{N}} \tag{9}$$

where N is the number of data pairs, M_i is the measured value, and P_i is the predicted (simulated) value. *RMSE* represents the standard deviation of the differences between predicted and measured values.

The percentage error (*PE*) is defined as

$$PE(\%) = \frac{100}{N}\sum_{i=1}^{N}\left(\frac{P_i - M_i}{M_i}\right) \tag{10}$$

which is the average error over the period of comparison.

The scatter index (*SI*) is defined as the *RMSE* normalized by the average of all measured values over the period of comparison:

$$SI = \frac{RMSE}{\overline{M}}, \tag{11}$$

where the overbar indicates the mean of the measured values. Being a normalized quantity, *SI*, allows comparison of model performance across regions that have different wave climates.

Model bias is defined as follows:

$$Bias = \frac{1}{N}\sum_{i=1}^{N}(P_i - M_i). \tag{12}$$

A negative (positive) model bias indicates model underprediction (overprediction) tendency. Percentage bias, which normalizes the bias by the magnitude of the measurements, is defined as

$$Bias(\%) = \frac{\sum_{i=1}^{N} P_i - \sum_{i=1}^{N} M_i}{\sum_{i=1}^{N} M_i} \cdot 100. \tag{13}$$

The linear correlation coefficient, R, is defined as follows:

$$R = \frac{\sum_{i=1}^{N}(M_i - \overline{M})(P_i - \overline{P})}{\sqrt{\left(\sum_{i=1}^{N}(M_i - \overline{M})^2\right)\left(\sum_{i=1}^{N}(P_i - \overline{P})^2\right)}} \tag{14}$$

and is a measure of the linear relationship between the predicted and measured values.

Directional errors are treated differently because directions are a periodic quantity in which 0° and 360° have the same meaning. In computing error statistics for these variables, the angular bias ($bias_\theta$) and the circular correlation (R_θ) are introduced following Hanson et al. (2009) and Bowers et al. (2000), respectively:

$$bias_\theta = \tan^{-1}\frac{\sum_{i=1}^{N}\sin|P_i - M_i|}{\sum_{i=1}^{N}\cos|P_i - M_i|} \tag{15}$$

$$R_\theta = \frac{\sum_{i=1}^{N}\sin(M_i - \bar{M})\sin(P_i - \bar{P})}{\sqrt{\left(\sum_{i=1}^{N}(\sin(M_i - \bar{M}))^2\right)\left(\sum_{i=1}^{N}(\sin(P_i - \bar{P}))^2\right)}} \tag{16}$$

4.2.1 Buoy-Based Model Validation

In situ model-data comparisons were performed off the east shore of Guam. A 1-year comparison in Figure 4.8 shows the model performance across different seasons. The model reproduces the seasonal variability of the wave resource including the magnitude and directional characteristics. Despite underestimation of the peak wave height and power for the extreme events, the model accurately resolves the general characteristics of the wave resource. Figures for all years with available data are provided in Appendix A.

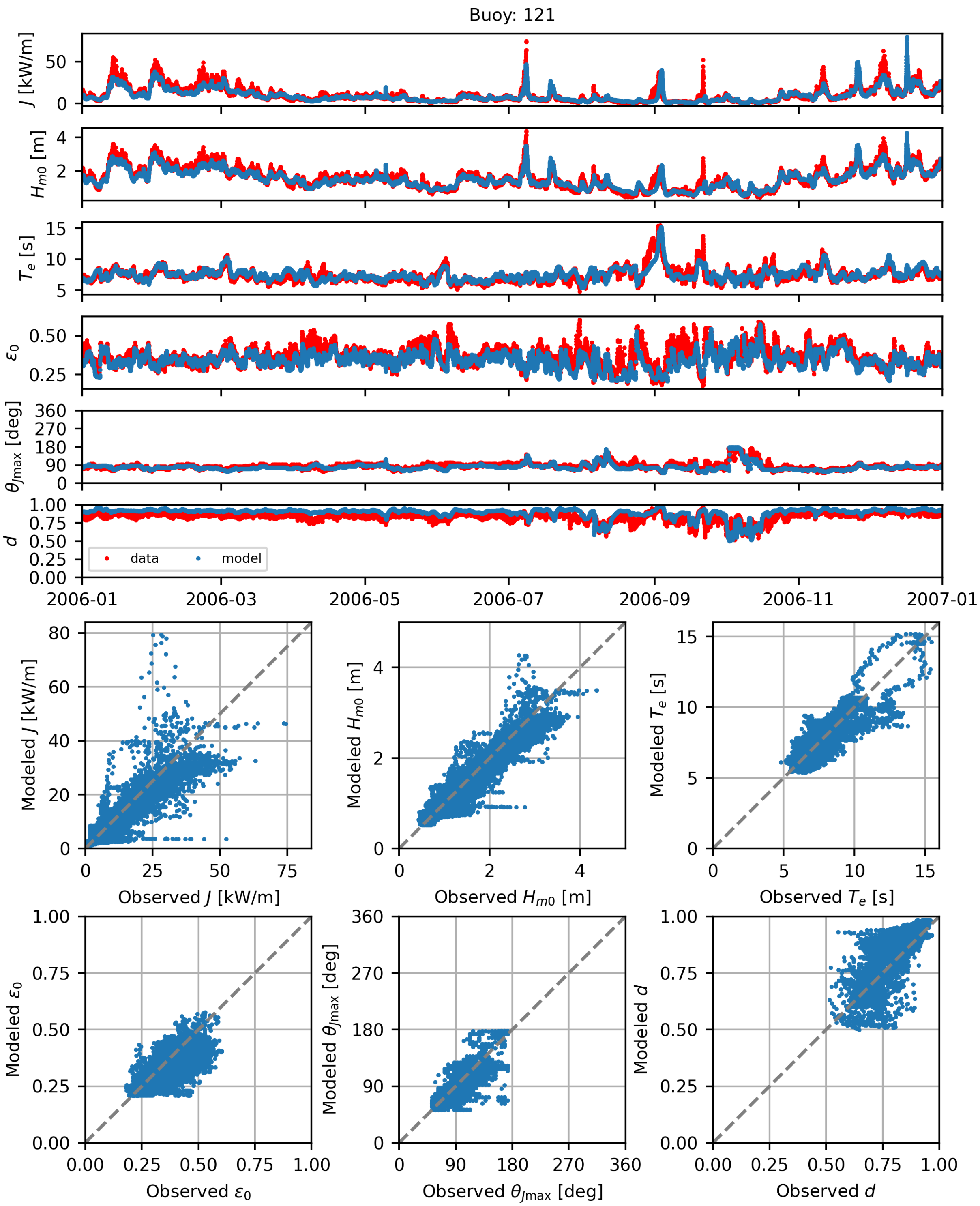

Figure 4.8. Time series (top) and scatter plots (bottom) of the six modeled and observed IEC-recommended wave energy characterization parameters during 2006 at Buoy 121 near Ipan, Guam.

Yearly error statistics are computed and shown in Appendix D and the overall statistics are shown in Table 4.1. Model performance across all parameters is very good with a slight underprediction of the significant wave height (as evident from the time-series comparisons) and overprediction of the energy period which is common for spectral wave models.

Table 4.1. Model performance metrics from 2003 through 2008 at Buoy 121. Number of hindcast and buoy data pairs is 85,131. The error statistics for θ_{Jmax} are computed with the angular formulas.

Parameter	RMSE	PE (%)	SI	Bias	Bias (%)	R
J (kW/m)	4.2	2.0	0.40	-0.9	-8.8	0.91
H_{m0} (m)	0.22	-1.6	0.14	-0.1	-4.3	0.95
T_e (s)	0.6	2.0	0.08	0.2	2.4	0.84
ϵ_0 (-)	0.06	-6.7	0.15	-0.03	-7.5	0.66
θ_{Jmax} (deg)	-	-	-	7.6	-	0.74
d (-)	0.09	8.4	0.10	0.07	7.9	0.60

4.2.2 Altimetry-Based Model Validation

The hindcast significant wave height is interpolated to match the time and location of each available altimetry observation. The hindcast and observed data pairs are binned on to a spatial grid for computation of error metrics. RMSE, bias, and linear correlation coefficient for each domain are shown in Figure 4.9 through Figure 4.15. The RMSE of significant wave height is around 30 cm for most of the islands. The CNMI-Guam region has the largest uncertainties with RMSE reaching 50 cm for some bins. Model bias is generally small with absolute values less than 20 cm. Overall, the correlation coefficients are high throughout all regions.

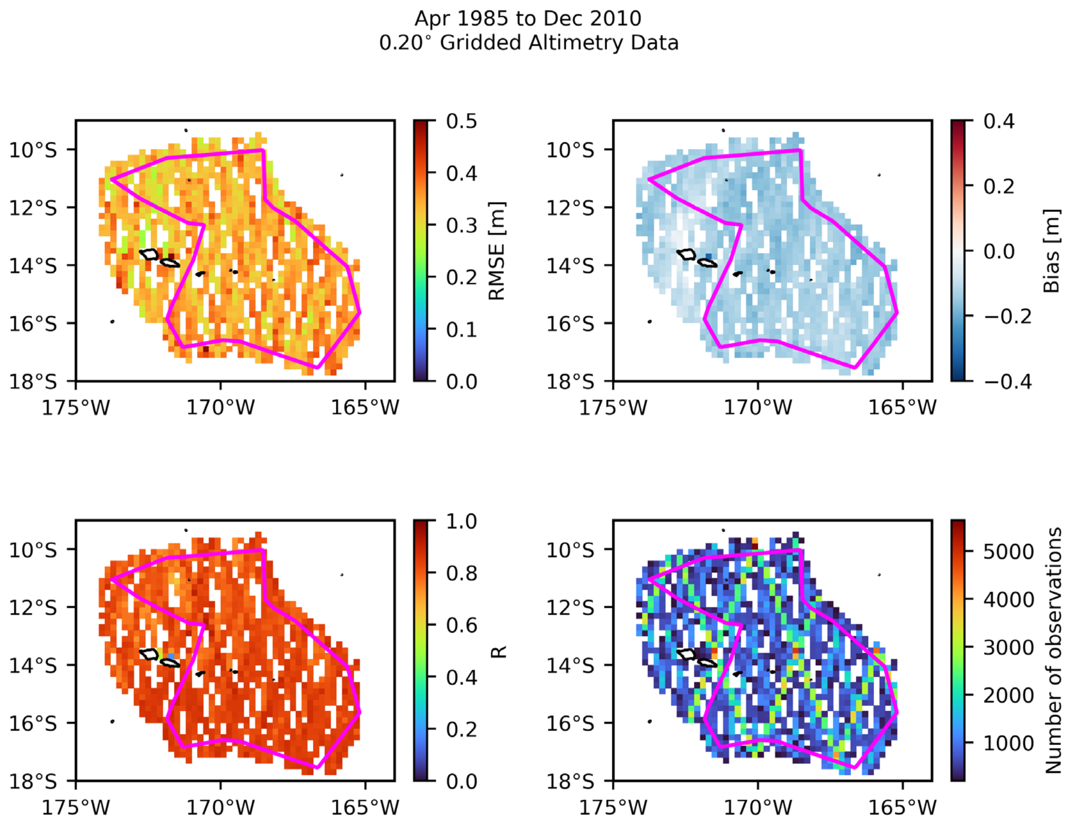

Figure 4.9. Error metrics of hindcast significant wave height compared to altimetry-based observations for American Samoa. The Exclusive Economic Zone is outlined in magenta. A minimum of 200 observations in each bin are required for generating error metrics.

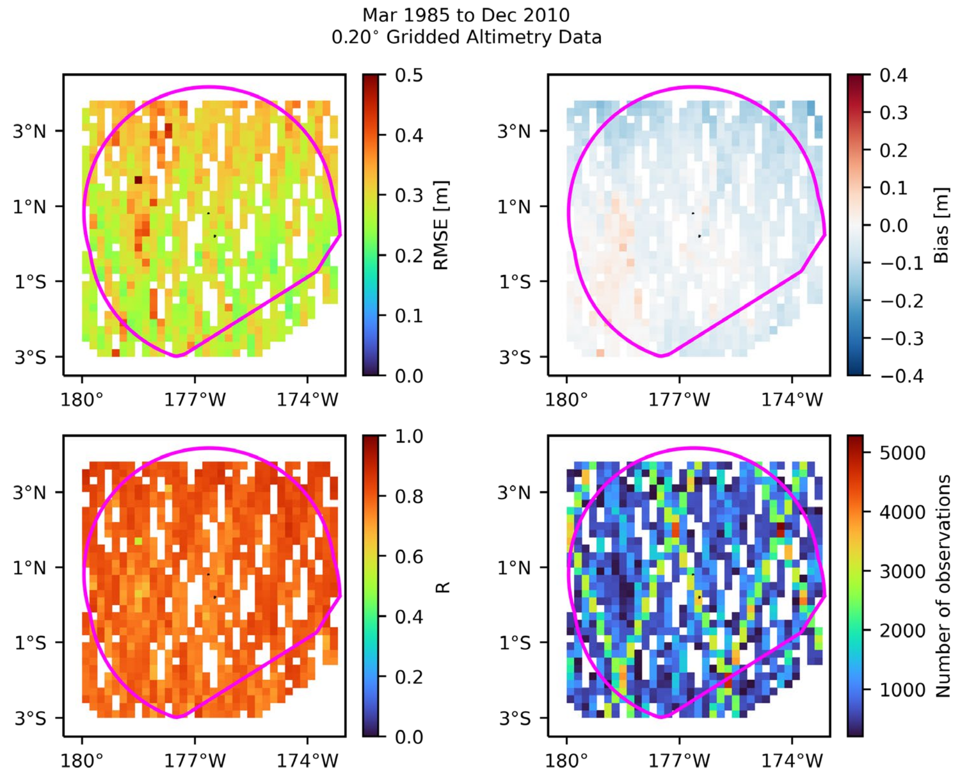

Figure 4.10. Error metrics of hindcast significant wave height compared to the altimetry-based observations for Baker and Howland Islands. The Exclusive Economic Zone is outlined in magenta. A minimum of 200 observations are required for generating error metrics.

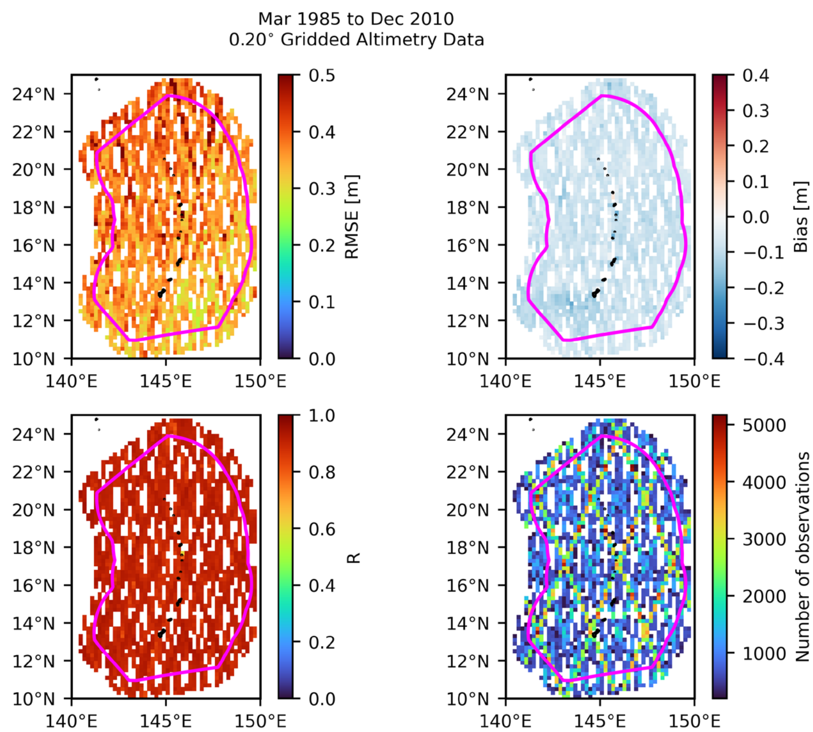

Figure 4.11. Error metrics of hindcast significant wave height compared to the altimetry-based observations for the Commonwealth of Northern Mariana Islands and Guam. The Exclusive Economic Zone is outlined in magenta. A minimum of 200 observations are required for generating error metrics.

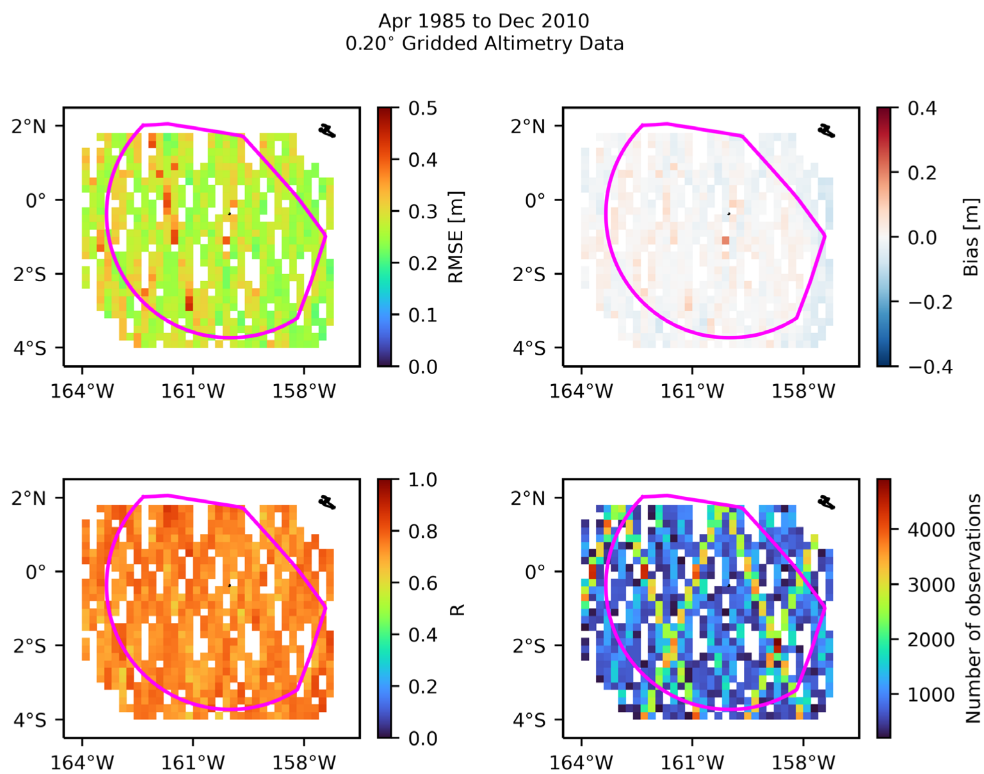

Figure 4.12. Error metrics of hindcast significant wave height compared to altimetry-based observations for the Jarvis Island. The Exclusive Economic Zone is outlined in magenta. A minimum of 200 observations are required for generating error metrics.

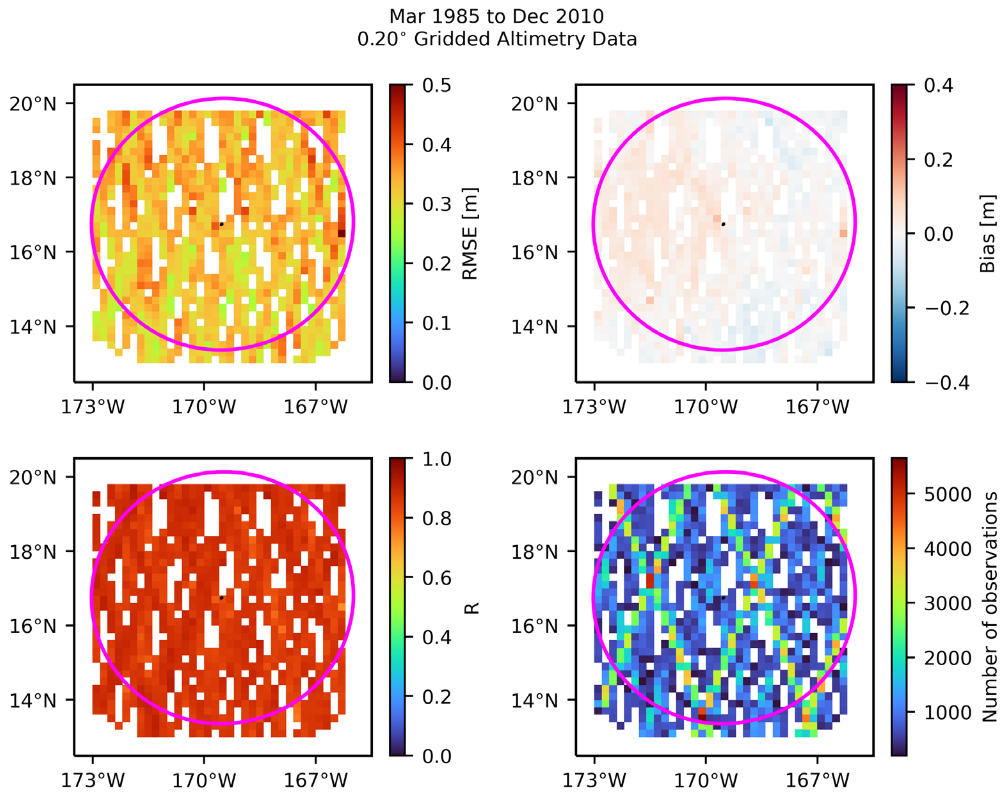

Figure 4.13. Error metrics of hindcast significant wave height compared to altimetry-based observations for the Johnston Atoll. The Exclusive Economic Zone is outlined in magenta. A minimum of 200 observations are required for generating error metrics.

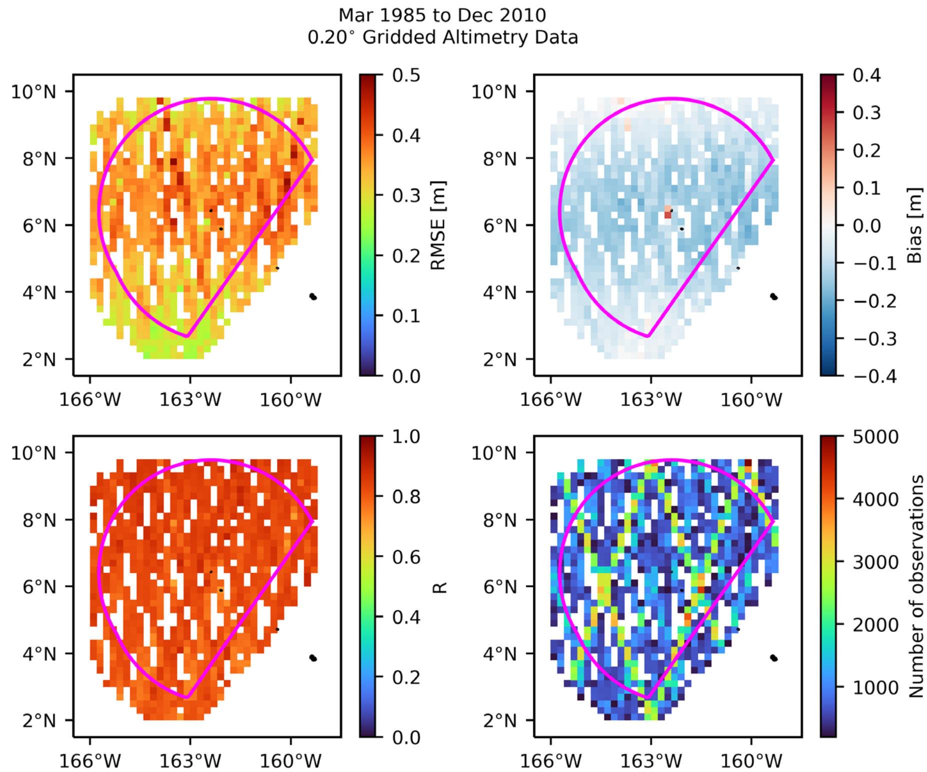

Figure 4.14. Error metrics of hindcast significant wave height compared to altimetry-based observations for the Palmyra Atoll and Kingman Reef. The Exclusive Economic Zone is outlined in magenta. A minimum of 200 observations are required for generating error metrics.

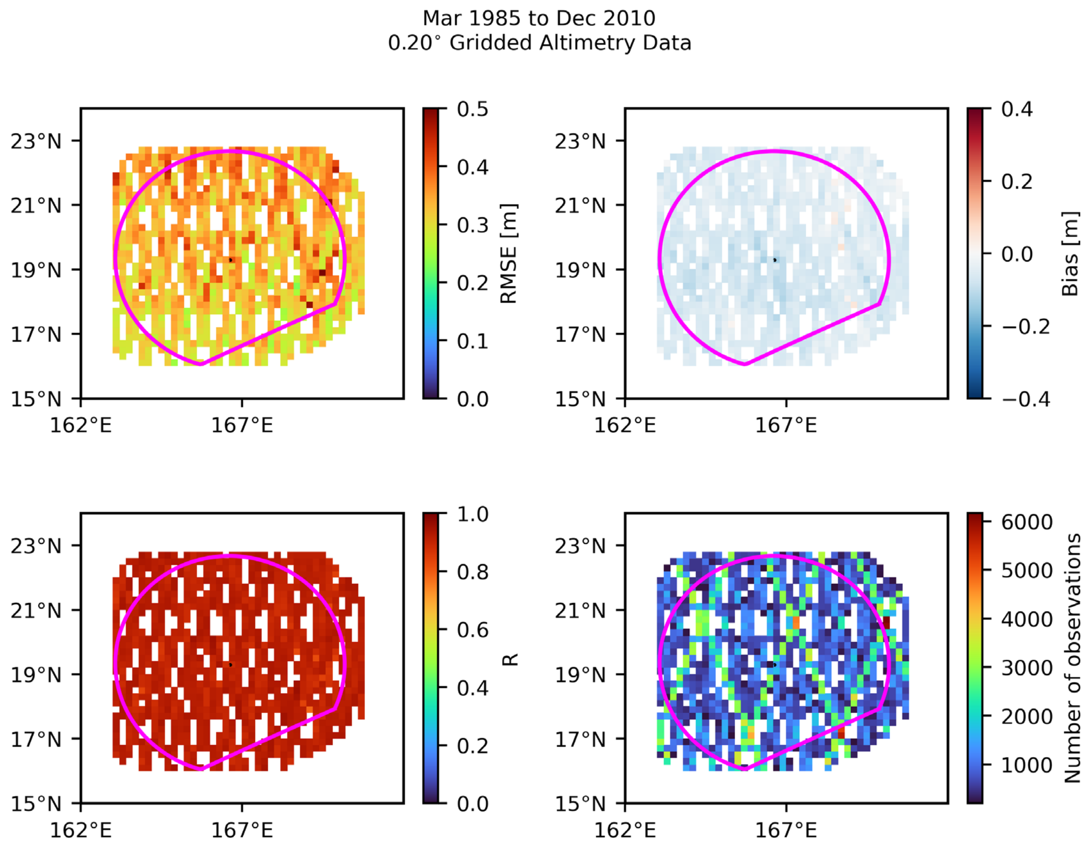

Figure 4.15. Error metrics of hindcast significant wave height compared to altimetry-based observations for the Wake Island. The Exclusive Economic Zone is outlined in magenta. A minimum of 200 observations are required for generating error metrics.

4.3 Data Output

Bulk and partitioned wave parameters were output at 3-hour intervals for all the computational grid over the 32-year hindcast. The parameters are stored in separate files for each month following the Climate and Forecast convention. In addition, hourly frequency-direction spectra are output at locations based on distance from shoreline and depth criteria. The number of output points is listed in Table 4.2. As an example, the location map of the spectral output stations is shown in Figure 4.16.

Table 4.2. Output inventory.

Type	Grid	Number of Points							Temporal Resolution
		AS	BI	JA	JI	MI	PA	WI	
Bulk wave parameters	Computational	452,579	127,059	145,448	58,400	450,688	141,680	69,947	3 h
Spectral partitions	Computational	452,579	127,059	145,448	58,400	450,688	141,680	69,947	3 h
Wave Spectra	100 m isobath	239	22	65	14	629	86	23	1h

Type	Grid	Number of Points							Temporal Resolution
		AS	BI	JA	JI	MI	PA	WI	
Wave Spectra	2 km from shore	106	19	16	11	330	15	16	1h
Wave Spectra	5 km from shore	61	38	25	20	184	24	25	1h

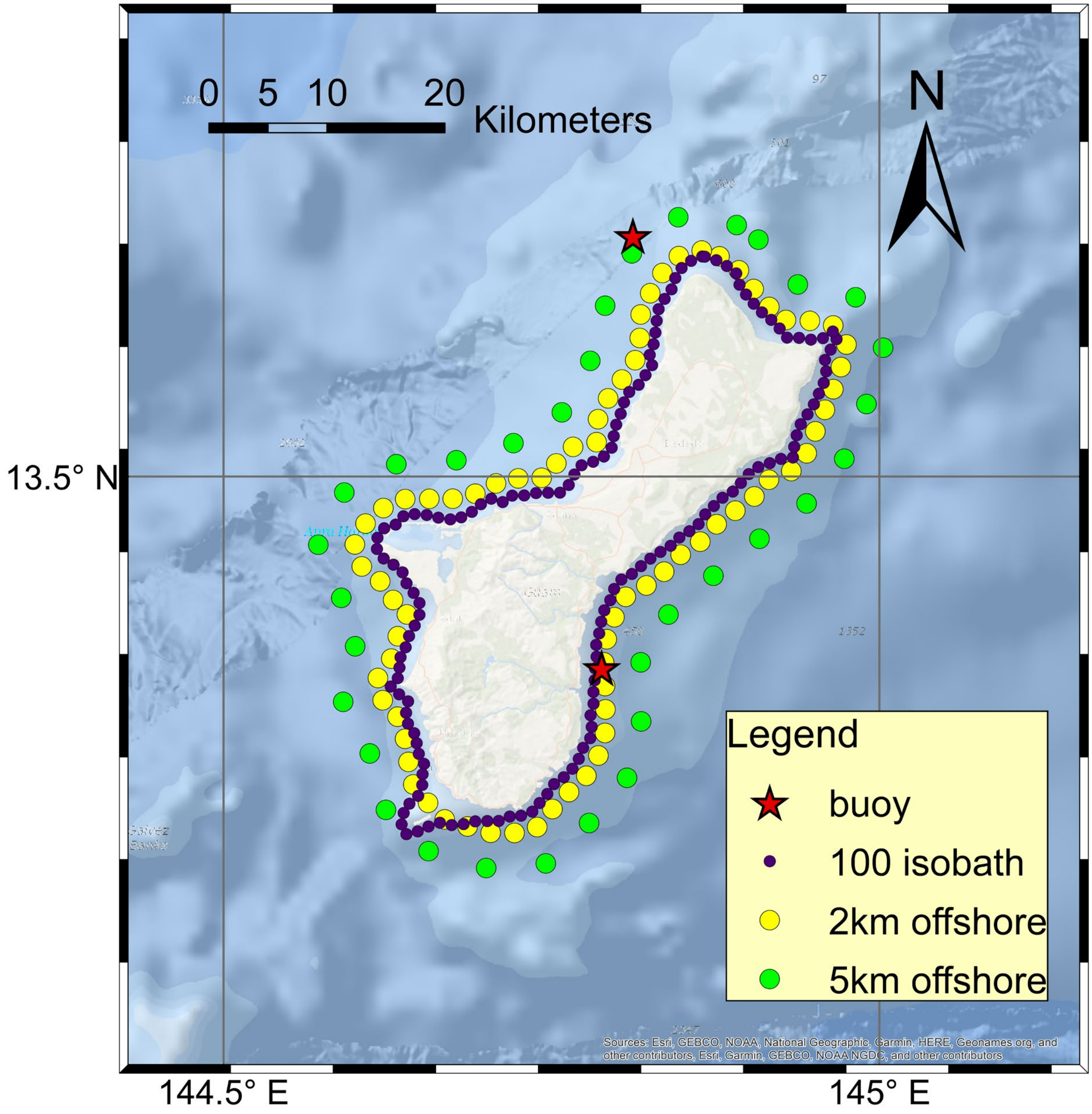

Figure 4.16. Spectral output locations near Guam.

A database with total size of 77.3 TB in NetCDF format was produced for all the seven regions during the 32 years of hindcast period. Table 4.3 shows the output size for each model.

Table 4.3. Archived data size.

Region	Output Size for 32 Years NetCDF Files (TB)
American Samoa	26.0
Baker and Howland Islands	5.0
Jarvis Island	2.5
Johnston Atoll	5.8
Commonwealth of Northern Mariana Island and Guam	29.0
Palmyra Atoll and Kingman Reef	6.0
Wake Island	3.0

5.0 Conclusions

A high-resolution wave hindcast spanning the period from 1979 to 2010 and covering the EEZs around the U.S. Pacific Island territories has been developed. The hindcast includes the six IEC-recommended parameters for wave energy characterization at 3-hour intervals over the computational grids. Wave spectra are also output at selected locations around the islands and atolls to provide more detailed information to end users. The numerical models show good performance based on comparisons with in-situ and satellite-borne measurements. The long-term dataset provides important information to aid development and planning for marine energy harvesting. The results from this study will be used to update the DOE Marine and Hydrokinetic Energy Atlas.

6.0 References

Ahn, Seongho, Kevin A. Haas, and Vincent S. Neary. 2020. "Wave Energy Resource Characterization and Assessment for Coastal Waters of the United States." *Applied Energy* 267 (June): 114922. https://doi.org/10.1016/j.apenergy.2020.114922.

Allahdadi, M. Nabi, Budi Gunawan, Jonathan Lai, Ruoying He, and Vincent S. Neary. 2019. "Development and Validation of a Regional-Scale High-Resolution Unstructured Model for Wave Energy Resource Characterization along the US East Coast." *Renewable Energy* 136 (June): 500–511. https://doi.org/10.1016/j.renene.2019.01.020.

Amante, C., and B. W. Eakins. 2009. "ETOPO1 1 Arc-Minute Global Relief Model: Procedures, Data Sources and Analysis." NOAA Technical Memorandum NESDIS NGDC-24.

Ardhuin, Fabrice, Erick Rogers, Alexander V. Babanin, Jean-François Filipot, Rudy Magne, Aaron Roland, Andre van der Westhuysen, et al. 2010. "Semiempirical Dissipation Source Functions for Ocean Waves. Part I: Definition, Calibration, and Validation." *Journal of Physical Oceanography* 40 (9): 1917–41. https://doi.org/10.1175/2010JPO4324.1.

Battjes, J. A., and J. P. F. M. Janssen. 1978. "Energy Loss and Set-up Due to Breaking of Random Waves." In *16th International Conference on Coastal Engineering*, 569–87. Hamburg, Germany: ASCE.

Bowers, JA, ID Morton, and GI Mould. 2000. "Directional Statistics of the Wind and Waves." *Applied Ocean Research* 22 (1): 13–30.

Dutheil, Cyril, S. Jullien, J. Aucan, C. Menkes, R. Le Gendre, and S. Andréfouët. 2021. "The Wave Regimes of the Central Pacific Ocean with a Focus on Pearl Farming Atolls." *Marine Pollution Bulletin* 162 (January): 111751. https://doi.org/10.1016/j.marpolbul.2020.111751.

Eldeberky, Y. 1996. "Nonlinear Transformation of Wave Spectra in the Nearshore Zone (Ph. D. Thesis)." *Netherlands: Delft University of Technology, Department of Civil Engineering*.

García-Medina, G., Z. Yang, N. Li, K. F. Cheung, T. Wang, and W. Wu. 2019. "High-Resolution Regional Wave Hindcast for Hawaii." https://doi.org/10.2172/1572913.

García-Medina, G., Z. Yang, W. Wu, and T. Wang. 2021. "Wave Resource Characterization at Regional and Nearshore Scales for the U.S. Alaska Coast Based on a 32-Year High-Resolution Hindcast." *Renewable Energy* 170 (June): 595–612. https://doi.org/10.1016/j.renene.2021.02.005.

Hagerman, G., and G. Scott. 2011. "Mapping and Assessment of the United States Ocean Wave Energy Resource." https://doi.org/10.2172/1219363.

Hanson, Jeffrey L., Barbara A. Tracy, Hendrik L. Tolman, and R. Douglas Scott. 2009. "Pacific Hindcast Performance of Three Numerical Wave Models." *Journal of Atmospheric and Oceanic Technology* 26 (8): 1614–33. https://doi.org/10.1175/2009JTECHO650.1.

Hasselmann, K., T. P. Barnett, E. Bouws, H. Carlson, D. E. Cartwright, K. Enke, J. A. Ewing, et al. 1973. "Measurements of Wind-Wave Growth and Swell Decay during the Joint North Sea

Wave Project (JONSWAP).” *Ergaenzungsheft Zur Deutschen Hydrographischen Zeitschrift* A (12): 95 pp.

Hasselmann, S., K. Hasselmann, J. H. Allender, and T. P. Barnett. 1985. “Computations and Parameterizations of the Nonlinear Energy Transfer in a Gravity-Wave Specturm. Part II: Parameterizations of the Nonlinear Energy Transfer for Application in Wave Models.” *Journal of Physical Oceanography* 15 (November): 1378–91. https://doi.org/10.1175/1520-0485(1985)015<1378:CAPOTN>2.0.CO;2.

IEC TS 62600-101. 2015. “Marine Energy - Wave, Tidal and Other Water Current Converters - Part 101: Wave Energy Resource Assessment and Characterization.” Geneva, Switzerland: International Electrotechnical Commission.

Komen, G. J., K. Hasselmann, and K. Hasselmann. 1984. “On the Existence of a Fully Developed Wind-Sea Spectrum.” *Journal of Physical Oceanography* 14 (8): 1271–85. https://doi.org/10.1175/1520-0485(1984)014<1271:OTEOAF>2.0.CO;2.

Li, N., K. F. Cheung, J. E. Stopa, F. Hsiao, Y. Chen, L. Vega, and P. Cross. 2016. “Thirty-Four Years of Hawaii Wave Hindcast from Downscaling of Climate Forecast System Reanalysis.” *Ocean Modelling* 100 (April): 78–95. https://doi.org/10.1016/j.ocemod.2016.02.001.

Li, N., G. García-Medina, K. F. Cheung, and Z. Yang. 2021. “Wave Energy Resources Assessment for the Multi-Modal Sea State of Hawaii.” *Renewable Energy* 174: 1036 – 1055. https://doi.org/10.1016/j.renene.2021.03.116.

Lim, E, L. A. Taylor, B. W. Eakins, K. S. Carignan, P. R. Grothe, and R.J. Caldwell. 2010. “Digital Elevation Models of Pago Pago, American Samoa: Procedures, Data Sources and Analysis. Boulder, Colorado: National Geophysical Data Center.” NOAA Technical Memorandum NESDIS NGDC-36. Boulder, Colorado: NOAA National Geophysical Data Center.

Lokuliyana, R. L. K., M. Folley, S. D. G. S. P. Gunawardane, and P. N. Wickramanayake. 2020. “Sri Lankan Wave Energy Resource Assessment and Characterisation Based on IEC Standards.” Renewable Energy 162 (December): 1255 – 1272. https://doi.org/10.1016/j.renene.2020.08.005.

NOAA National Centers for Environmental Information. 2004. “Multibeam Bathymetry Database (MBBDB).” NOAA National Centers for Environmental Information. Accessed May 2020. https://doi.org/10.7289/V56T0JNC.

NOAA National Geophysical Data Center. 2009a. “Wake Island 1/3 Arc-Second MHW Coastal Digital Elevation Model.” NOAA National Centers for Environmental Information. Accessed April 2020.

———. 2009b. “Wake Island 3 Arc-Second MHW Coastal Digital Elevation Model.” NOAA National Centers for Environmental Information. Accessed April 2020.

Ribal, A., and I. R. Young. 2019. “33 Years of Globally Calibrated Wave Height and Wind Speed Data Based on Altimeter Observations.” Scientific Data 6 (1): 1–15. https://doi.org/10.1038/s41597-019-0083-9.

Robertson, B. , C. E. Hiles, and B. J. Buckham. 2014. "Characterizing the near Shore Wave Energy Resource on the West Coast of Vancouver Island, Canada." *Renewable Energy* 71 (November): 665–78. https://doi.org/10.1016/j.renene.2014.06.006.

Saha, S., S. Moorthi, H. Pan, X. Wu, J. Wang, S. Nadiga, P. Tripp, et al. 2010. "The NCEP Climate Forecast System Reanalysis." *Bulletin of the American Meteorological Society* 91 (8): 1015–58. https://doi.org/10.1175/2010BAMS3001.1.

Sosa, J., L. Cavaleri, and J. Portilla-Yandún. 2017. "On the Interaction between Ocean Surface Waves and Seamounts." *Ocean Dynamics* 67 (12): 1553–65. https://doi.org/10.1007/s10236-017-1107-7.

Stopa, J. E., and K. F. Cheung. 2014. "Intercomparison of Wind and Wave Data from the ECMWF Reanalysis Interim and the NCEP Climate Forecast System Reanalysis." *Ocean Modelling* 75 (March): 65–83. https://doi.org/10.1016/j.ocemod.2013.12.006.

Stopa, J. E., K. F. Cheung, and Y. Chen. 2011. "Assessment of Wave Energy Resources in Hawaii." *Renewable Energy* 36 (2): 554–67. https://doi.org/10.1016/j.renene.2010.07.014.

The WAVEWATCH III® Development Group (WW3DG), 2016. "User manual and system documentation of WAVEWATCH III® version 5.16. Technical Note 329, NOAA/NWS/NCEP/MMAB, College Park, MD, USA, 326 pp.

Wu, W., T. Wang, Z. Yang, and G. García-Medina. 2020. "Development and Validation of a High-Resolution Regional Wave Hindcast Model for U.S. West Coast Wave Resource Characterization." *Renewable Energy* 152 (June): 736–53. https://doi.org/10.1016/j.renene.2020.01.077.

Wu, W., Z. Yang, and T. Wang. 2018. "Wave Resource Characterization Using an Unstructured Grid Modeling Approach." *Energies* 11 (3): 605. https://doi.org/10.3390/en11030605.

Yang, Z., G. García-Medina, W. Wu, and T. Wang. 2020. "Characteristics and Variability of the Nearshore Wave Resource on the U.S. West Coast." *Energy* 203 (July): 117818. https://doi.org/10.1016/j.energy.2020.117818.

Yang, Z., V. S. Neary, T. Wang, B. Gunawan, A. R. Dallman, and W. Wu. 2017. "A Wave Model Test Bed Study for Wave Energy Resource Characterization." *Renewable Energy*, Wave and Tidal Resource Characterization, 114 (December): 132–44. https://doi.org/10.1016/j.renene.2016.12.057.

Yang, Z., W. Wu, T. Wang, and L. Castrucci. 2018. "High-Resolution Regional Wave Hindcast for the U.S. West Coast." https://doi.org/10.2172/1573061.

Yang, Z., W. Wu, T. Wang, G. García Medina, and L. Castrucci. 2019. "High-Resolution Regional Wave Hindcast for the U.S. Alaska Coast." https://doi.org/10.2172/1579259.

Zijlema, M. 2010. "Computation of Wind-Wave Spectra in Coastal Waters with SWAN on Unstructured Grids." *Coastal Engineering* 57 (3): 267–77. https://doi.org/10.1016/j.coastaleng.2009.10.011.

Appendix A – Monthly Distributions of IEC Wave Resource Parameters from 1979–2010

A.1 American Samoa

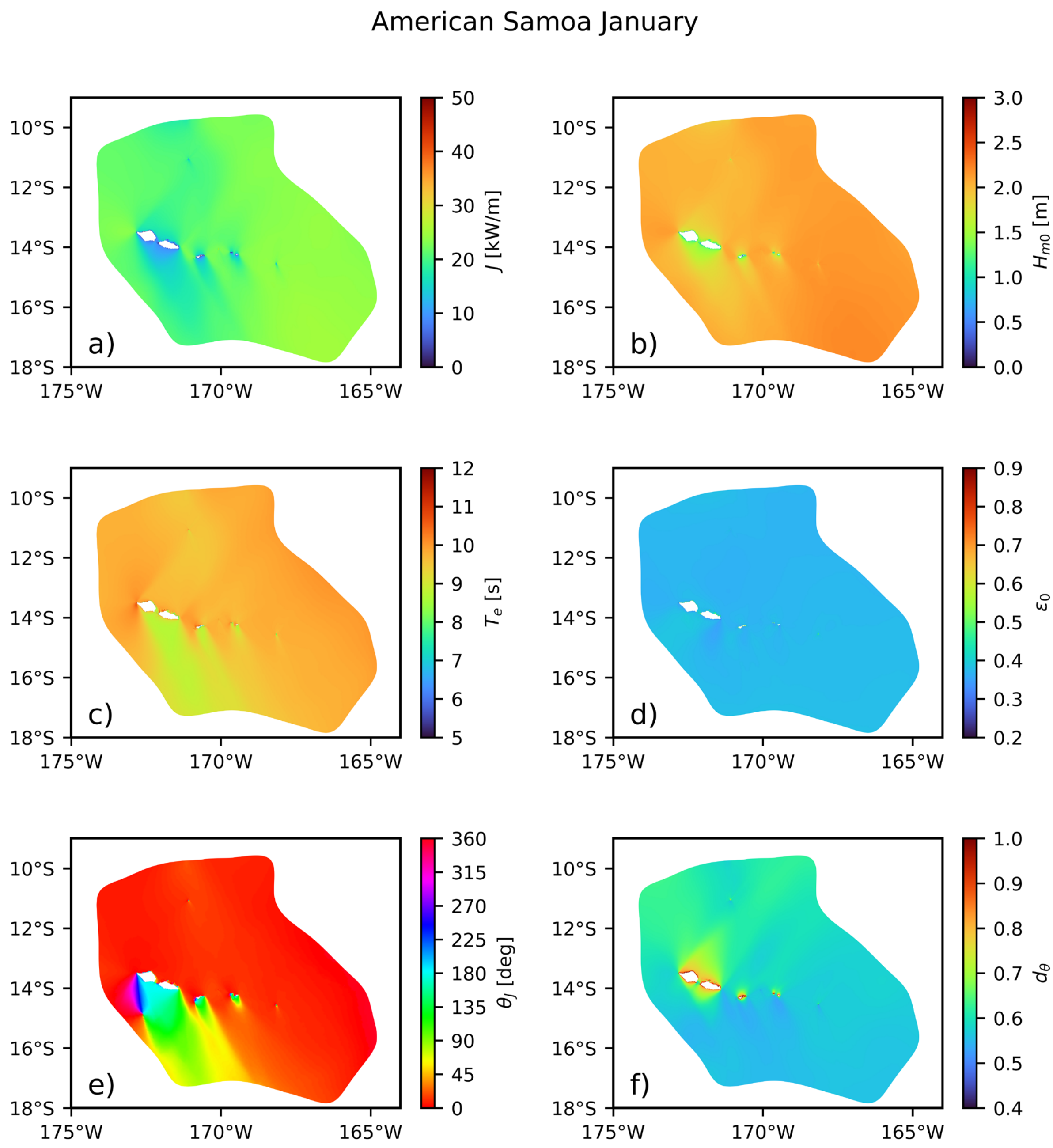

Figure A.1. Monthly distributions of six IEC parameters around American Samoa in January: (a) omnidirectional wave power, (b) significant wave height, (c) energy period, (d) spectral width, (e) direction of maximum directionally resolved wave power, and (f) directionality coefficient.

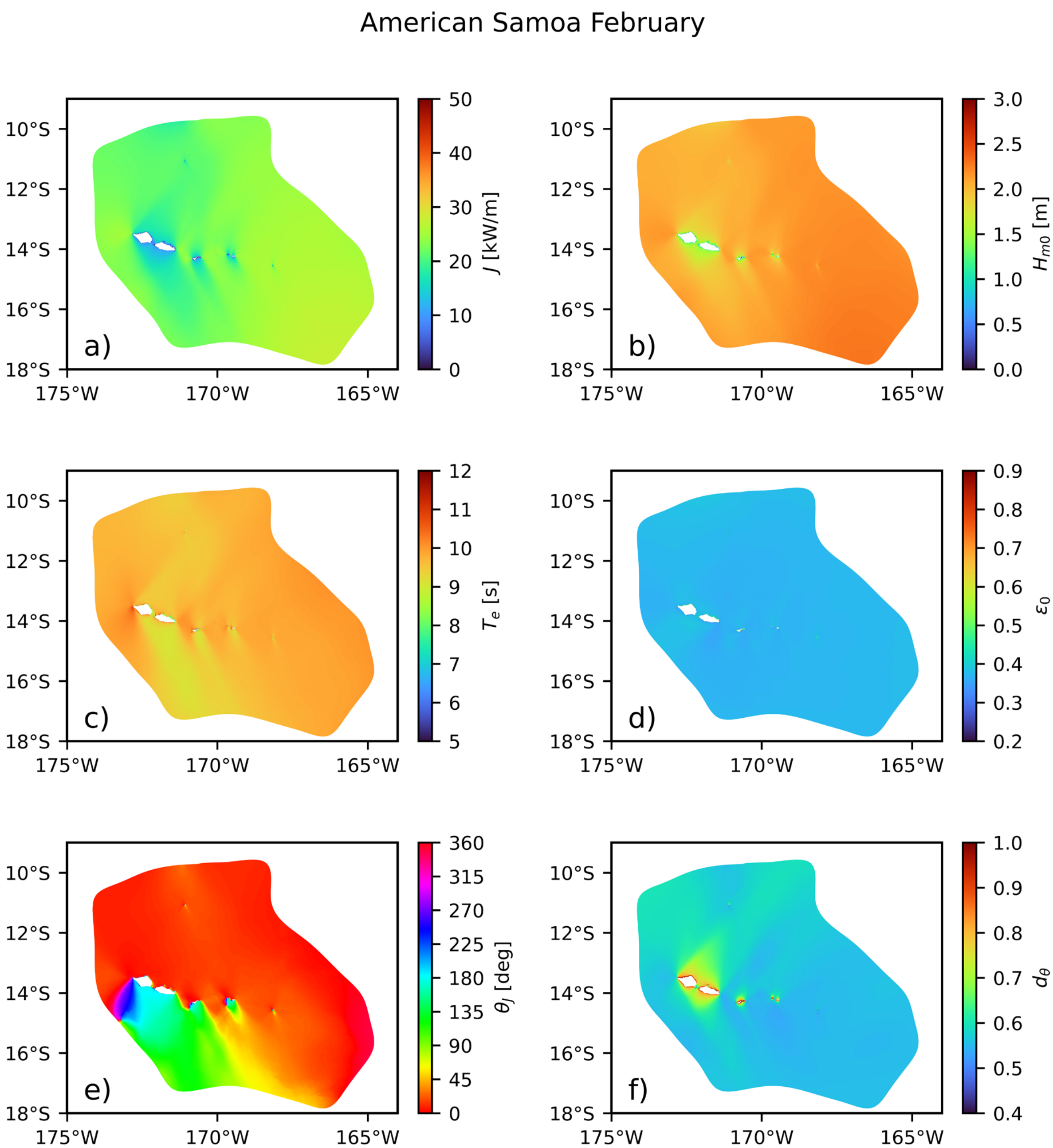

Figure A.2. Monthly distributions of six IEC parameters around American Samoa in February: (a) omnidirectional wave power, (b) significant wave height, (c) energy period, (d) spectral width, (e) direction of maximum directionally resolved wave power, and (f) directionality coefficient.

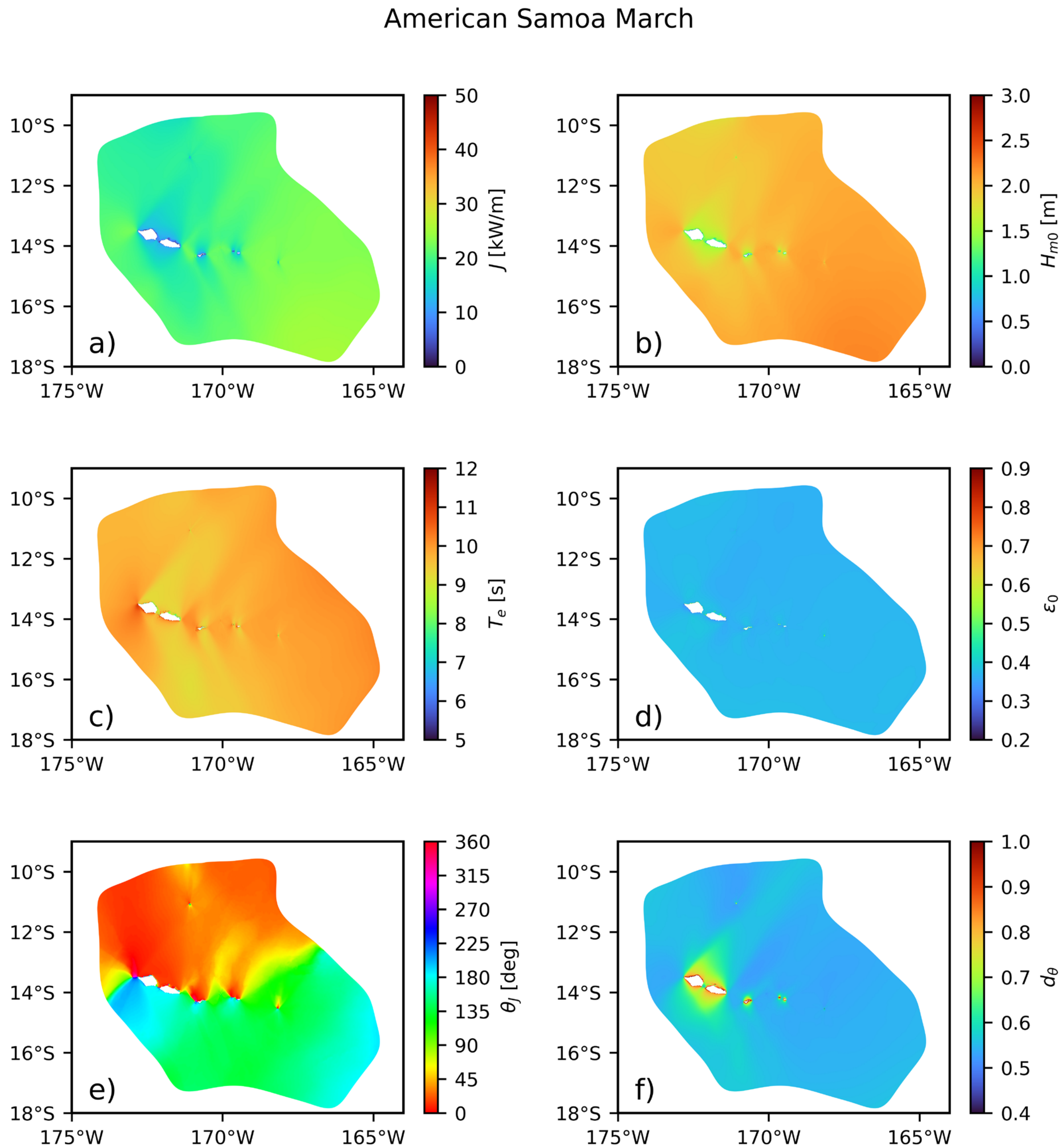

Figure A.3. Monthly distributions of six IEC parameters around American Samoa in March: (a) omnidirectional wave power, (b) significant wave height, (c) energy period, (d) spectral width, (e) direction of maximum directionally resolved wave power, and (f) directionality coefficient.

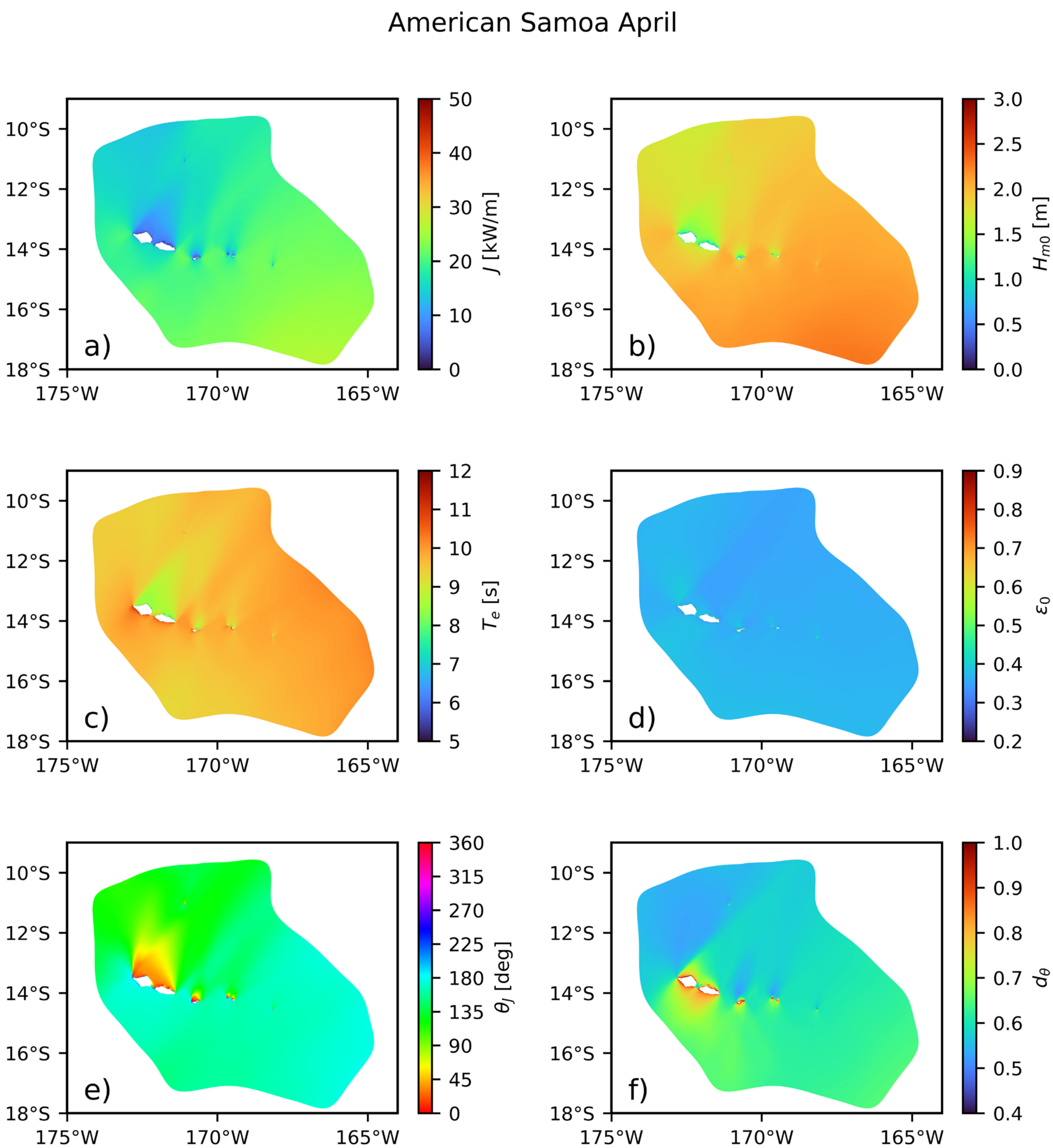

Figure A.4. Monthly distributions of six IEC parameters around American Samoa in April: (a) omnidirectional wave power, (b) significant wave height, (c) energy period, (d) spectral width, (e) direction of maximum directionally resolved wave power, and (f) directionality coefficient.

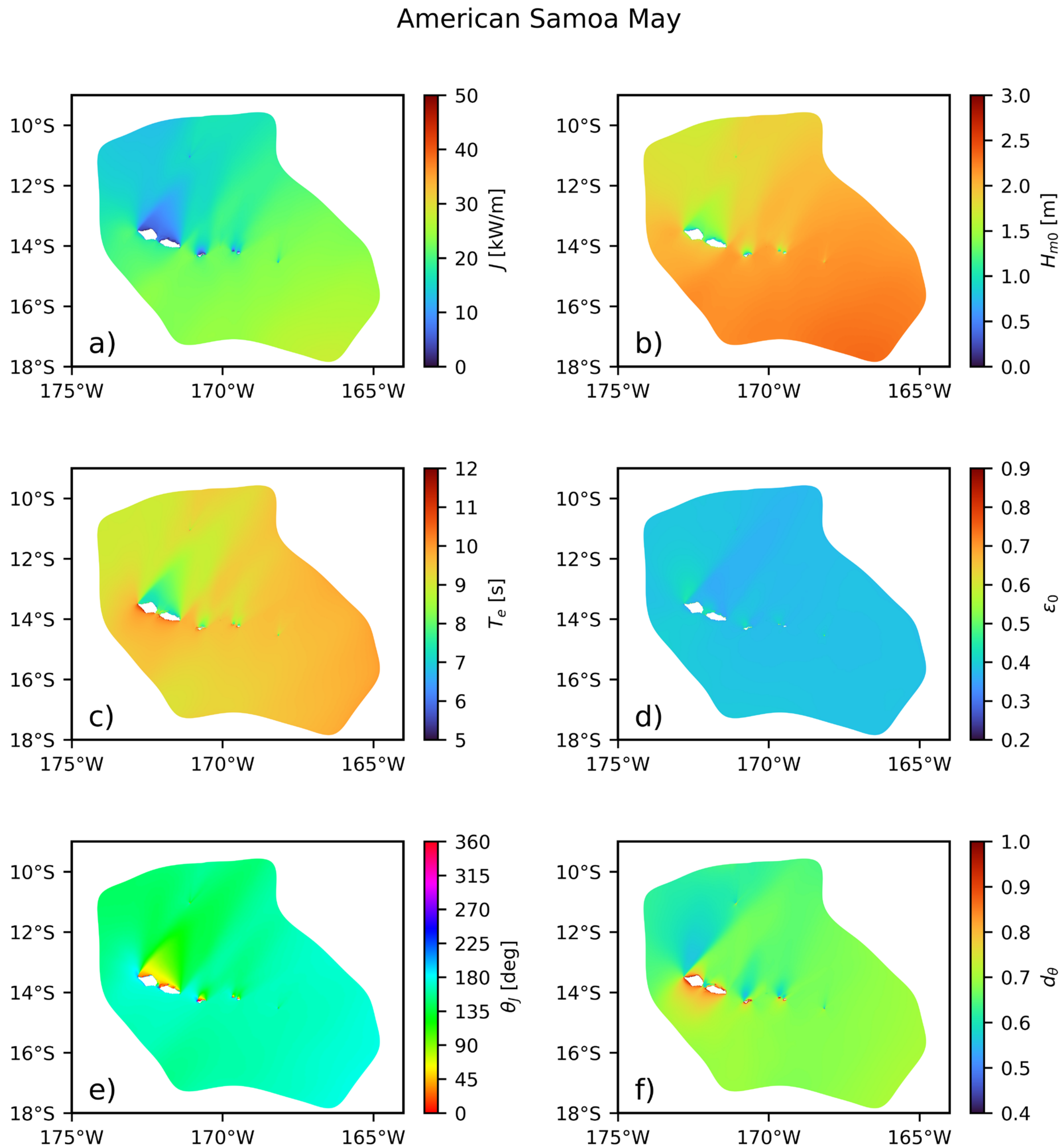

Figure A.5. Monthly distributions of six IEC parameters around American Samoa in May: (a) omnidirectional wave power, (b) significant wave height, (c) energy period, (d) spectral width, (e) direction of maximum directionally resolved wave power, and (f) directionality coefficient.

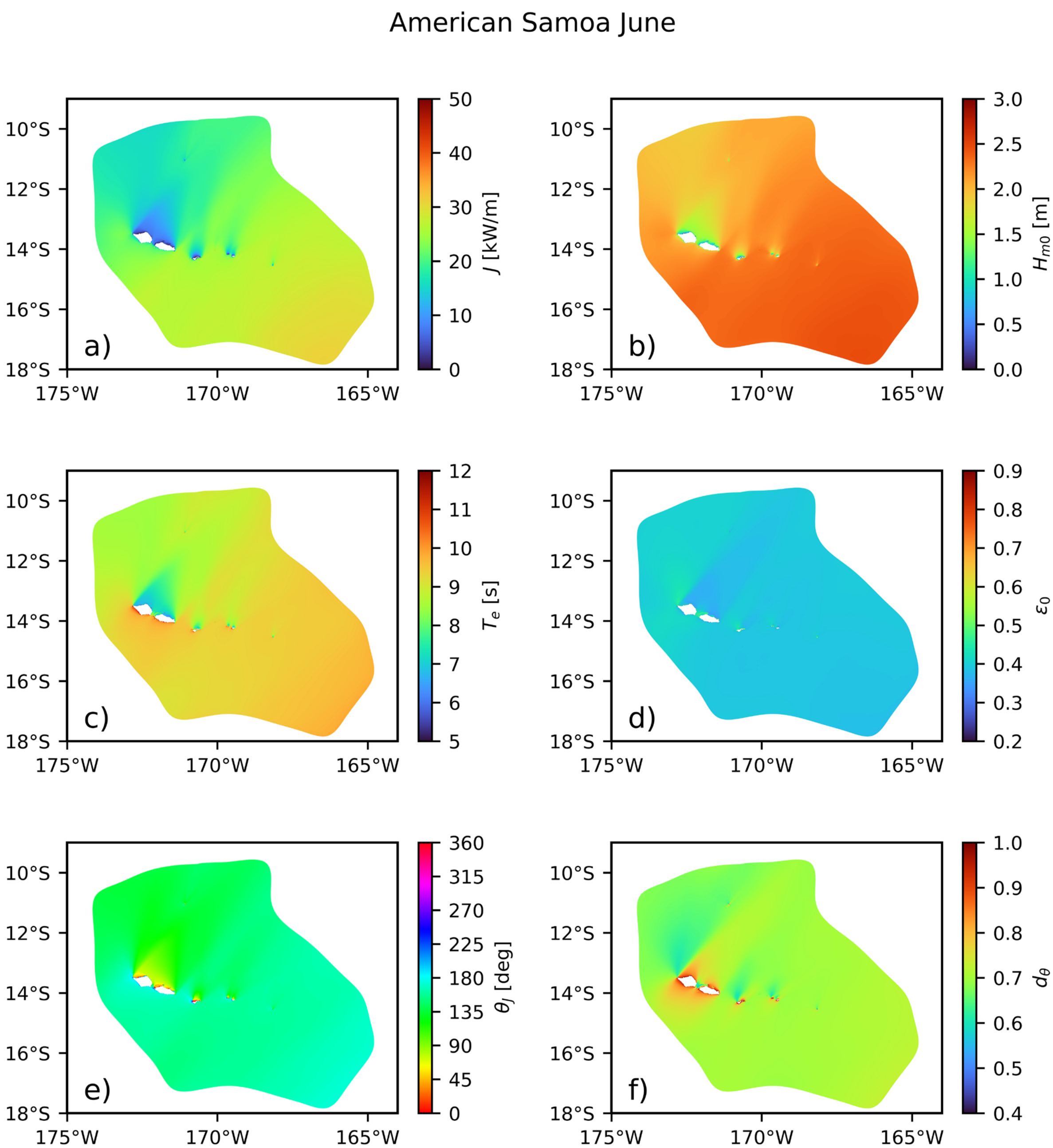

Figure A.6. Monthly distributions of six IEC parameters around American Samoa in June: (a) omnidirectional wave power, (b) significant wave height, (c) energy period, (d) spectral width, (e) direction of maximum directionally resolved wave power, and (f) directionality coefficient.

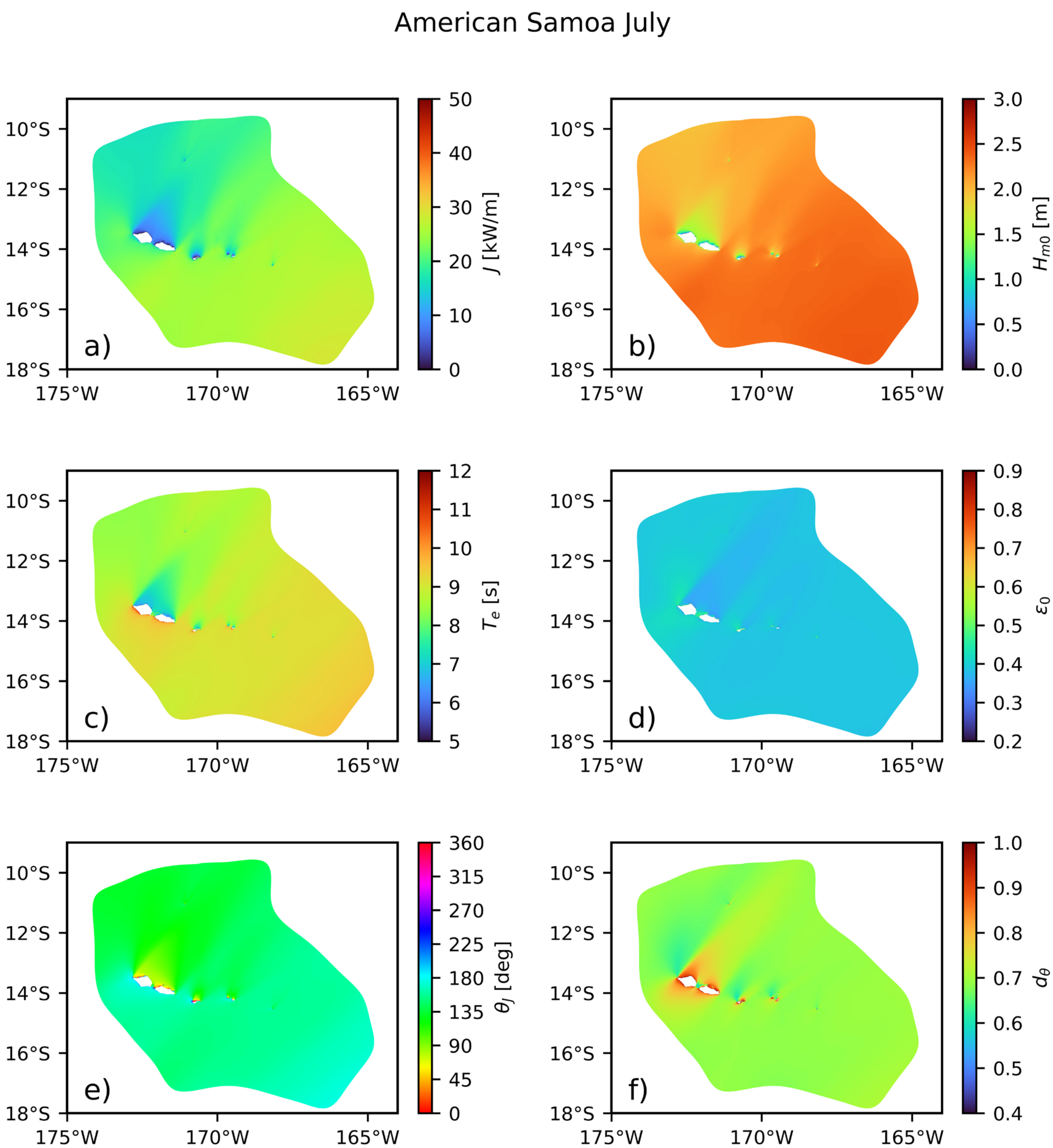

Figure A.7. Monthly distributions of six IEC parameters around American Samoa in July: (a) omnidirectional wave power, (b) significant wave height, (c) energy period, (d) spectral width, (e) direction of maximum directionally resolved wave power, and (f) directionality coefficient.

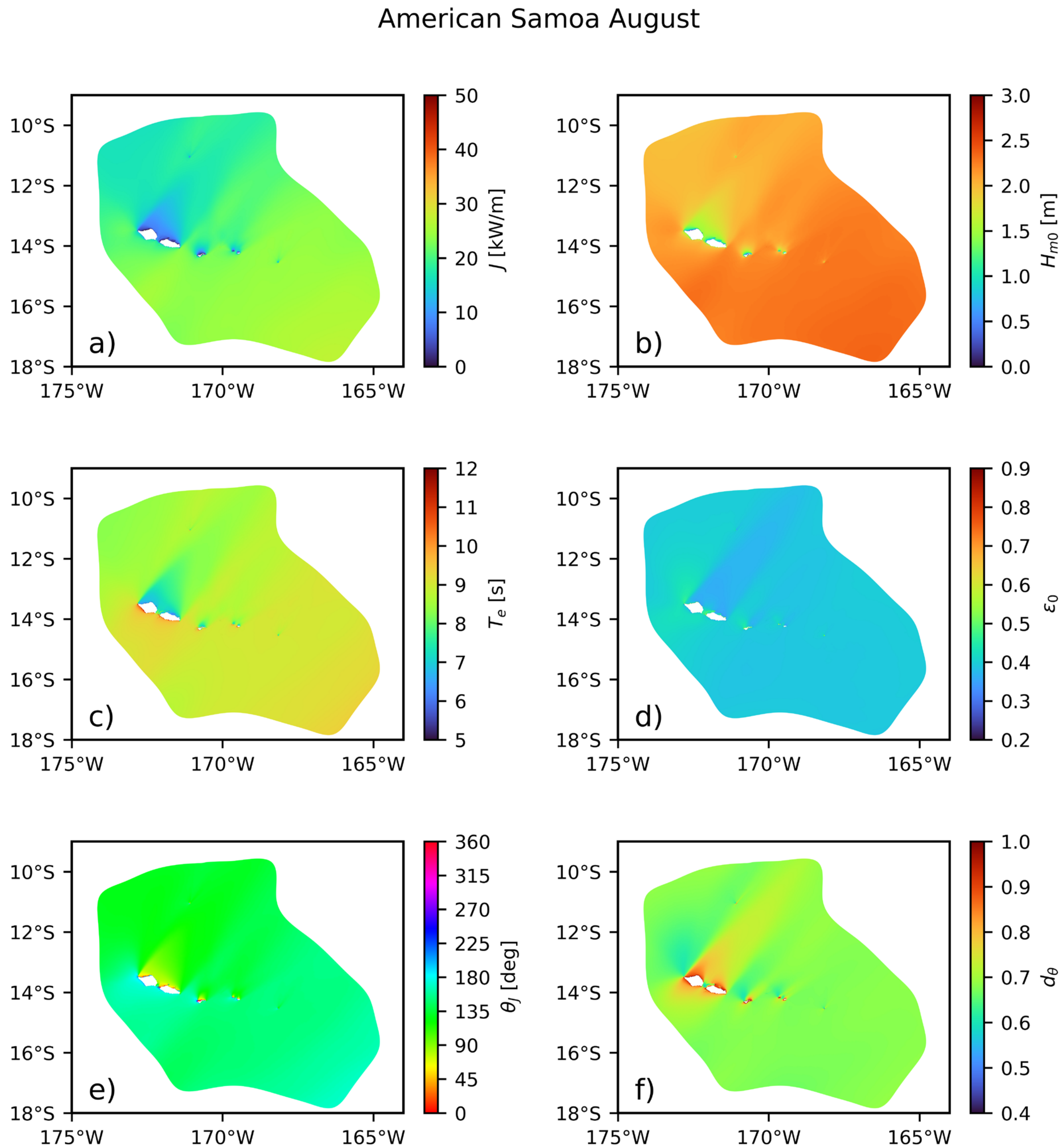

Figure A.8. Monthly distributions of six IEC parameters around American Samoa in August: (a) omnidirectional wave power, (b) significant wave height, (c) energy period, (d) spectral width, (e) direction of maximum directionally resolved wave power, and (f) directionality coefficient.

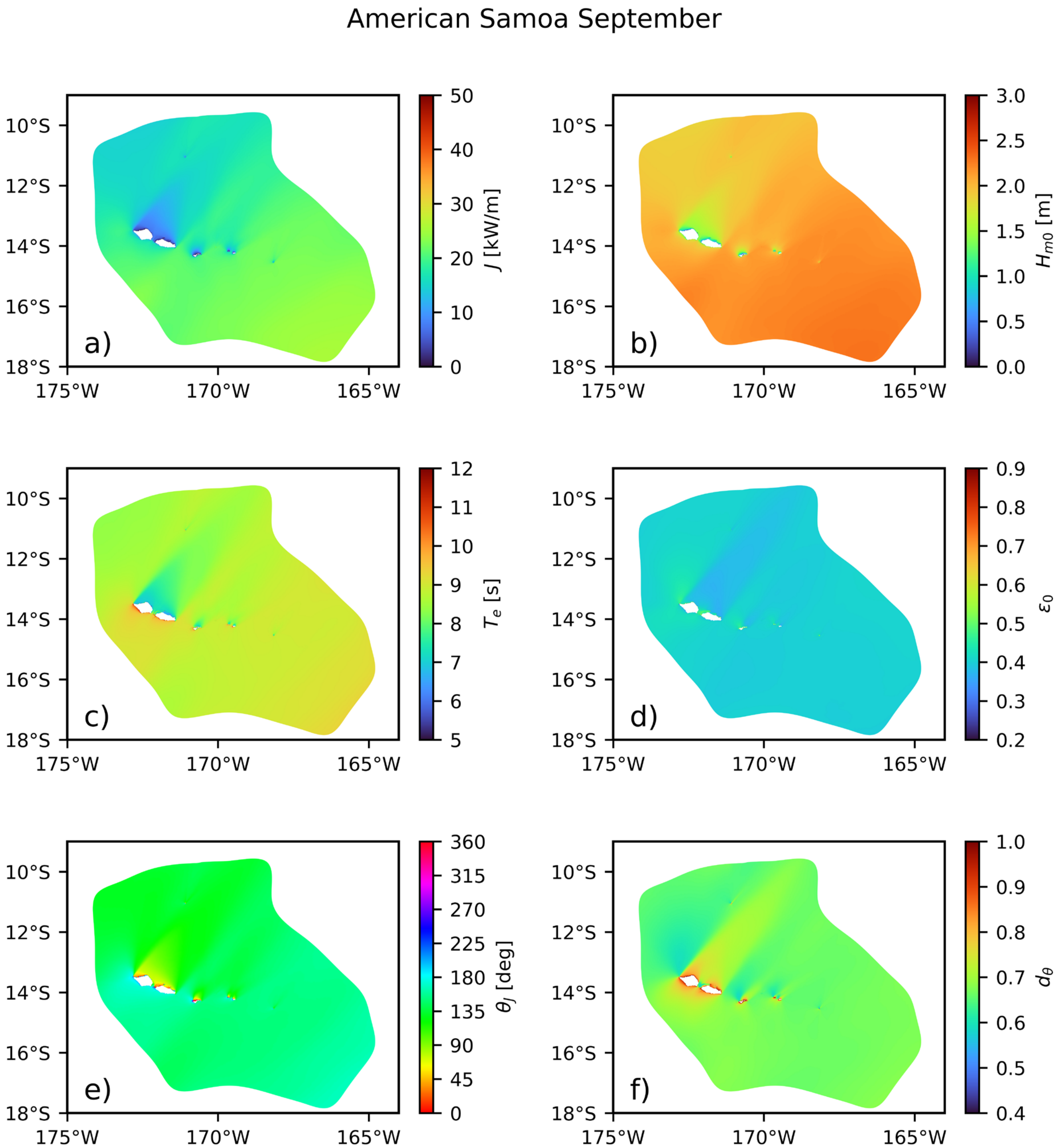

Figure A.9. Monthly distributions of six IEC parameters around American Samoa in September: (a) omnidirectional wave power, (b) significant wave height, (c) energy period, (d) spectral width, (e) direction of maximum directionally resolved wave power, and (f) directionality coefficient.

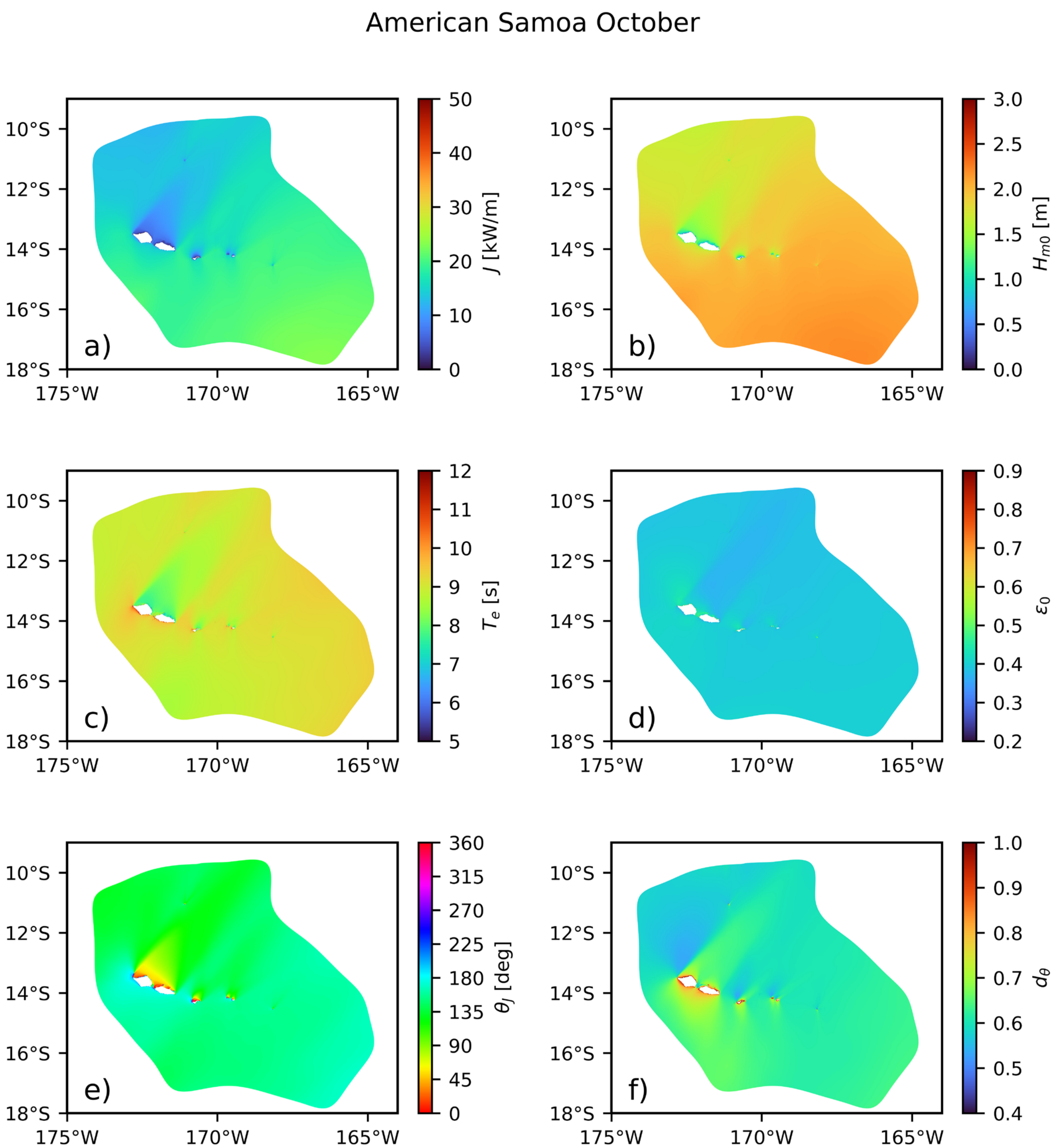

Figure A.10. Monthly distributions of six IEC parameters around American Samoa in October: (a) omnidirectional wave power, (b) significant wave height, (c) energy period, (d) spectral width, (e) direction of maximum directionally resolved wave power, and (f) directionality coefficient.

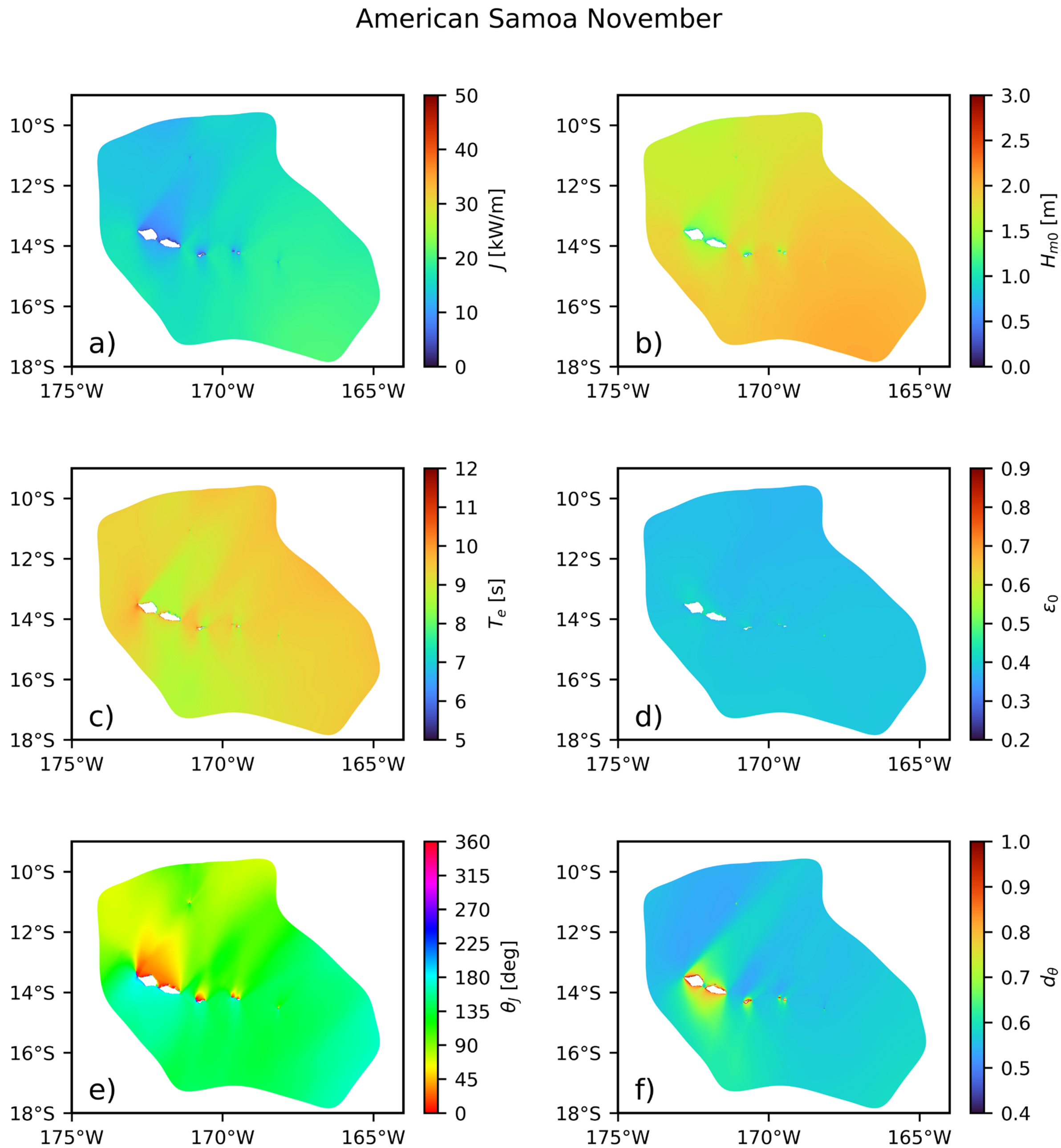

Figure A.11. Monthly distributions of six IEC parameters around American Samoa in November: (a) omnidirectional wave power, (b) significant wave height, (c) energy period, (d) spectral width, (e) direction of maximum directionally resolved wave power, and (f) directionality coefficient.

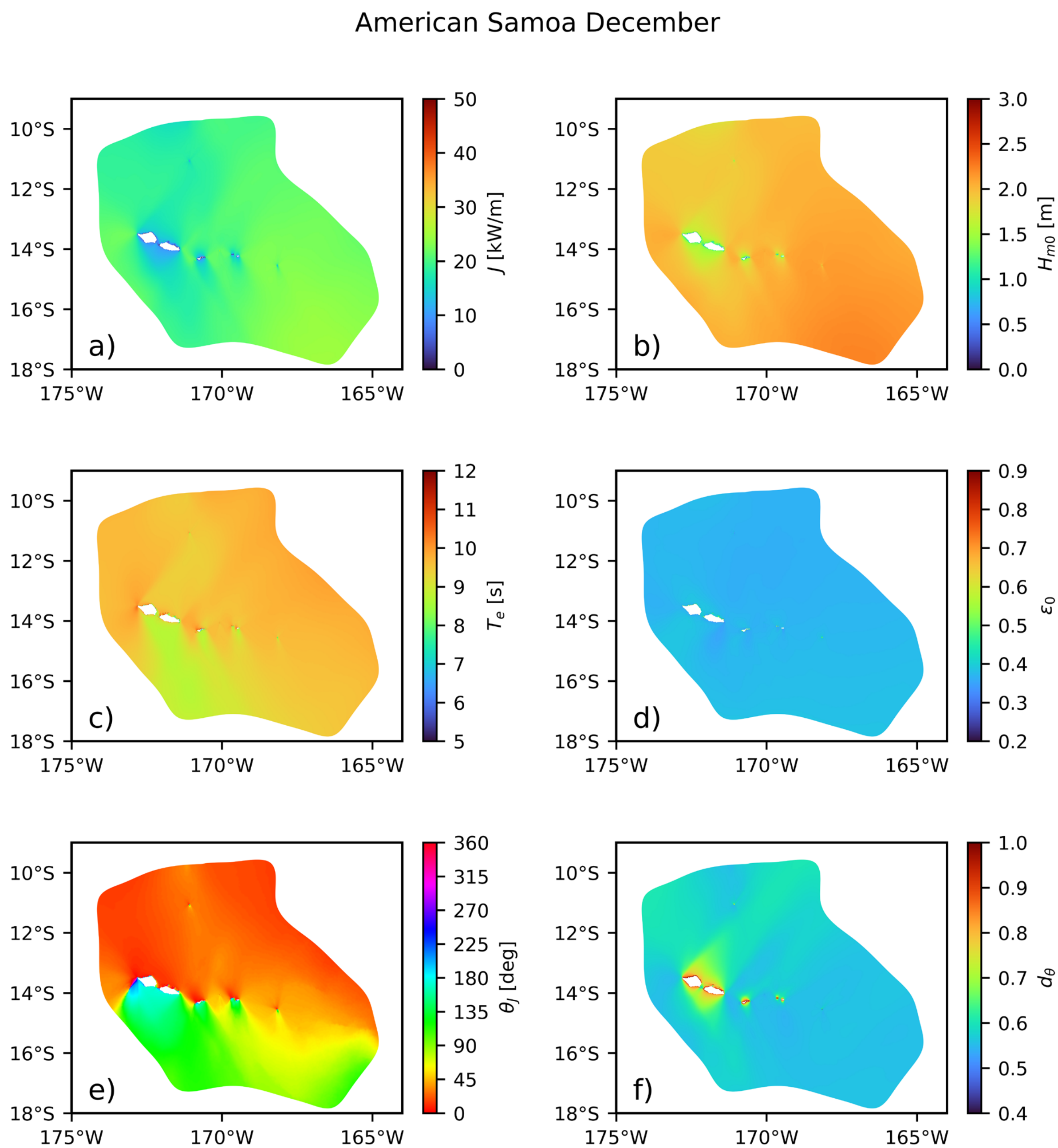

Figure A.12. Monthly distributions of six IEC parameters around American Samoa in December: (a) omnidirectional wave power, (b) significant wave height, (c) energy period, (d) spectral width, (e) direction of maximum directionally resolved wave power, and (f) directionality coefficient.

A.2 Baker and Howland Islands

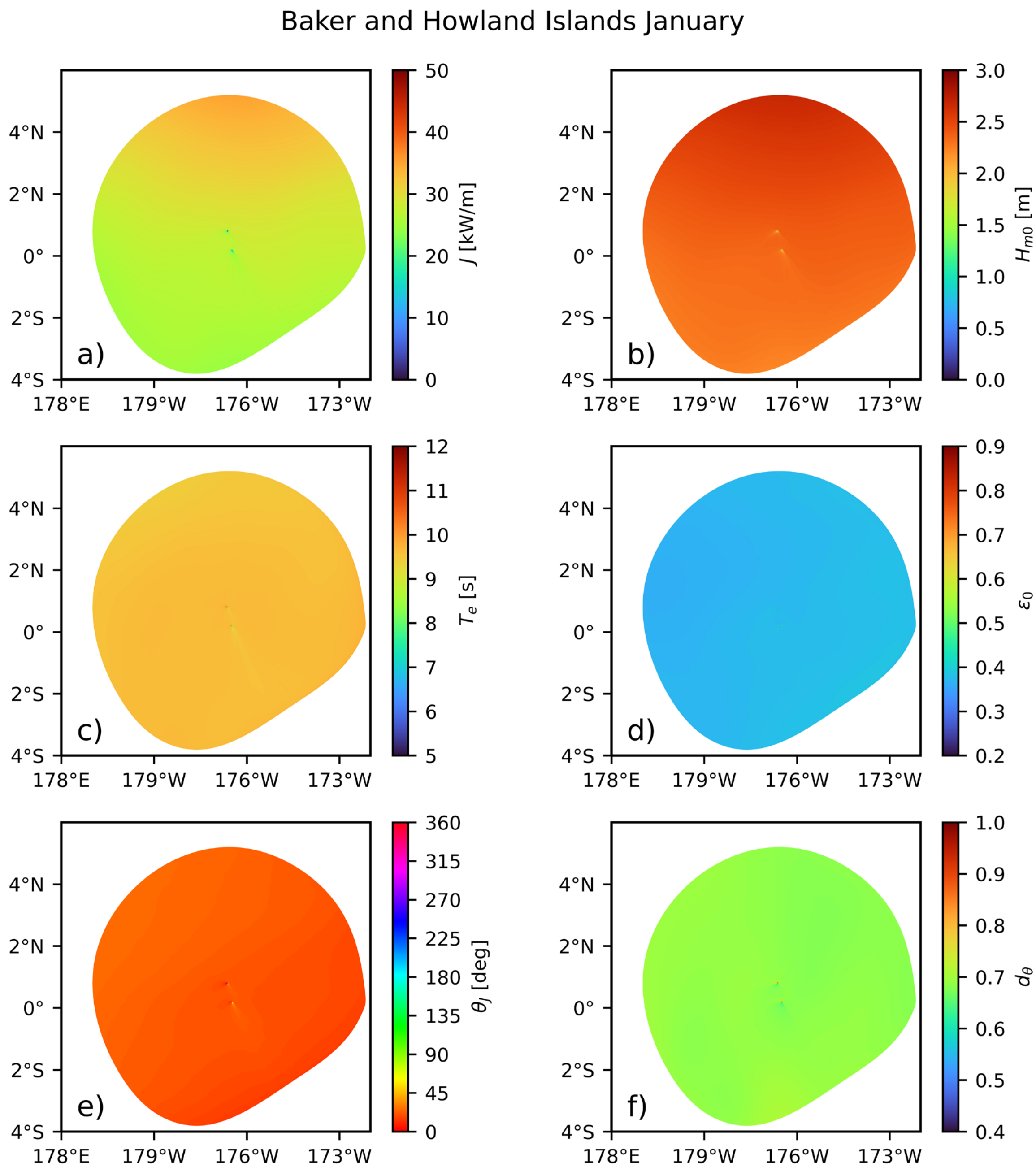

Figure A.13. Monthly distributions of six IEC parameters around Baker and Howland Islands in January: (a) omnidirectional wave power, (b) significant wave height, (c) energy period, (d) spectral width, (e) direction of maximum directionally resolved wave power, and (f) directionality coefficient.

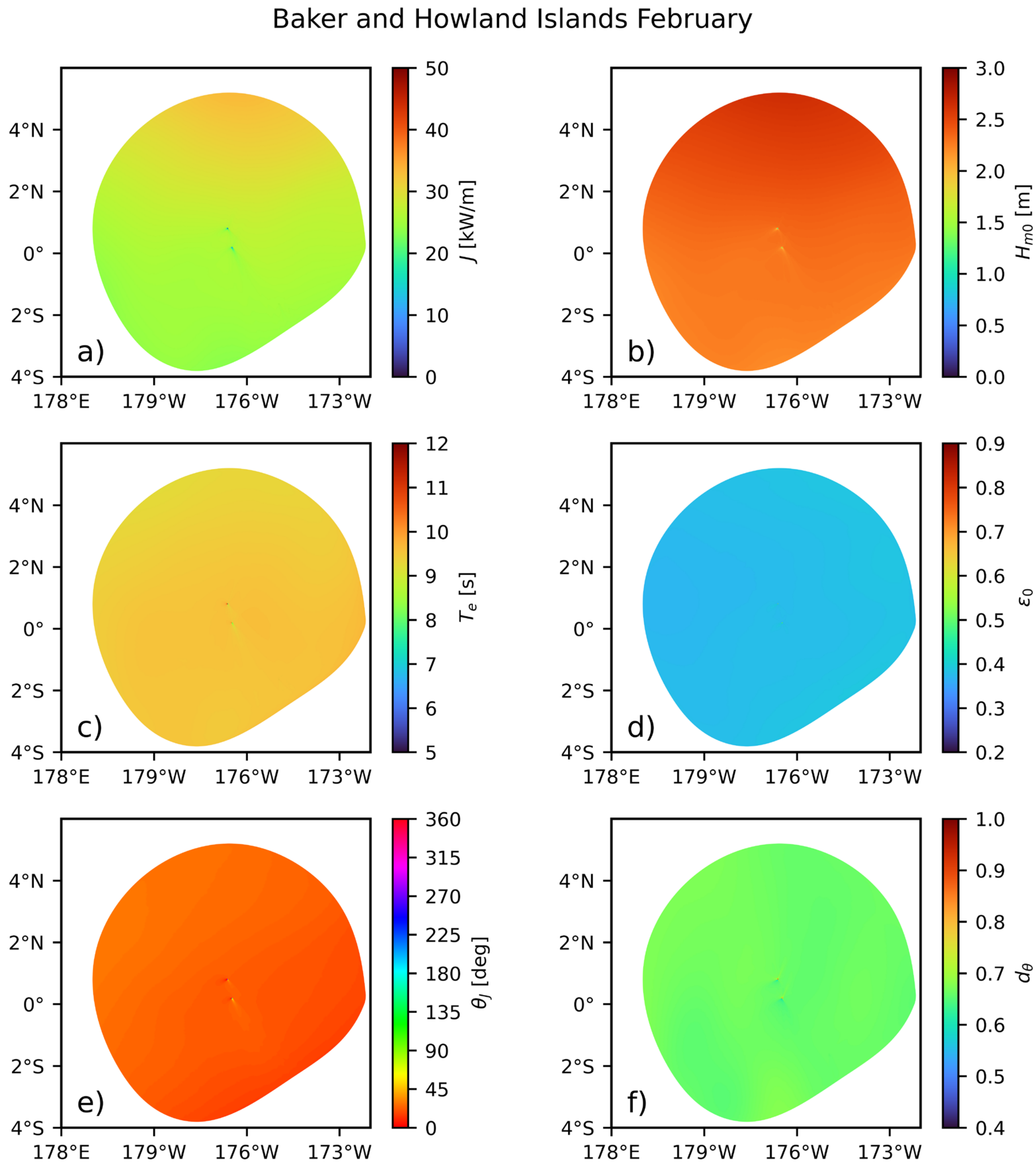

Figure A.14. Monthly distributions of six IEC parameters around Baker and Howland Islands in February: (a) omnidirectional wave power, (b) significant wave height, (c) energy period, (d) spectral width, (e) direction of maximum directionally resolved wave power, and (f) directionality coefficient.

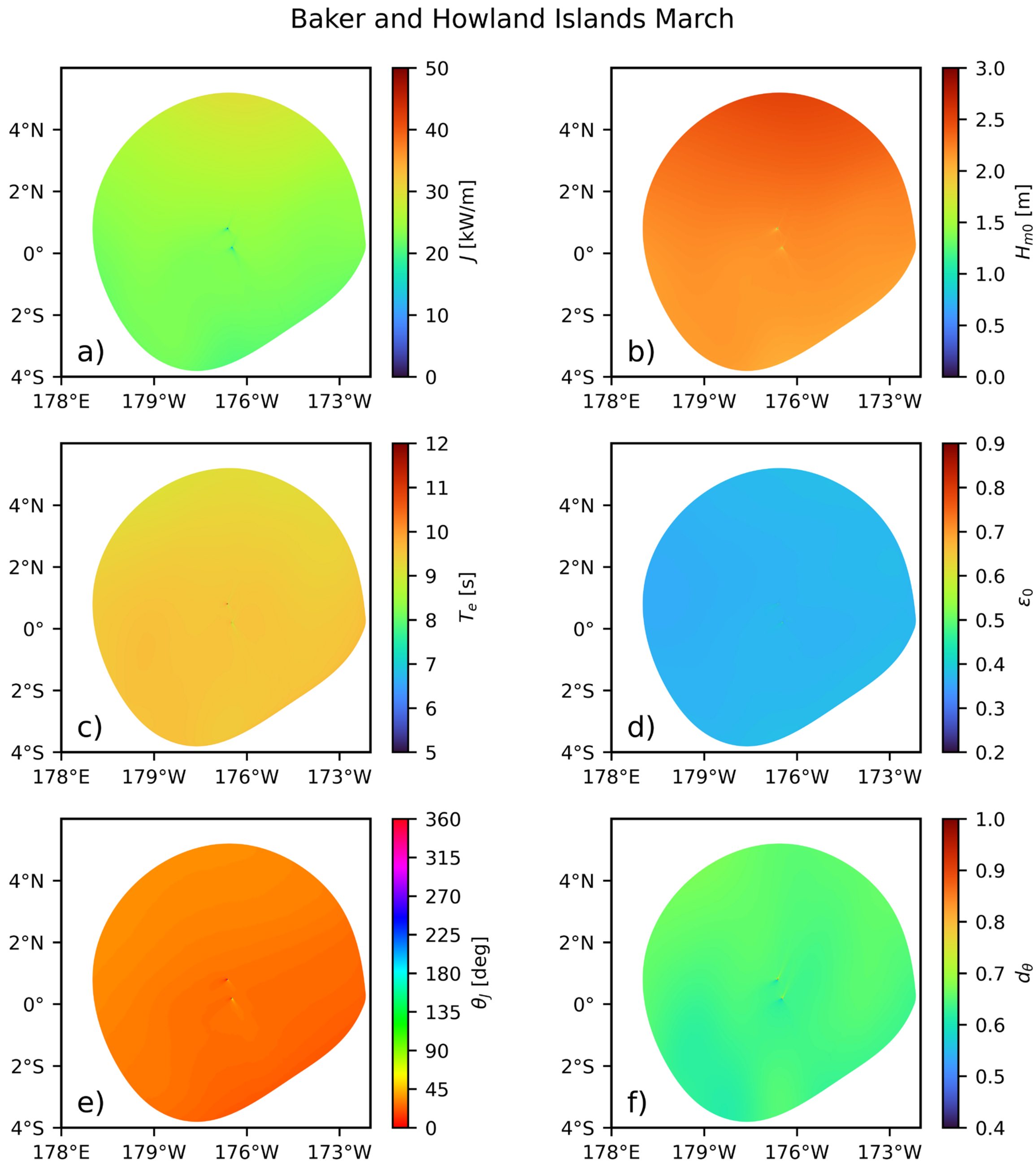

Figure A.15. Monthly distributions of six IEC parameters around Baker and Howland Islands in March: (a) omnidirectional wave power, (b) significant wave height, (c) energy period, (d) spectral width, (e) direction of maximum directionally resolved wave power, and (f) directionality coefficient.

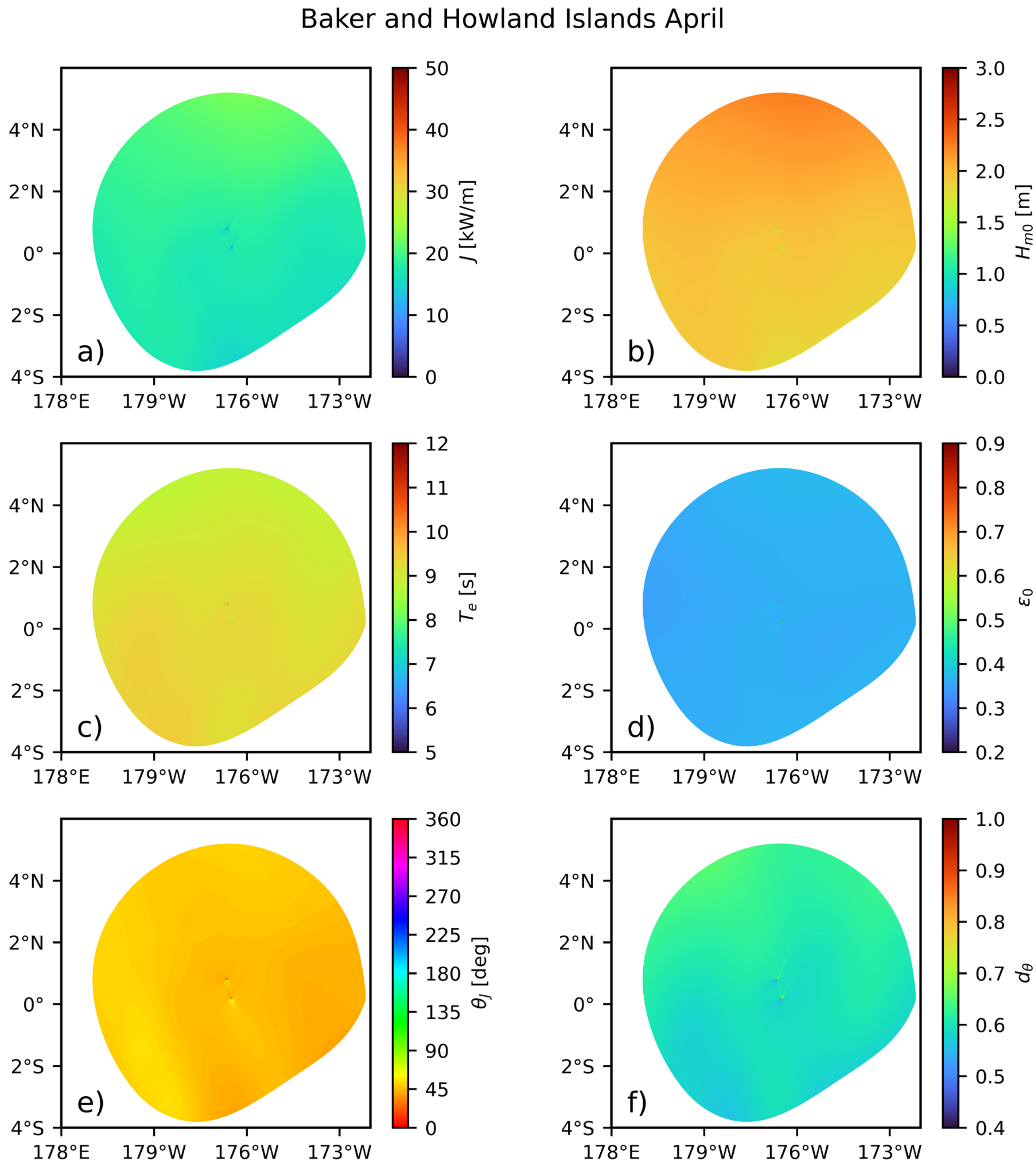

Figure A.16. Monthly distributions of six IEC parameters around Baker and Howland Islands in April: (a) omnidirectional wave power, (b) significant wave height, (c) energy period, (d) spectral width, (e) direction of maximum directionally resolved wave power, and (f) directionality coefficient.

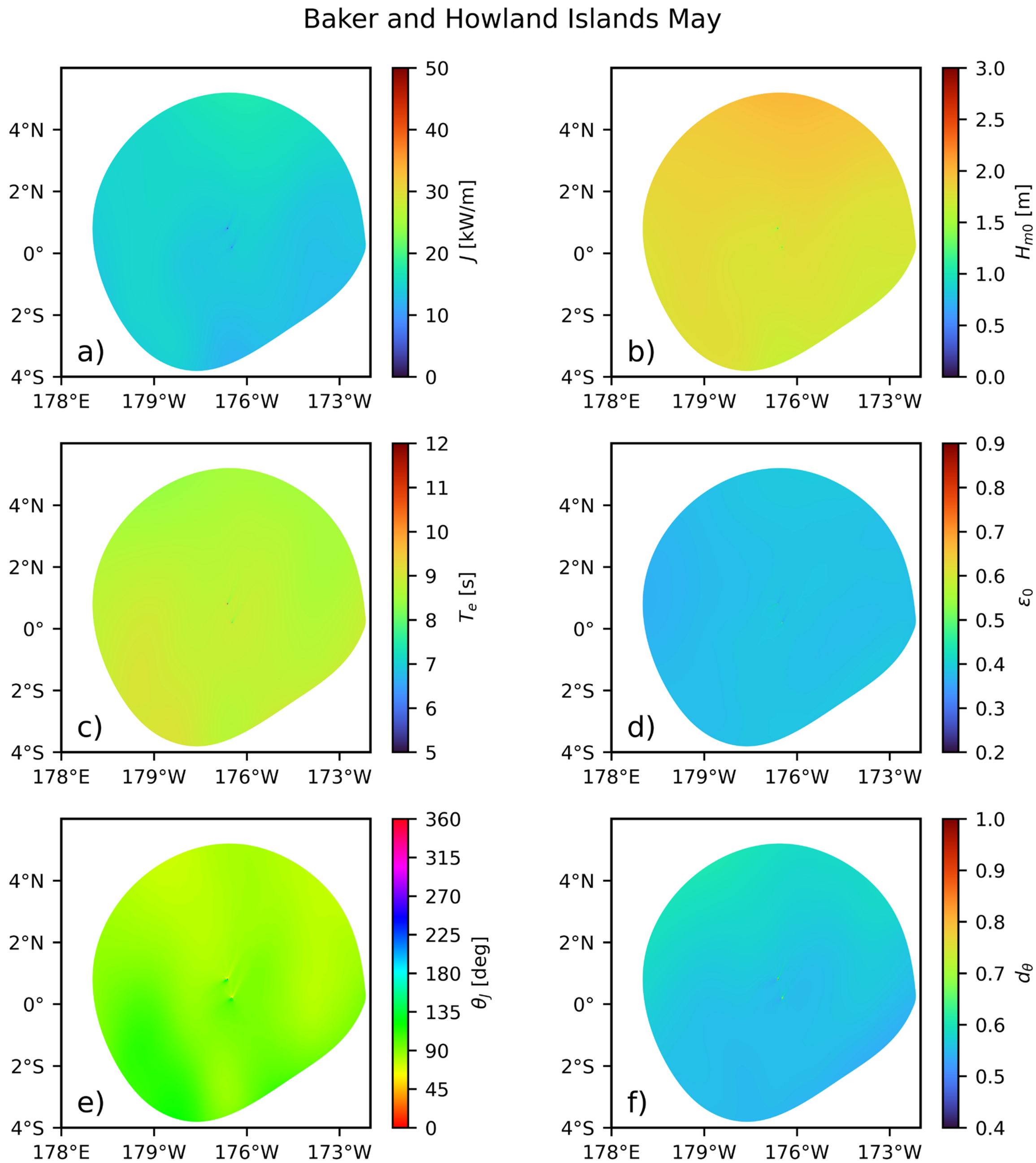

Figure A.17. Monthly distributions of six IEC parameters around Baker and Howland Islands in May: (a) omnidirectional wave power, (b) significant wave height, (c) energy period, (d) spectral width, (e) direction of maximum directionally resolved wave power, and (f) directionality coefficient.

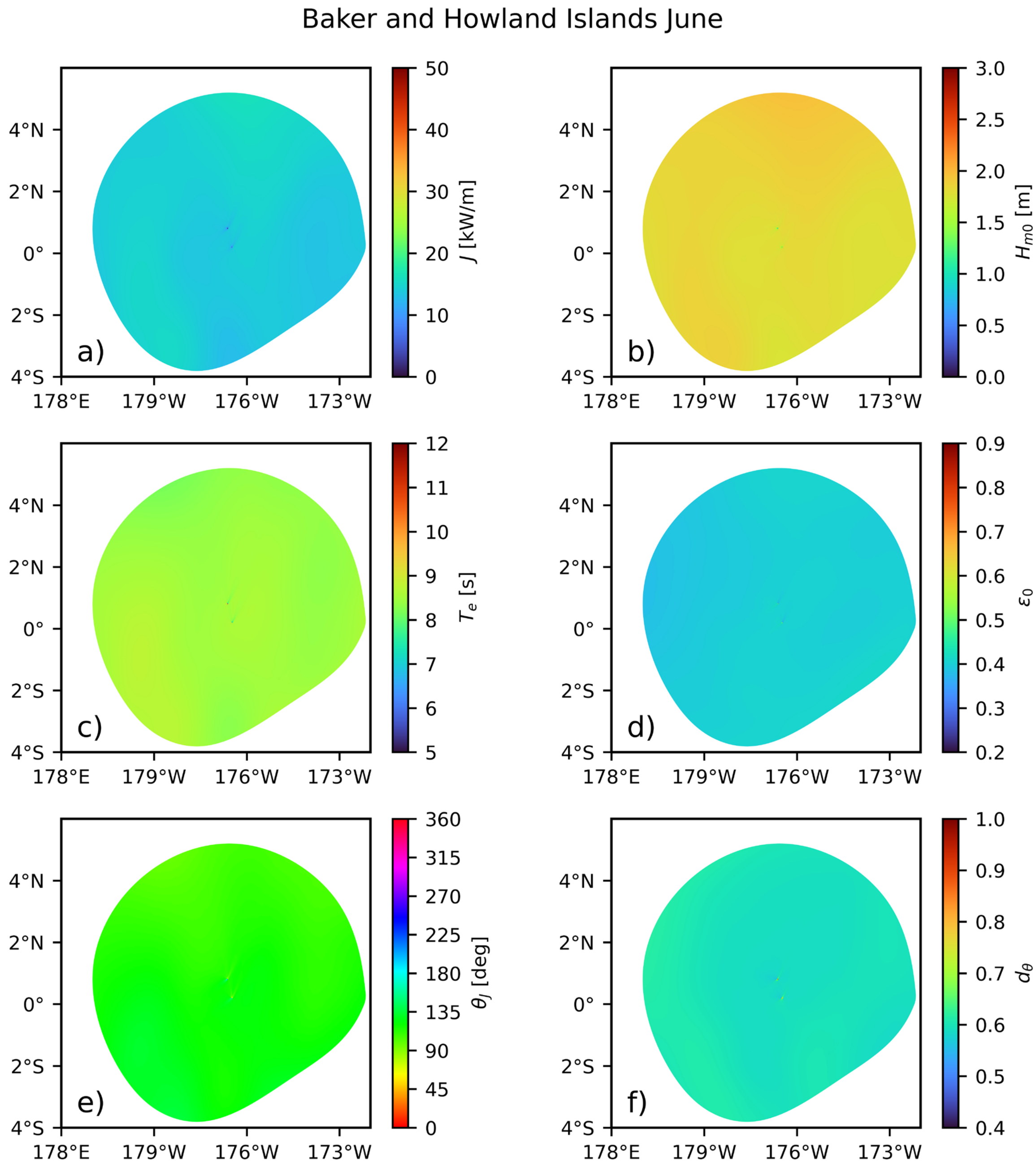

Figure A.18. Monthly distributions of six IEC parameters around Baker and Howland Islands in June: (a) omnidirectional wave power, (b) significant wave height, (c) energy period, (d) spectral width, (e) direction of maximum directionally resolved wave power, and (f) directionality coefficient.

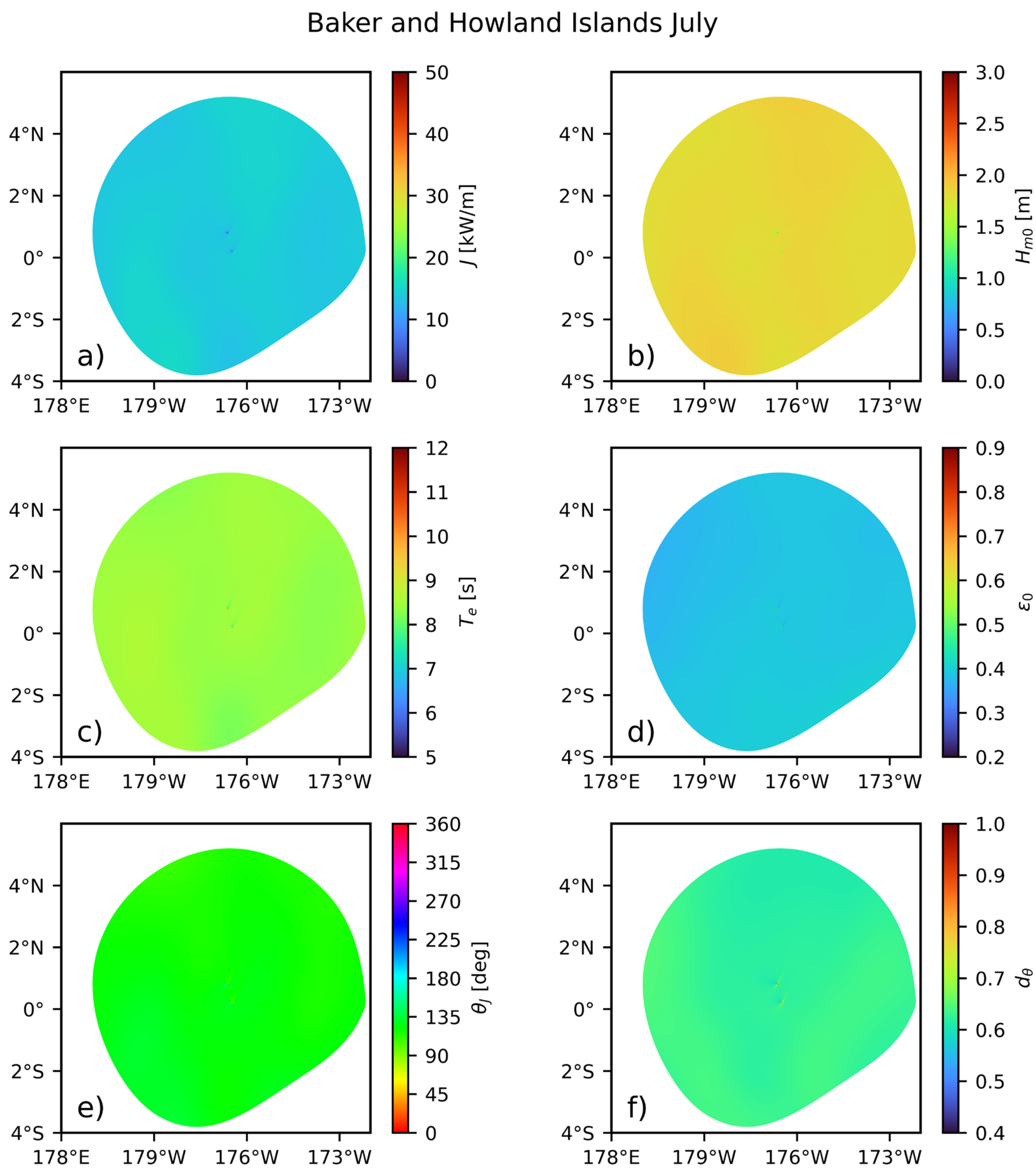

Figure A.19. Monthly distributions of six IEC parameters around Baker and Howland Islands in July: (a) omnidirectional wave power, (b) significant wave height, (c) energy period, (d) spectral width, (e) direction of maximum directionally resolved wave power, and (f) directionality coefficient.

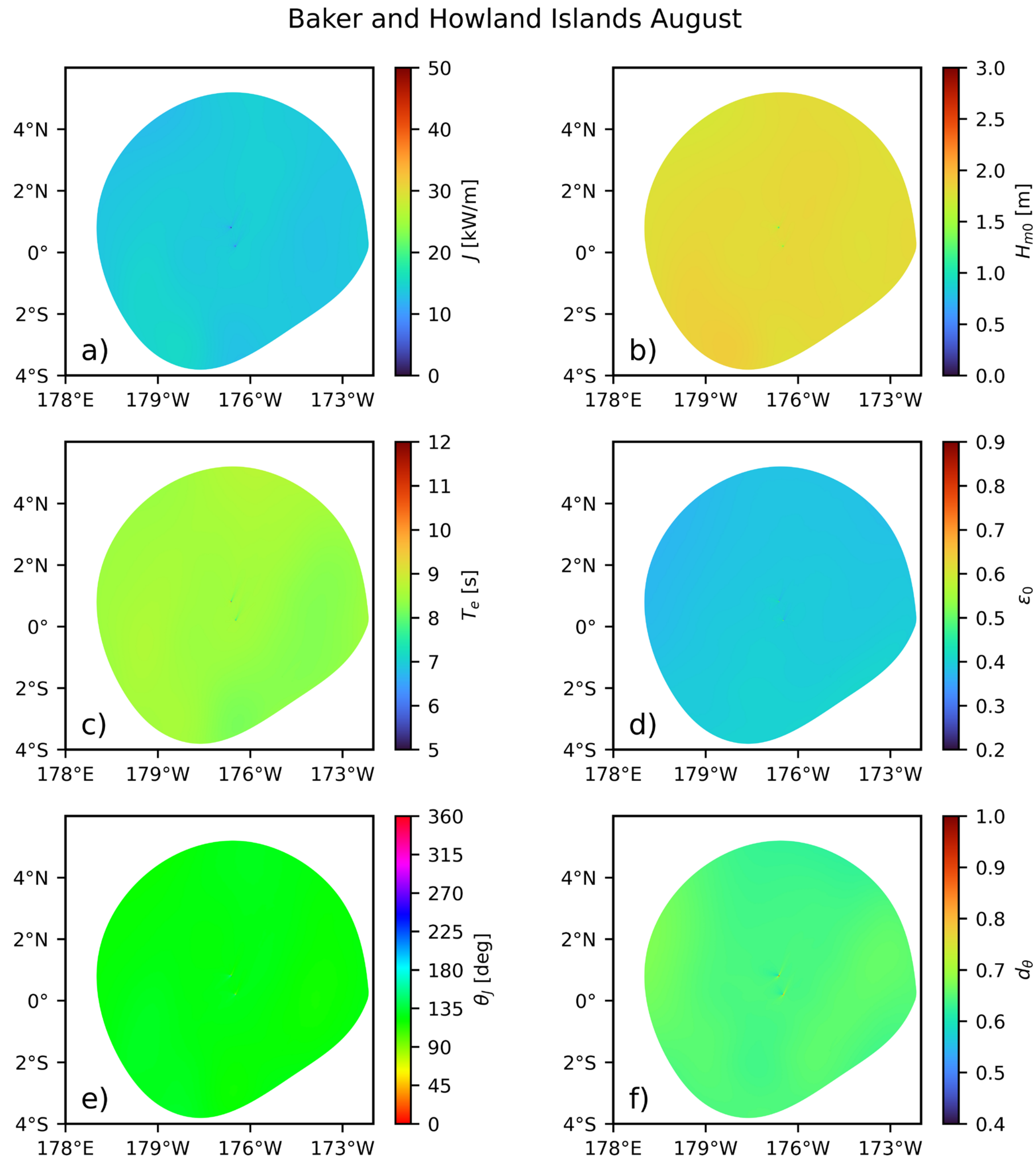

Figure A.20. Monthly distributions of six IEC parameters around Baker and Howland Islands in August: (a) omnidirectional wave power, (b) significant wave height, (c) energy period, (d) spectral width, (e) direction of maximum directionally resolved wave power, and (f) directionality coefficient.

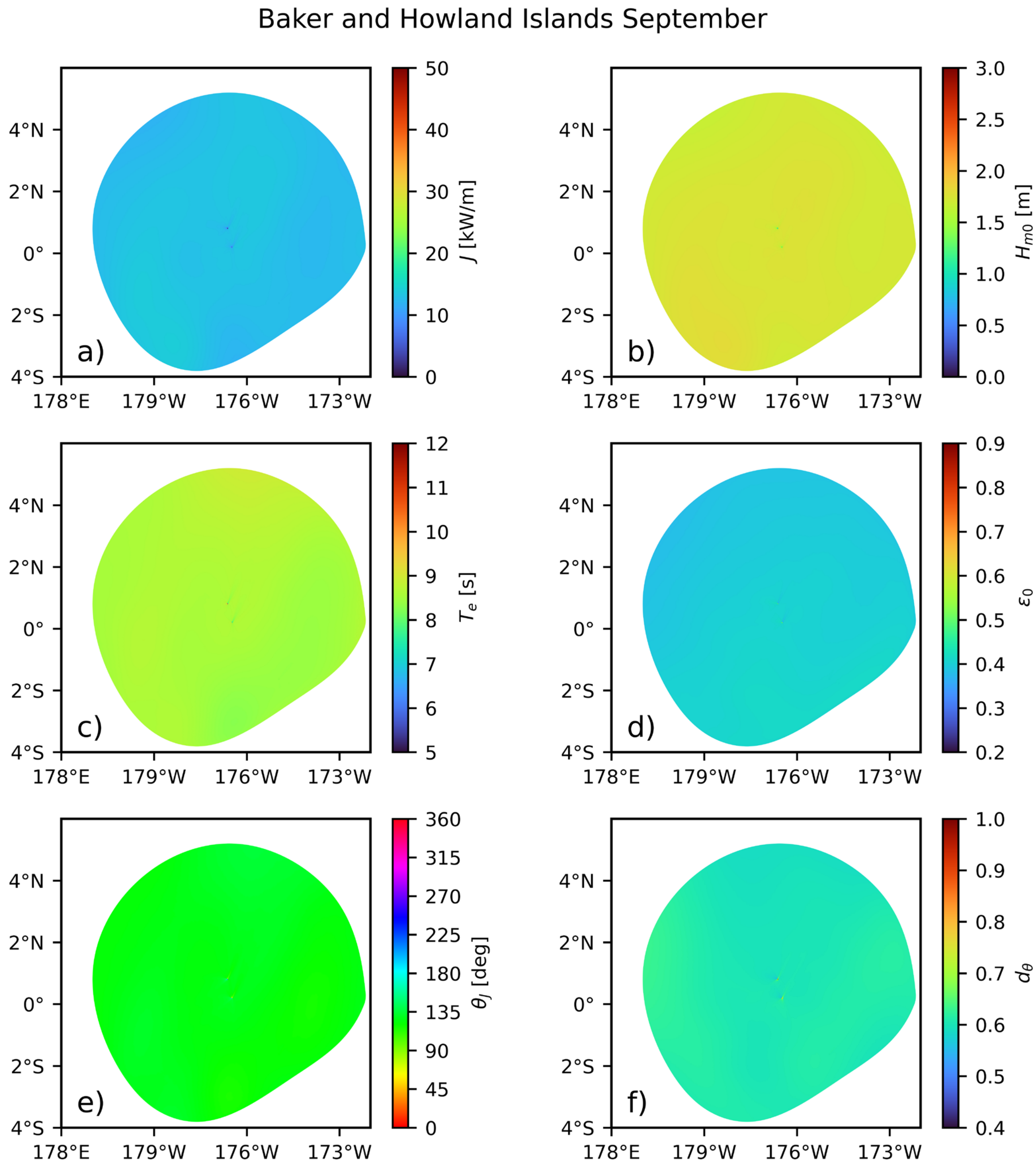

Figure A.21. Monthly distributions of six IEC parameters around Baker and Howland Islands in September: (a) omnidirectional wave power, (b) significant wave height, (c) energy period, (d) spectral width, (e) direction of maximum directionally resolved wave power, and (f) directionality coefficient.

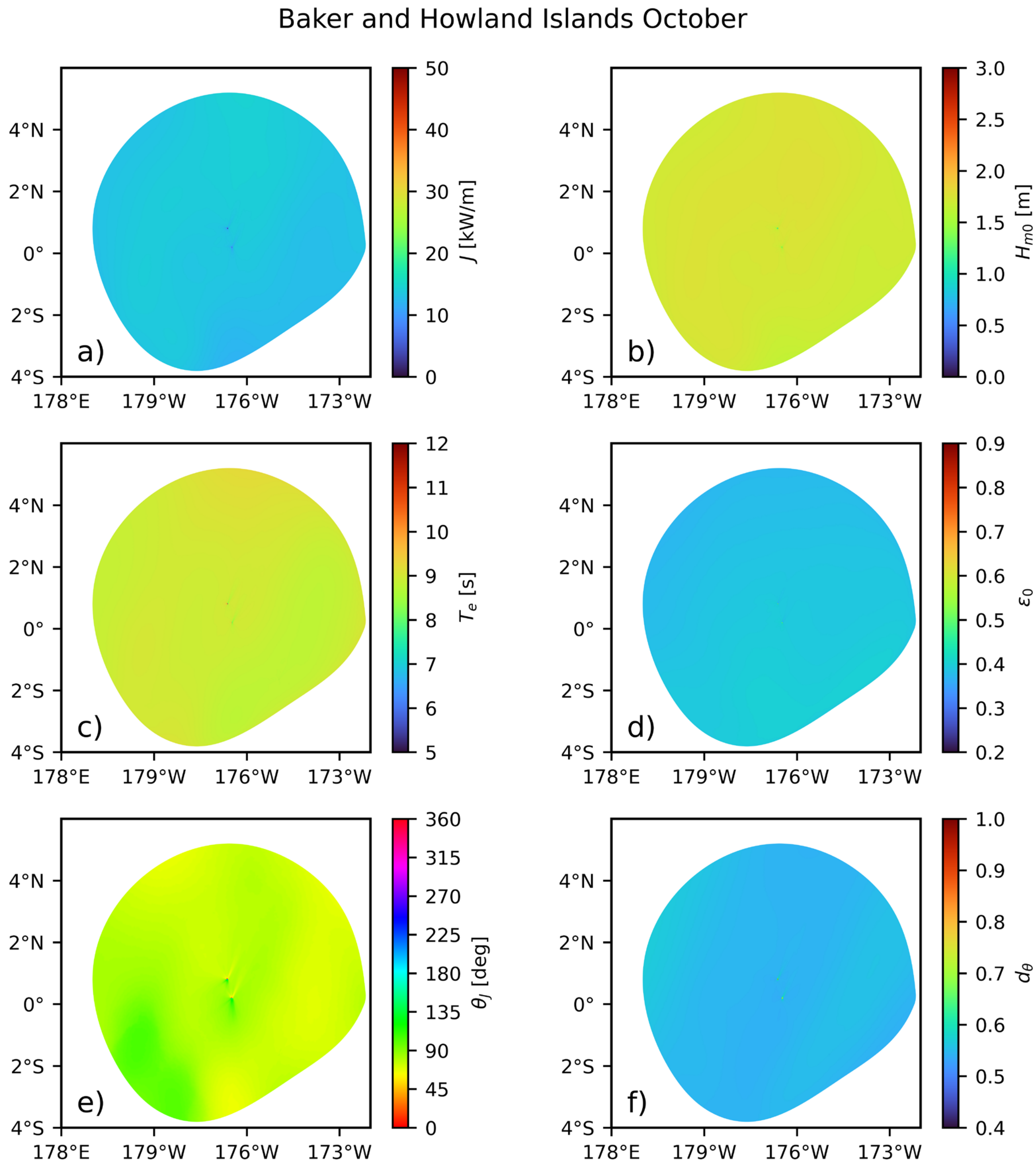

Figure A.22. Monthly distributions of six IEC parameters around Baker and Howland Islands in September: (a) omnidirectional wave power, (b) significant wave height, (c) energy period, (d) spectral width, (e) direction of maximum directionally resolved wave power, and (f) directionality coefficient.

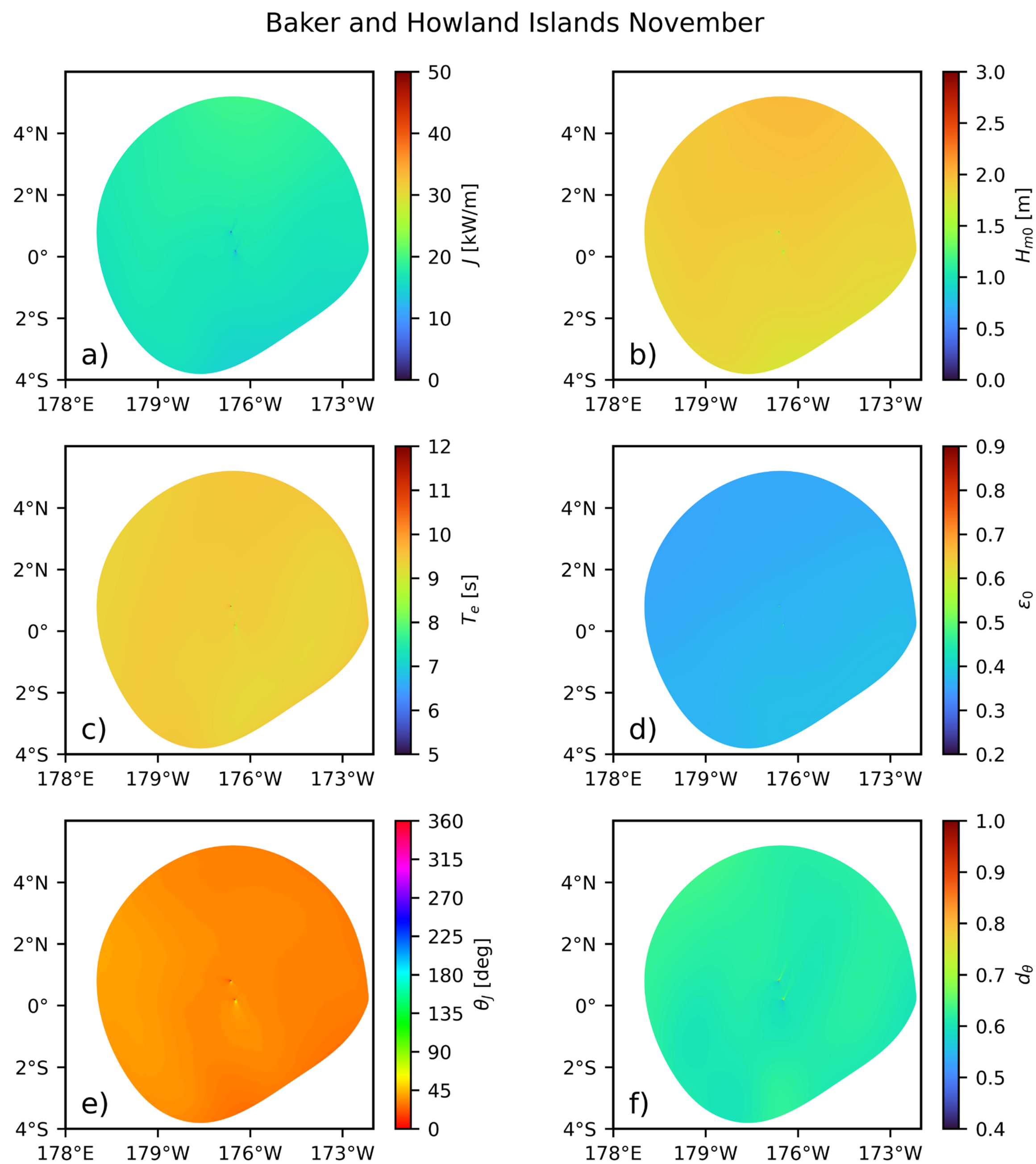

Figure A.23. Monthly distributions of six IEC parameters around Baker and Howland Islands in November: (a) omnidirectional wave power, (b) significant wave height, (c) energy period, (d) spectral width, (e) direction of maximum directionally resolved wave power, and (f) directionality coefficient.

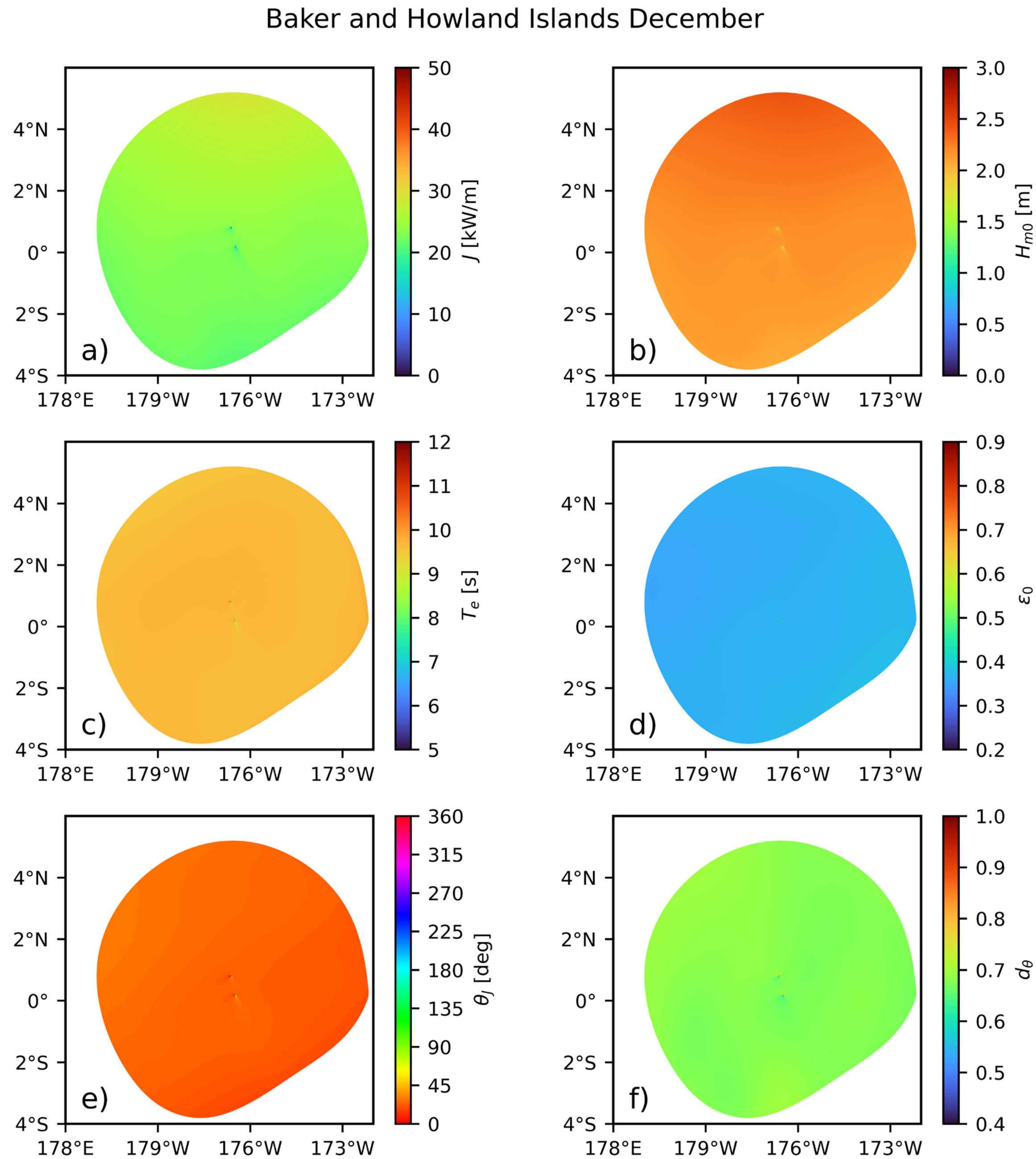

Figure A.24. Monthly distributions of six IEC parameters around Baker and Howland Islands in December: (a) omnidirectional wave power, (b) significant wave height, (c) energy period, (d) spectral width, (e) direction of maximum directionally resolved wave power, and (f) directionality coefficient.

A.3 Commonwealth of Northern Mariana Islands and Guam

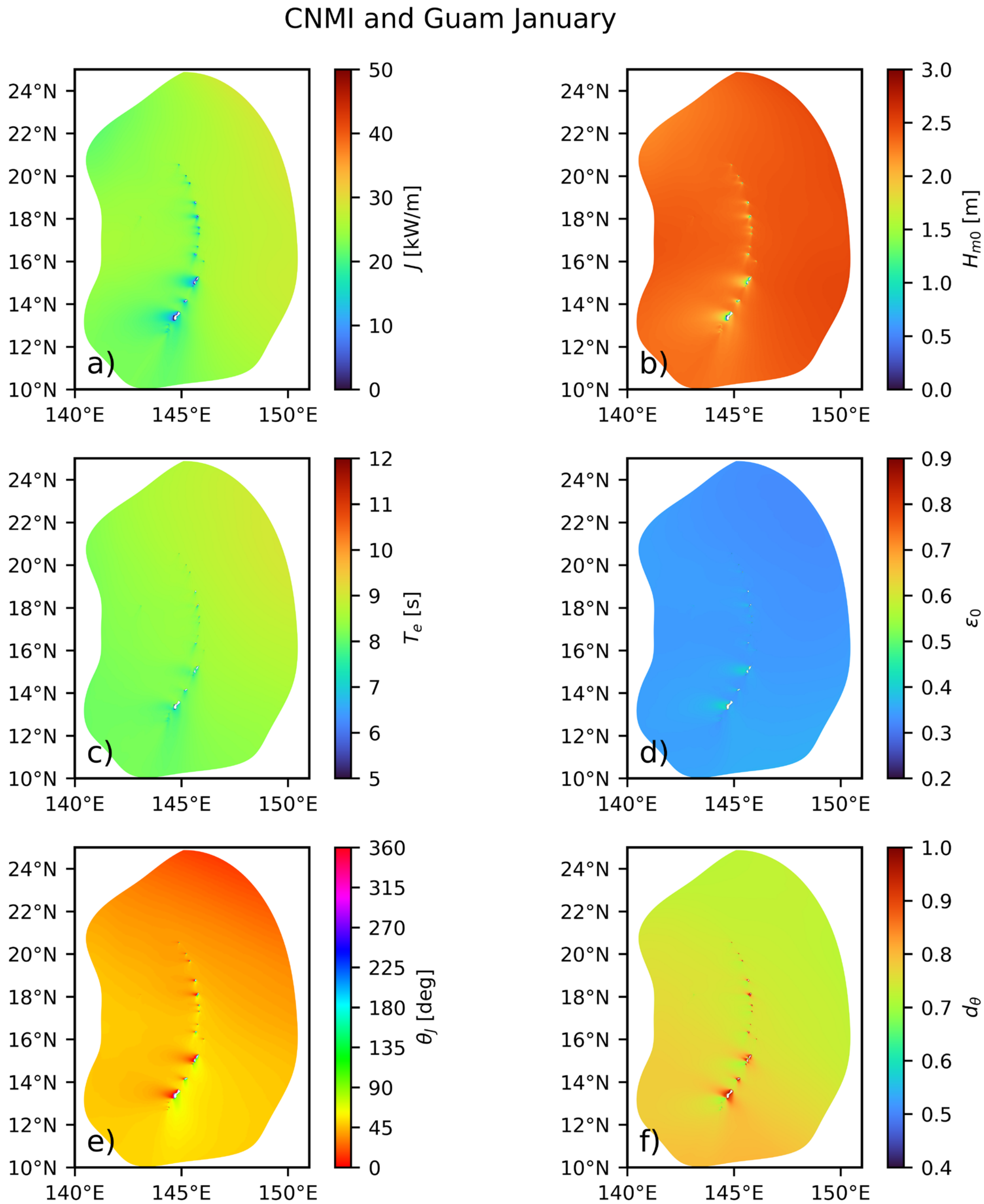

Figure A.25. Monthly distributions of six IEC parameters around the Commonwealth of Northern Mariana Islands and Guam in January: (a) omnidirectional wave power, (b) significant wave height, (c) energy period, (d) spectral width, (e) direction of maximum directionally resolved wave power, and (f) directionality coefficient.

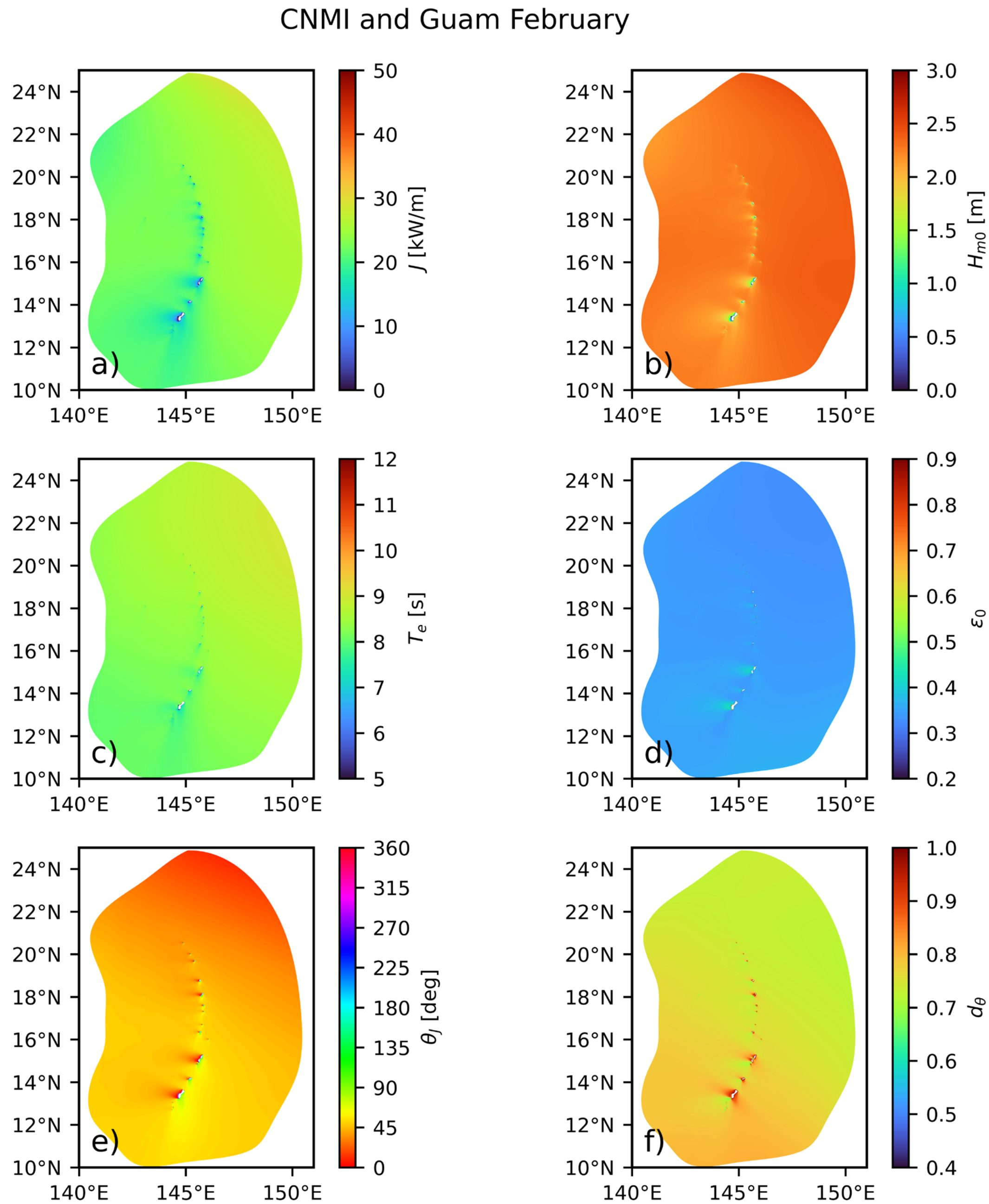

Figure A.26. Monthly distributions of six IEC parameters around the Commonwealth of Northern Mariana Islands and Guam in February: (a) omnidirectional wave power, (b) significant wave height, (c) energy period, (d) spectral width, (e) direction of maximum directionally resolved wave power, and (f) directionality coefficient.

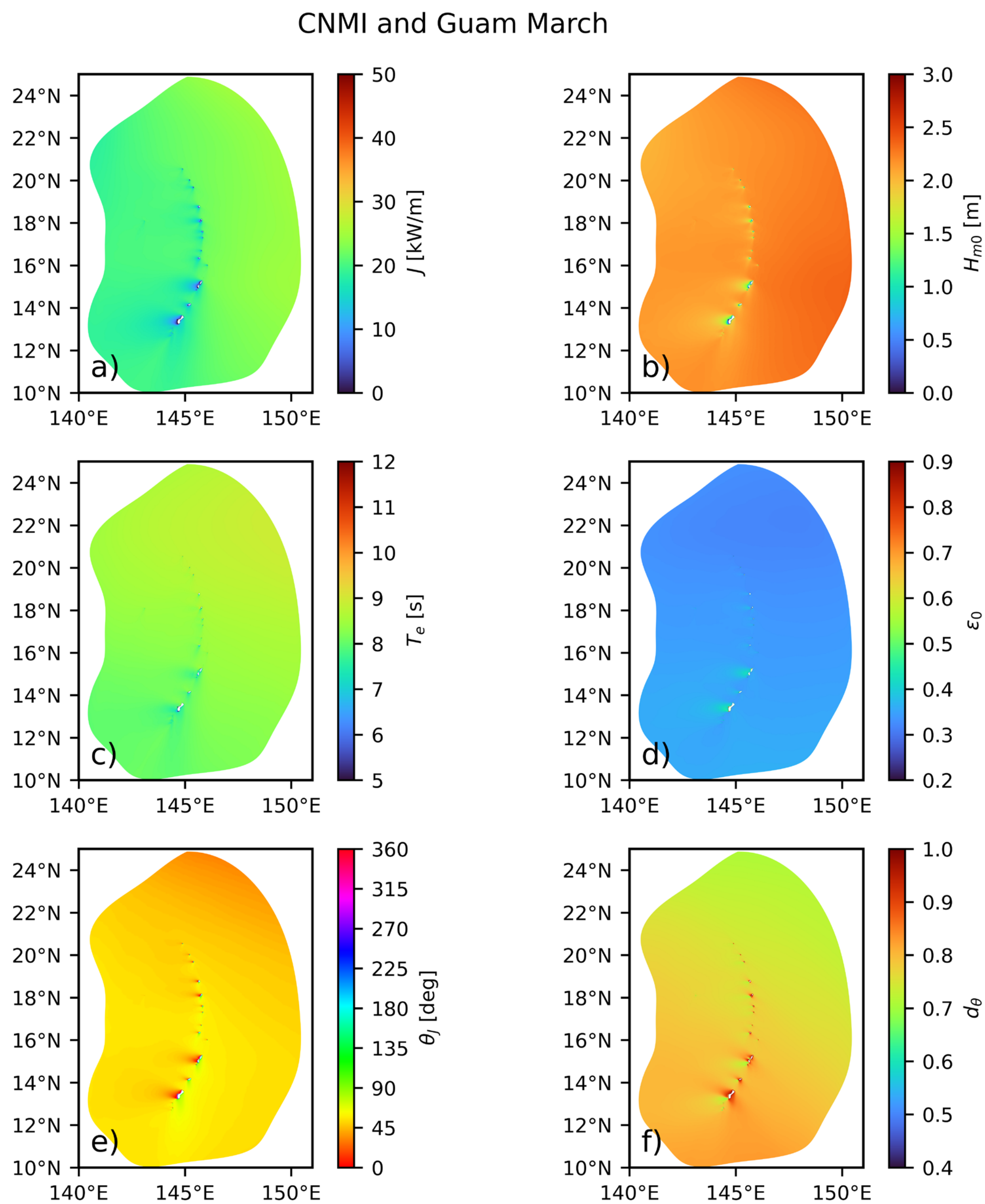

Figure A.27. Monthly distributions of six IEC parameters around the Commonwealth of Northern Mariana Islands and Guam in March: (a) omnidirectional wave power, (b) significant wave height, (c) energy period, (d) spectral width, (e) direction of maximum directionally resolved wave power, and (f) directionality coefficient.

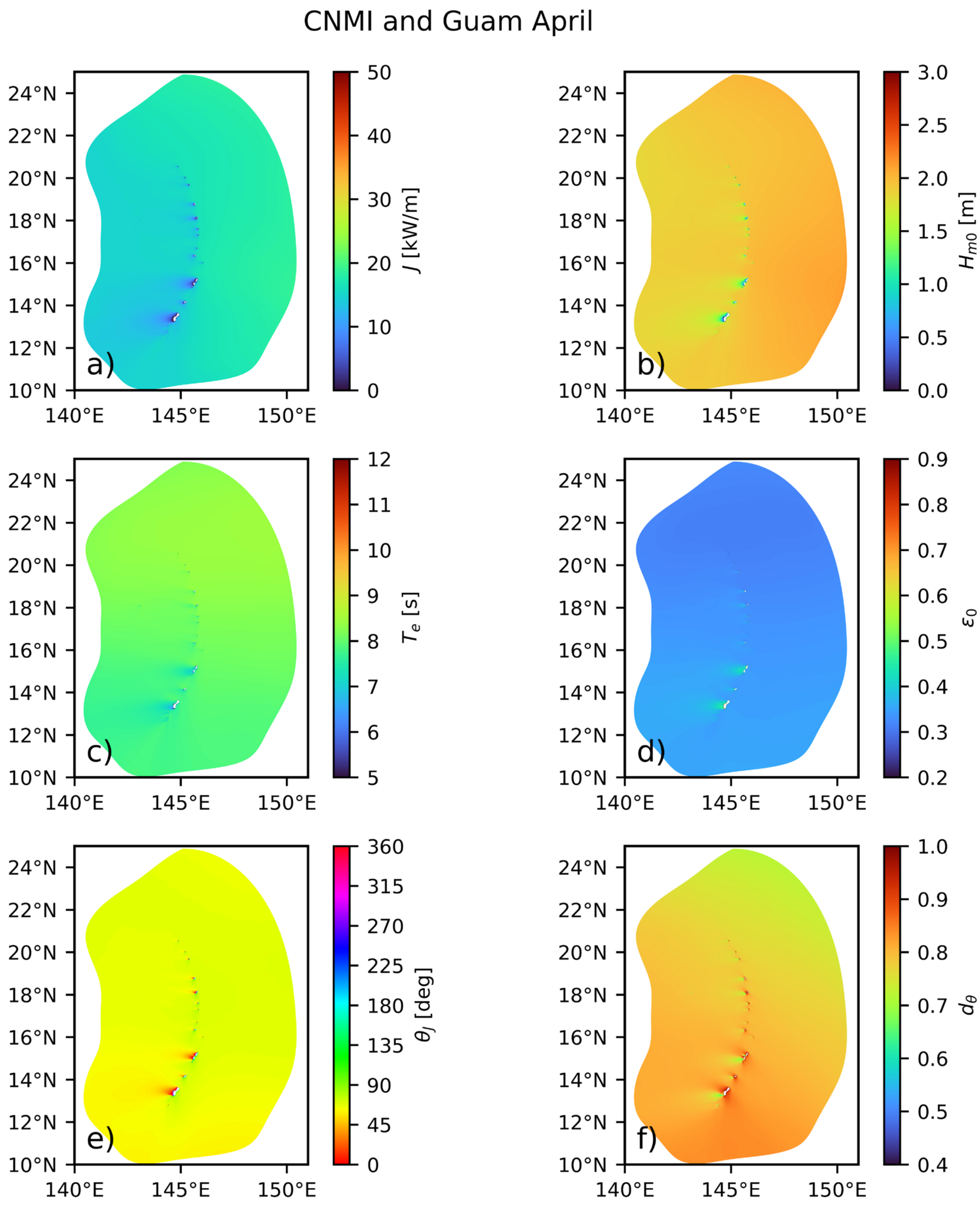

Figure A.28. Monthly distributions of six IEC parameters around the Commonwealth of Northern Mariana Islands and Guam in April: (a) omnidirectional wave power, (b) significant wave height, (c) energy period, (d) spectral width, (e) direction of maximum directionally resolved wave power, and (f) directionality coefficient.

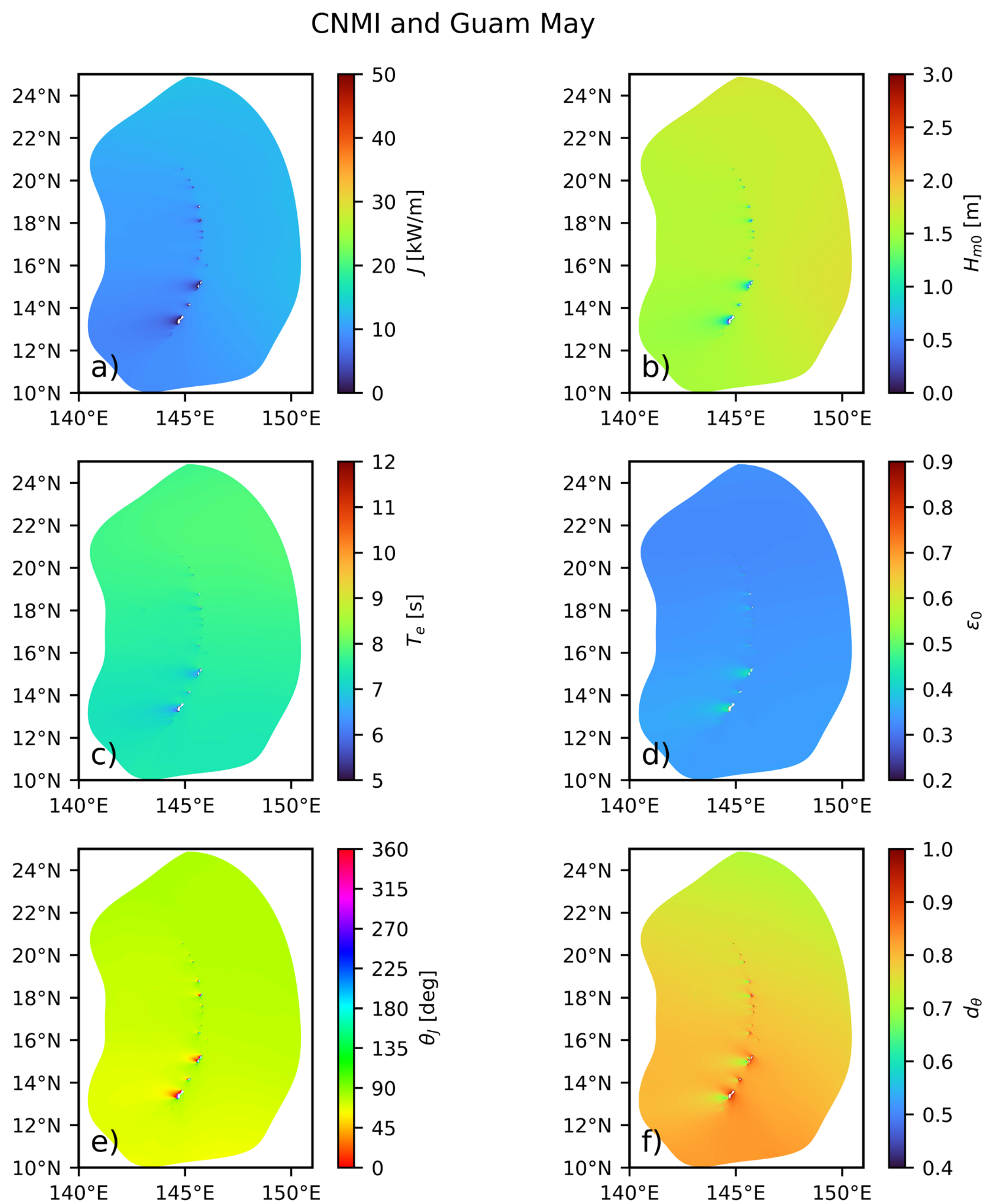

Figure A.29. Monthly distributions of six IEC parameters around the Commonwealth of Northern Mariana Islands and Guam in May: (a) omnidirectional wave power, (b) significant wave height, (c) energy period, (d) spectral width, (e) direction of maximum directionally resolved wave power, and (f) directionality coefficient.

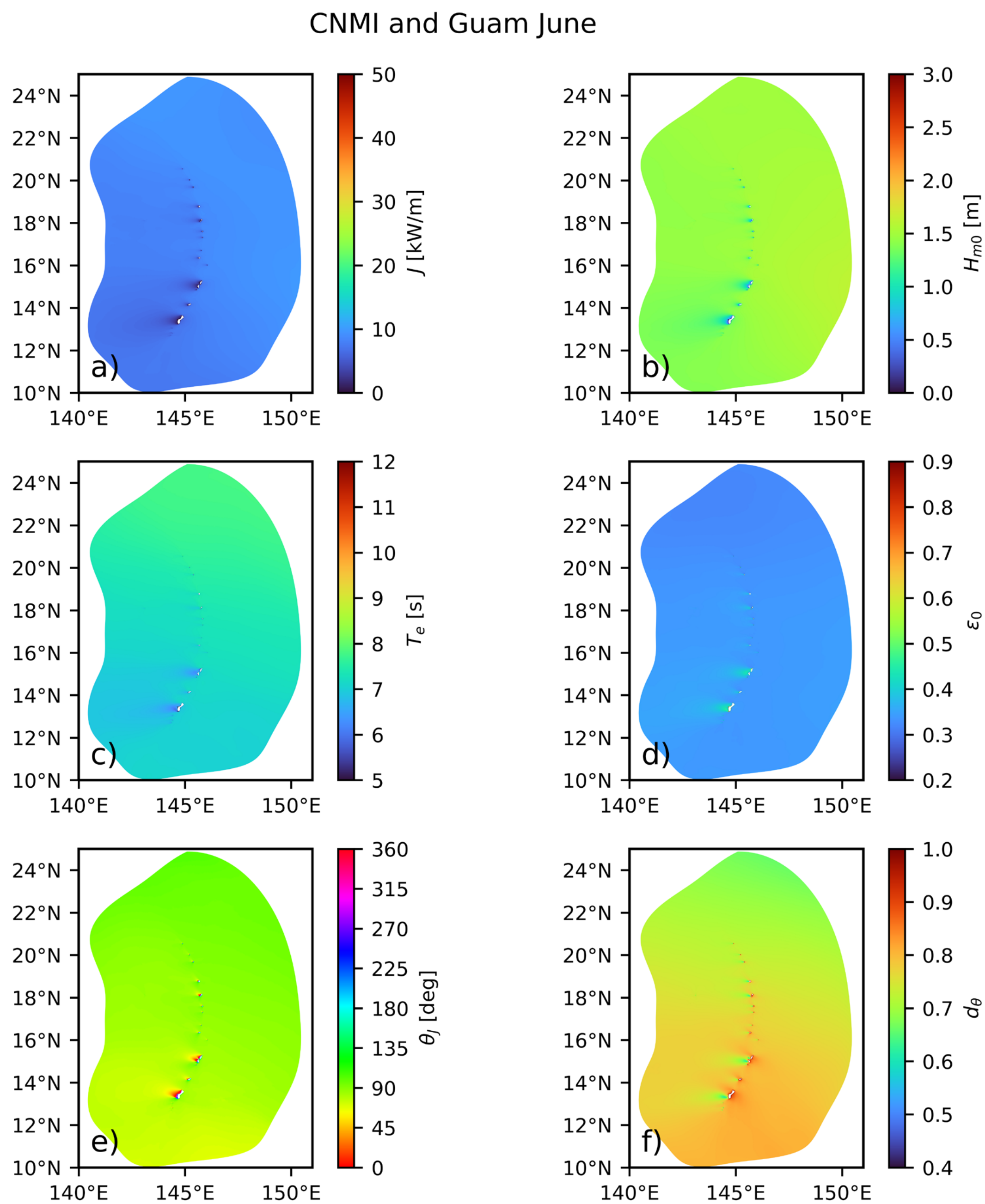

Figure A.30. Monthly distributions of six IEC parameters around the Commonwealth of Northern Mariana Islands and Guam in June: (a) omnidirectional wave power, (b) significant wave height, (c) energy period, (d) spectral width, (e) direction of maximum directionally resolved wave power, and (f) directionality coefficient.

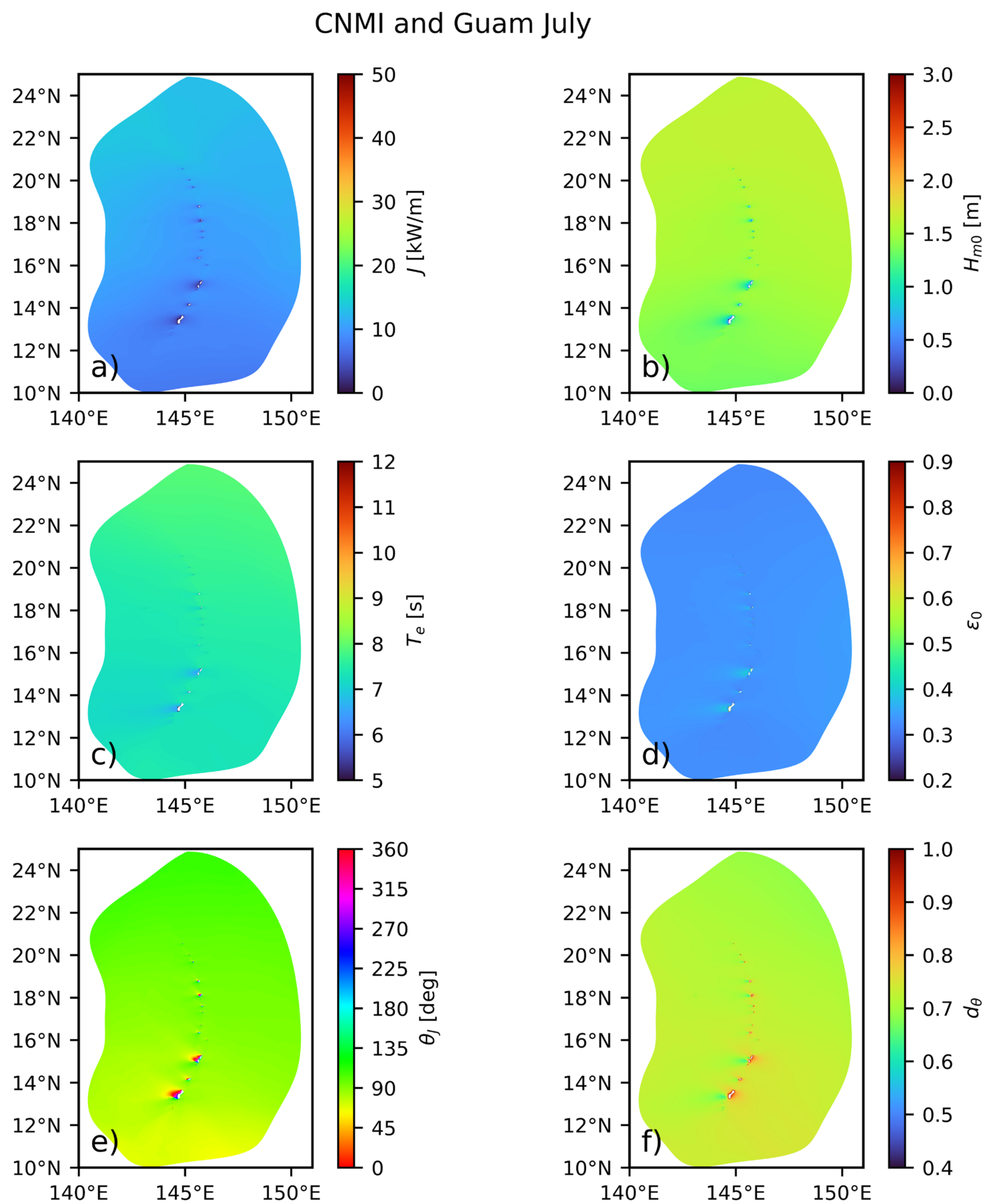

Figure A.31. Monthly distributions of six IEC parameters around the Commonwealth of Northern Mariana Islands and Guam in July: (a) omnidirectional wave power, (b) significant wave height, (c) energy period, (d) spectral width, (e) direction of maximum directionally resolved wave power, and (f) directionality coefficient.

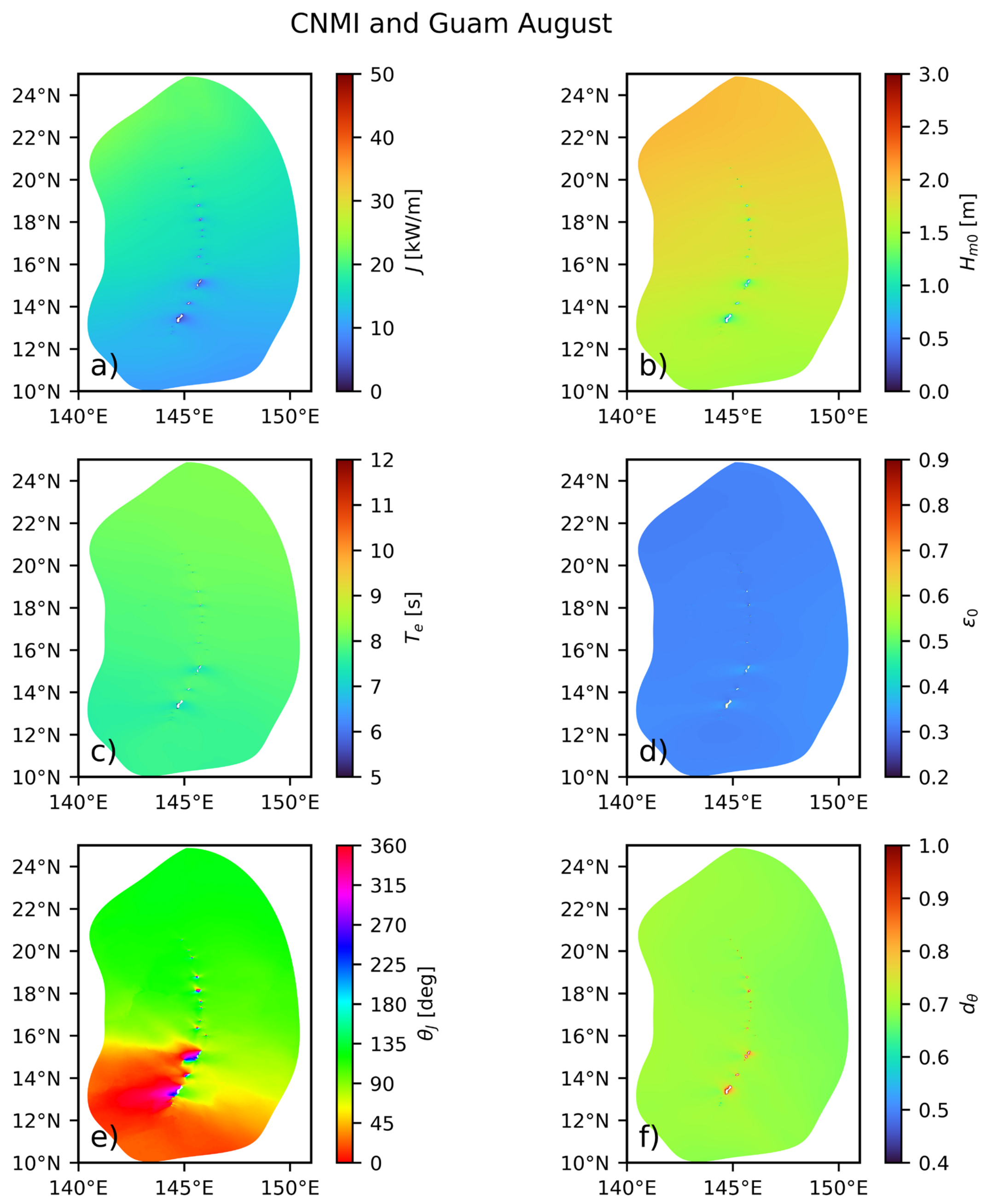

Figure A.32. Monthly distributions of six IEC parameters around the Commonwealth of Northern Mariana Islands and Guam in August: (a) omnidirectional wave power, (b) significant wave height, (c) energy period, (d) spectral width, (e) direction of maximum directionally resolved wave power, and (f) directionality coefficient.

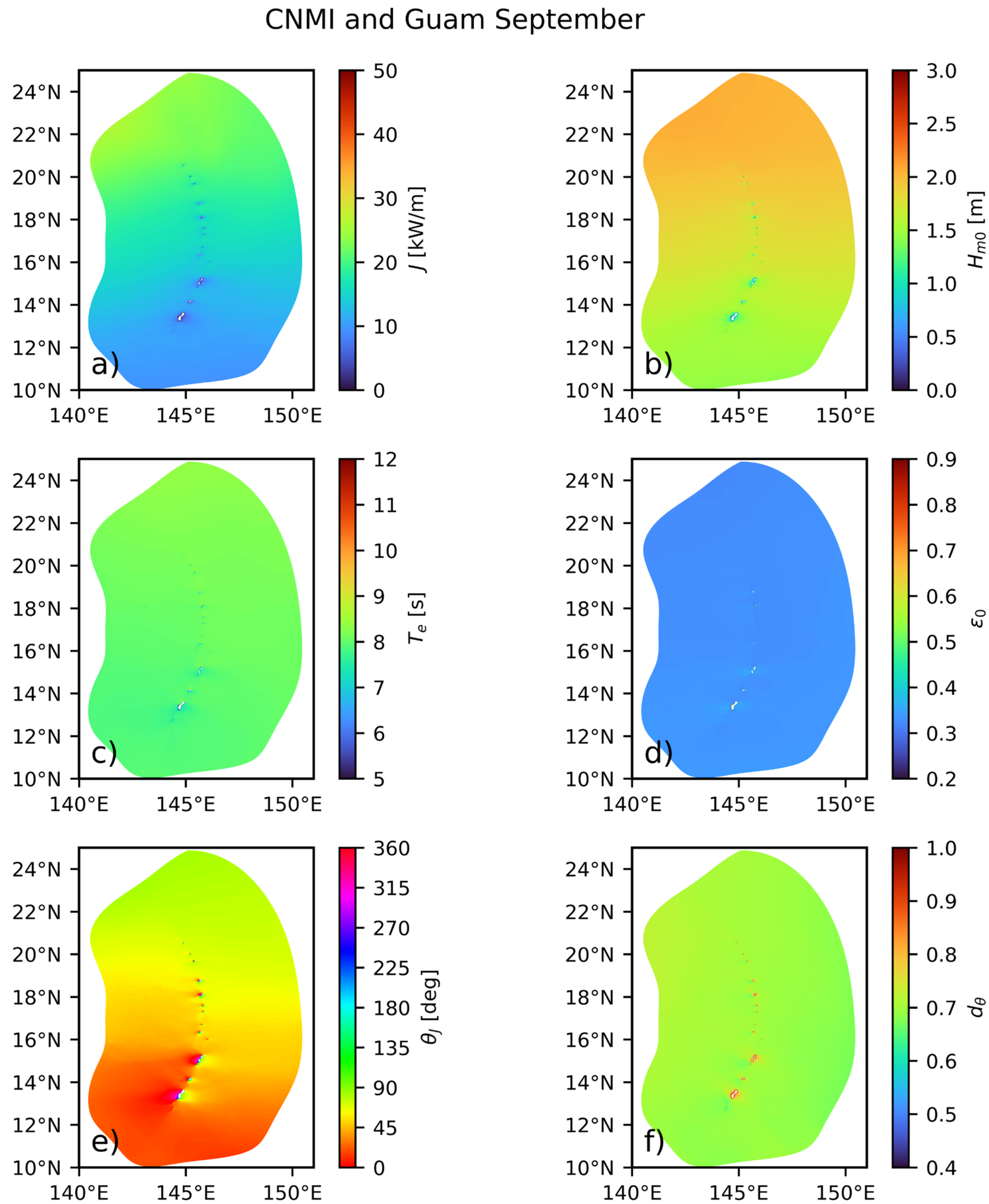

Figure A.33. Monthly distributions of six IEC parameters around the Commonwealth of Northern Mariana Islands and Guam in September: (a) omnidirectional wave power, (b) significant wave height, (c) energy period, (d) spectral width, (e) direction of maximum directionally resolved wave power, and (f) directionality coefficient.

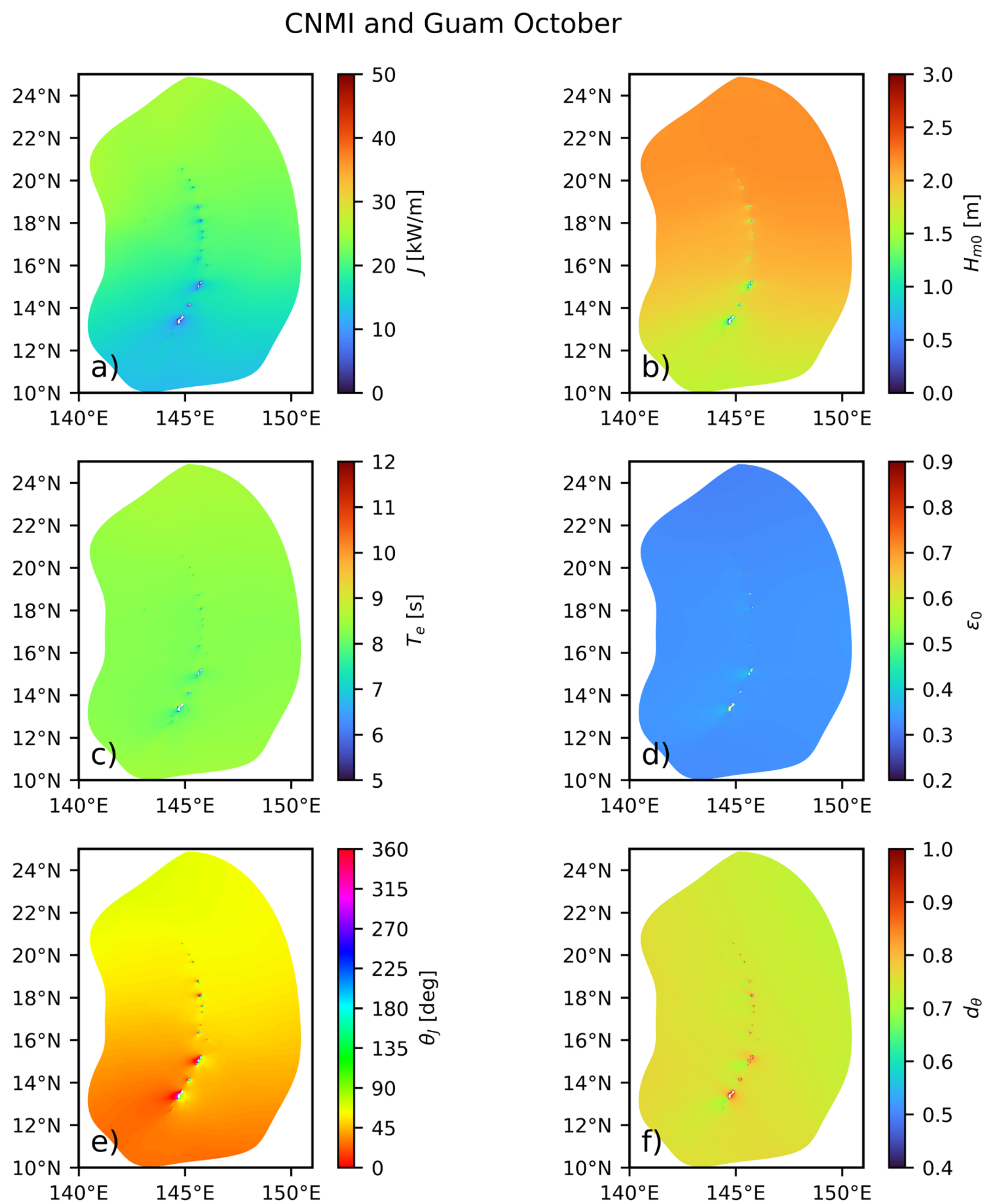

Figure A.34. Monthly distributions of six IEC parameters around the Commonwealth of Northern Mariana Islands and Guam in October: (a) omnidirectional wave power, (b) significant wave height, (c) energy period, (d) spectral width, (e) direction of maximum directionally resolved wave power, and (f) directionality coefficient.

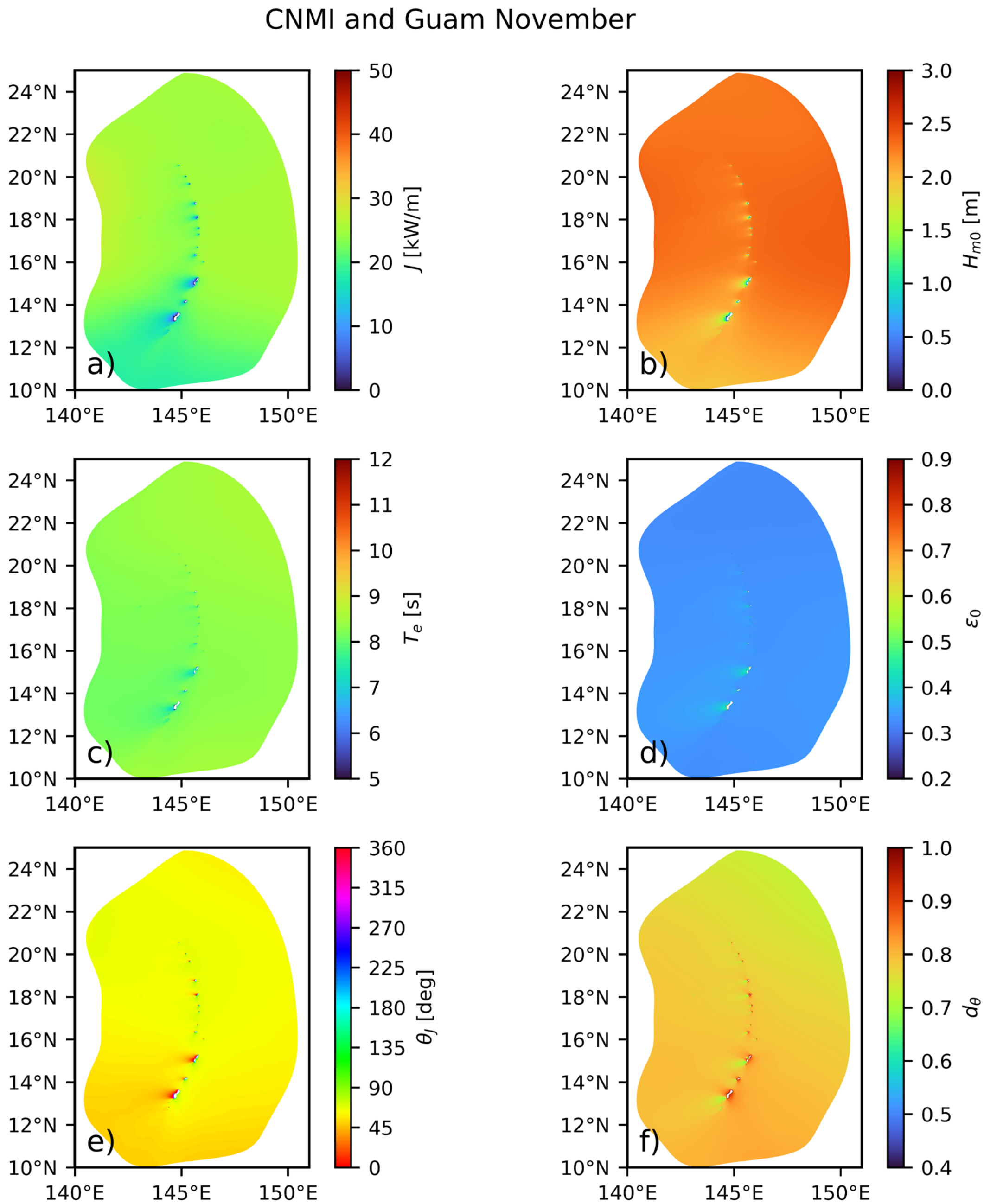

Figure A.35. Monthly distributions of six IEC parameters around the Commonwealth of Northern Mariana Islands and Guam in November: (a) omnidirectional wave power, (b) significant wave height, (c) energy period, (d) spectral width, (e) direction of maximum directionally resolved wave power, and (f) directionality coefficient.

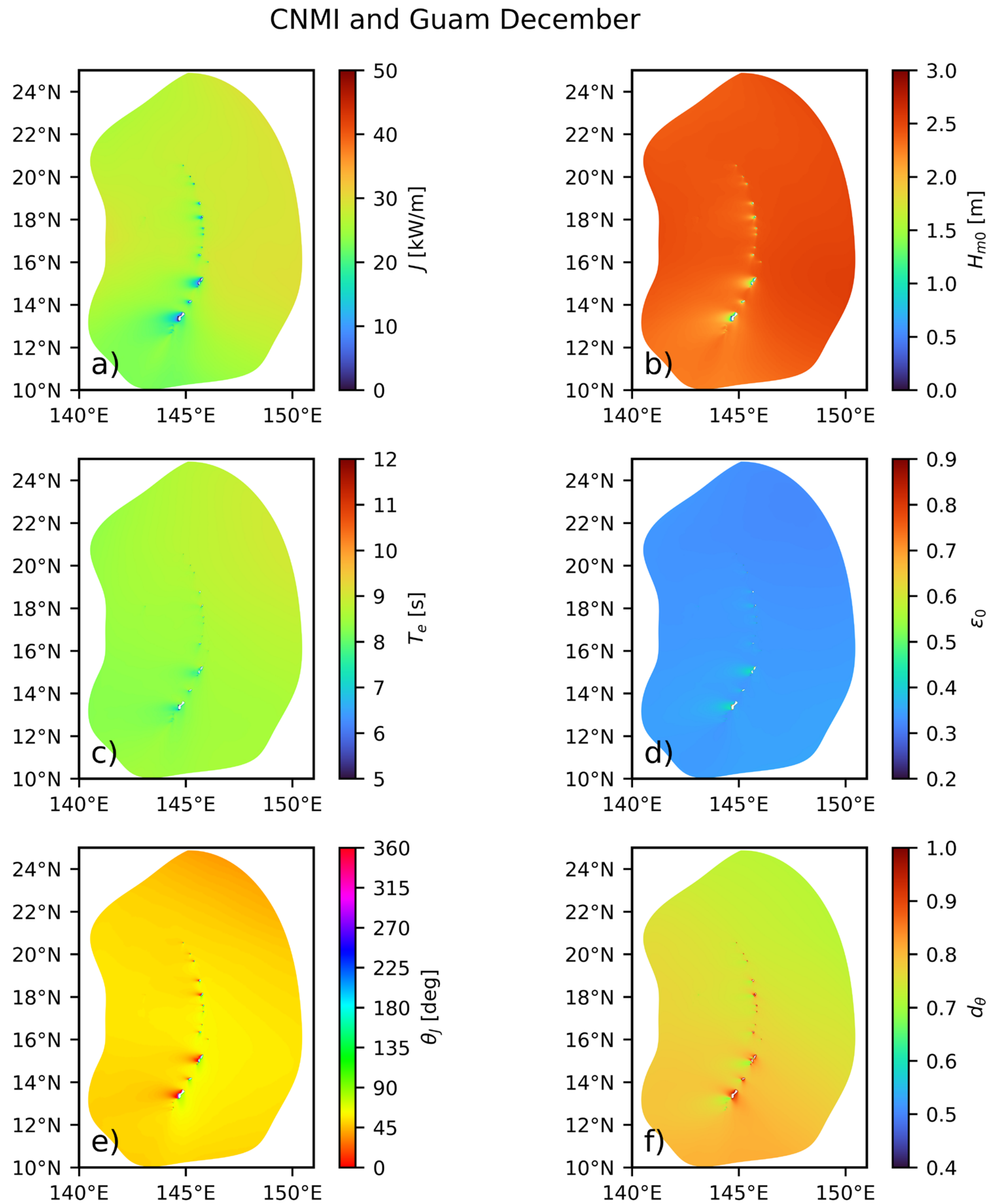

Figure A.36. Monthly distributions of six IEC parameters around the Commonwealth of Northern Mariana Islands and Guam in December: (a) omnidirectional wave power, (b) significant wave height, (c) energy period, (d) spectral width, (e) direction of maximum directionally resolved wave power, and (f) directionality coefficient.

A.4 Jarvis Island

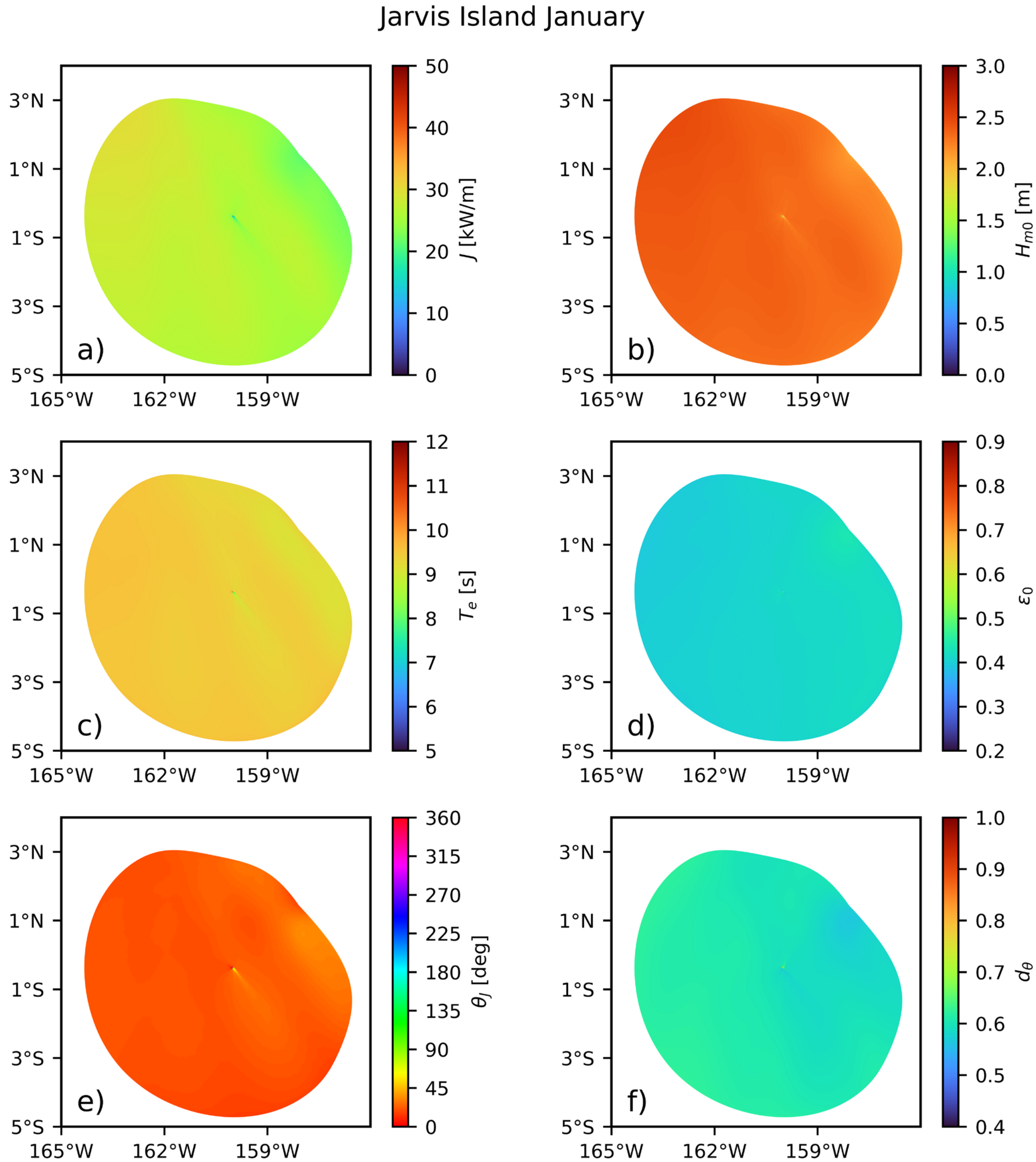

Figure A.37. Monthly distributions of six IEC parameters around Jarvis Island in January: (a) omnidirectional wave power, (b) significant wave height, (c) energy period, (d) spectral width, (e) direction of maximum directionally resolved wave power, and (f) directionality coefficient.

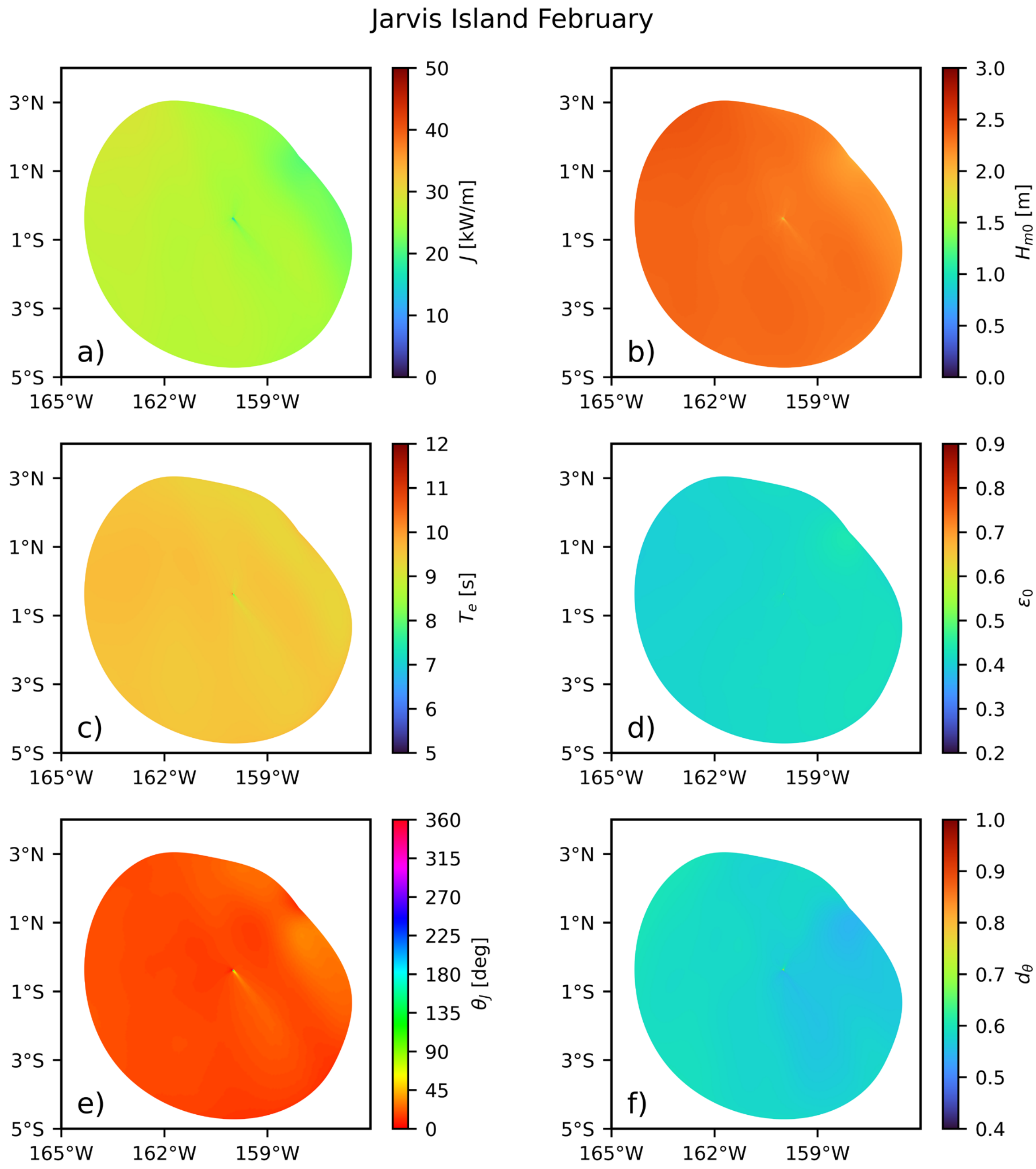

Figure A.38. Monthly distributions of six IEC parameters around Jarvis Island in February: (a) omnidirectional wave power, (b) significant wave height, (c) energy period, (d) spectral width, (e) direction of maximum directionally resolved wave power, and (f) directionality coefficient.

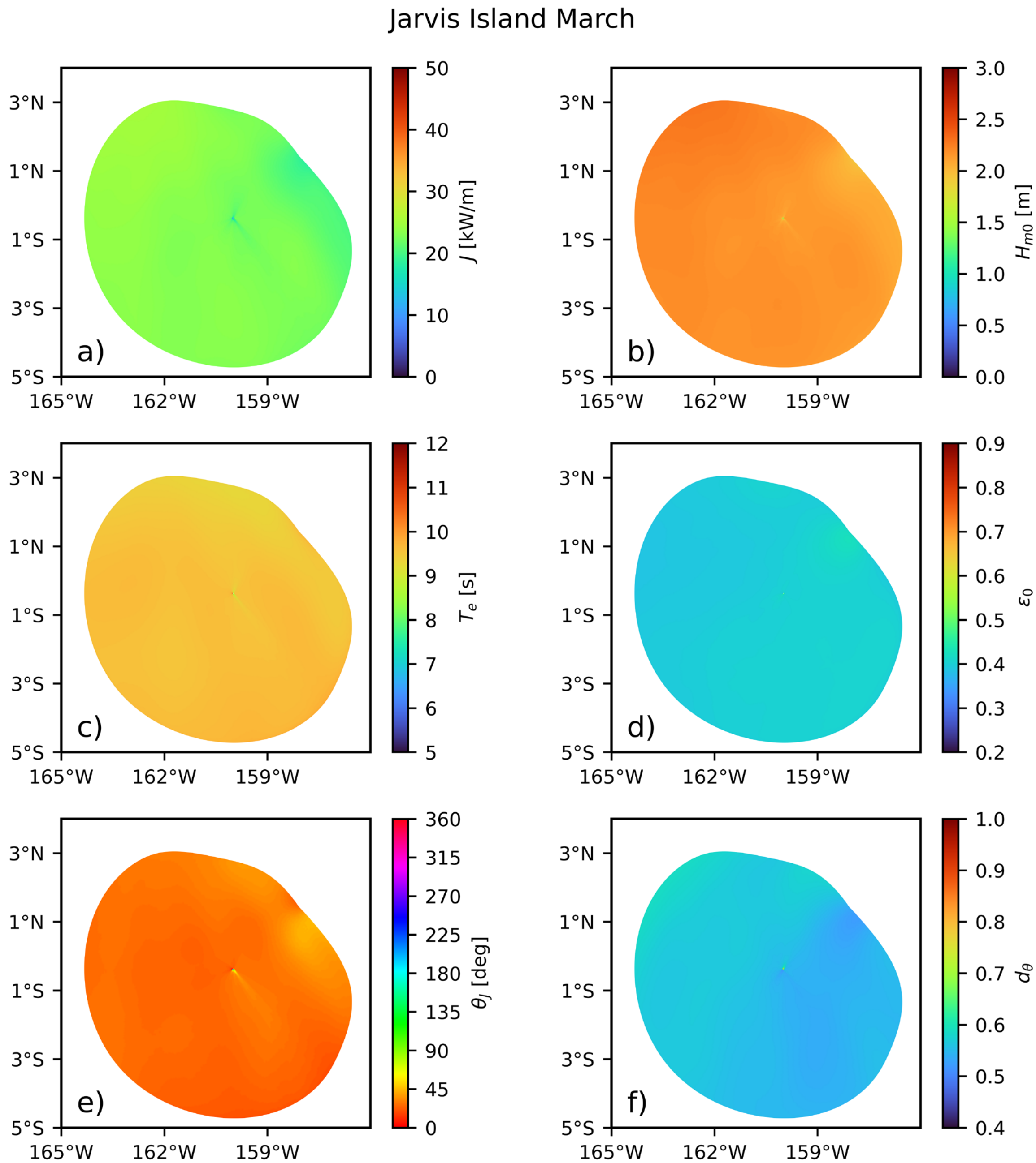

Figure A.39. Monthly distributions of six IEC parameters around Jarvis Island in March: (a) omnidirectional wave power, (b) significant wave height, (c) energy period, (d) spectral width, (e) direction of maximum directionally resolved wave power, and (f) directionality coefficient.

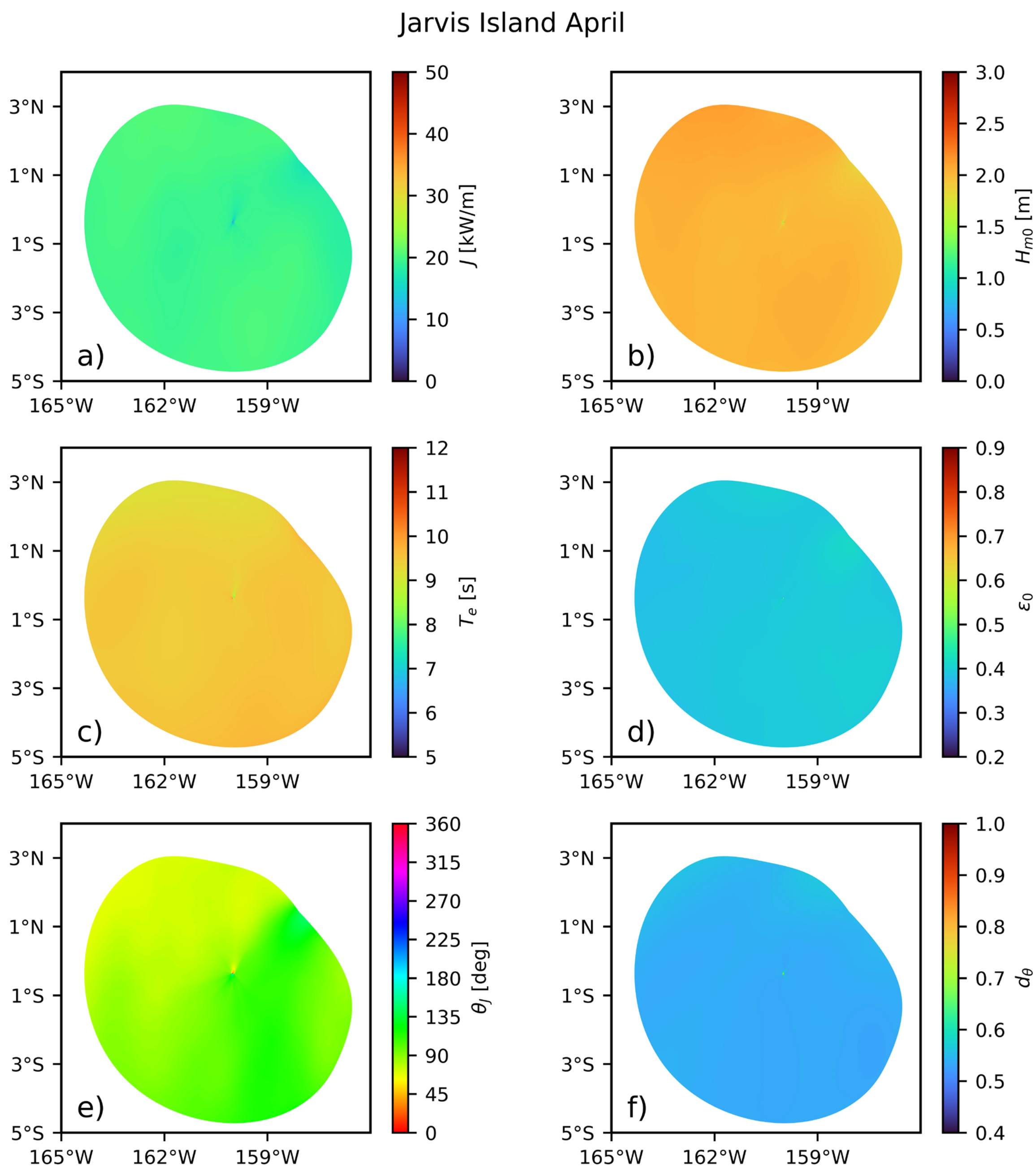

Figure A.40. Monthly distributions of six IEC parameters around Jarvis Island in April: (a) omnidirectional wave power, (b) significant wave height, (c) energy period, (d) spectral width, (e) direction of maximum directionally resolved wave power, and (f) directionality coefficient.

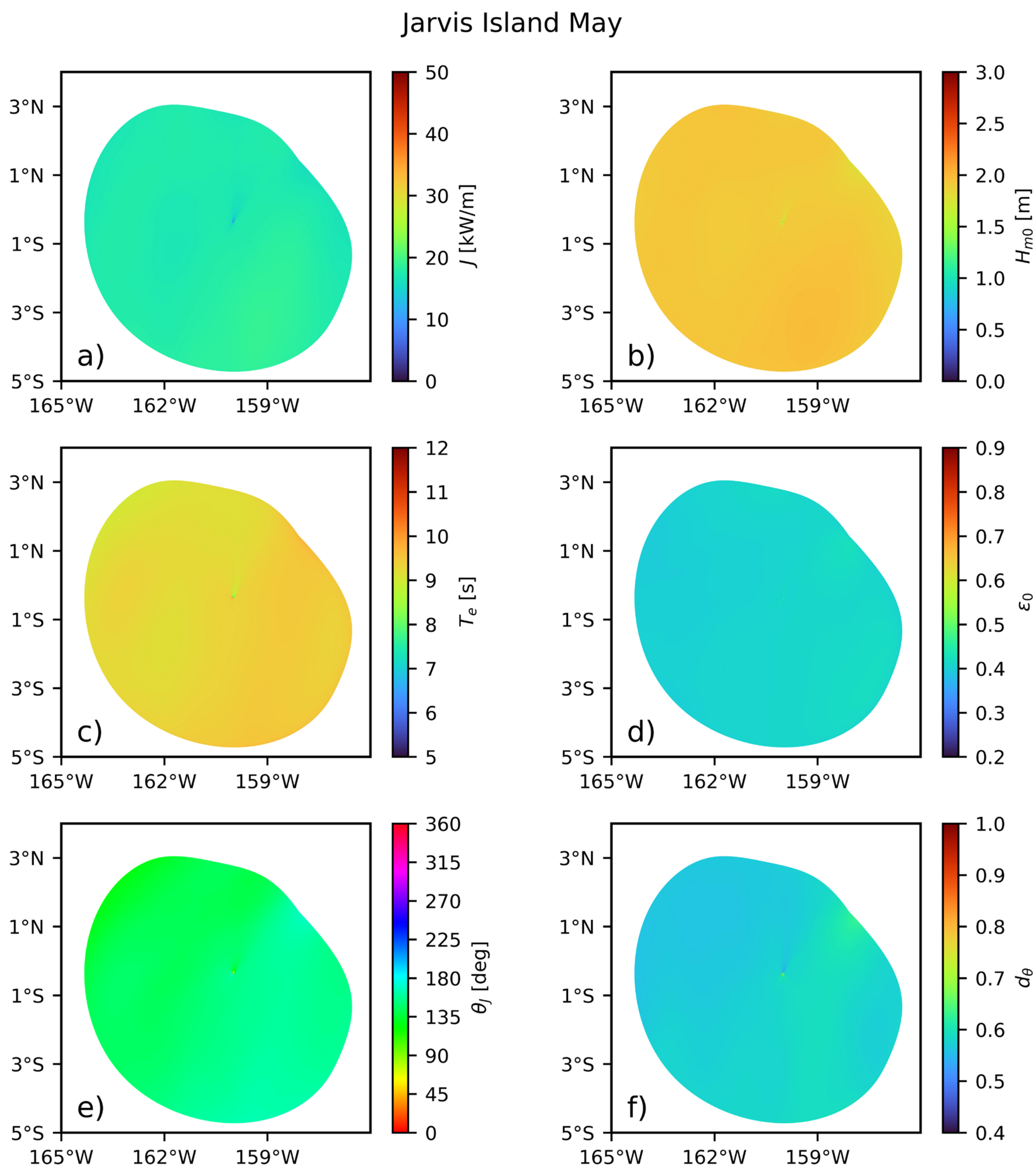

Figure A.41. Monthly distributions of six IEC parameters around Jarvis Island in May: (a) omnidirectional wave power, (b) significant wave height, (c) energy period, (d) spectral width, (e) direction of maximum directionally resolved wave power, and (f) directionality coefficient.

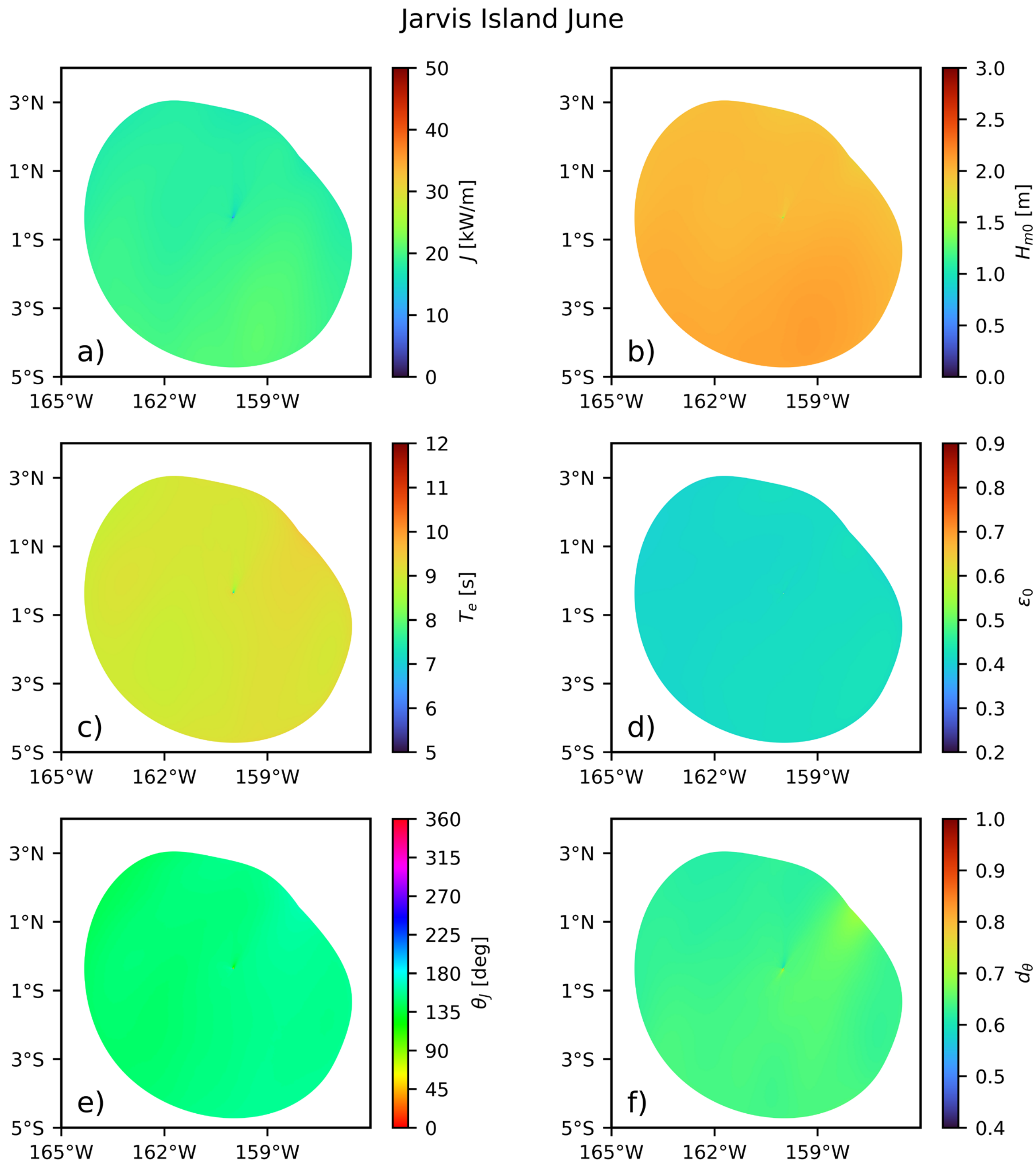

Figure A.42. Monthly distributions of six IEC parameters around Jarvis Island in June: (a) omnidirectional wave power, (b) significant wave height, (c) energy period, (d) spectral width, (e) direction of maximum directionally resolved wave power, and (f) directionality coefficient.

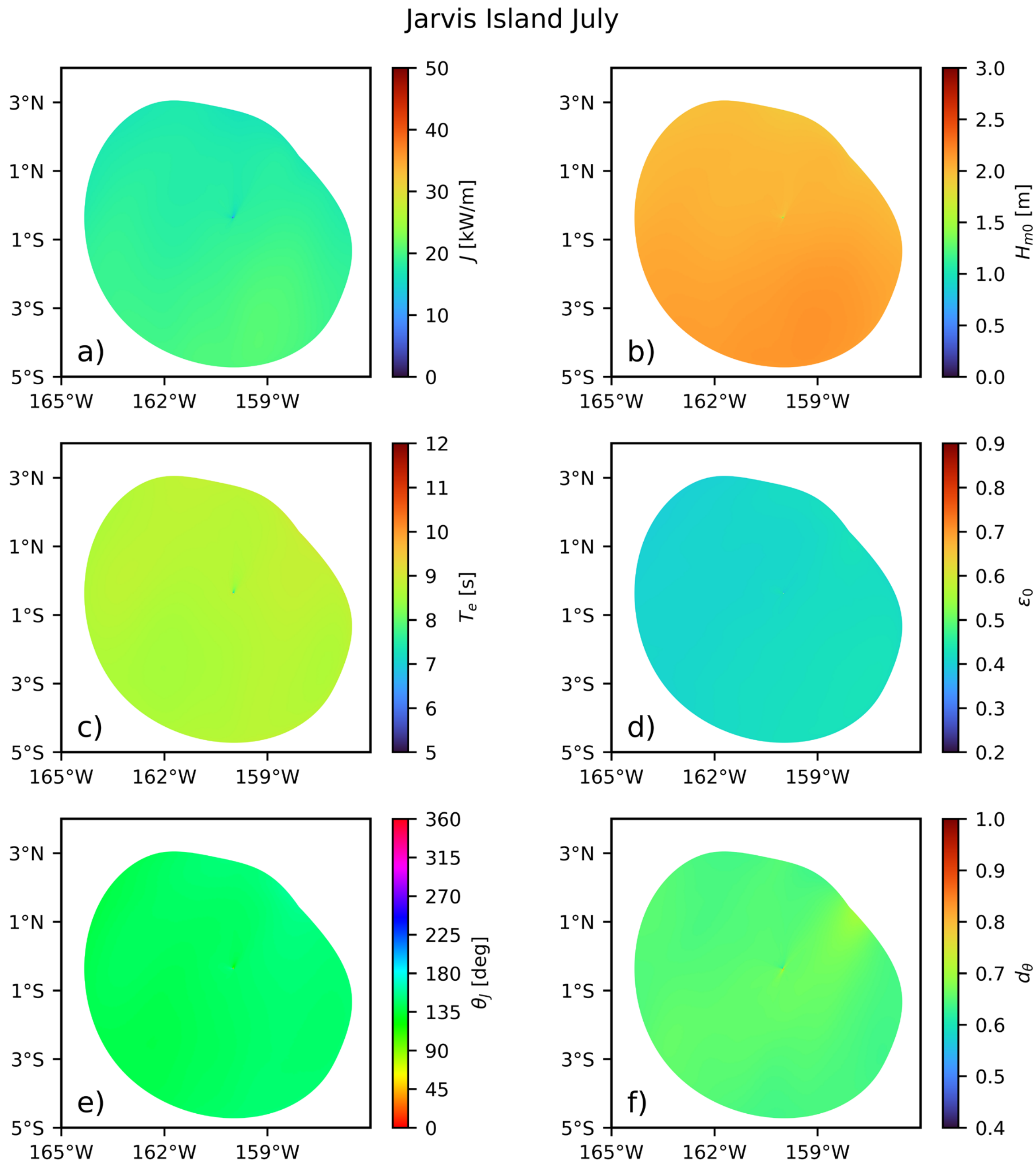

Figure A.43. Monthly distributions of six IEC parameters around Jarvis Island in July: (a) omnidirectional wave power, (b) significant wave height, (c) energy period, (d) spectral width, (e) direction of maximum directionally resolved wave power, and (f) directionality coefficient.

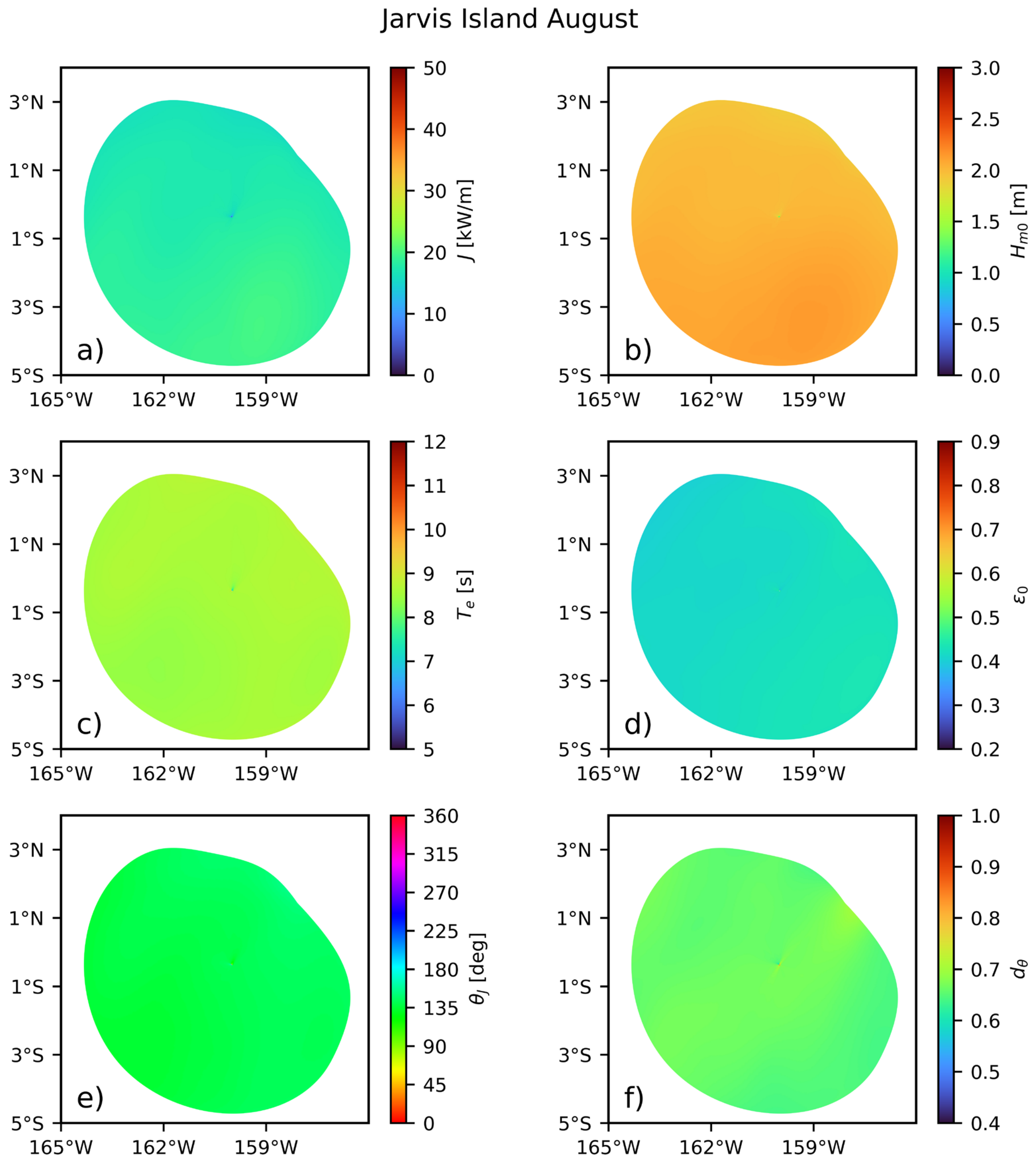

Figure A.44. Monthly distributions of six IEC parameters around Jarvis Island in August: (a) omnidirectional wave power, (b) significant wave height, (c) energy period, (d) spectral width, (e) direction of maximum directionally resolved wave power, and (f) directionality coefficient.

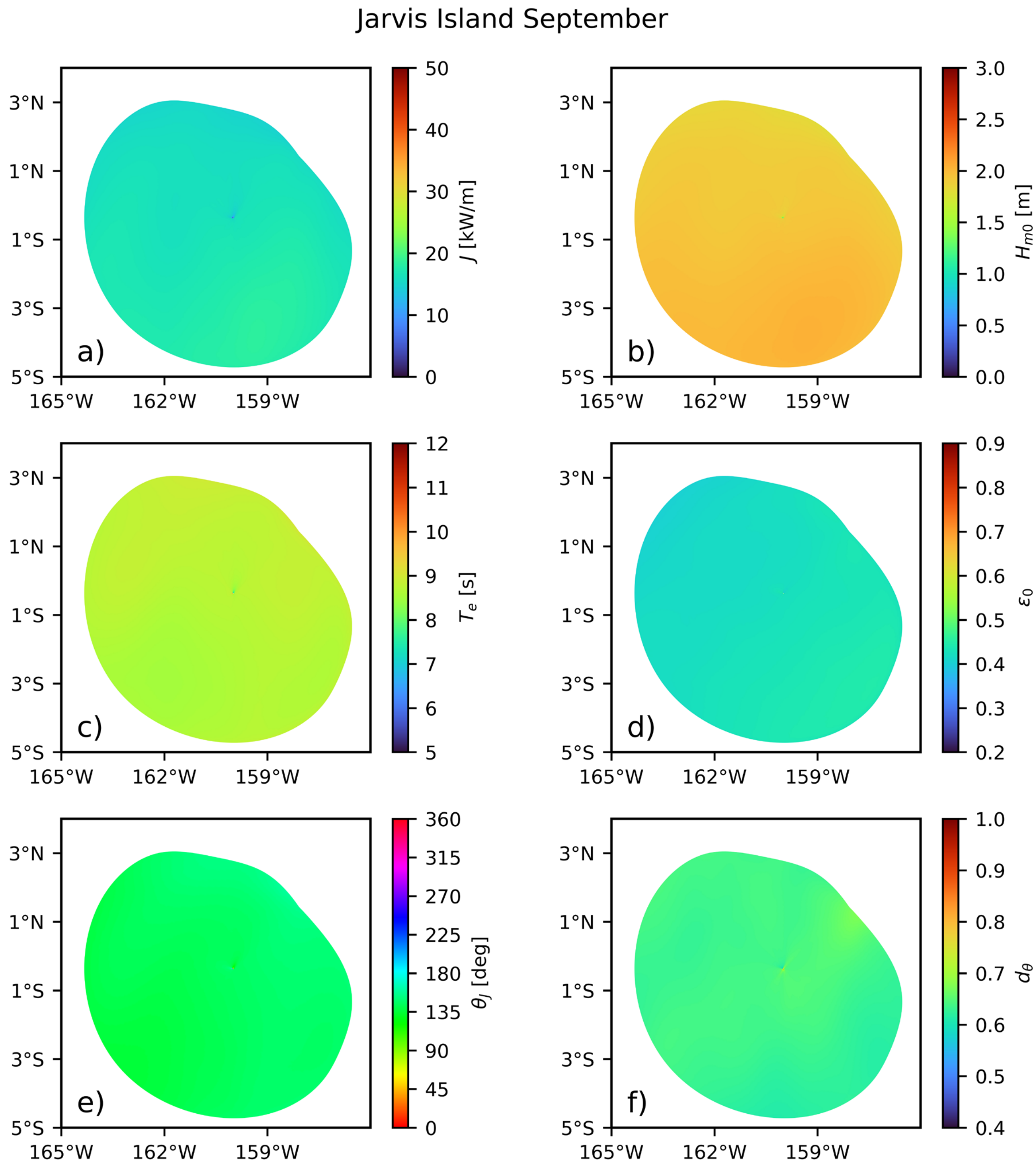

Figure A.45. Monthly distributions of six IEC parameters around Jarvis Island in September: (a) omnidirectional wave power, (b) significant wave height, (c) energy period, (d) spectral width, (e) direction of maximum directionally resolved wave power, and (f) directionality coefficient.

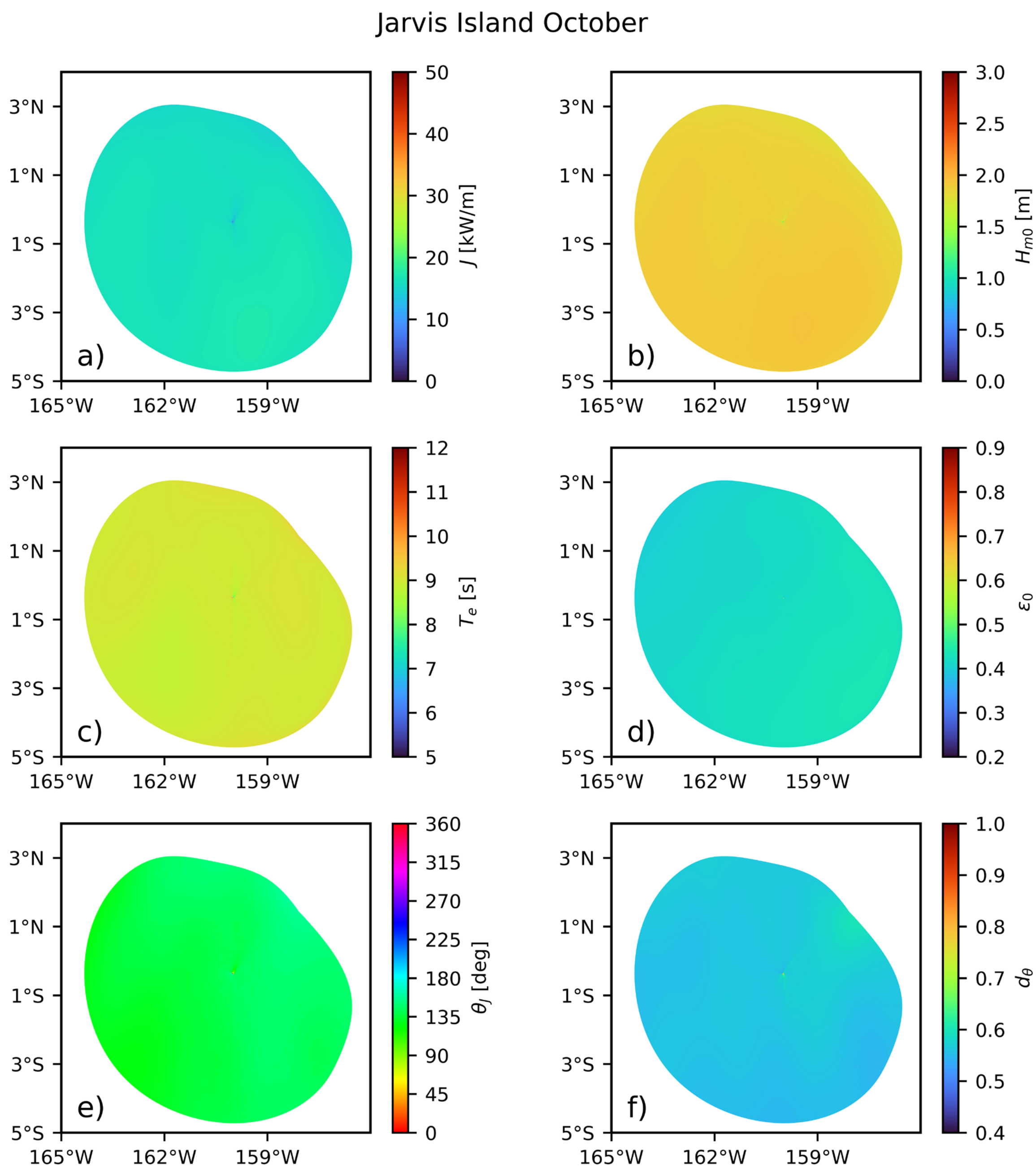

Figure A.46. Monthly distributions of six IEC parameters around Jarvis Island in October: (a) omnidirectional wave power, (b) significant wave height, (c) energy period, (d) spectral width, (e) direction of maximum directionally resolved wave power, and (f) directionality coefficient.

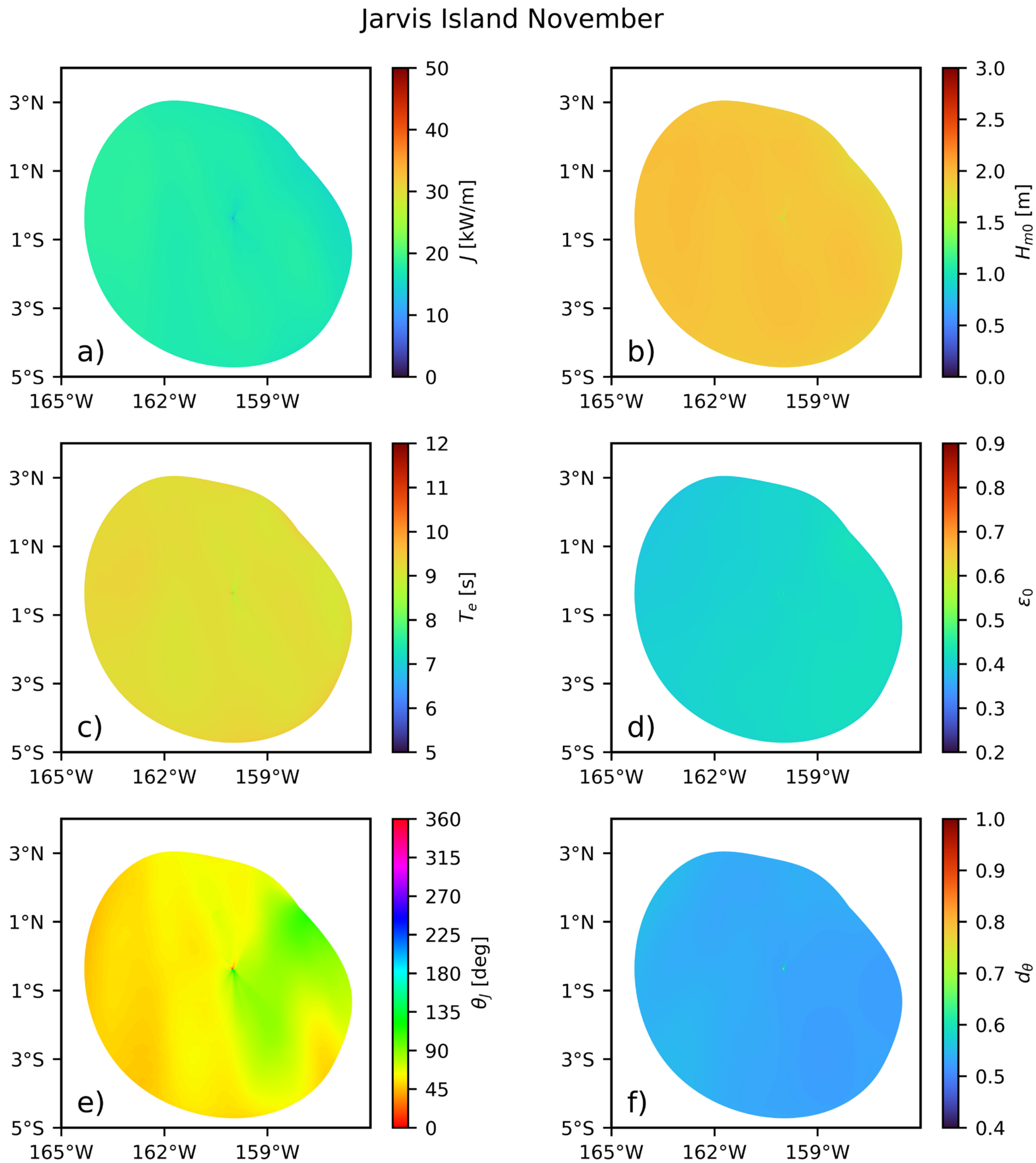

Figure A.47. Monthly distributions of six IEC parameters around Jarvis Island in November: (a) omnidirectional wave power, (b) significant wave height, (c) energy period, (d) spectral width, (e) direction of maximum directionally resolved wave power, and (f) directionality coefficient.

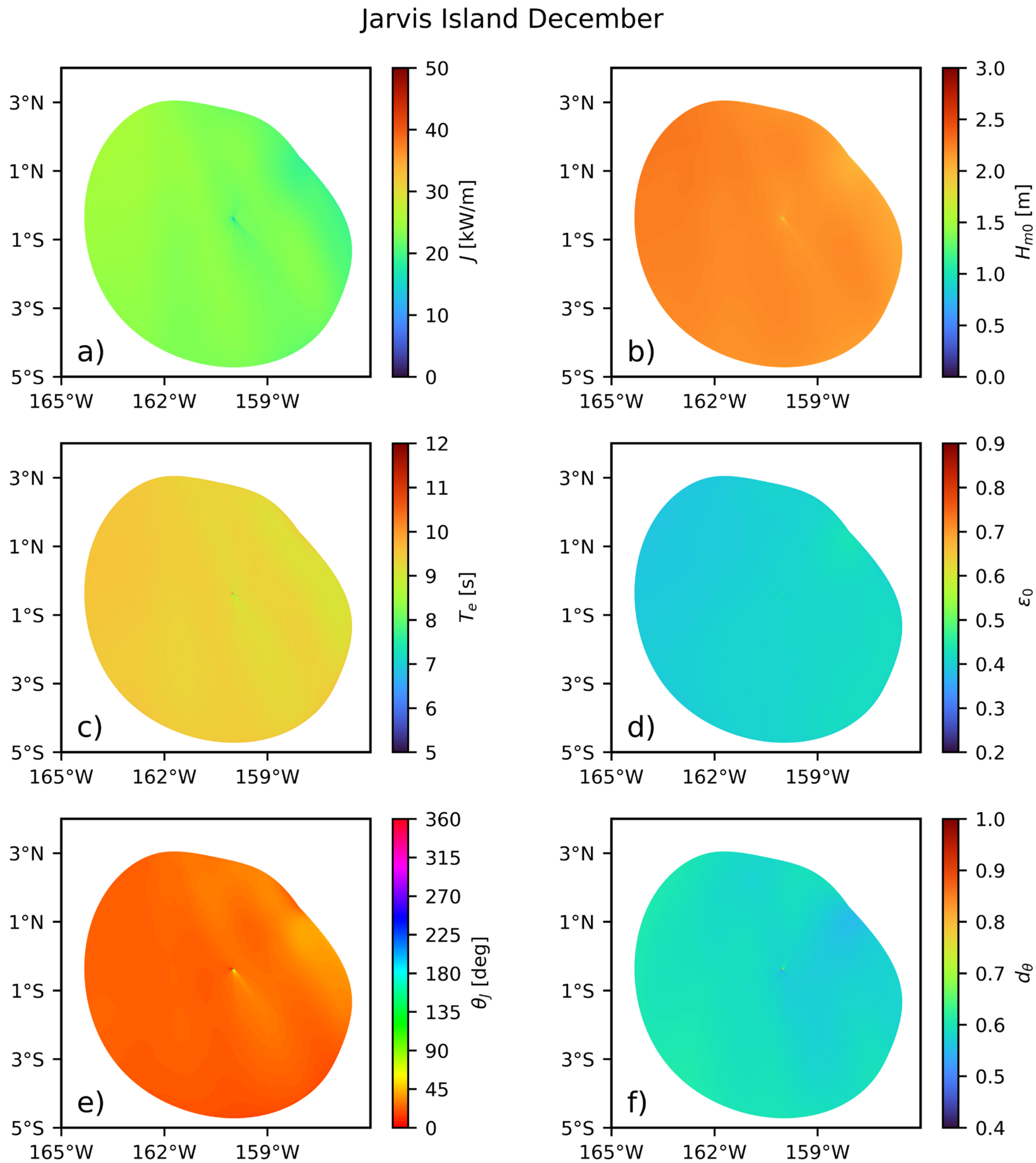

Figure A.48. Monthly distributions of six IEC parameters around Jarvis Island in December: (a) omnidirectional wave power, (b) significant wave height, (c) energy period, (d) spectral width, (e) direction of maximum directionally resolved wave power, and (f) directionality coefficient.

A.5 Johnston Atoll

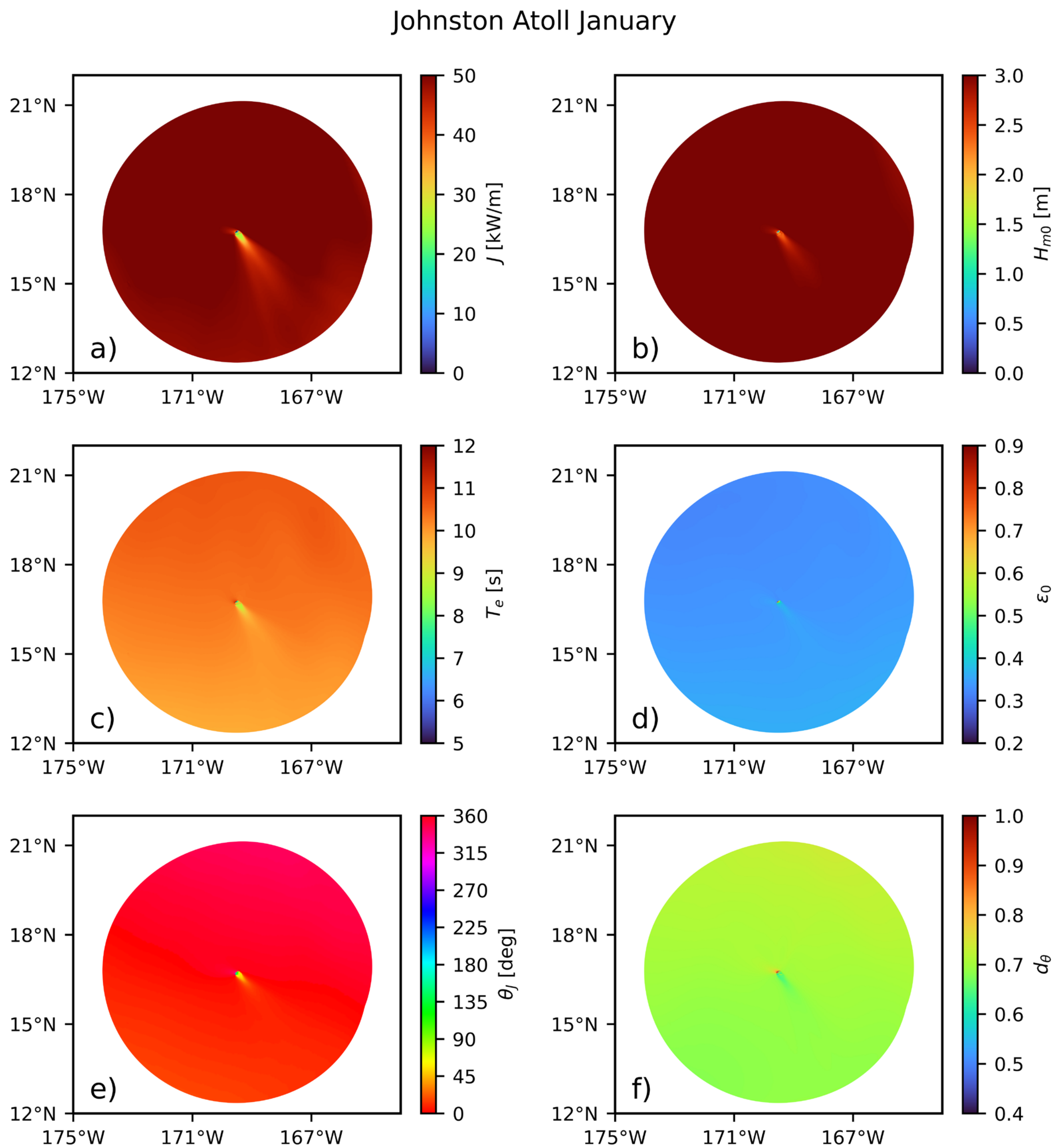

Figure A.49. Monthly distributions of six IEC parameters around Johnston Atoll in January: (a) omnidirectional wave power, (b) significant wave height, (c) energy period, (d) spectral width, (e) direction of maximum directionally resolved wave power, and (f) directionality coefficient.

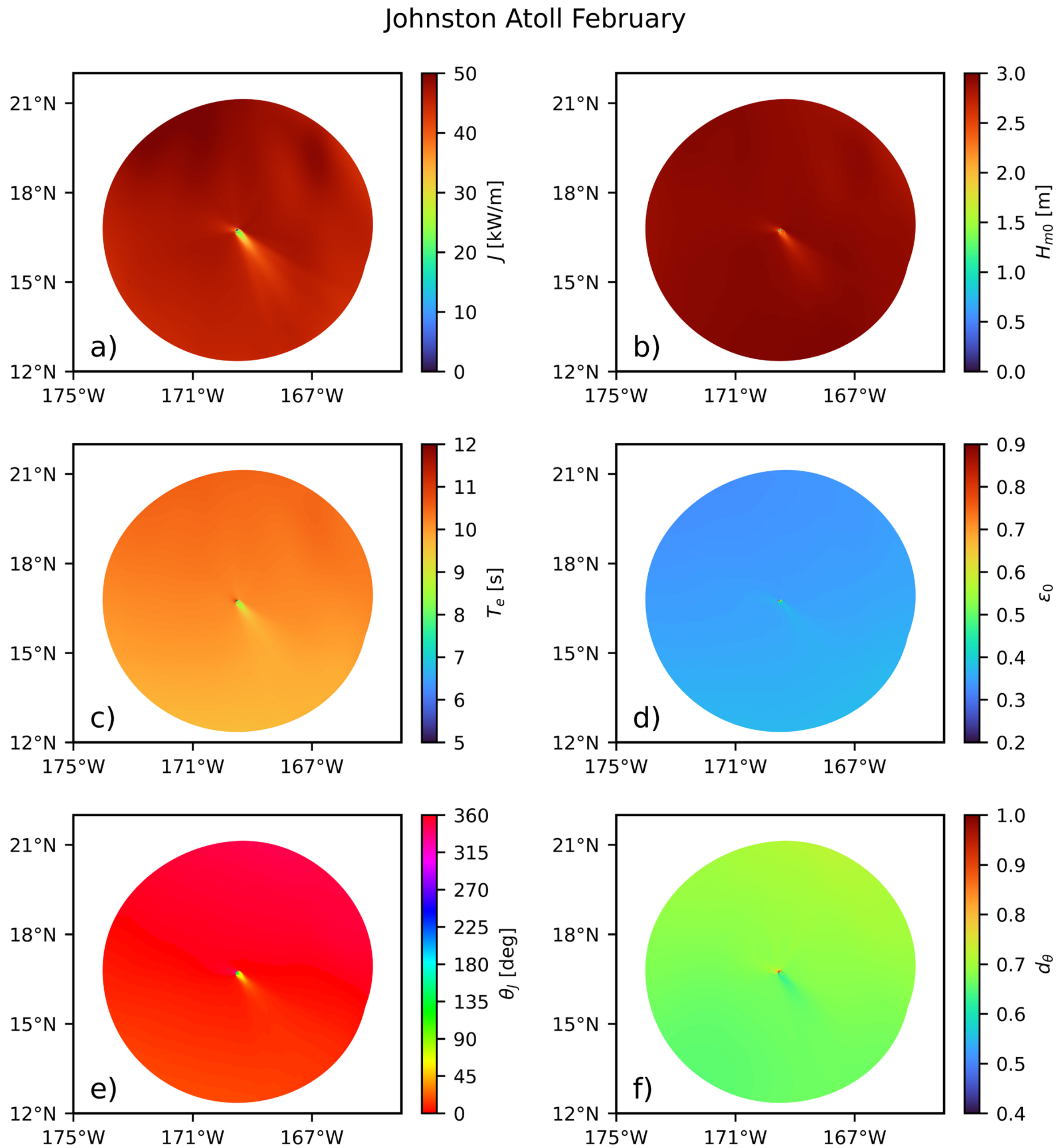

Figure A.50. Monthly distributions of six IEC parameters around Johnston Atoll in February: (a) omnidirectional wave power, (b) significant wave height, (c) energy period, (d) spectral width, (e) direction of maximum directionally resolved wave power, and (f) directionality coefficient.

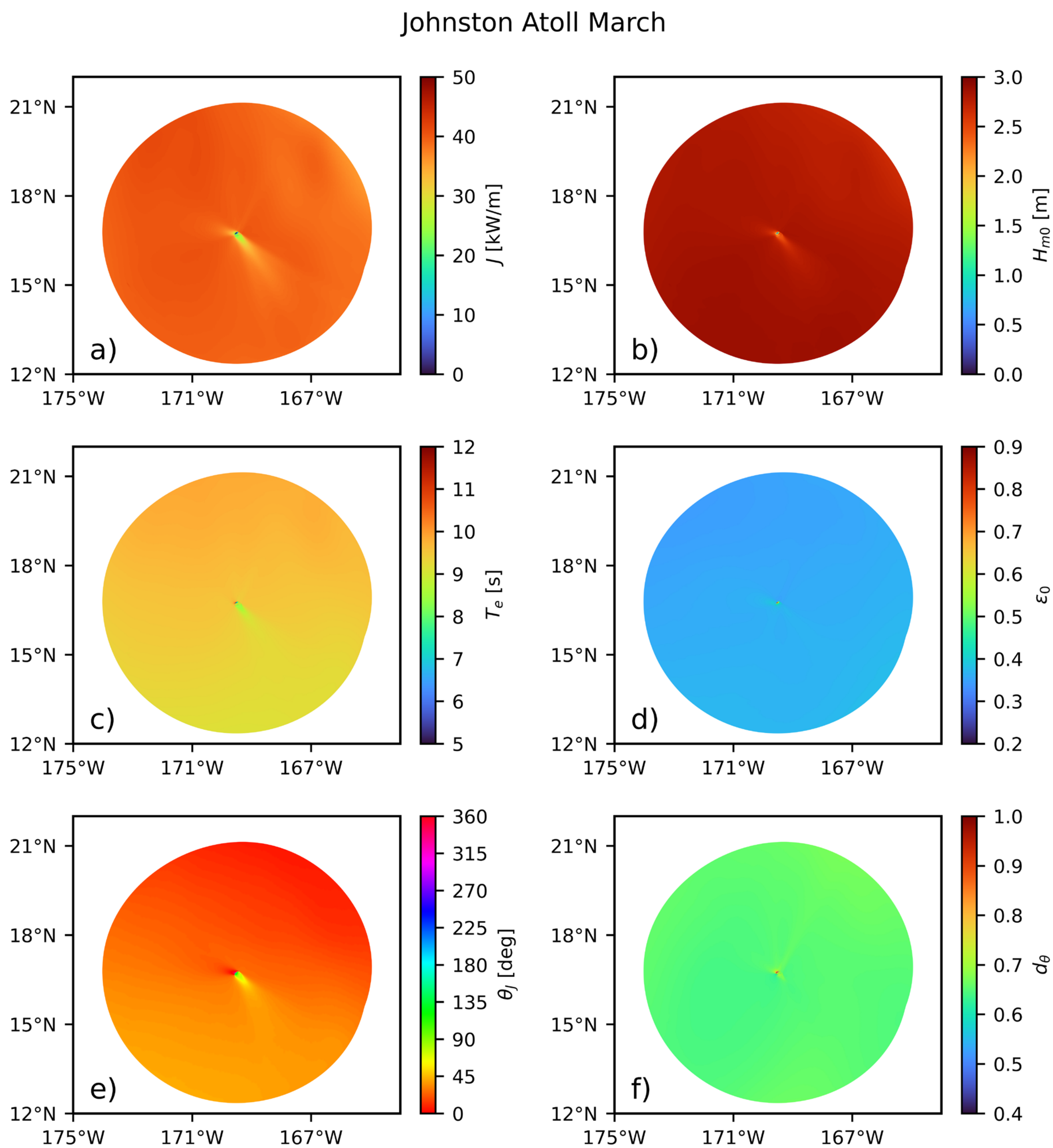

Figure A.51. Monthly distributions of six IEC parameters around Johnston Atoll in March: (a) omnidirectional wave power, (b) significant wave height, (c) energy period, (d) spectral width, (e) direction of maximum directionally resolved wave power, and (f) directionality coefficient.

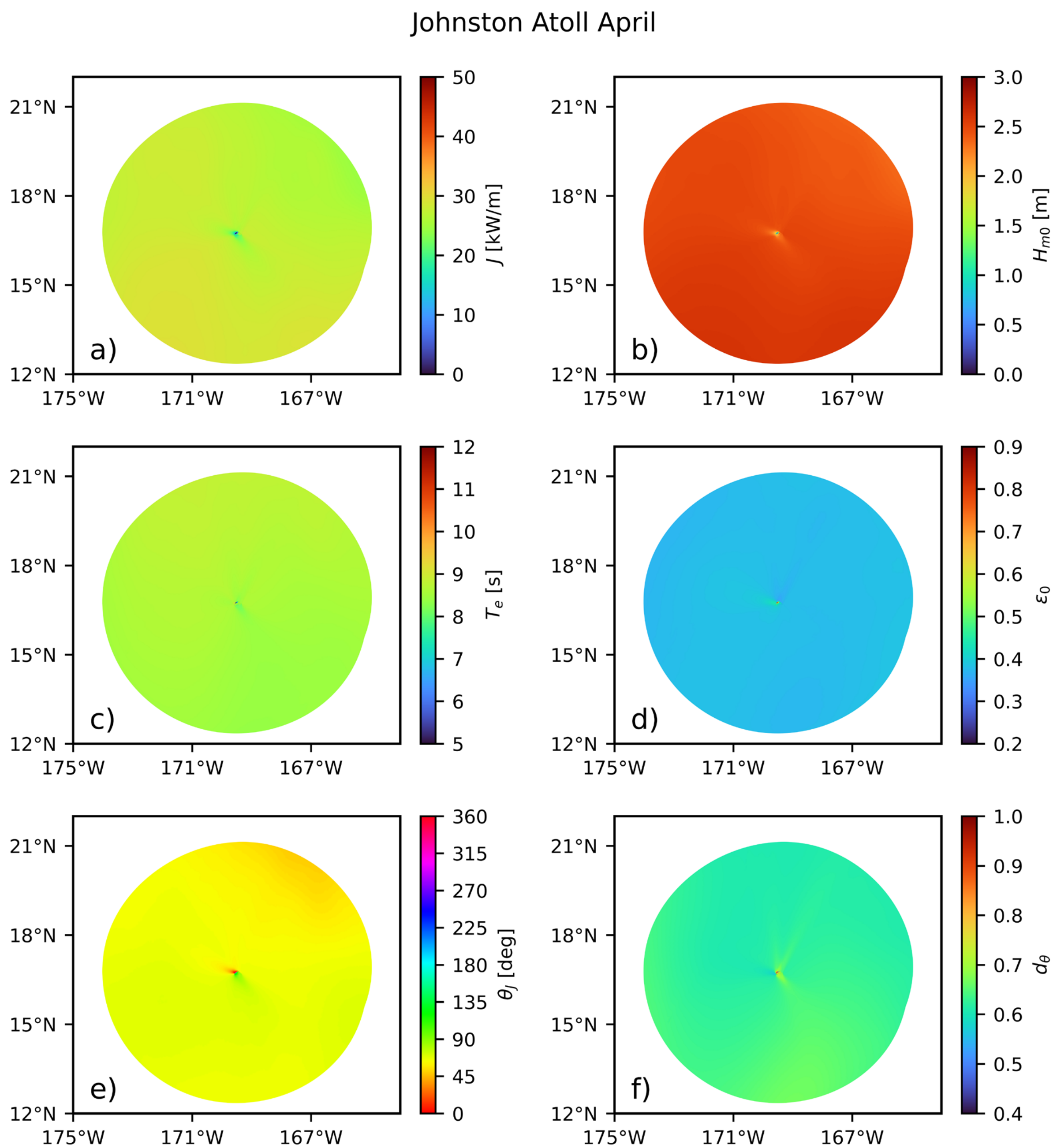

Figure A.52. Monthly distributions of six IEC parameters around Johnston Atoll in April: (a) omnidirectional wave power, (b) significant wave height, (c) energy period, (d) spectral width, (e) direction of maximum directionally resolved wave power, and (f) directionality coefficient.

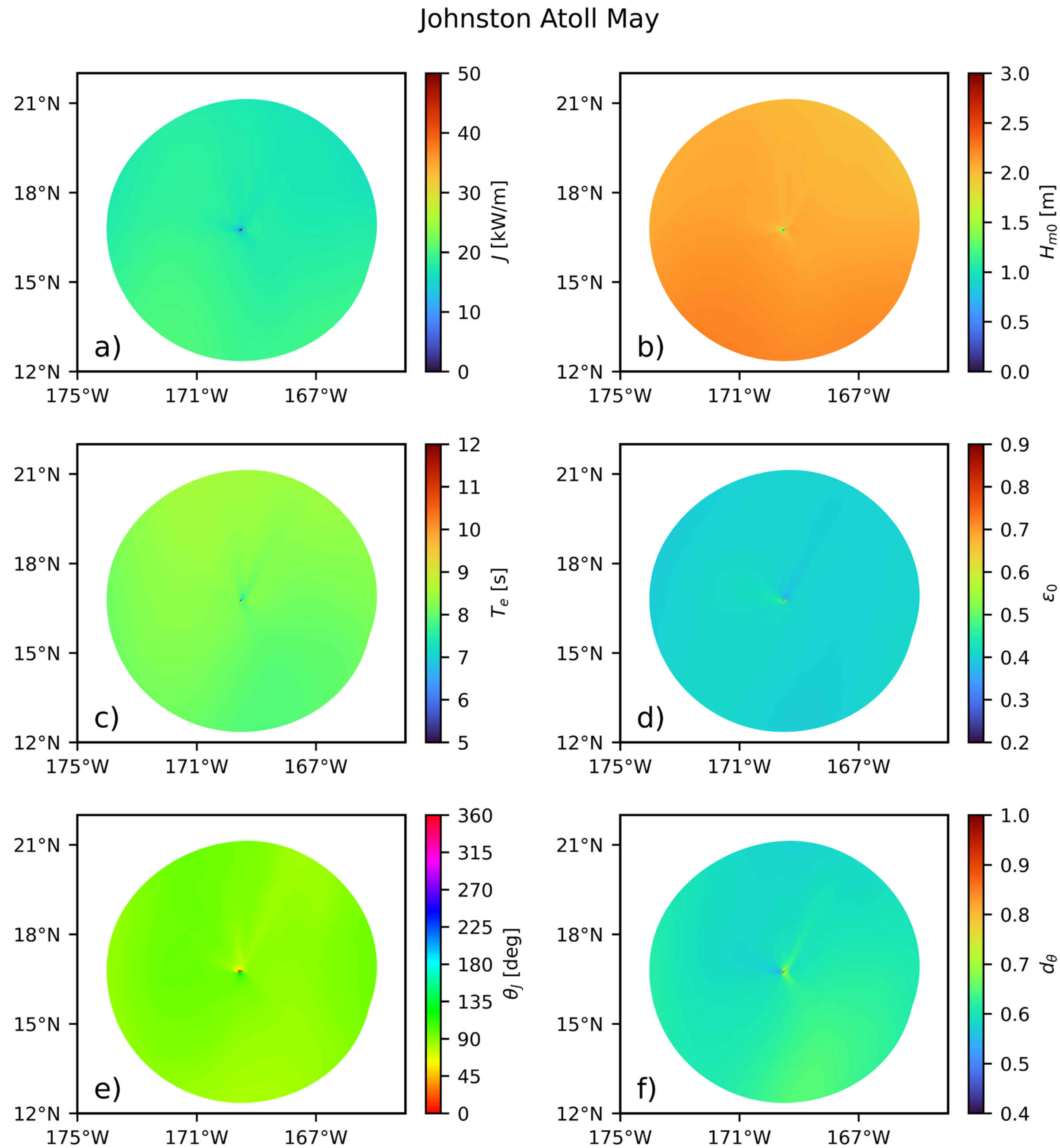

Figure A.53. Monthly distributions of six IEC parameters around Johnston Atoll in May: (a) omnidirectional wave power, (b) significant wave height, (c) energy period, (d) spectral width, (e) direction of maximum directionally resolved wave power, and (f) directionality coefficient.

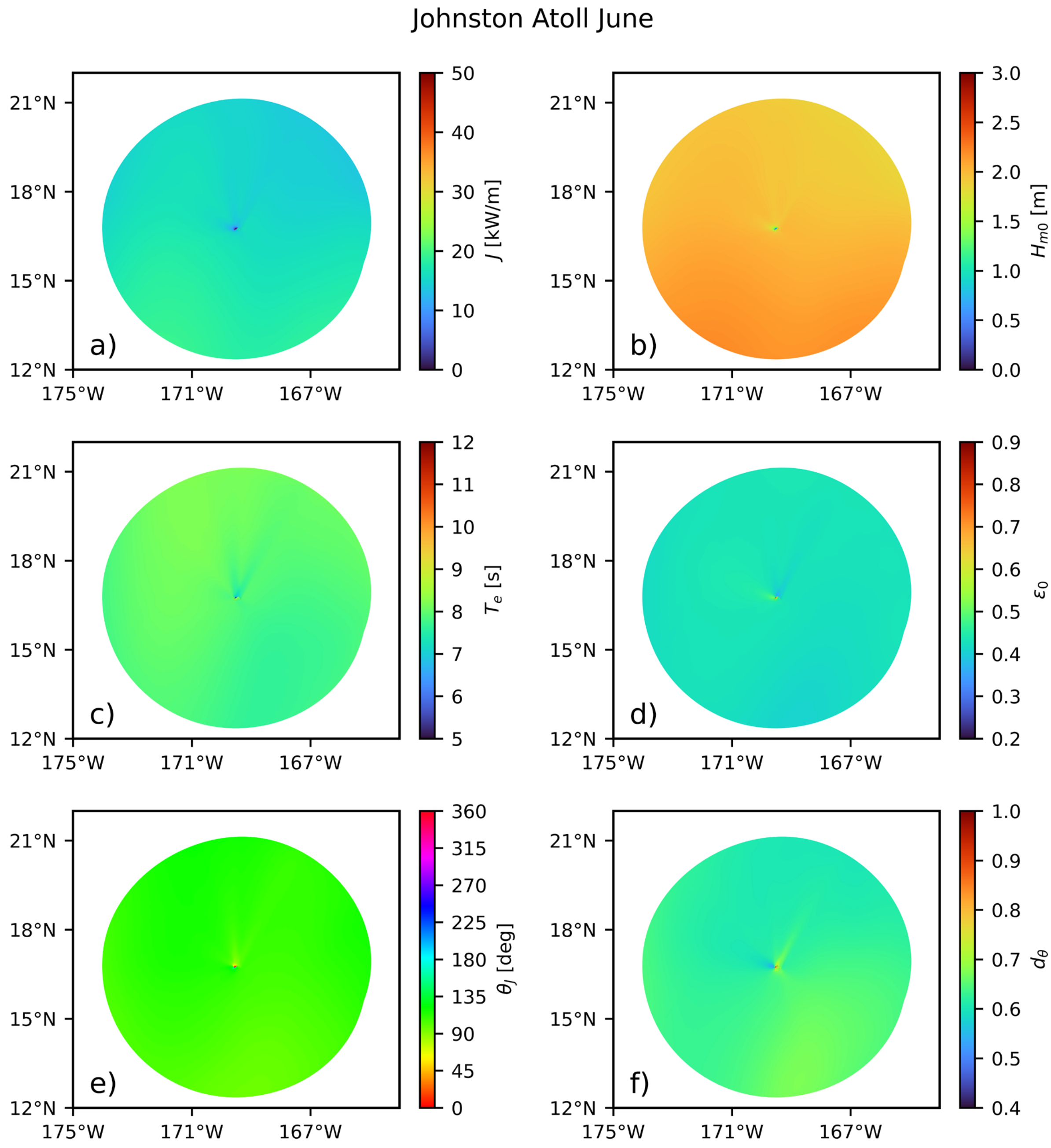

Figure A.54. Monthly distributions of six IEC parameters around Johnston Atoll in June: (a) omnidirectional wave power, (b) significant wave height, (c) energy period, (d) spectral width, (e) direction of maximum directionally resolved wave power, and (f) directionality coefficient.

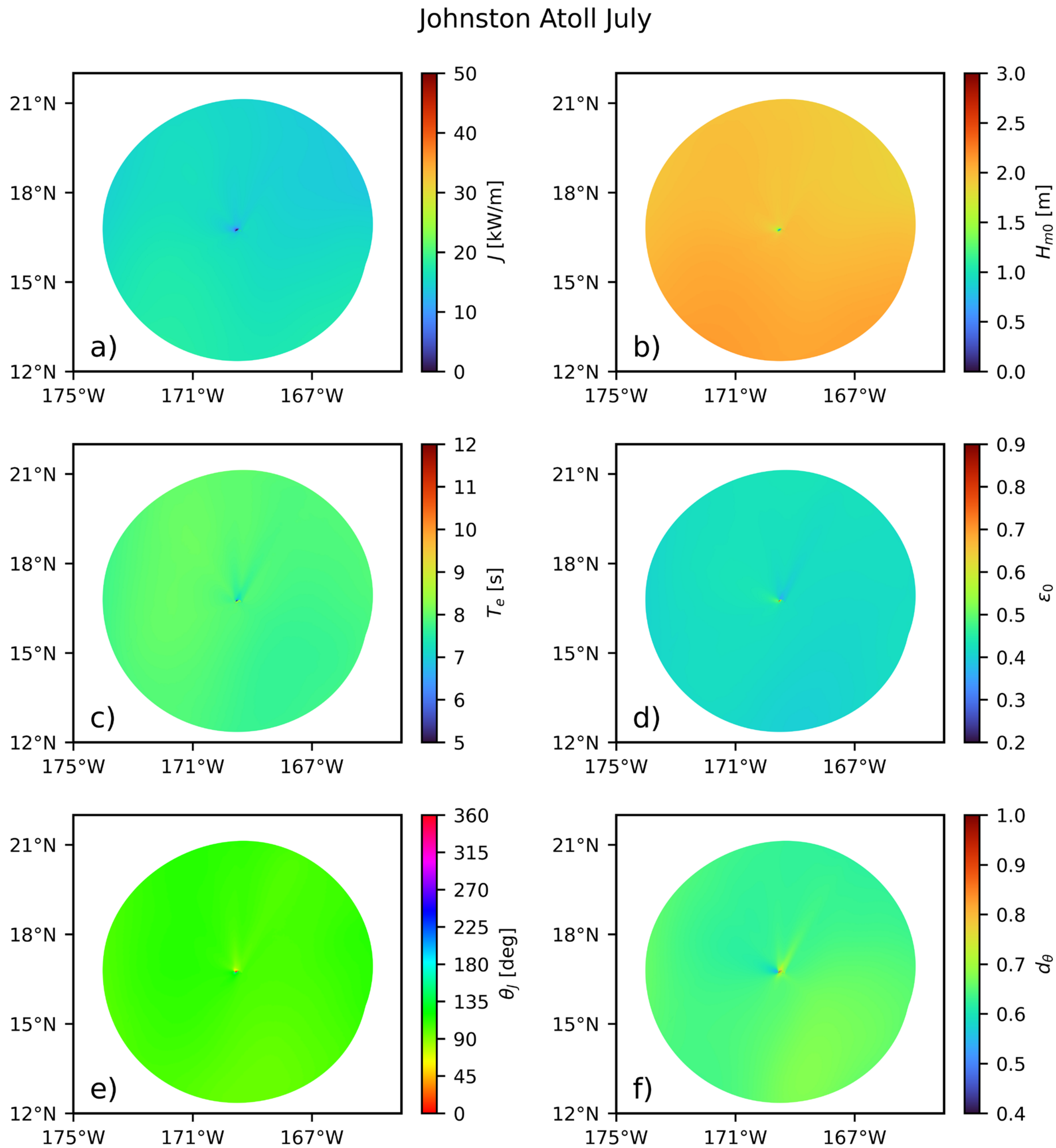

Figure A.55. Monthly distributions of six IEC parameters around Johnston Atoll in July: (a) omnidirectional wave power, (b) significant wave height, (c) energy period, (d) spectral width, (e) direction of maximum directionally resolved wave power, and (f) directionality coefficient.

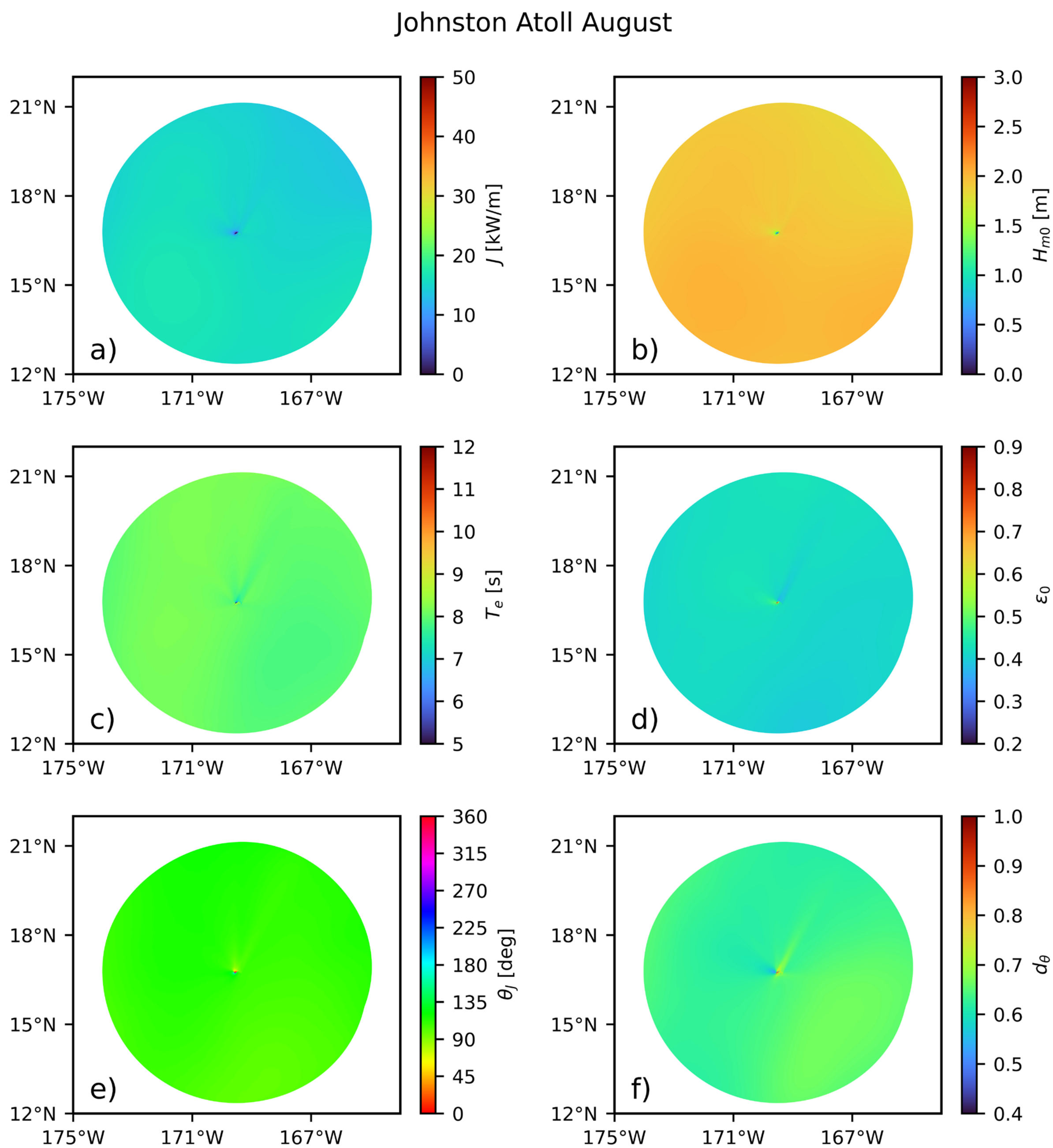

Figure A.56. Monthly distributions of six IEC parameters around Johnston Atoll in August: (a) omnidirectional wave power, (b) significant wave height, (c) energy period, (d) spectral width, (e) direction of maximum directionally resolved wave power, and (f) directionality coefficient.

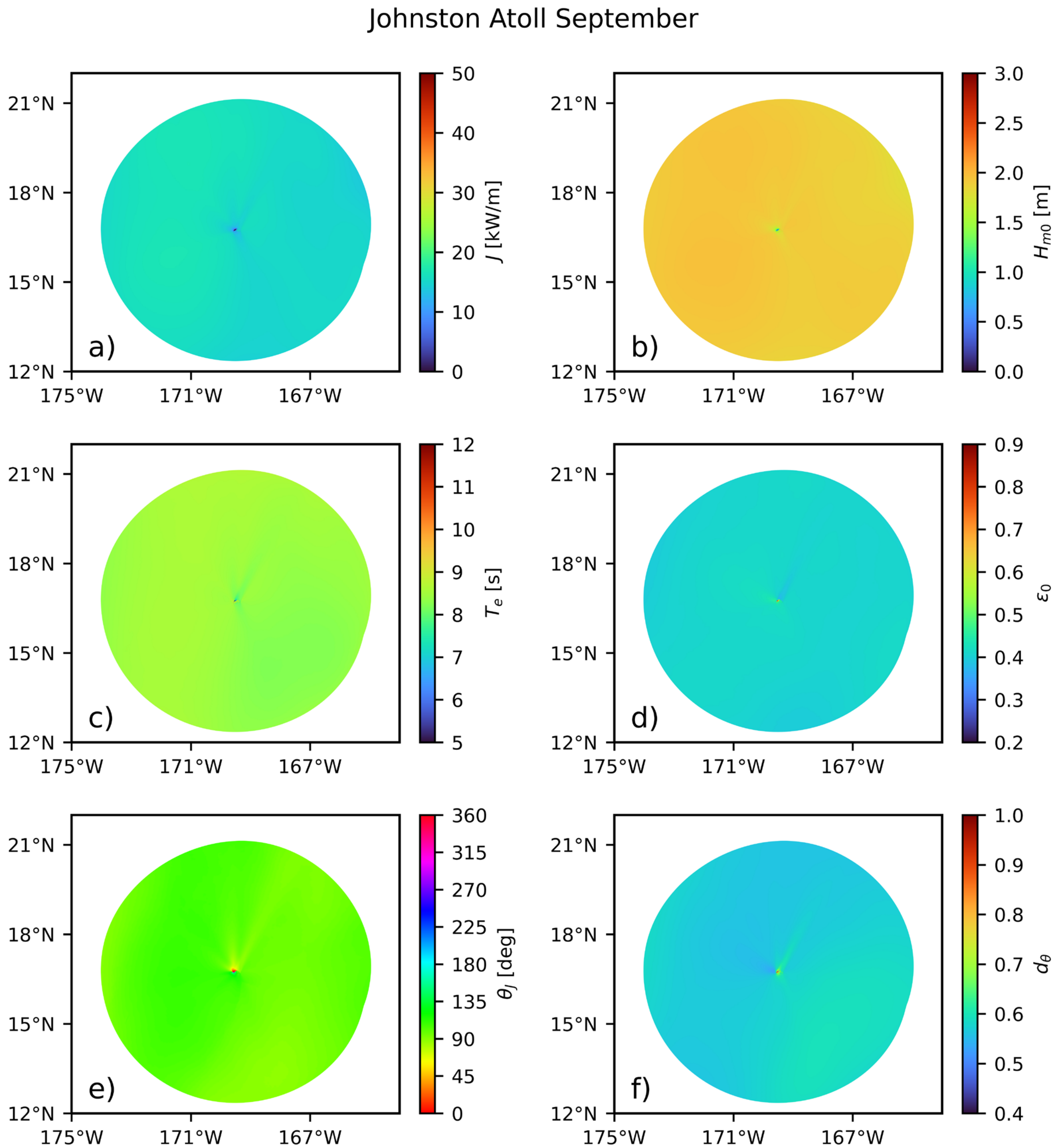

Figure A.57. Monthly distributions of six IEC parameters around Johnston Atoll in September: (a) omnidirectional wave power, (b) significant wave height, (c) energy period, (d) spectral width, (e) direction of maximum directionally resolved wave power, and (f) directionality coefficient.

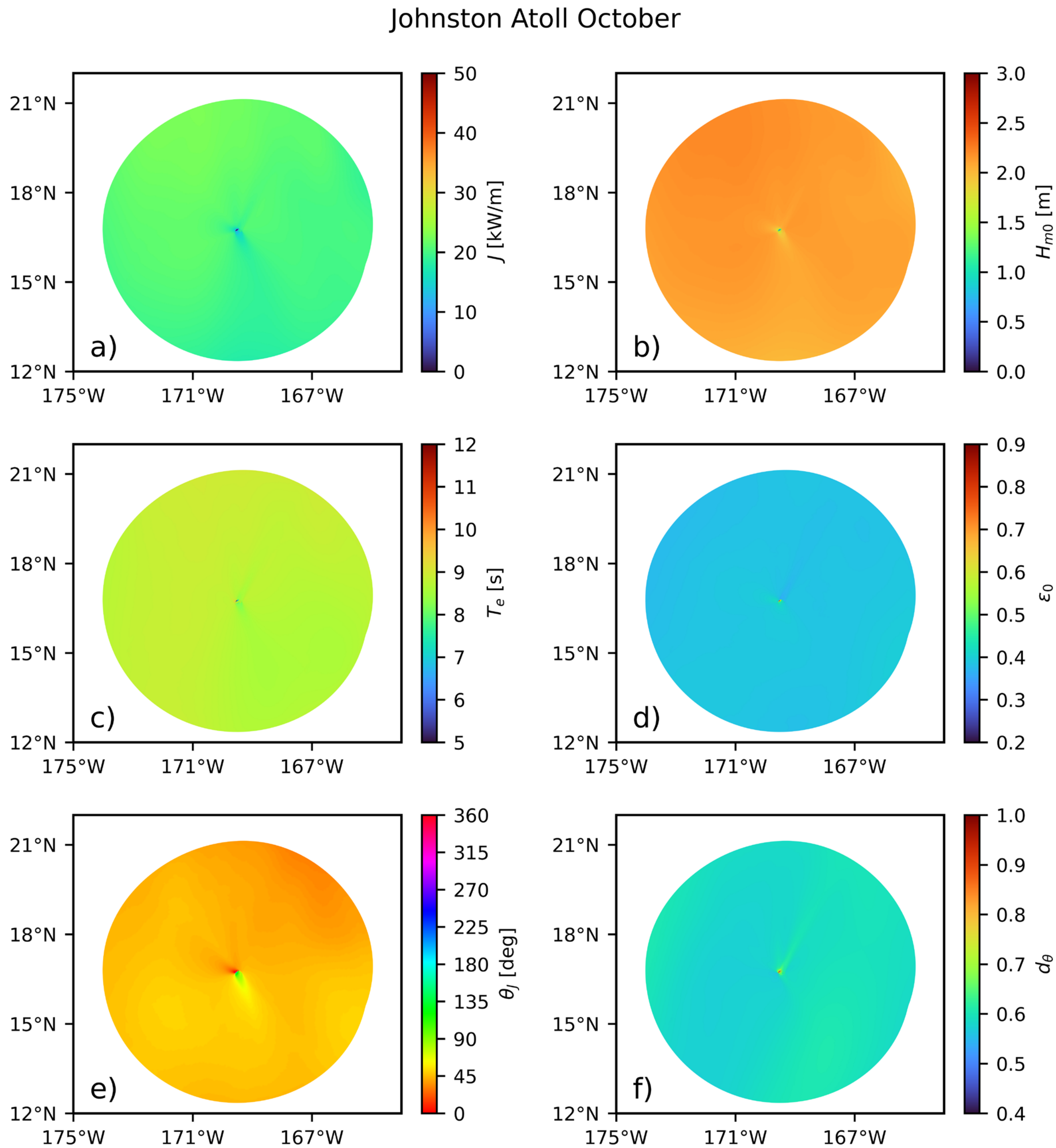

Figure A.58. Monthly distributions of six IEC parameters around Johnston Atoll in October: (a) omnidirectional wave power, (b) significant wave height, (c) energy period, (d) spectral width, (e) direction of maximum directionally resolved wave power, and (f) directionality coefficient.

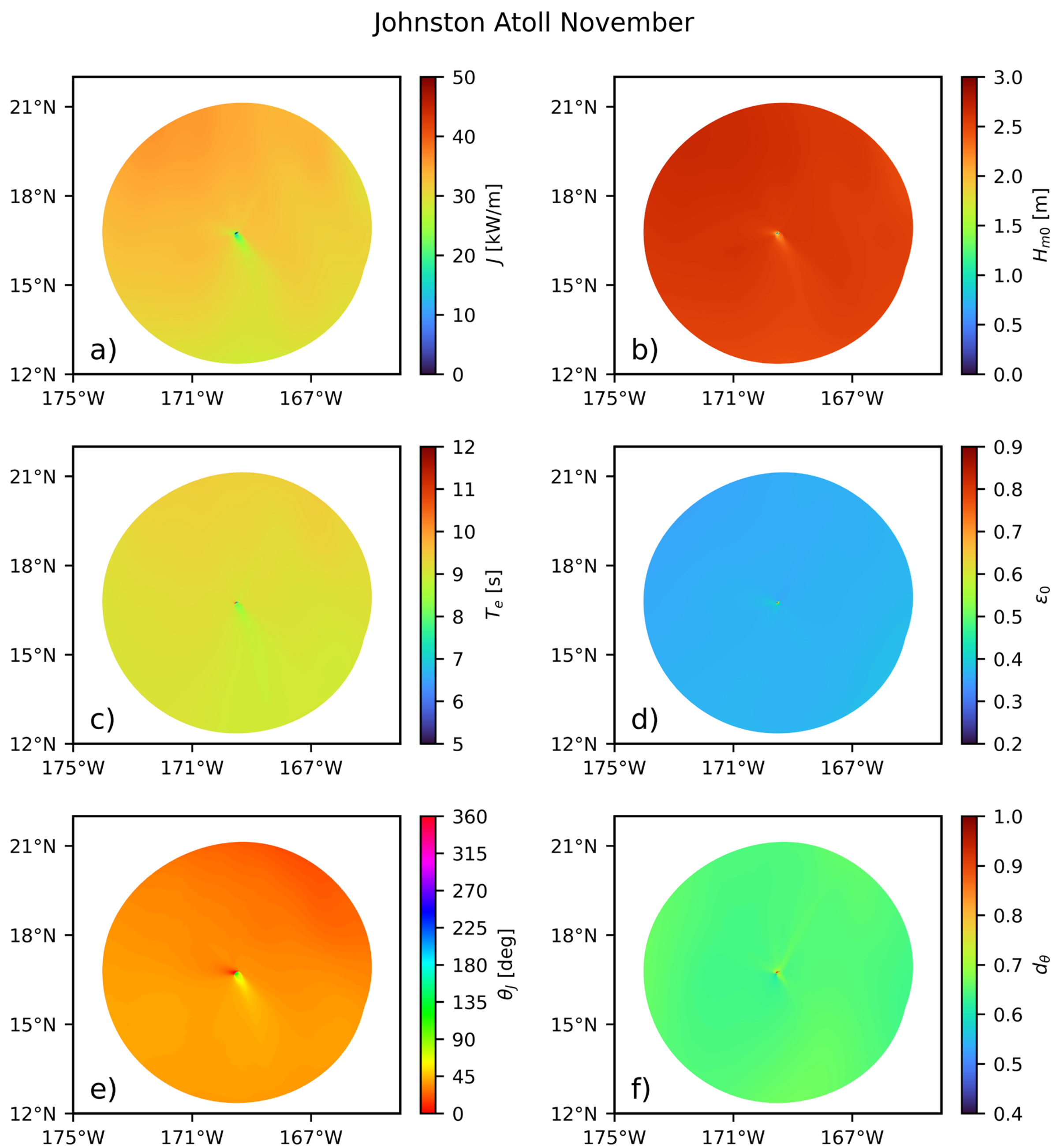

Figure A.59. Monthly distributions of six IEC parameters around Johnston Atoll in November: (a) omnidirectional wave power, (b) significant wave height, (c) energy period, (d) spectral width, (e) direction of maximum directionally resolved wave power, and (f) directionality coefficient.

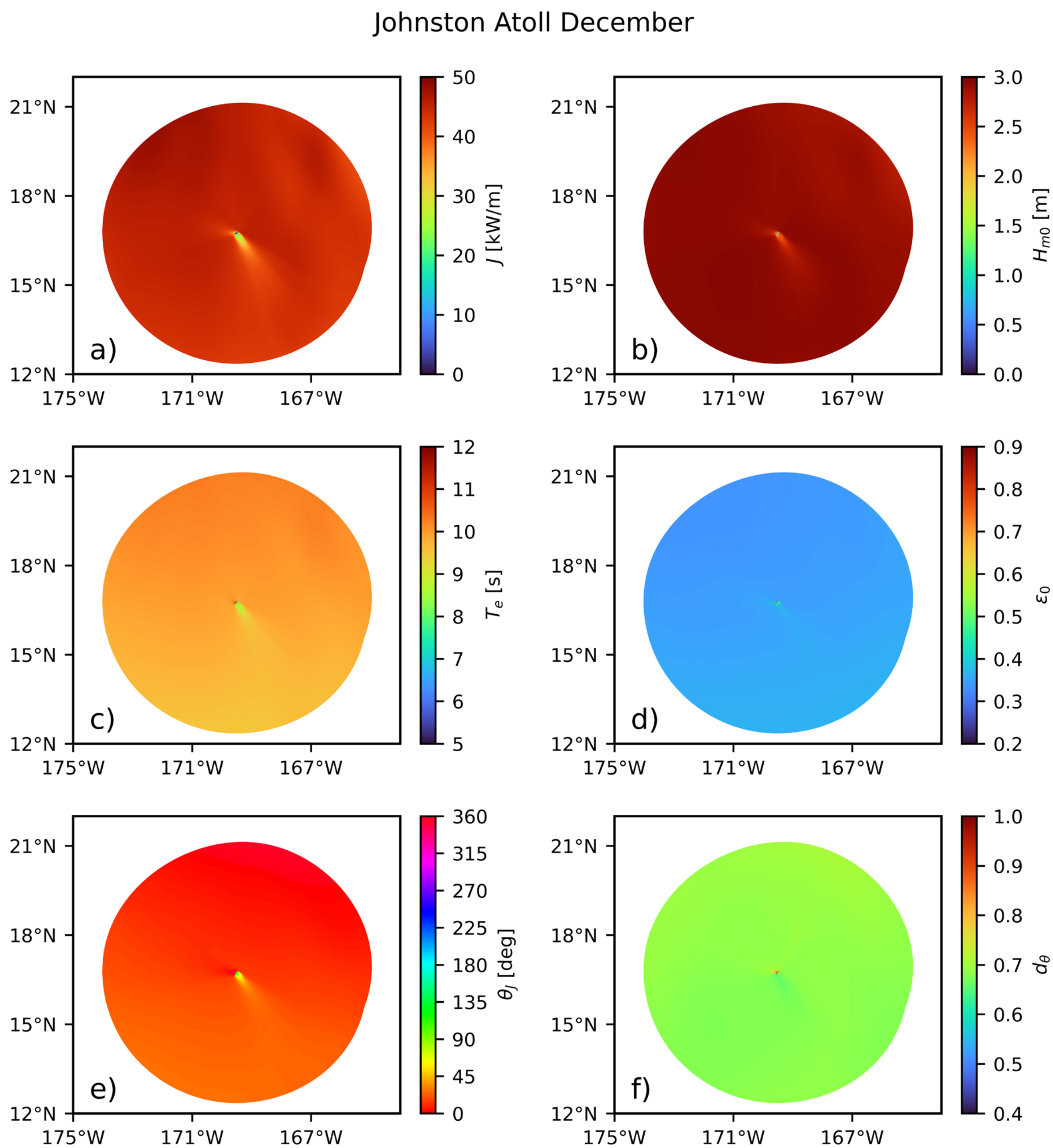

Figure A.60. Monthly distributions of six IEC parameters around Johnston Atoll.in December: (a) omnidirectional wave power, (b) significant wave height, (c) energy period, (d) spectral width, (e) direction of maximum directionally resolved wave power, and (f) directionality coefficient

A.6 Palmyra Atoll and Kingman Reef

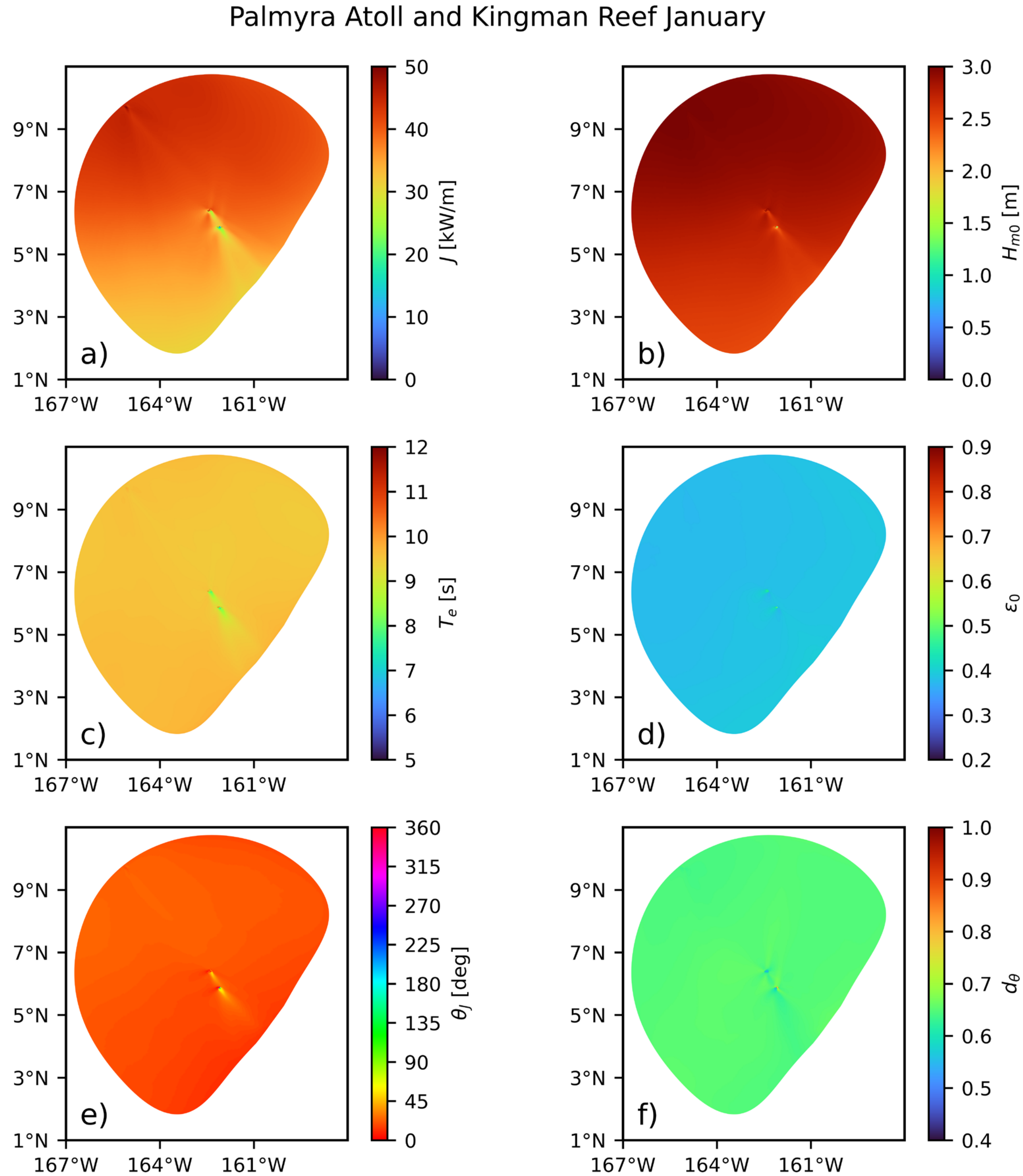

Figure A.61. Monthly distributions of six IEC parameters around Palmyra Atoll and Kingman Reef in January: (a) omnidirectional wave power, (b) significant wave height, (c) energy period, (d) spectral width, (e) direction of maximum directionally resolved wave power, and (f) directionality coefficient.

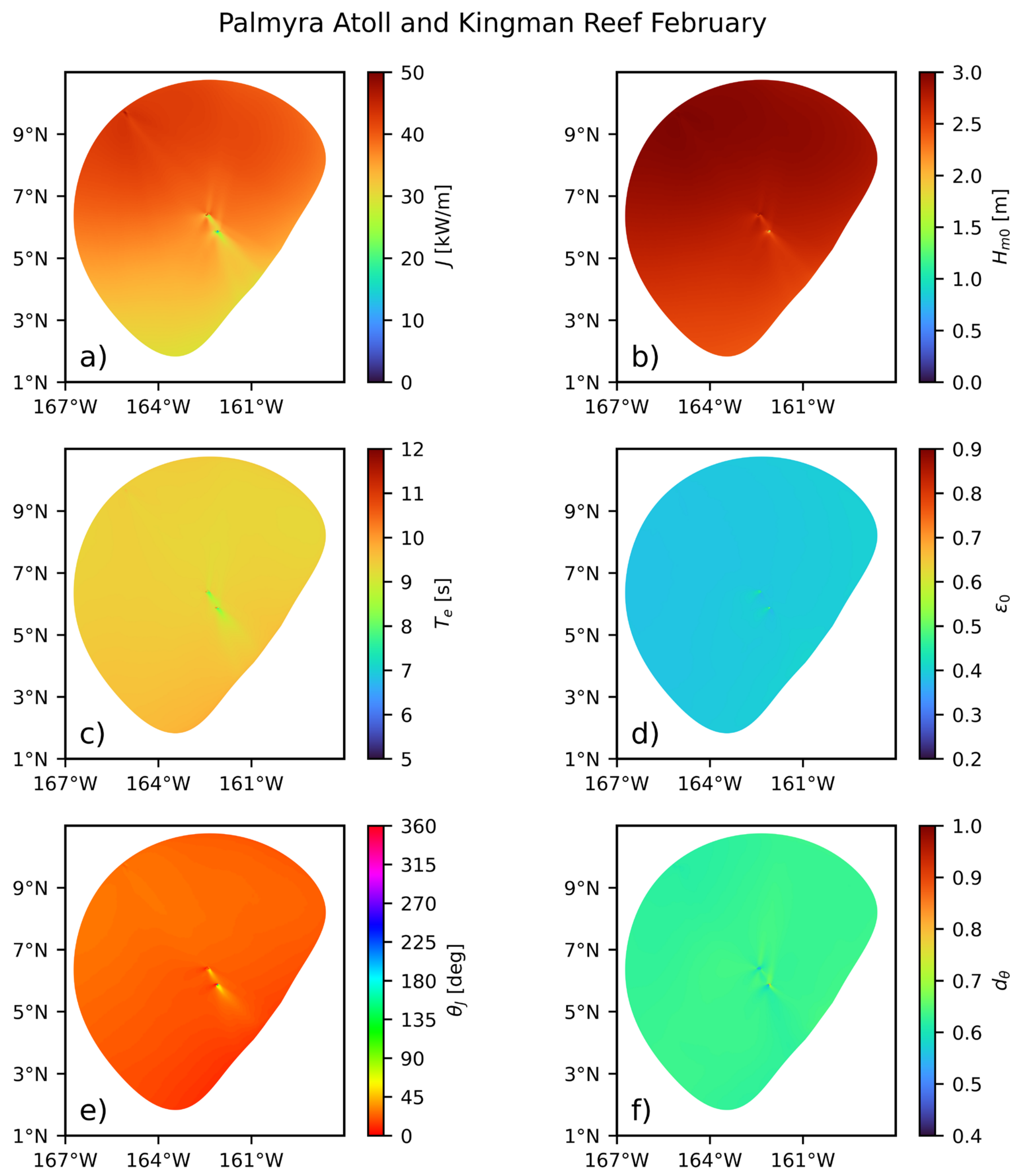

Figure A.62. Monthly distributions of six IEC parameters around Palmyra Atoll and Kingman Reef in February: (a) omnidirectional wave power, (b) significant wave height, (c) energy period, (d) spectral width, (e) direction of maximum directionally resolved wave power, and (f) directionality coefficient.

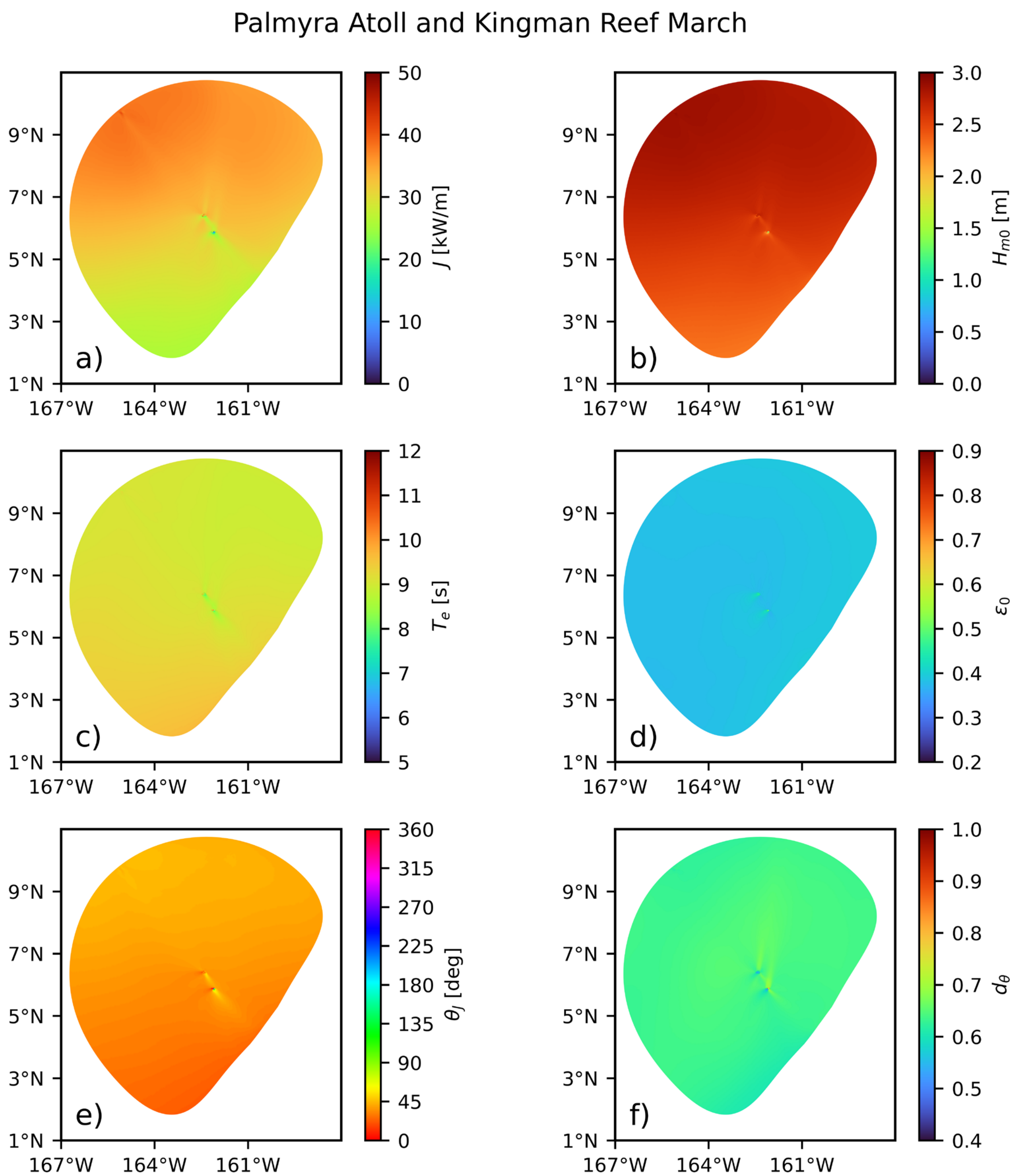

Figure A.63. Monthly distributions of six IEC parameters around Palmyra Atoll and Kingman Reef in March: (a) omnidirectional wave power, (b) significant wave height, (c) energy period, (d) spectral width, (e) direction of maximum directionally resolved wave power, and (f) directionality coefficient.

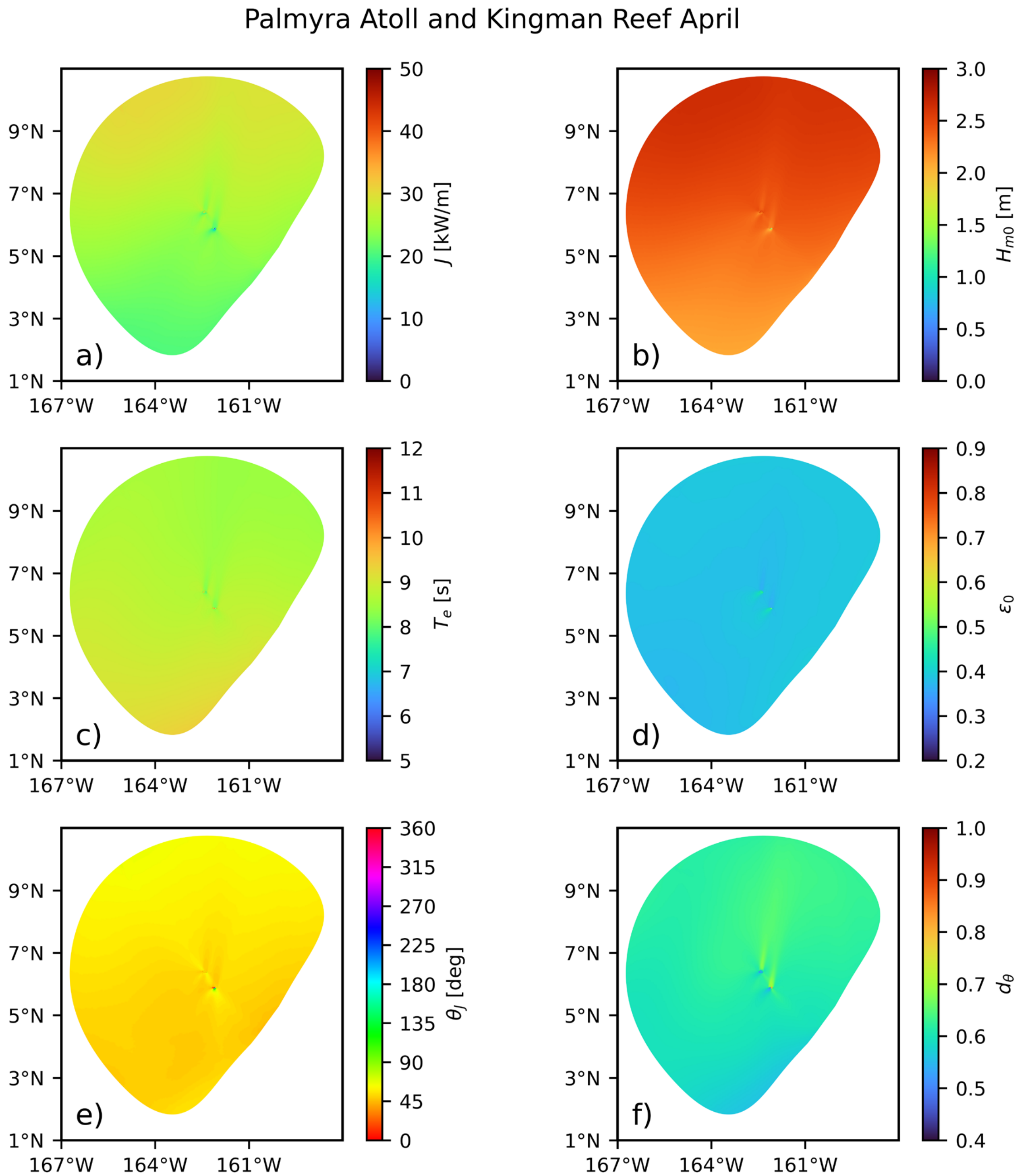

Figure A.64. Monthly distributions of six IEC parameters around Palmyra Atoll and Kingman Reef in April: (a) omnidirectional wave power, (b) significant wave height, (c) energy period, (d) spectral width, (e) direction of maximum directionally resolved wave power, and (f) directionality coefficient.

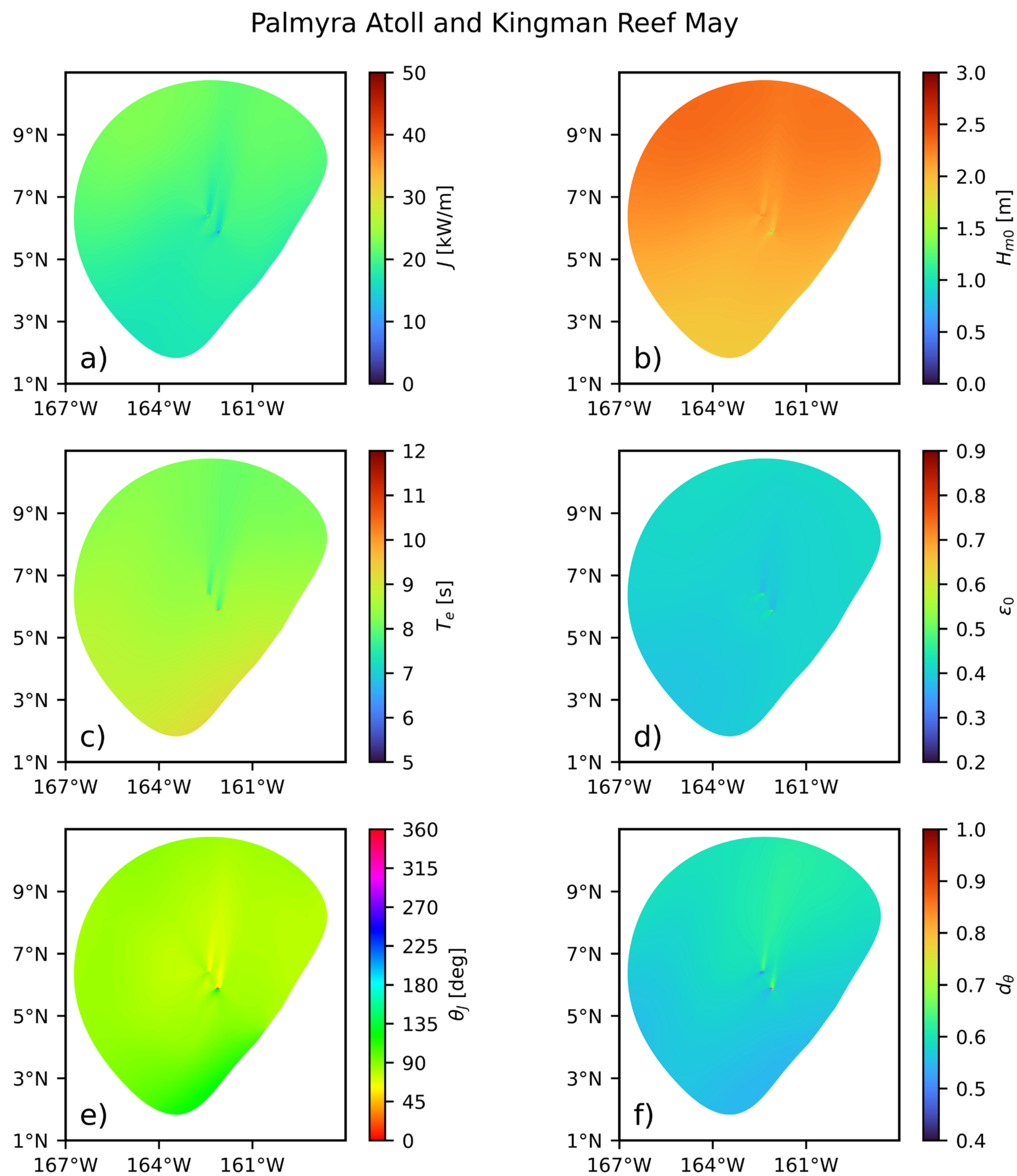

Figure A.65. Monthly distributions of six IEC parameters around Palmyra Atoll and Kingman Reef in May: (a) omnidirectional wave power, (b) significant wave height, (c) energy period, (d) spectral width, (e) direction of maximum directionally resolved wave power, and (f) directionality coefficient.

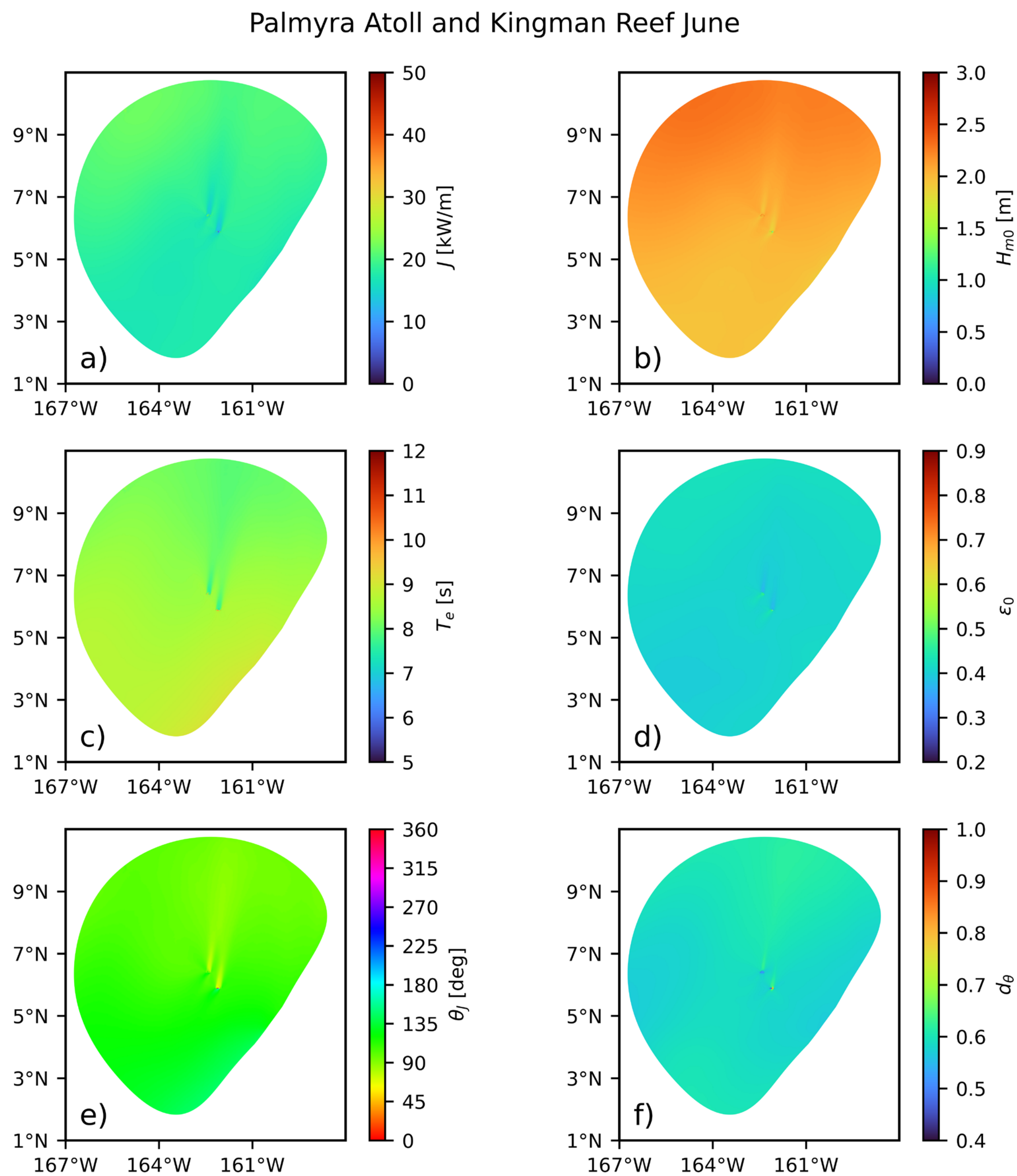

Figure A.66. Monthly distributions of six IEC parameters around Palmyra Atoll and Kingman Reef in June: (a) omnidirectional wave power, (b) significant wave height, (c) energy period, (d) spectral width, (e) direction of maximum directionally resolved wave power, and (f) directionality coefficient.

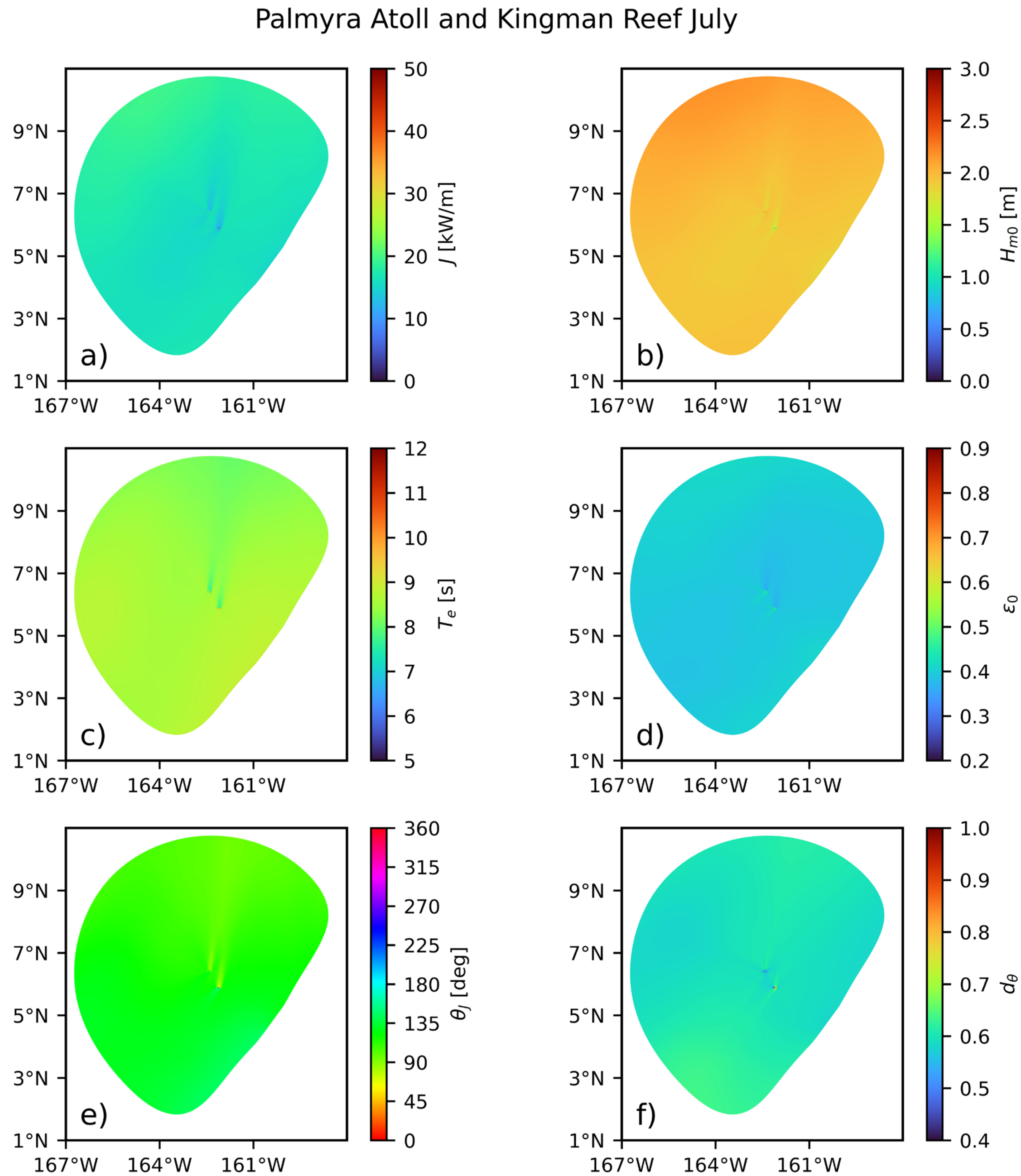

Figure A.67. Monthly distributions of six IEC parameters around Palmyra Atoll and Kingman Reef in July: (a) omnidirectional wave power, (b) significant wave height, (c) energy period, (d) spectral width, (e) direction of maximum directionally resolved wave power, and (f) directionality coefficient.

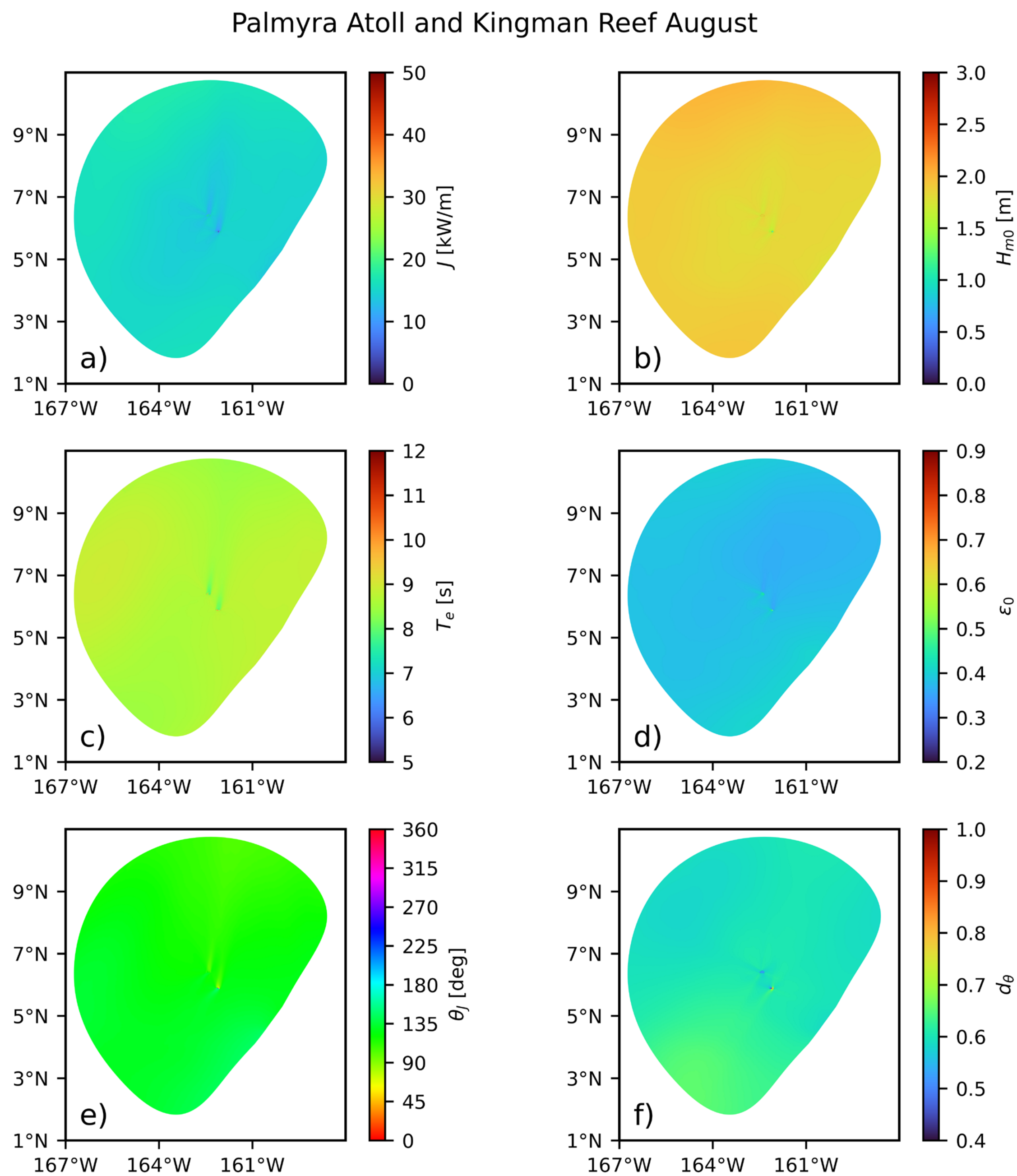

Figure A.68. Monthly distributions of six IEC parameters around Palmyra Atoll and Kingman Reef in August: (a) omnidirectional wave power, (b) significant wave height, (c) energy period, (d) spectral width, (e) direction of maximum directionally resolved wave power, and (f) directionality coefficient.

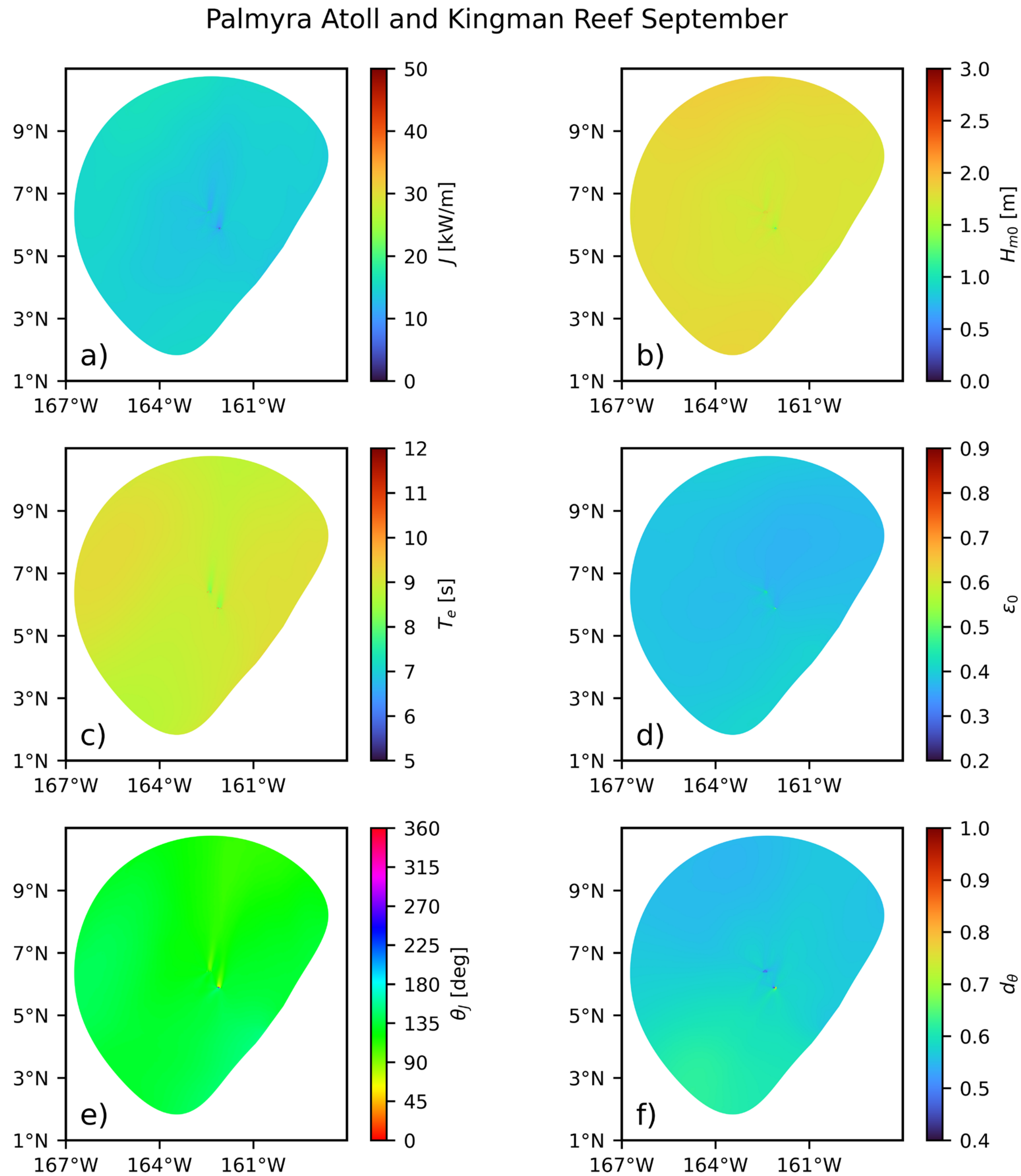

Figure A.69. Monthly distributions of six IEC parameters around Palmyra Atoll and Kingman Reef in September: (a) omnidirectional wave power, (b) significant wave height, (c) energy period, (d) spectral width, (e) direction of maximum directionally resolved wave power, and (f) directionality coefficient.

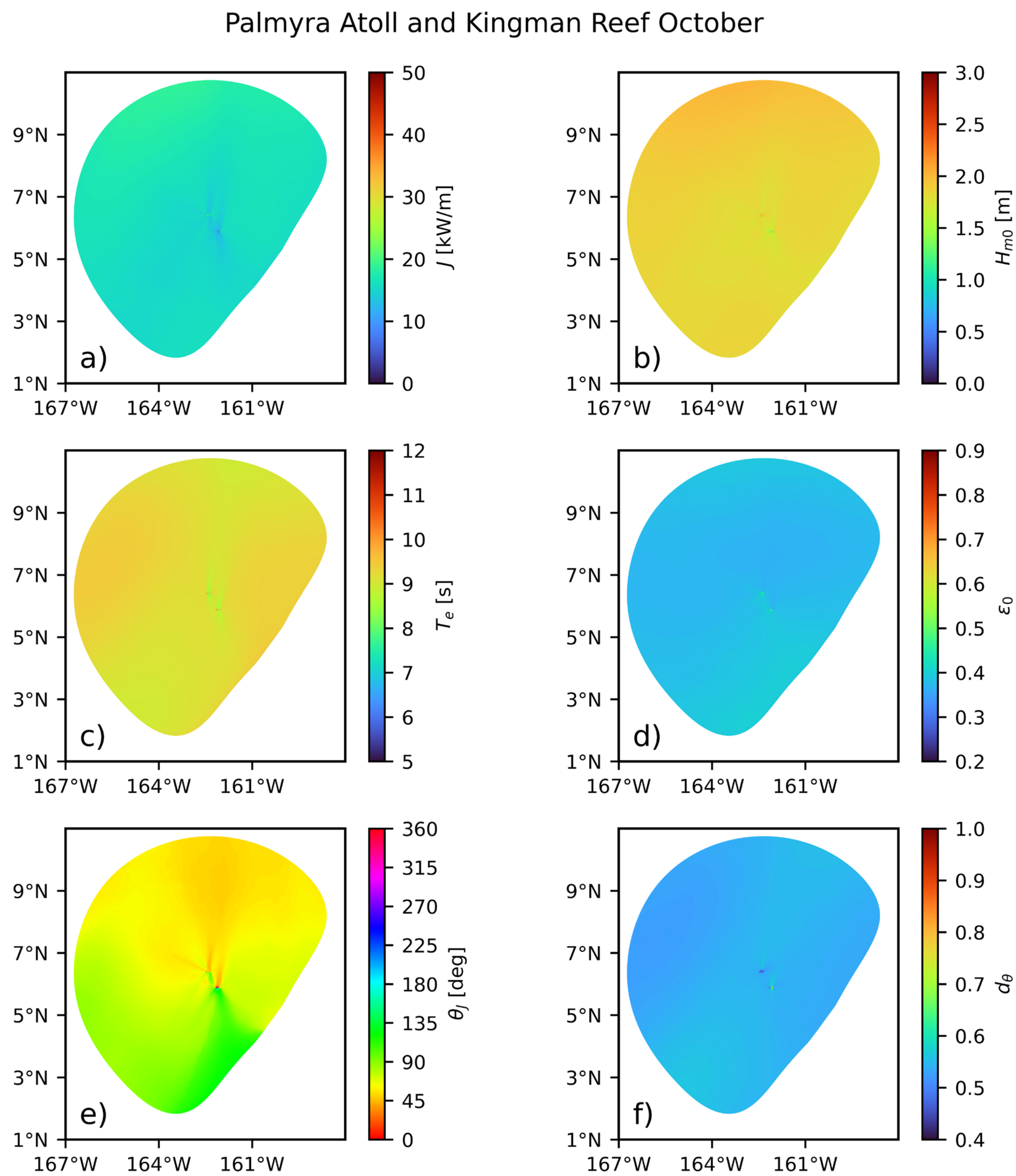

Figure A.70. Monthly distributions of six IEC parameters around Palmyra Atoll and Kingman Reef in October: (a) omnidirectional wave power, (b) significant wave height, (c) energy period, (d) spectral width, (e) direction of maximum directionally resolved wave power, and (f) directionality coefficient.

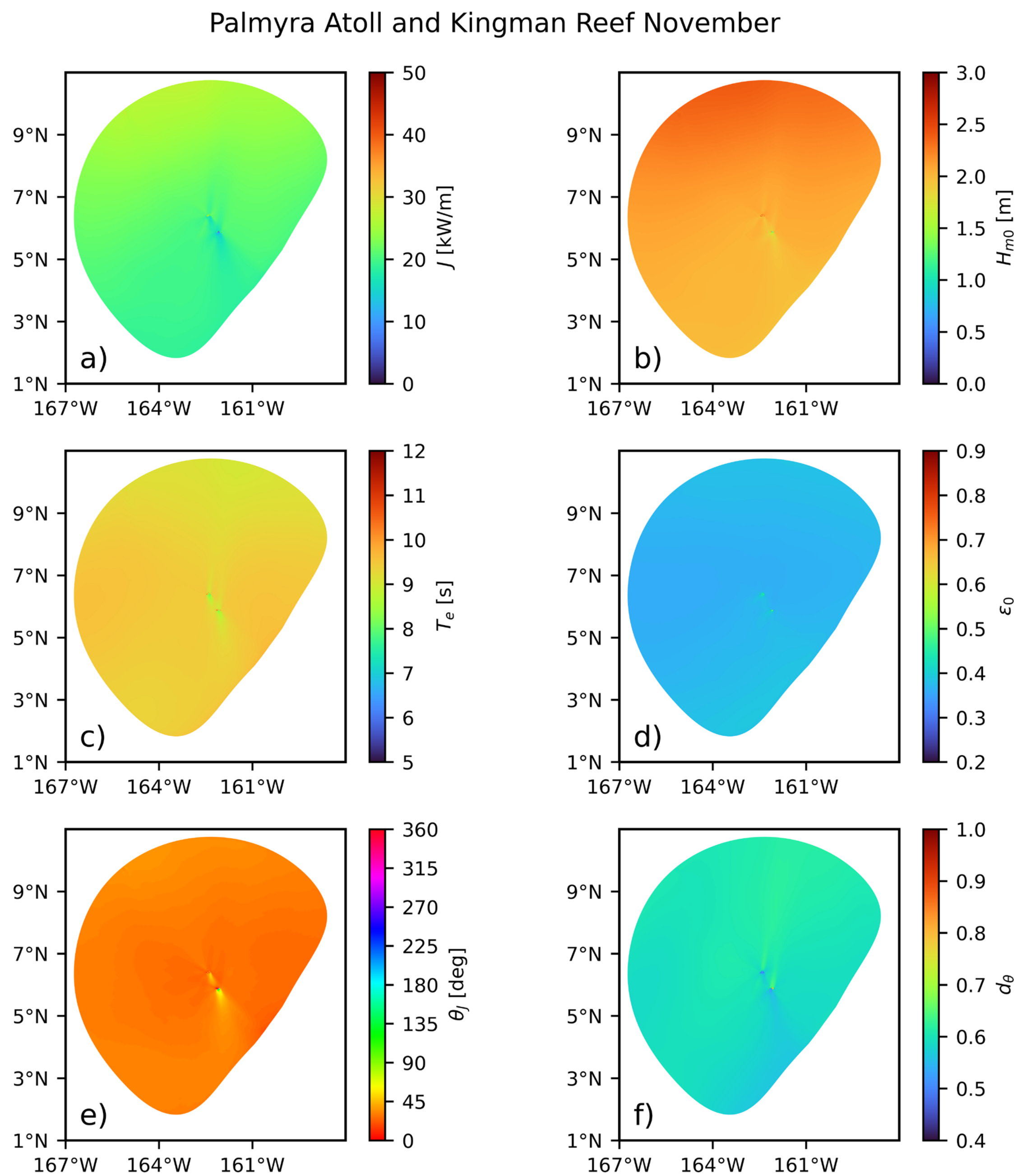

Figure A.71. Monthly distributions of six IEC parameters around Palmyra Atoll and Kingman Reef in November: (a) omnidirectional wave power, (b) significant wave height, (c) energy period, (d) spectral width, (e) direction of maximum directionally resolved wave power, and (f) directionality coefficient.

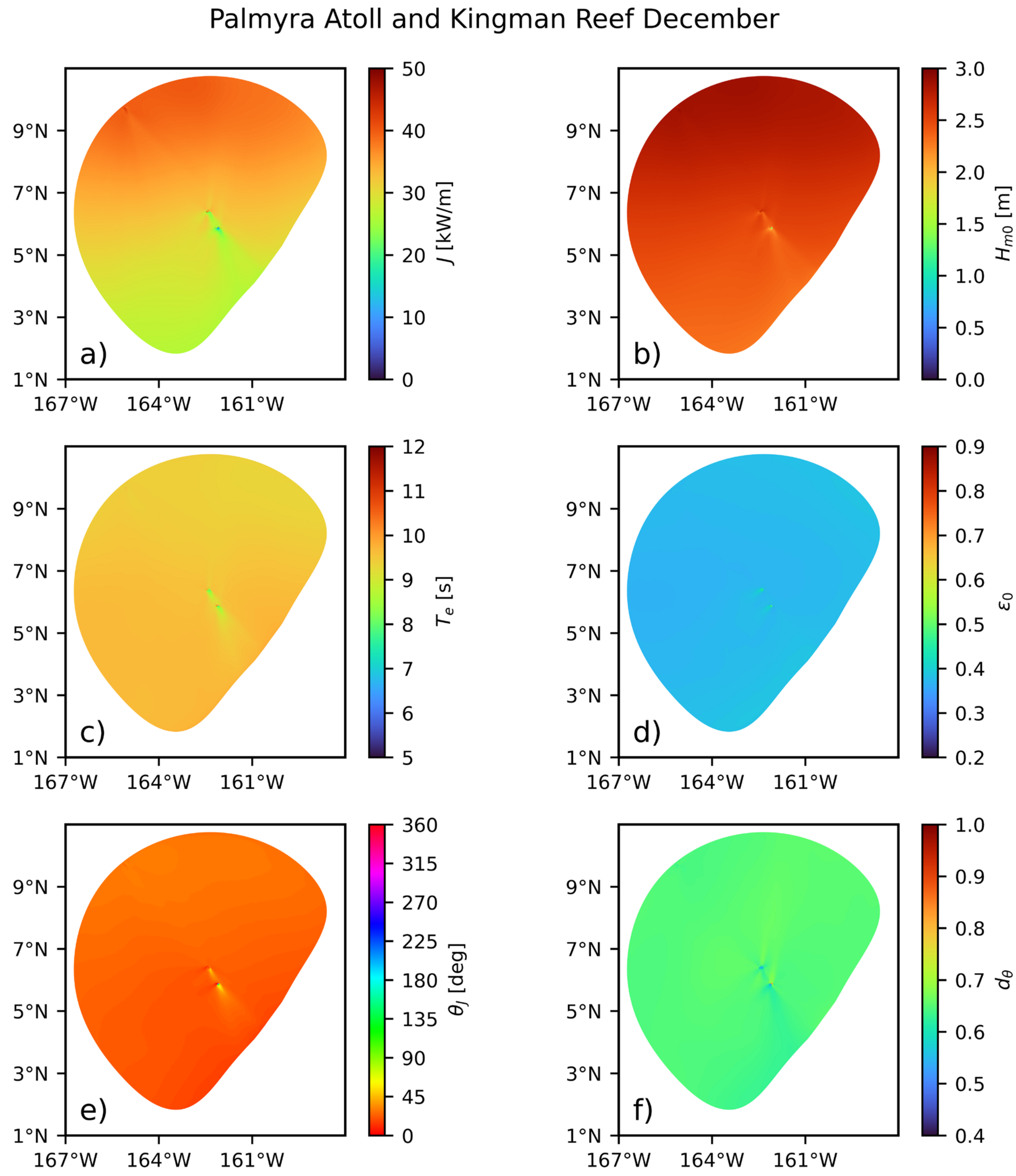

Figure A.72. Monthly distributions of six IEC parameters around Palmyra Atoll and Kingman Reef in December: (a) omnidirectional wave power, (b) significant wave height, (c) energy period, (d) spectral width, (e) direction of maximum directionally resolved wave power, and (f) directionality coefficient.

A.7 Wake Island

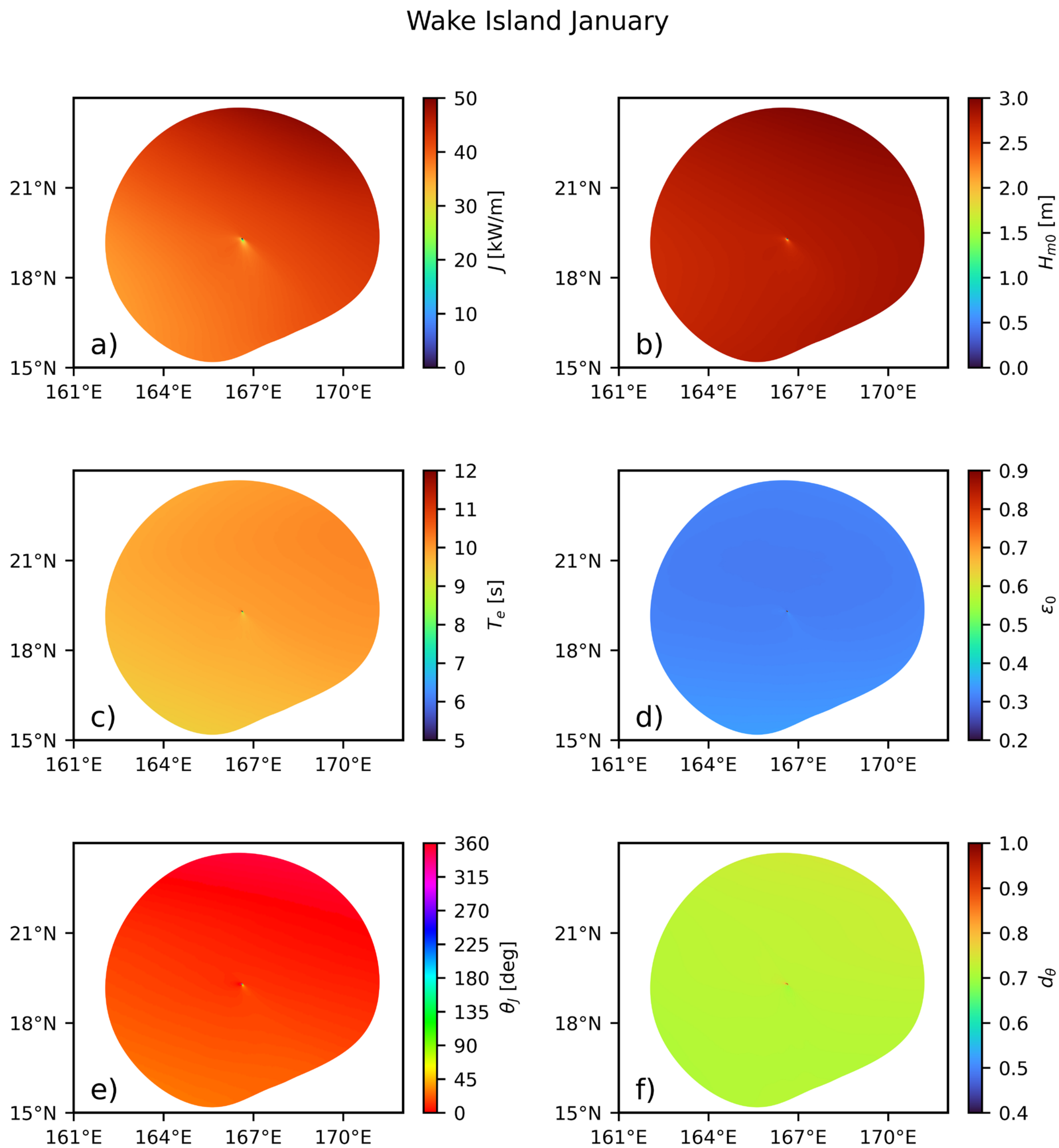

Figure A.73. Monthly distributions of six IEC parameters around Wake Island in January: (a) omnidirectional wave power, (b) significant wave height, (c) energy period, (d) spectral width, (e) direction of maximum directionally resolved wave power, and (f) directionality coefficient.

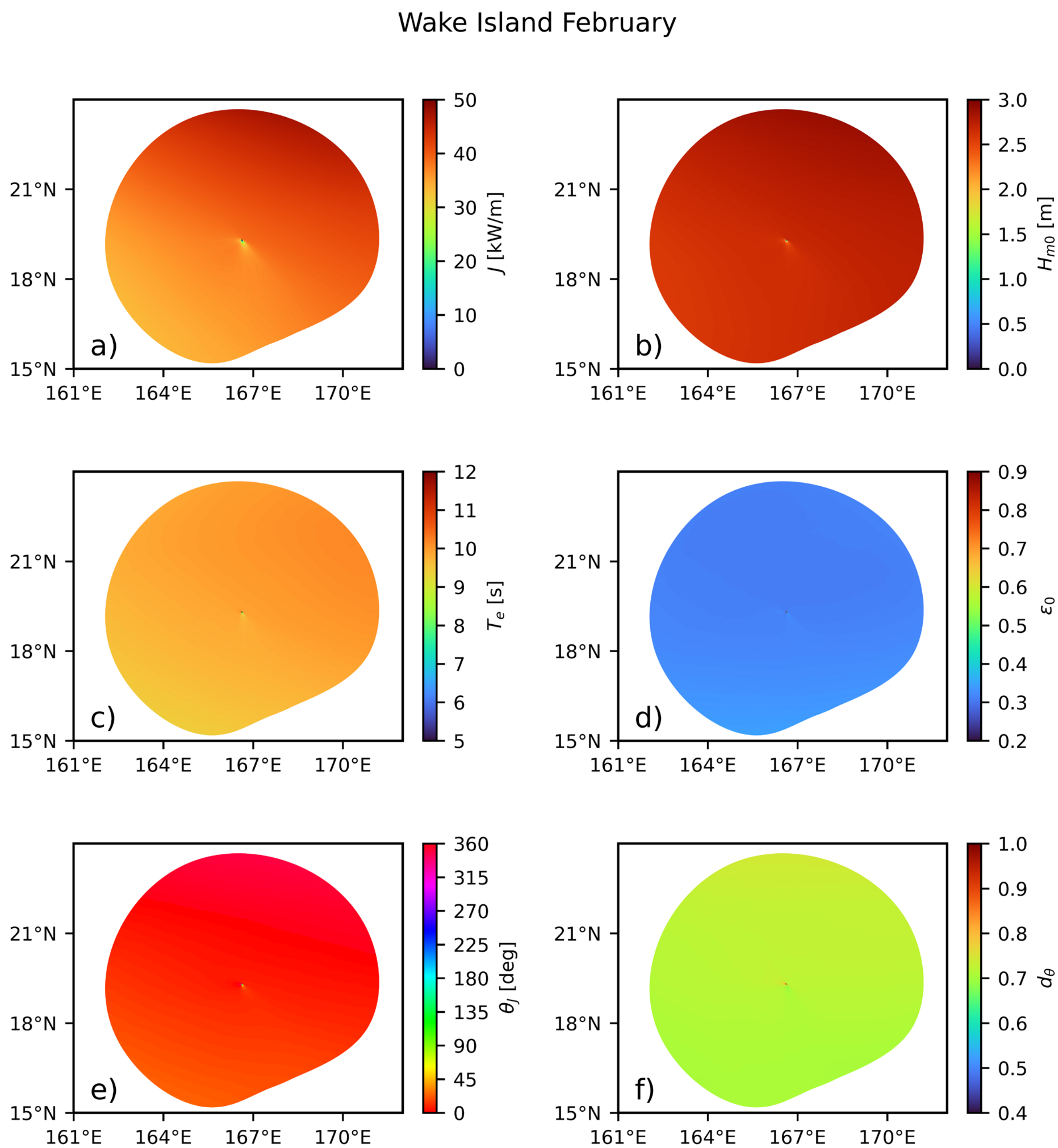

Figure A.74. Monthly distributions of six IEC parameters around Wake Island in February: (a) omnidirectional wave power, (b) significant wave height, (c) energy period, (d) spectral width, (e) direction of maximum directionally resolved wave power, and (f) directionality coefficient.

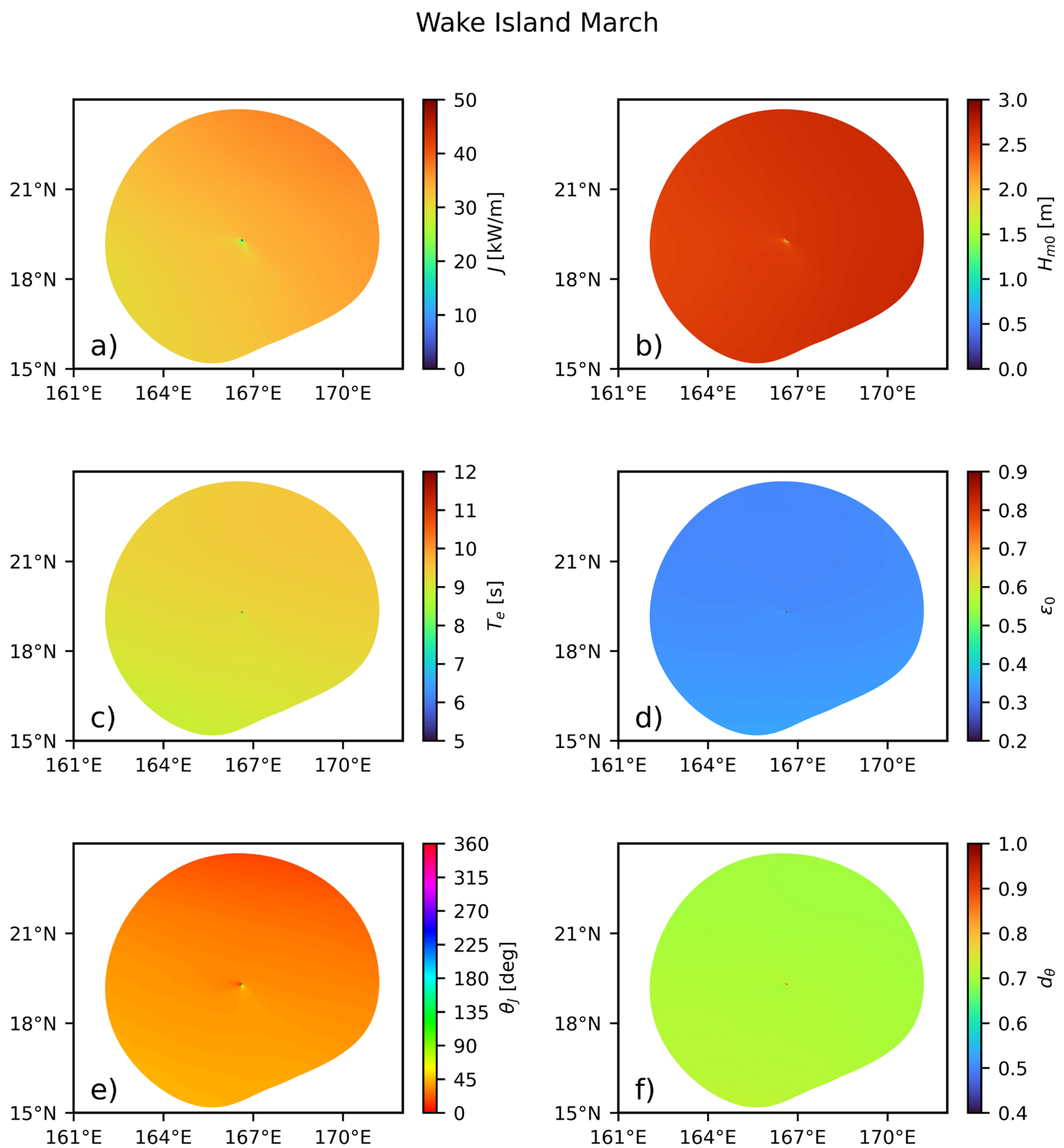

Figure A.75. Monthly distributions of six IEC parameters around Wake Island in March: (a) omnidirectional wave power, (b) significant wave height, (c) energy period, (d) spectral width, (e) direction of maximum directionally resolved wave power, and (f) directionality coefficient.

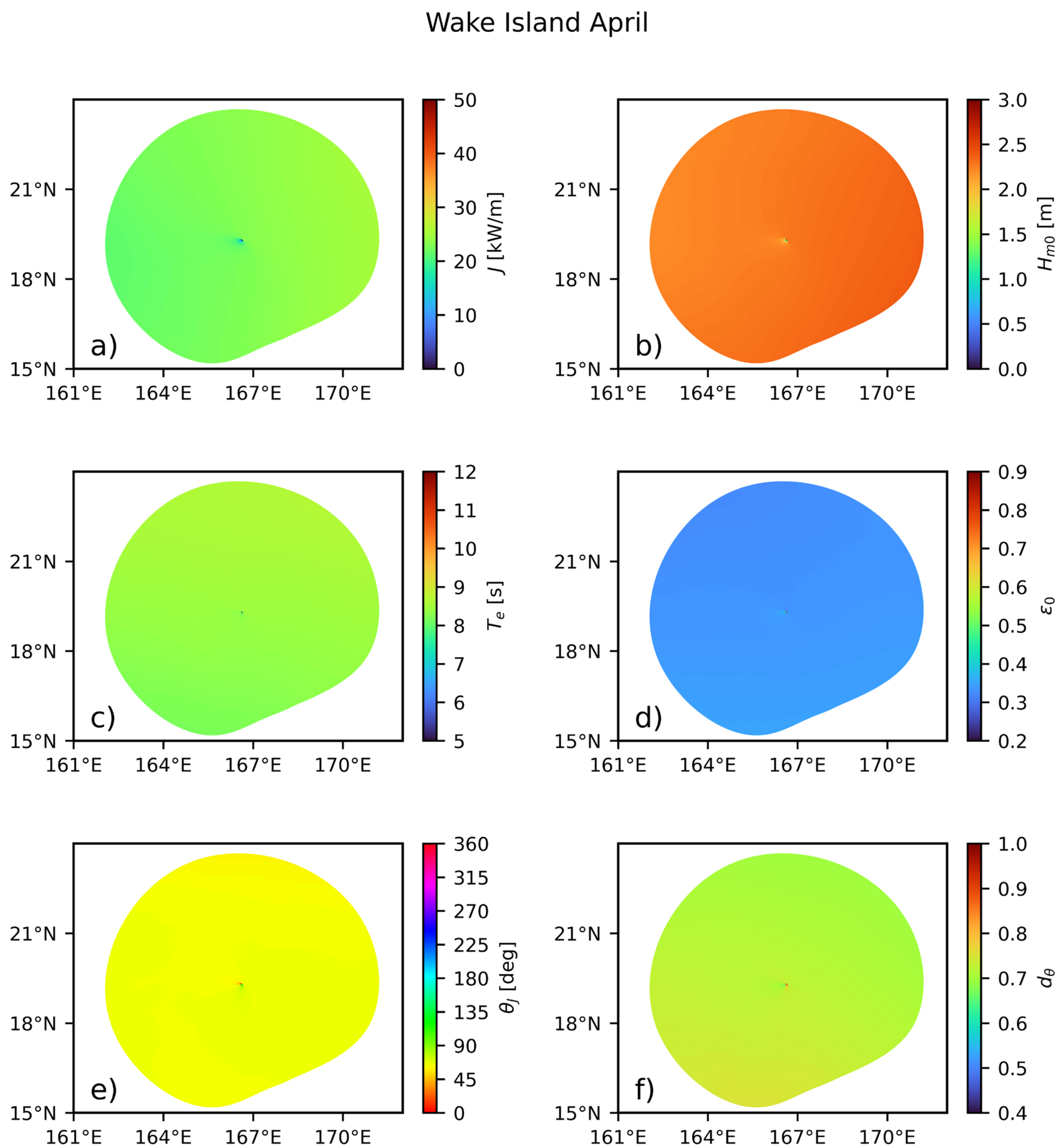

Figure A.76. Monthly distributions of six IEC parameters around Wake Island in April: (a) omnidirectional wave power, (b) significant wave height, (c) energy period, (d) spectral width, (e) direction of maximum directionally resolved wave power, and (f) directionality coefficient.

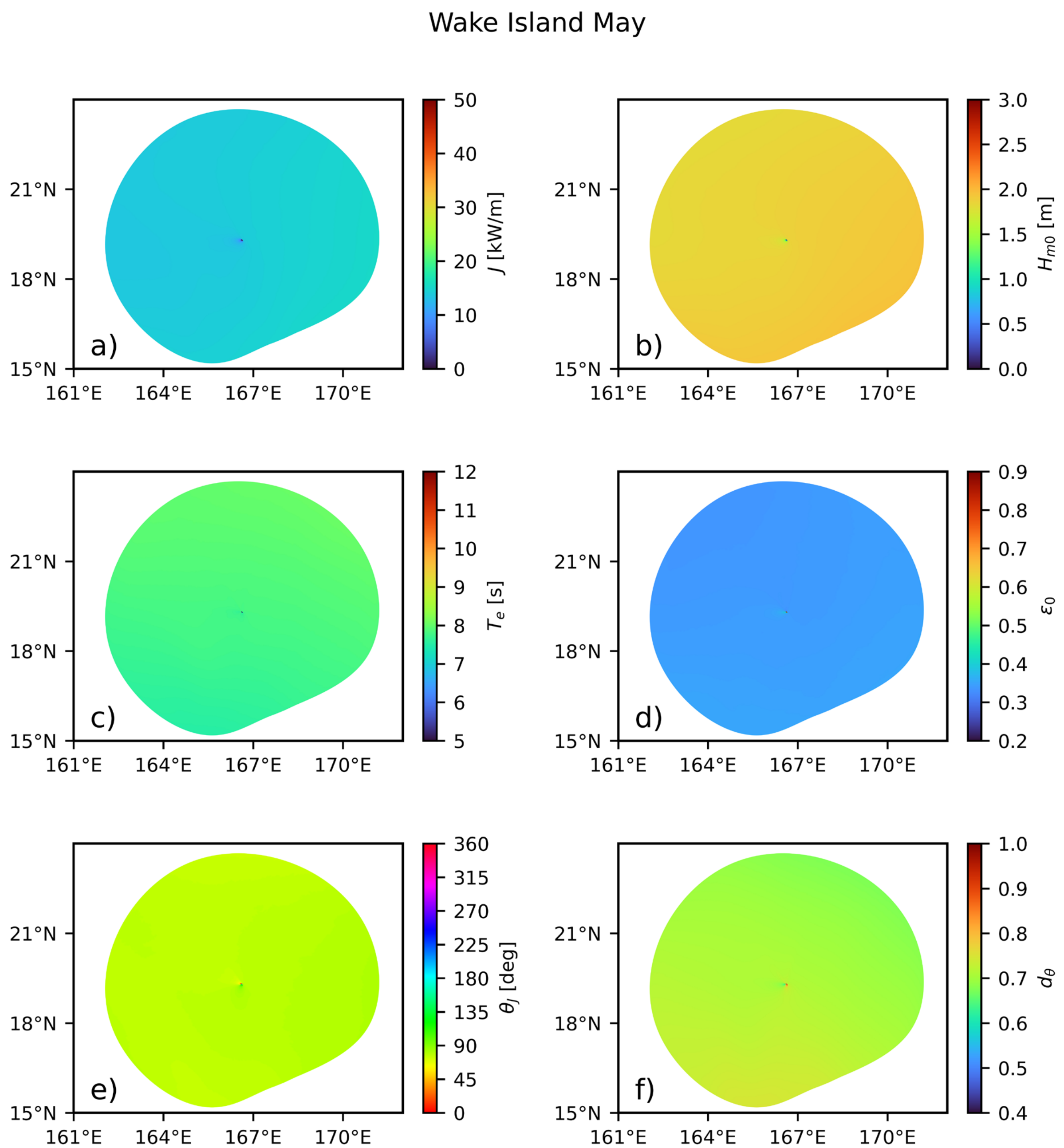

Figure A.77. Monthly distributions of six IEC parameters around Wake Island in May: (a) omnidirectional wave power, (b) significant wave height, (c) energy period, (d) spectral width, (e) direction of maximum directionally resolved wave power, and (f) directionality coefficient.

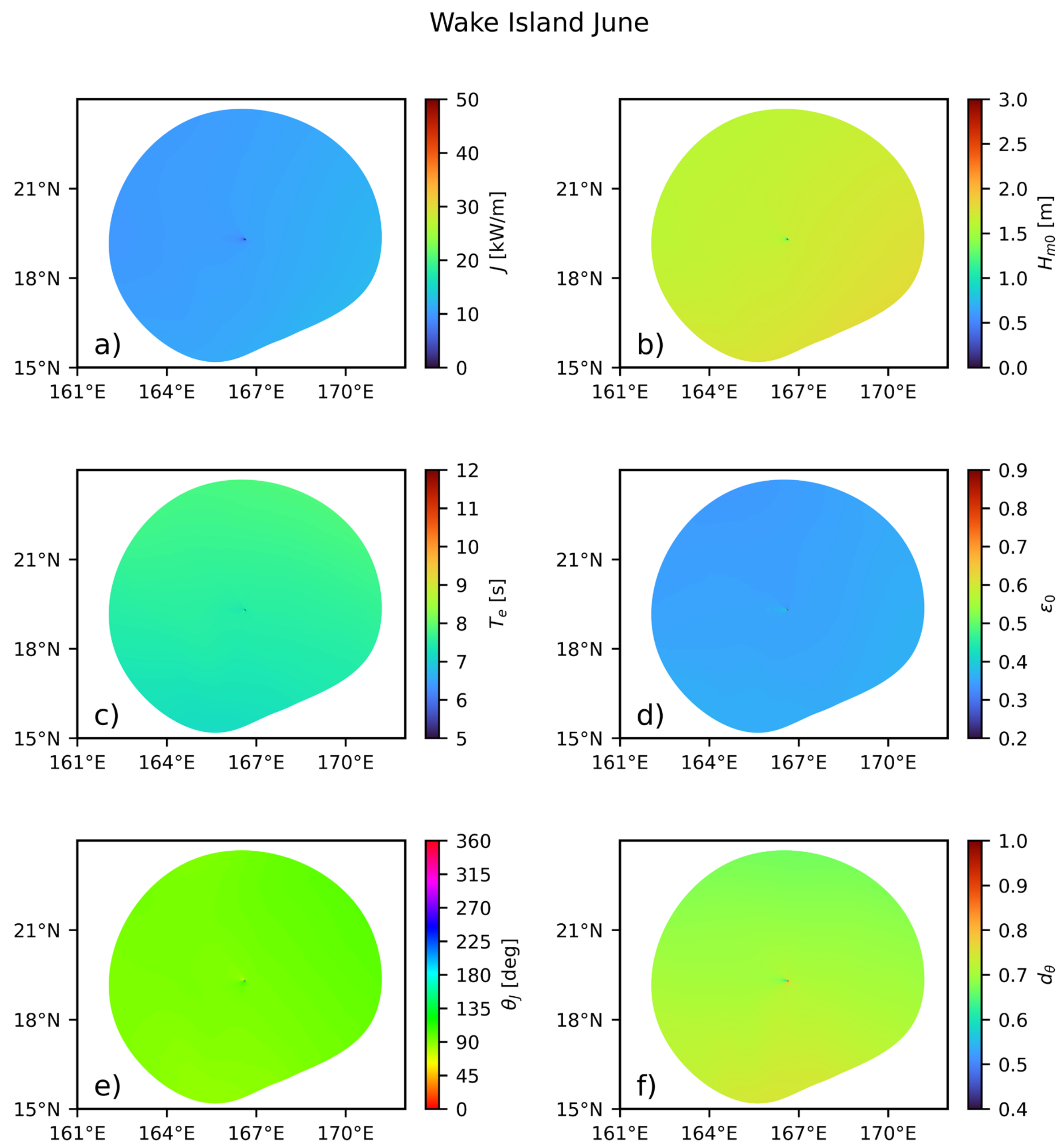

Figure A.78. Monthly distributions of six IEC parameters around Wake Island in June: (a) omnidirectional wave power, (b) significant wave height, (c) energy period, (d) spectral width, (e) direction of maximum directionally resolved wave power, and (f) directionality coefficient.

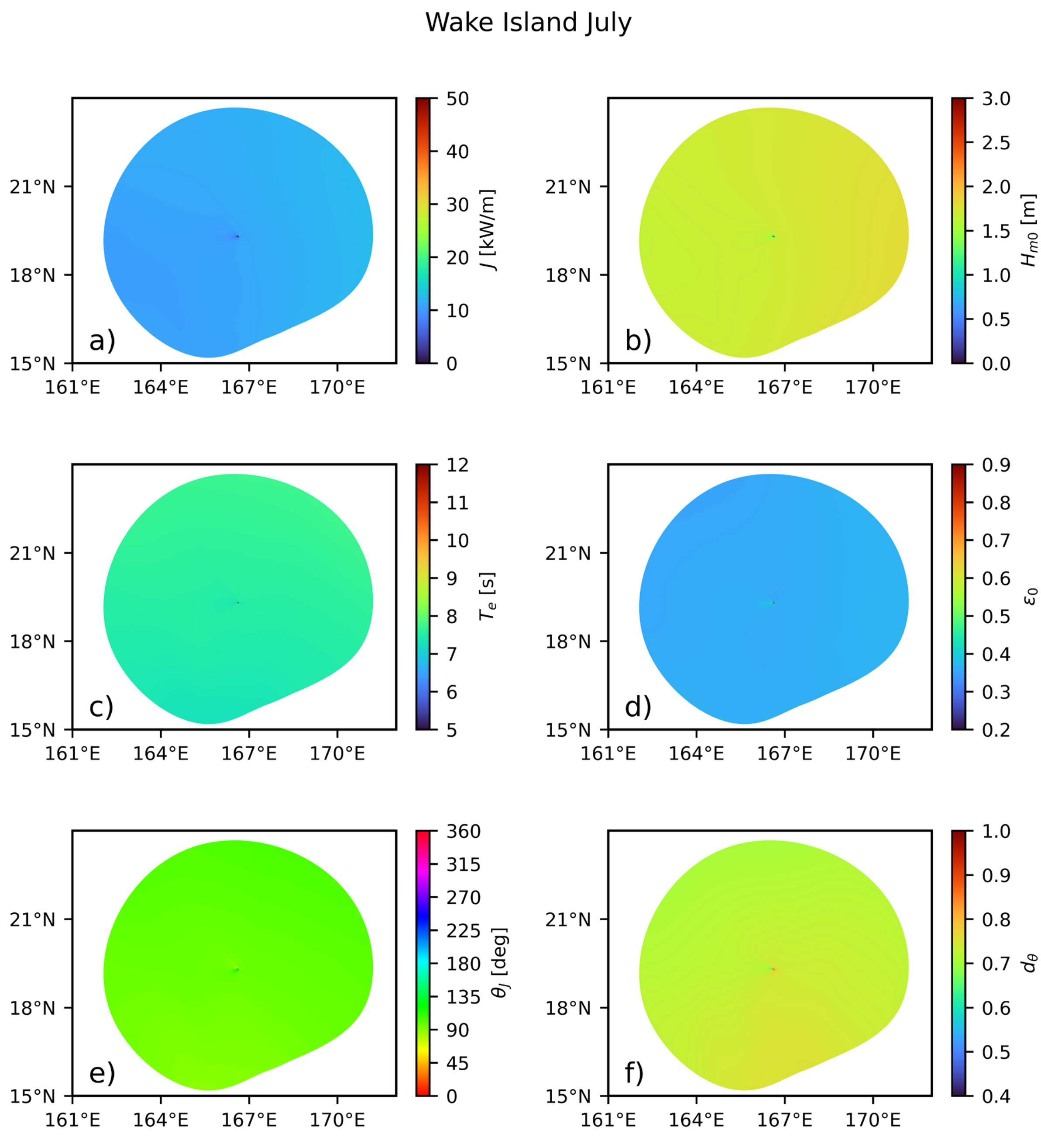

Figure A.79. Monthly distributions of six IEC parameters around Wake Island in July: (a) omnidirectional wave power, (b) significant wave height, (c) energy period, (d) spectral width, (e) direction of maximum directionally resolved wave power, and (f) directionality coefficient.

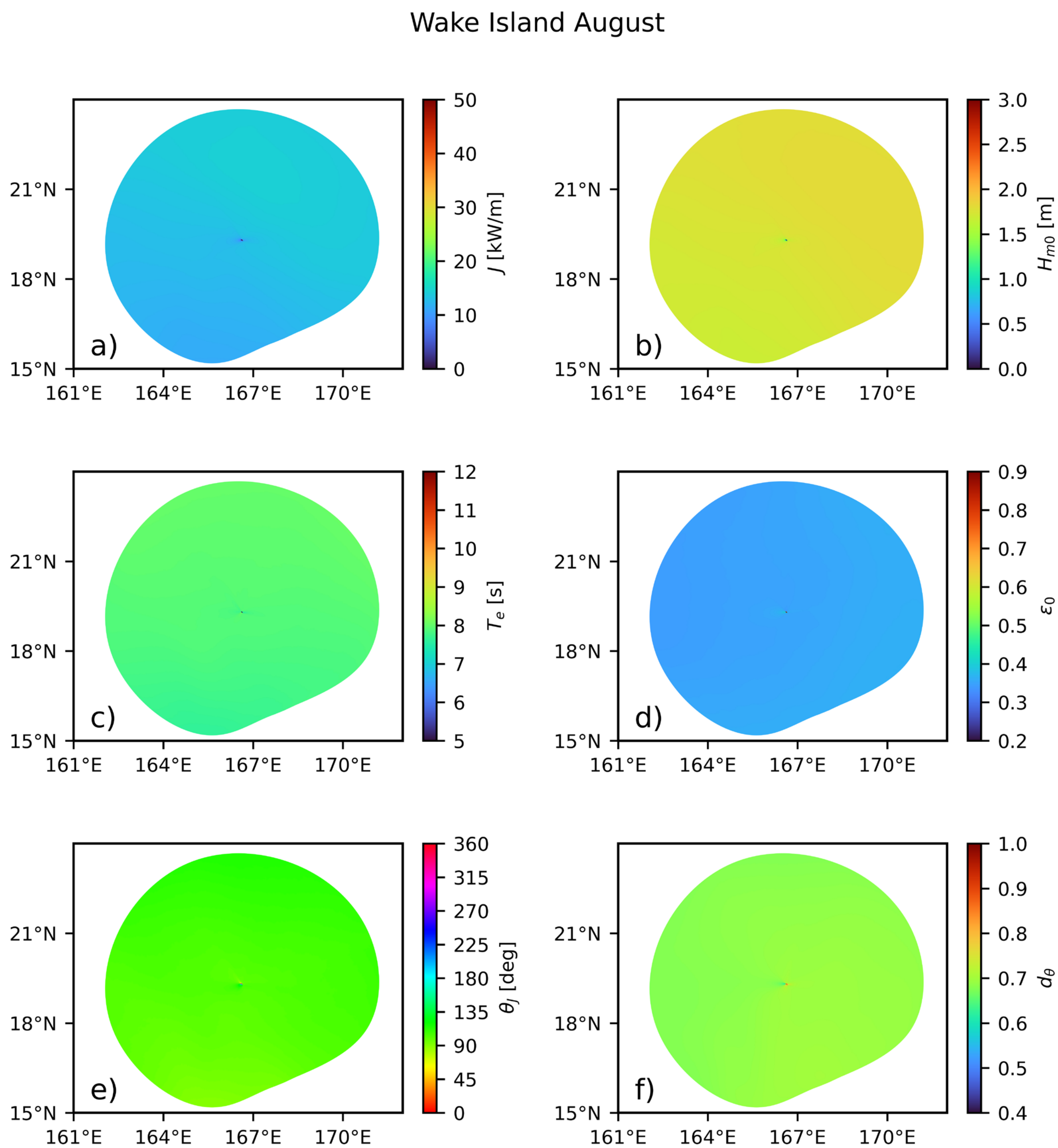

Figure A.80. Monthly distributions of six IEC parameters around Wake Island in August: (a) omnidirectional wave power, (b) significant wave height, (c) energy period, (d) spectral width, (e) direction of maximum directionally resolved wave power, and (f) directionality coefficient.

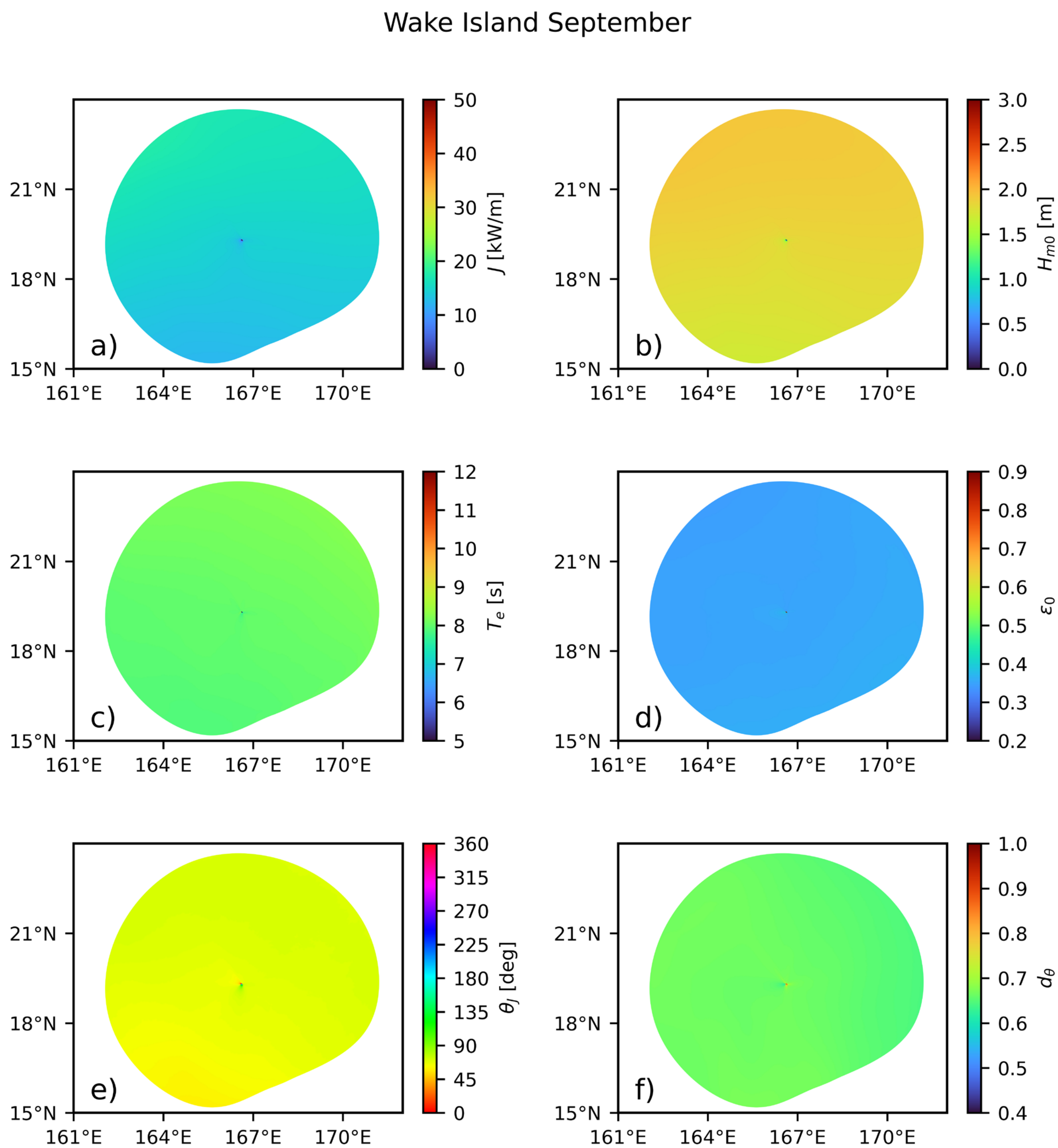

Figure A.81. Monthly distributions of six IEC parameters around Wake Island in September: (a) omnidirectional wave power, (b) significant wave height, (c) energy period, (d) spectral width, (e) direction of maximum directionally resolved wave power, and (f) directionality coefficient.

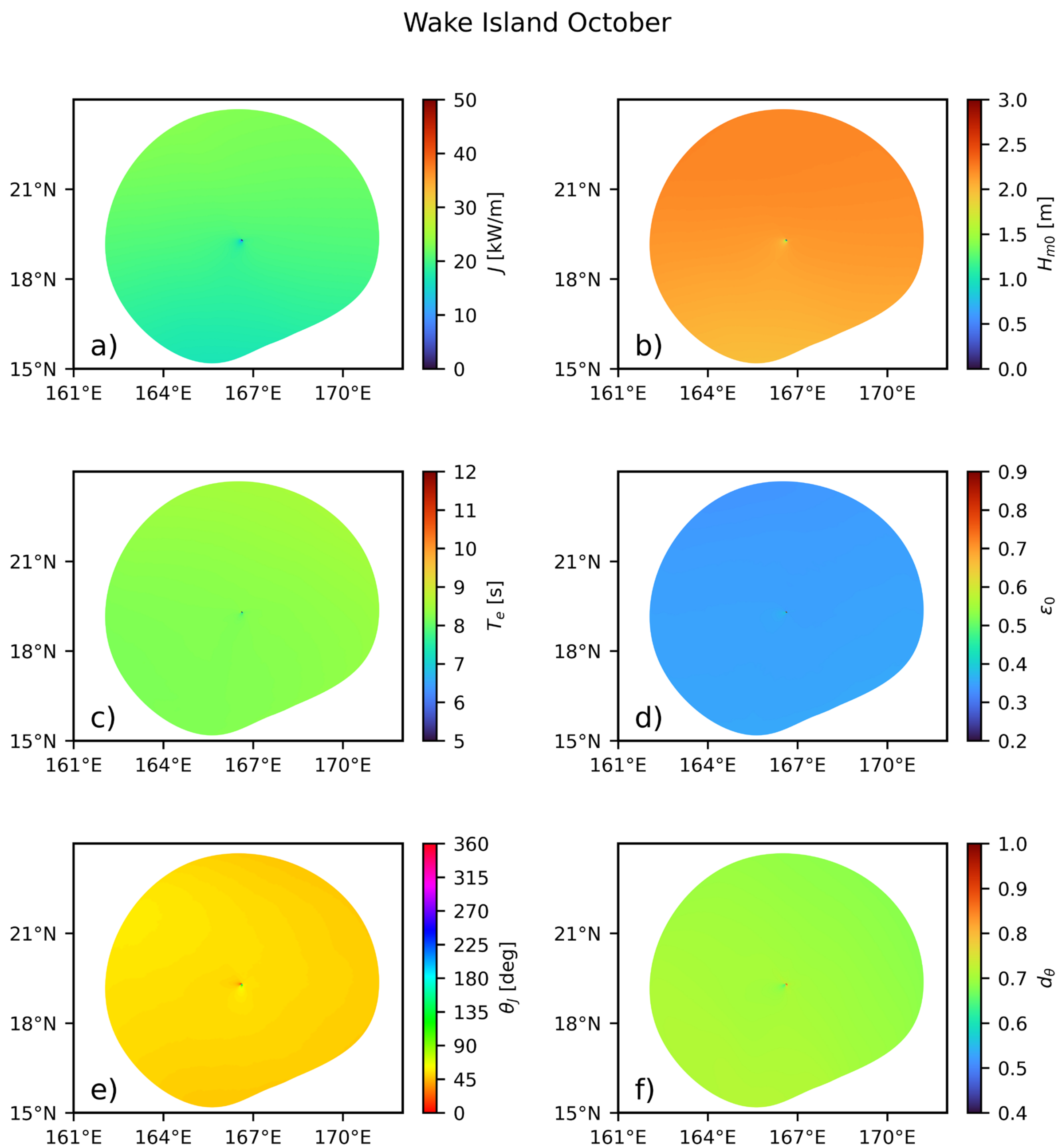

Figure A.82. Monthly distributions of six IEC parameters around Wake Island in October: (a) omnidirectional wave power, (b) significant wave height, (c) energy period, (d) spectral width, (e) direction of maximum directionally resolved wave power, and (f) directionality coefficient.

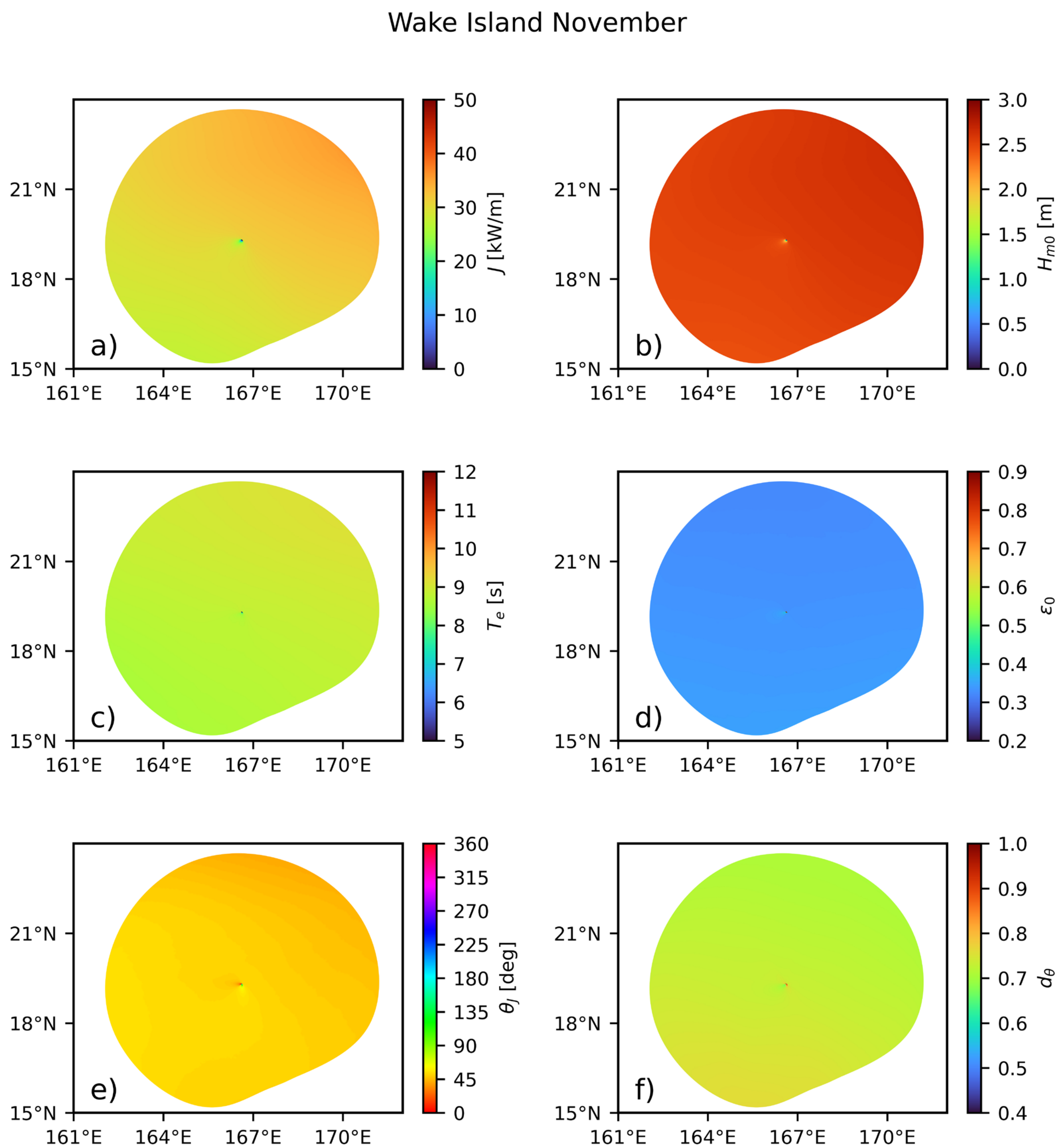

Figure A.83. Monthly distributions of six IEC parameters around Wake Island in November: (a) omnidirectional wave power, (b) significant wave height, (c) energy period, (d) spectral width, (e) direction of maximum directionally resolved wave power, and (f) directionality coefficient.

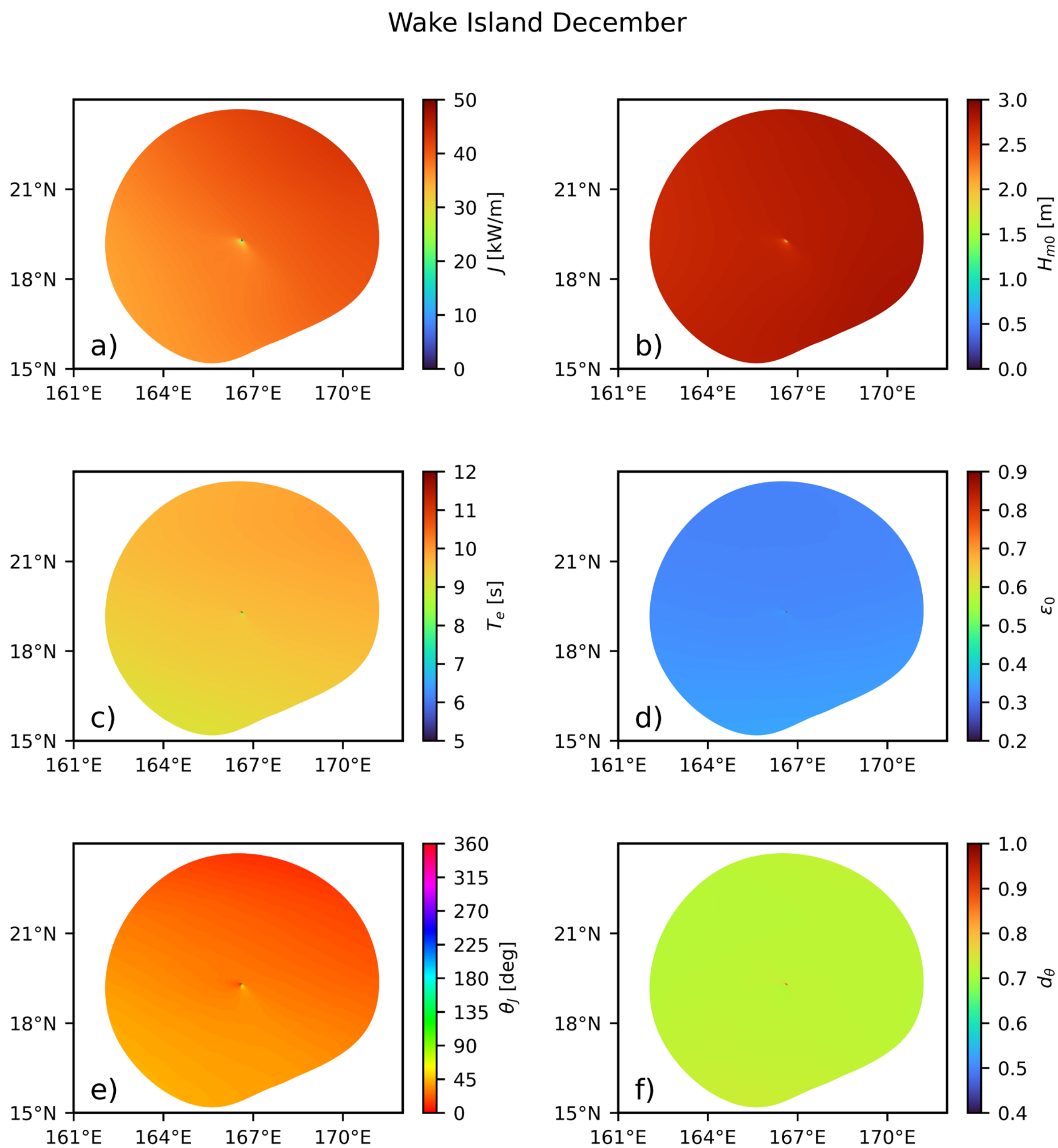

Figure A.84. Monthly distributions of six IEC parameters around Wake Island in December: (a) omnidirectional wave power, (b) significant wave height, (c) energy period, (d) spectral width, (e) direction of maximum directionally resolved wave power, and (f) directionality coefficient.

Appendix B – Model Sensitivity to Time Step

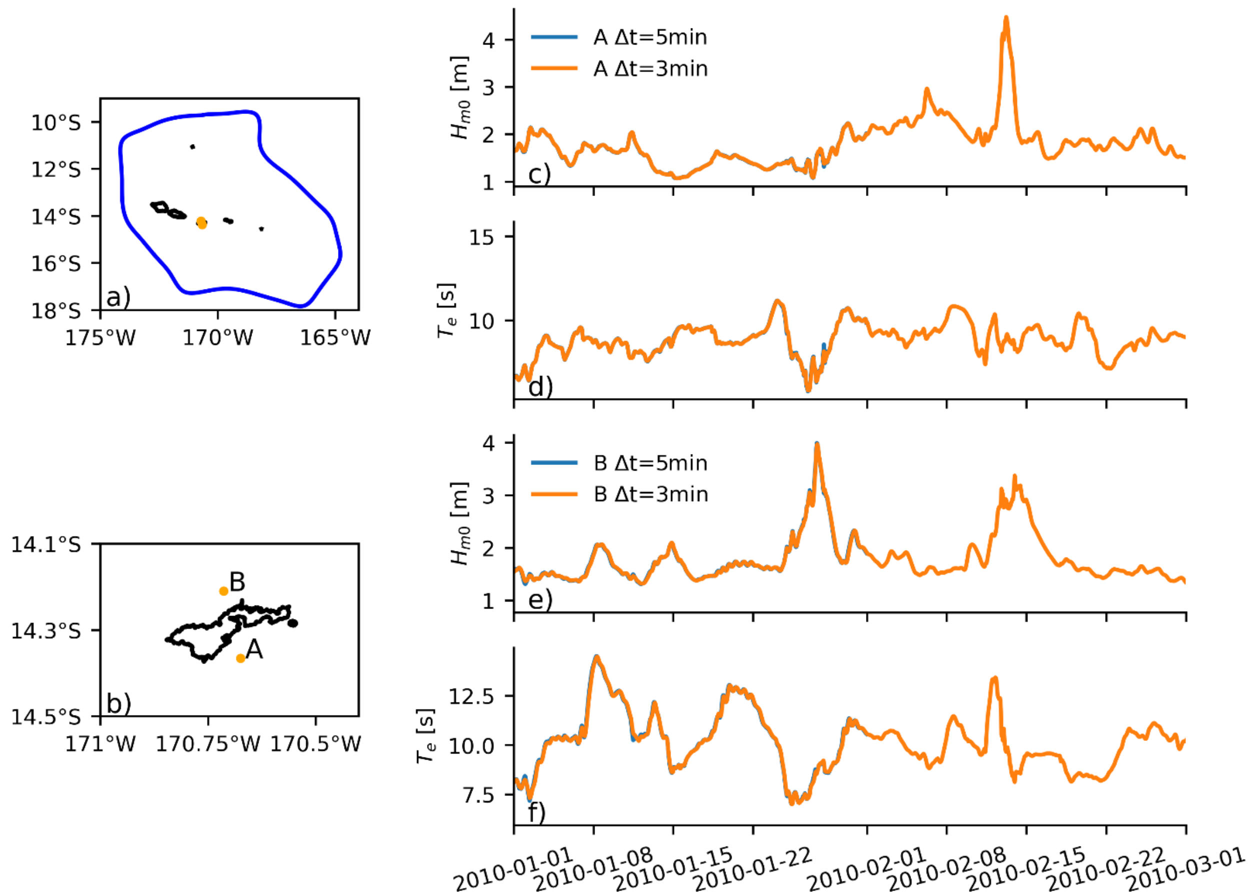

Figure B.1. Sensitivity to integration time step for the American Samoa model.

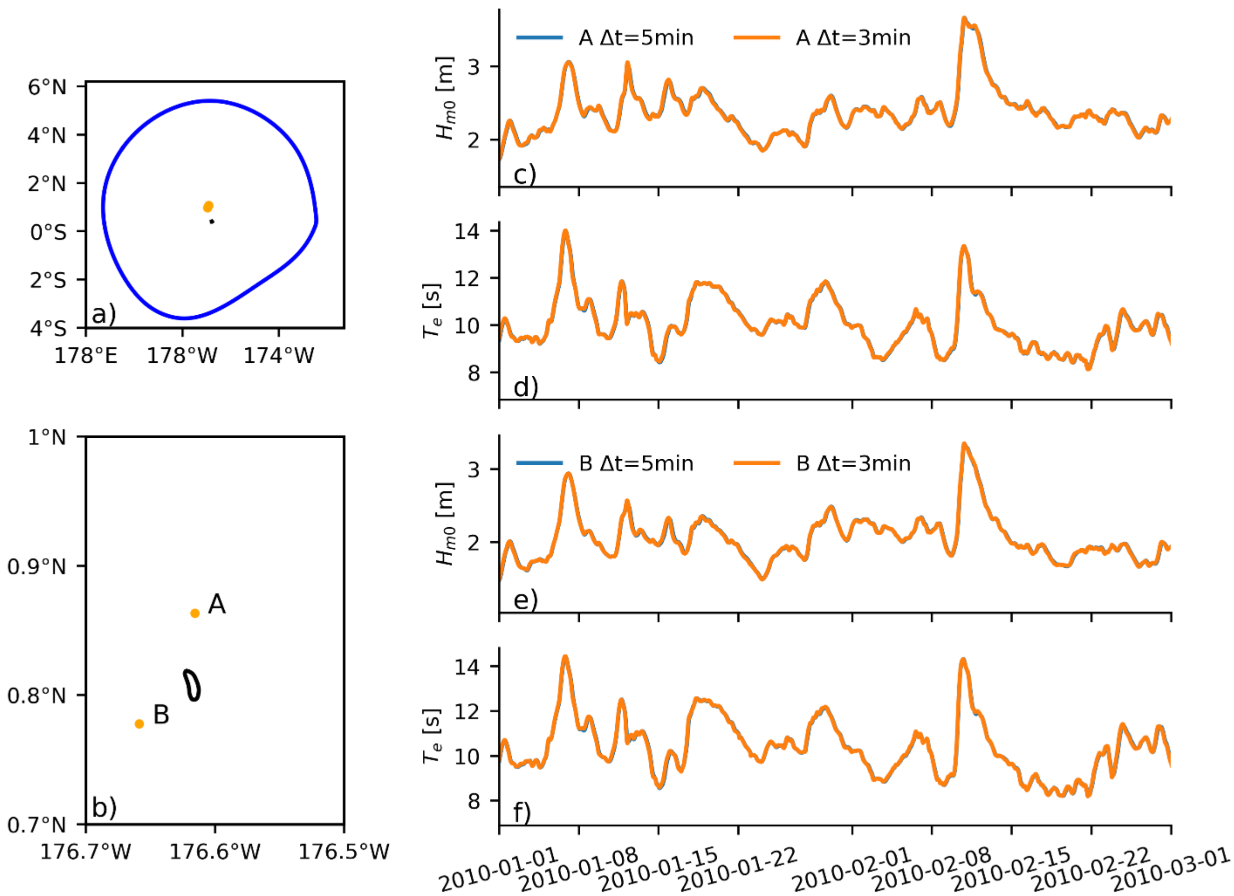

Figure B.2. Sensitivity to integration time step for the Baker and Howland Islands model.

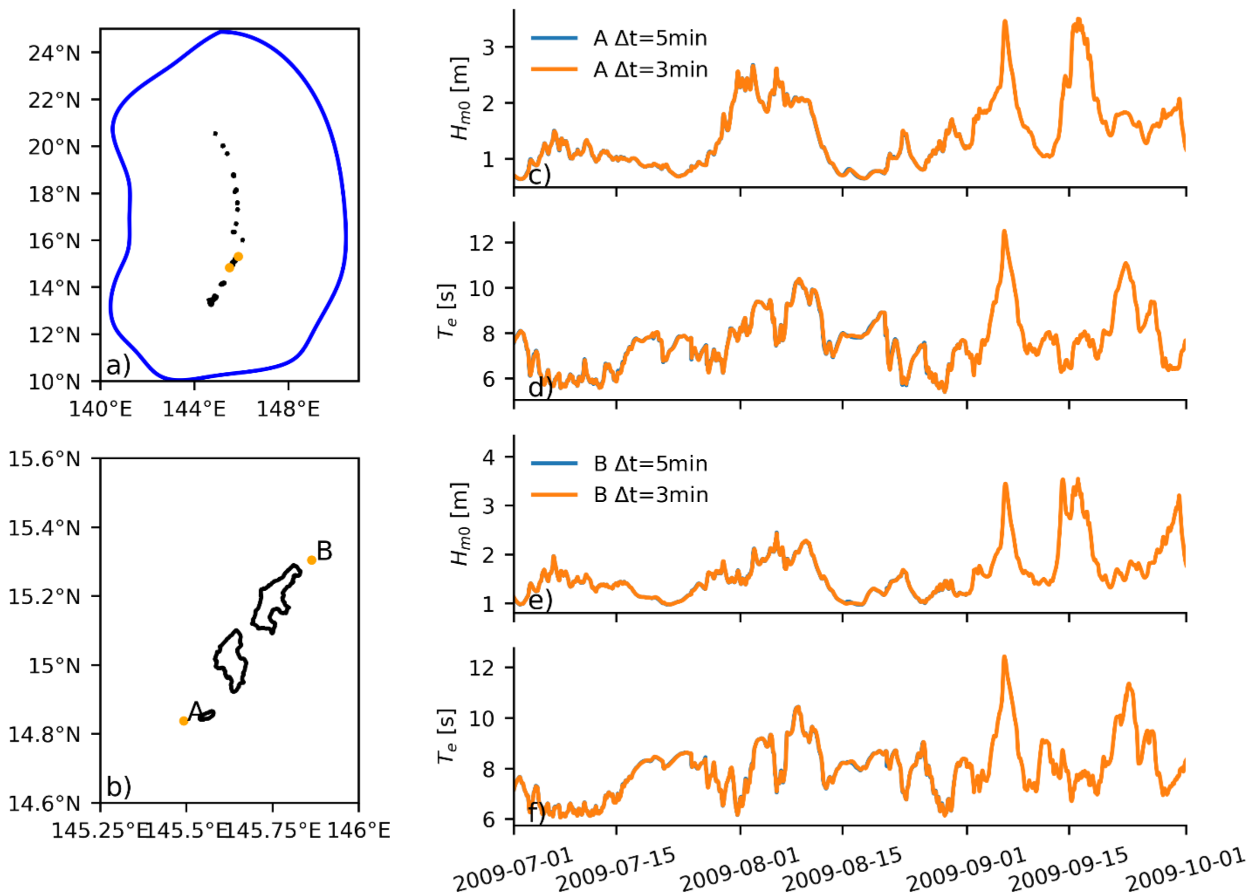

Figure B.3. Sensitivity to integration time step for the Commonwealth of Northern Mariana Islands and Guam model.

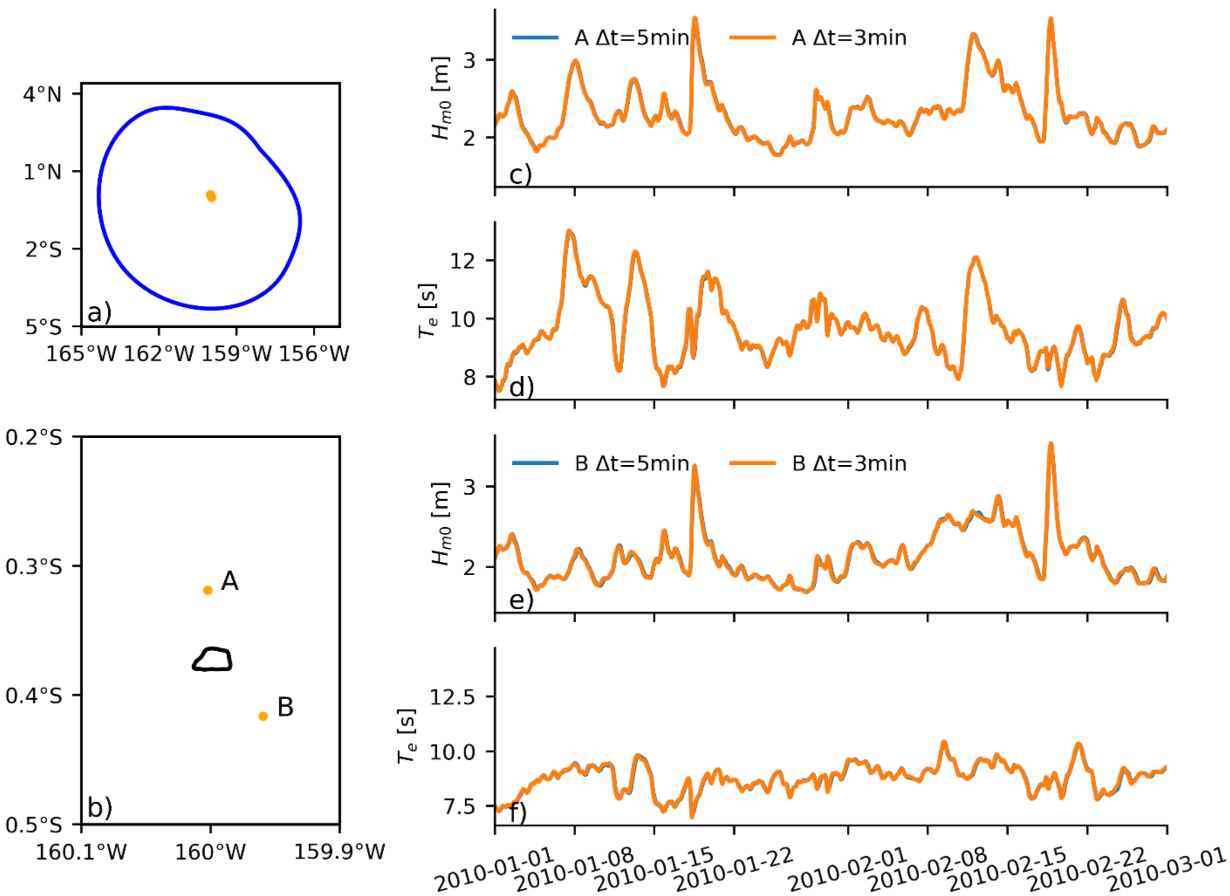

Figure B.4. Sensitivity to integration time step for the Jarvis Island model.

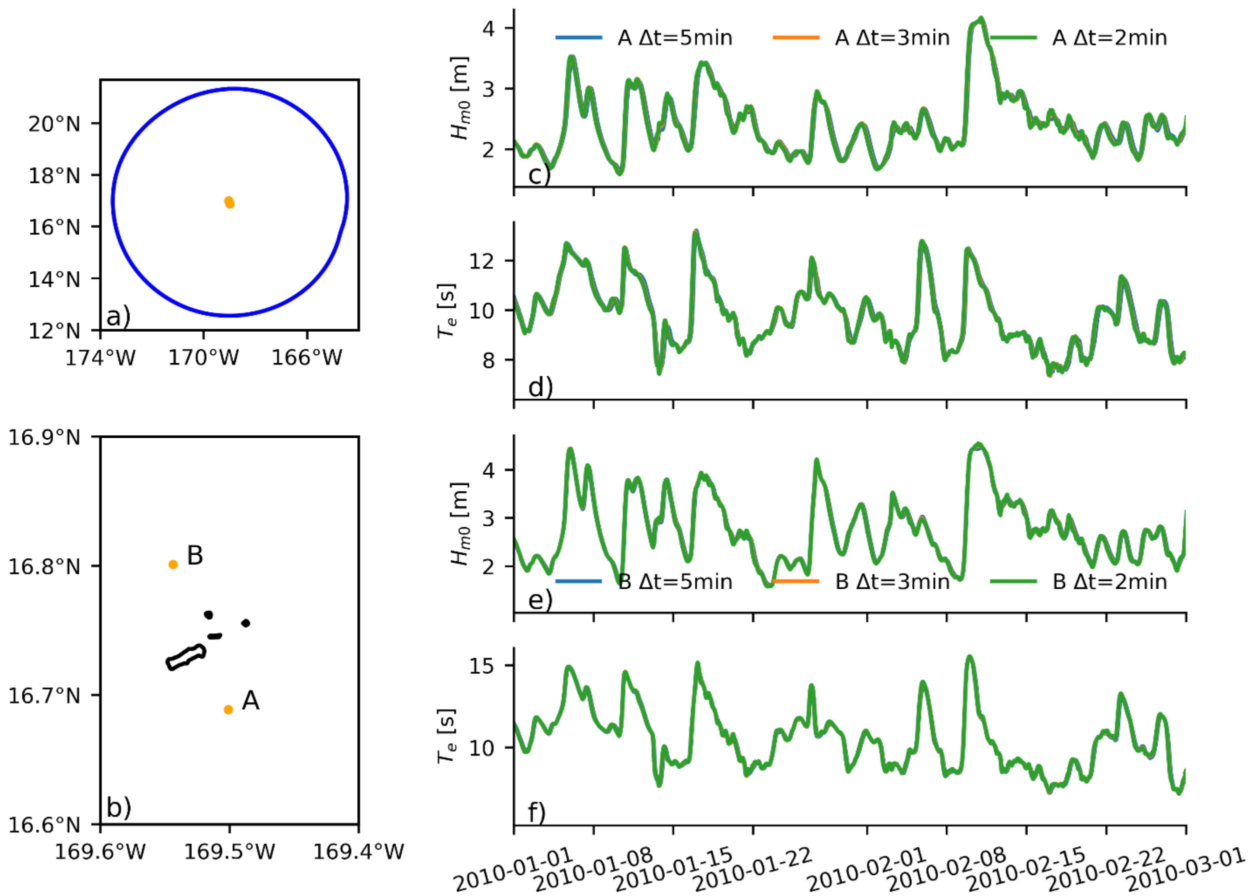

Figure B.5. Sensitivity to integration time step for the Johnston Atoll model.

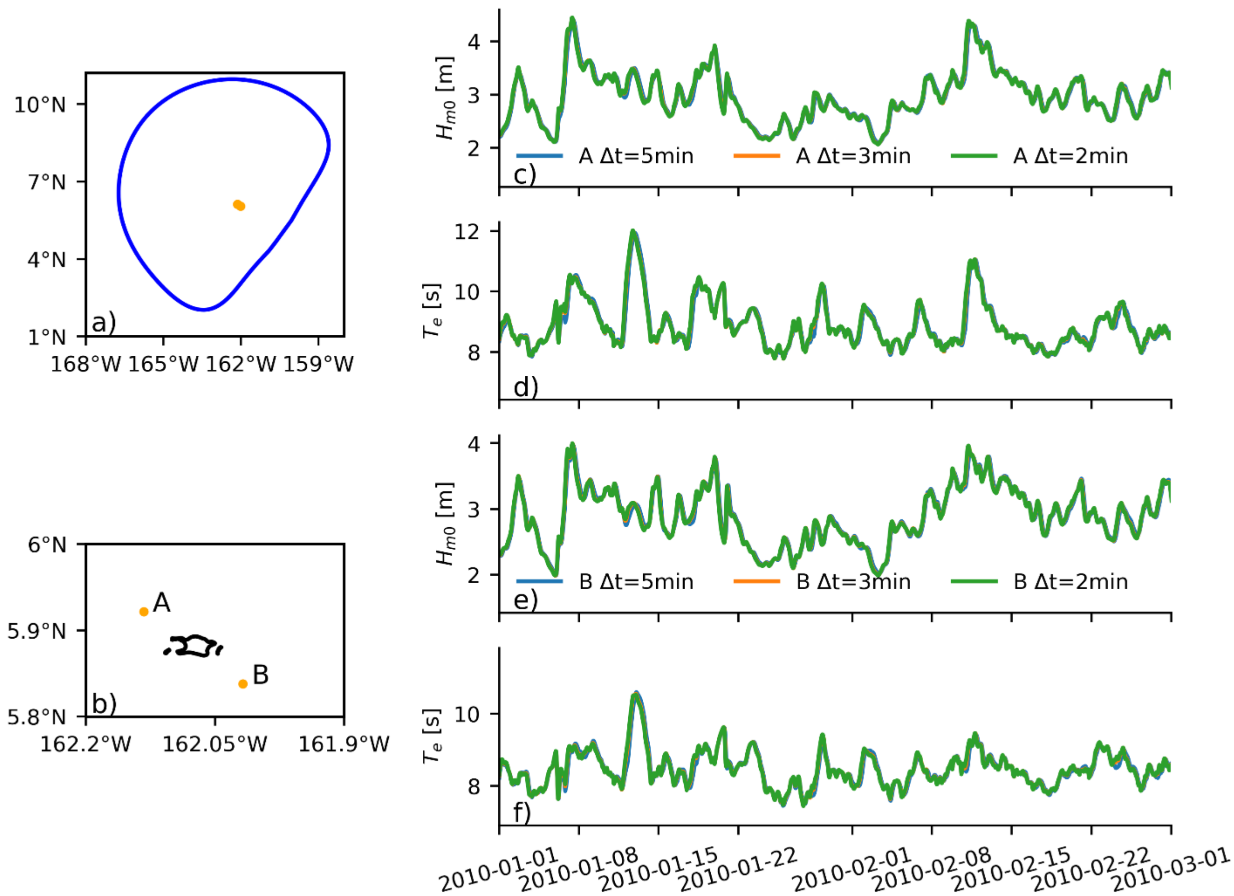

Figure B.6. Sensitivity to integration time step for the Palmyra Atoll and Kingman Reef model.

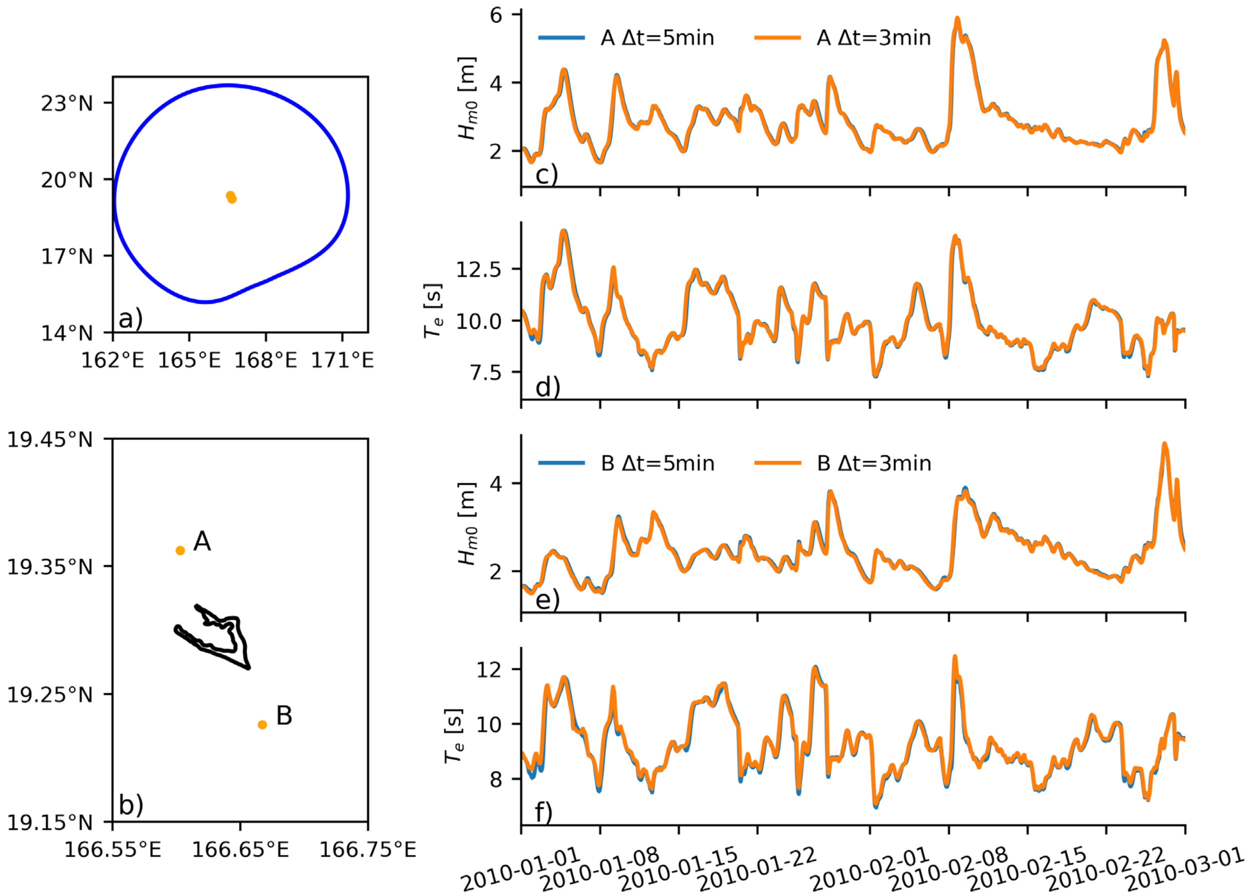

Figure B.7. Sensitivity to integration time step for the Wake Island model.

Appendix C – Comparisons of the Model-Simulated Six IEC Parameters with Observed Buoy Data

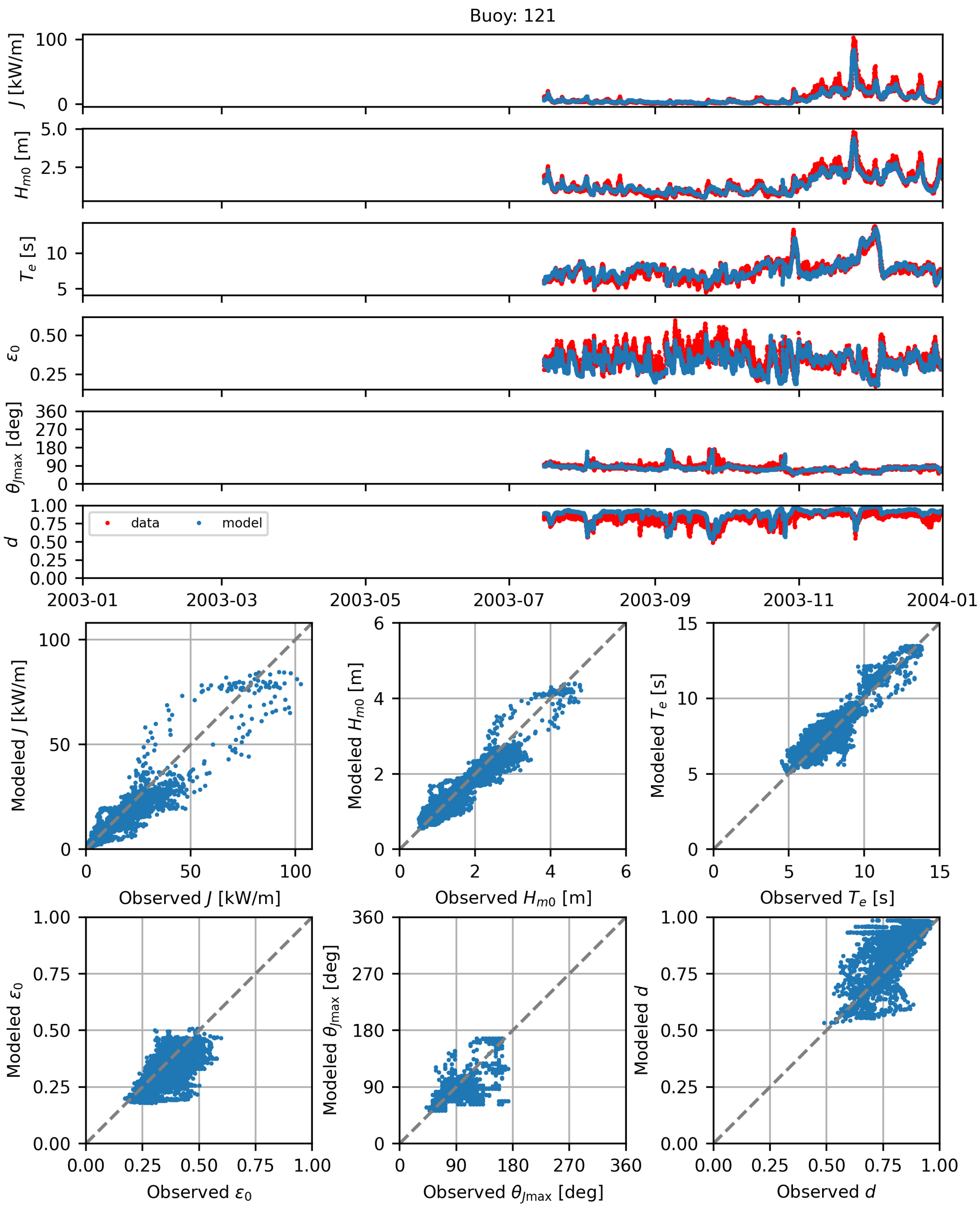

Figure C.1. Comparisons of time series (top) and scatter plots (bottom) of the six model-simulated IEC parameters with observed data at CDIP Buoy 121 for 2003.

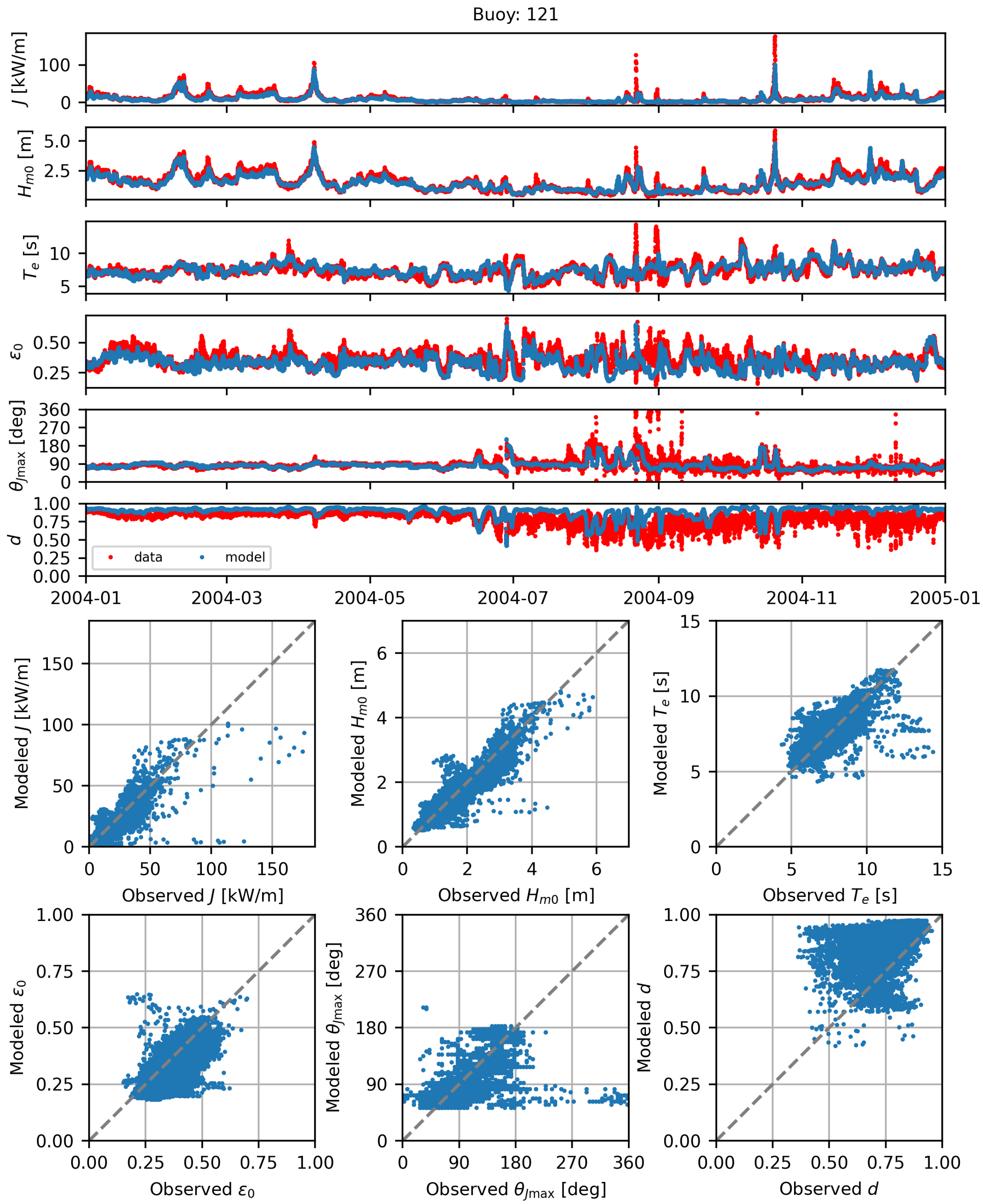

Figure C.2. Comparisons of time series (top) and scatter plots (bottom) of the six model-simulated IEC parameters with observed data at CDIP Buoy 121 for 2004.

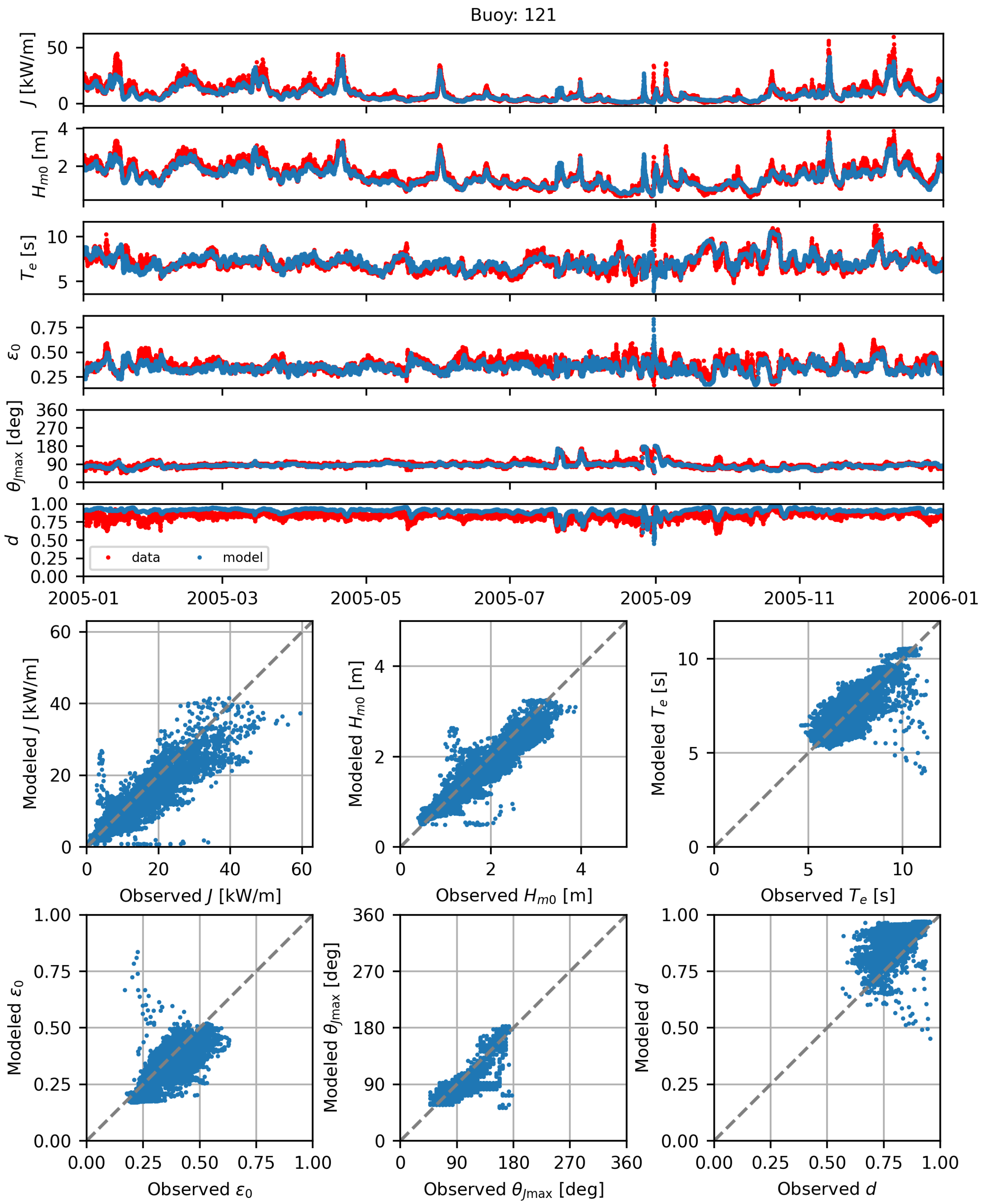

Figure C.3, Comparisons of time series (top) and scatter plots (bottom) of the six model-simulated IEC parameters with observed data at CDIP Buoy 121 for 2005.

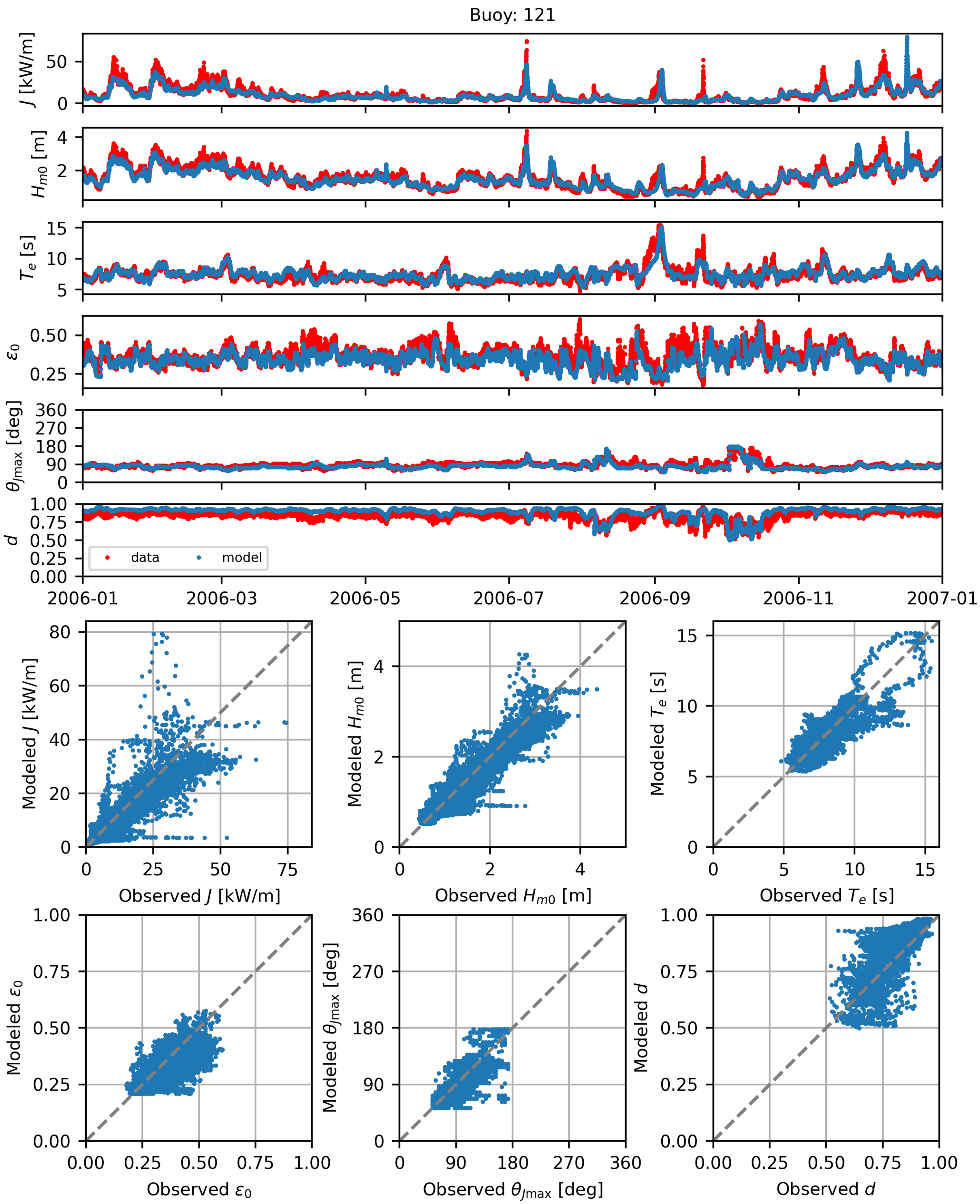

Figure C.4. Comparisons of time series (top) and scatter plots (bottom) of the six model-simulated IEC parameters with observed data at CDIP Buoy 121 for 2006.

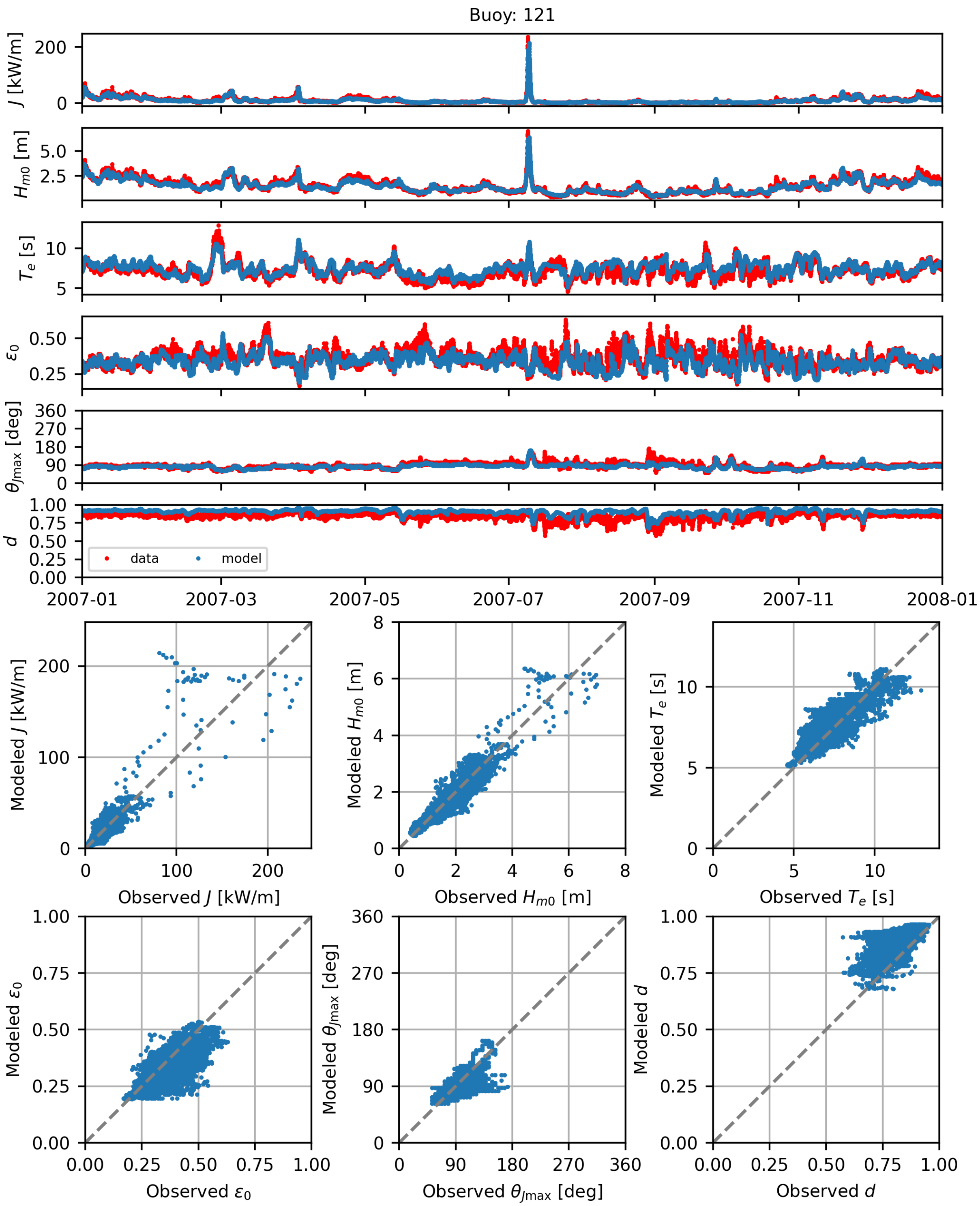

Figure C.5. Comparisons of time series (top) and scatter plots (bottom) of the six model-simulated IEC parameters with observed data at CDIP Buoy 121 for 2007.

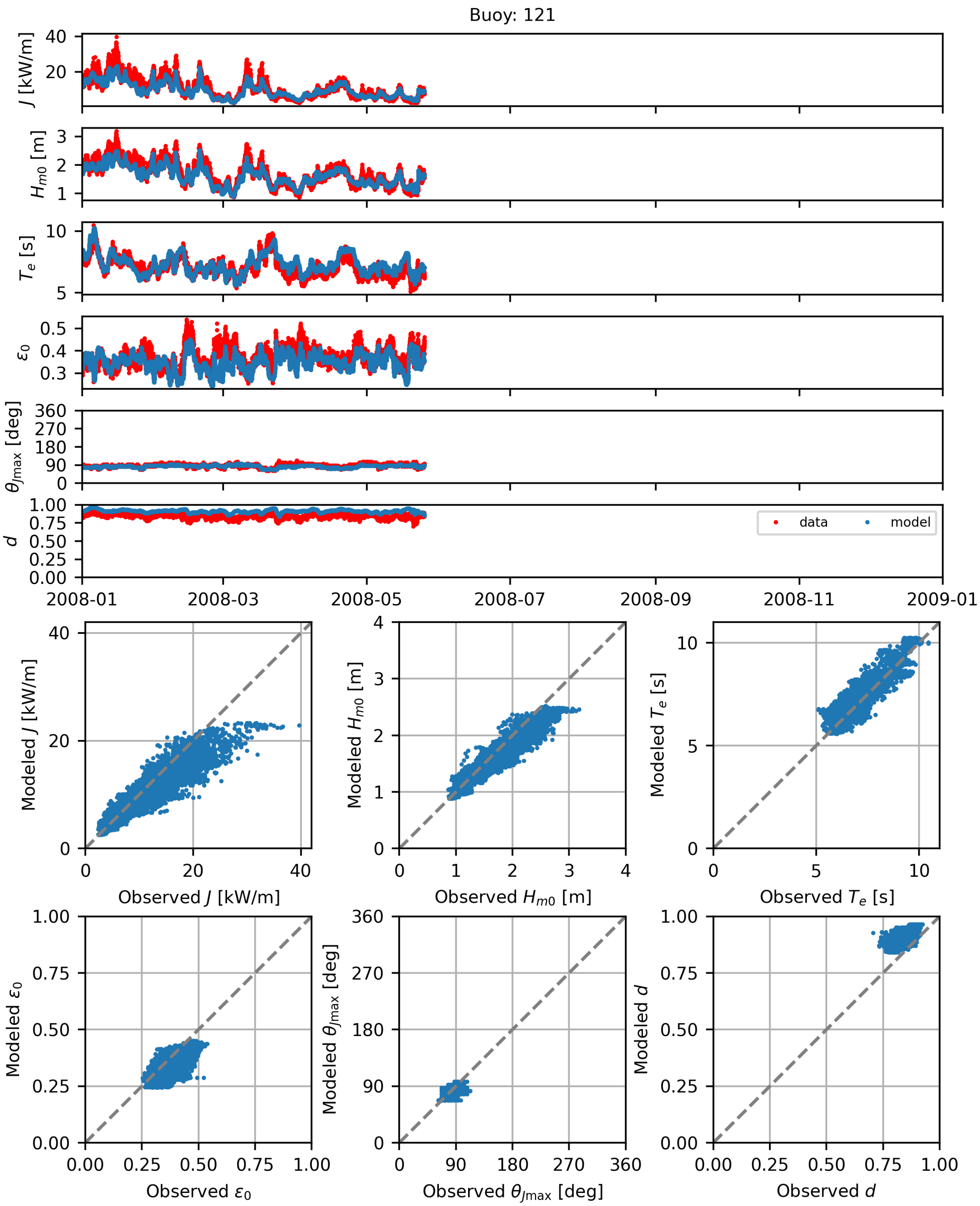

Figure C.6. Comparisons of time series (top) and scatter plots (bottom) of the six model-simulated IEC parameters with observed data at CDIP Buoy 121 for 2008.

Appendix D – Yearly Performance Metrics for Simulated IEC Resource Parameters at Buoy 121

Table D.1. Performance metrics for 2003.

Parameter	N	RMSE	PE (%)	SI	Bias	Bias (%)	R
J (kW/m)	8123	3.89	6.95	0.39	-0.71	-7.21	0.95
H_{m0} (m)	8123	0.21	0.90	0.14	-0.03	-2.35	0.96
T_e (s)	8123	0.59	2.75	0.08	0.17	2.25	0.92
ϵ_0 (-)	8123	0.06	-7.48	0.16	-0.03	-8.15	0.67
θ_{Jmax} (deg)	8123	-	-	-	7.61	-	0.72
d (-)	8123	0.08	6.91	0.09	0.06	6.73	0.74

Table D.2. Performance metrics for 2004.

Parameter	N	RMSE	PE (%)	SI	Bias	Bias (%)	R
J (kW/m)	17528	5.05	3.30	0.47	-1.22	-11.30	0.90
H_{m0} (m)	17528	0.25	-1.10	0.16	-0.07	-4.78	0.95
T_e (s)	17528	0.71	2.37	0.10	0.13	1.78	0.77
ϵ_0 (-)	17528	0.07	-8.21	0.18	-0.03	-9.26	0.61
θ_{Jmax} (deg)	17528	-	-	-	9.92	-	0.68
d (-)	17528	0.13	13.09	0.16	0.09	11.73	0.48

Table D.3. Performance metrics for 2005.

Parameter	N	RMSE	PE (%)	SI	Bias	Bias (%)	R
J (kW/m)	17491	3.03	-2.73	0.31	-1.16	-11.94	0.94
H_{m0} (m)	17491	0.21	-3.36	0.14	-0.09	-5.79	0.95
T_e (s)	17491	0.54	2.19	0.08	0.13	1.82	0.82
ϵ_0 (-)	17491	0.05	-6.48	0.15	-0.03	-7.25	0.69
θ_{Jmax} (deg)	17491	-	-	-	6.66	-	0.79
d (-)	17491	0.08	8.19	0.09	0.07	8.00	0.56

Table D.4. Performance metrics for 2006.

Parameter	N	RMSE	PE (%)	SI	Bias	Bias (%)	R
J (kW/m)	17494	3.97	2.91	0.38	-0.77	-7.25	0.90
H_{m0} (m)	17494	0.22	-0.96	0.14	-0.06	-3.62	0.94
T_e (s)	17494	0.66	2.28	0.09	0.13	1.74	0.83
ϵ_0 (-)	17494	0.05	-5.97	0.14	-0.02	-6.79	0.69
θ_{Jmax} (deg)	17494	-	-	-	7.62	-	0.78
d (-)	17494	0.07	6.28	0.08	0.05	6.21	0.77

Table D.5. Performance metrics for 2007.

Parameter	N	RMSE	PE (%)	SI	Bias	Bias (%)	R
J (kW/m)	17520	4.89	4.32	0.47	-0.54	-5.26	0.92
H_{m0} (m)	17520	0.21	-1.00	0.13	-0.06	-3.62	0.96
T_e (s)	17520	0.59	4.66	0.08	0.30	4.17	0.85
ϵ_0 (-)	17520	0.05	-5.95	0.14	-0.02	-6.76	0.67
θ_{Jmax} (deg)	17520	-	-	-	6.90	-	0.77
d (-)	17520	0.07	6.91	0.08	0.06	6.72	0.70

Table D.6. Performance metrics for 2008.

Parameter	N	RMSE	PE (%)	SI	Bias	Bias (%)	R
J (kW/m)	6975	2.60	-3.35	0.24	-1.03	-9.62	0.93
H_{m0} (m)	6975	0.18	-3.88	0.11	-0.09	-5.18	0.94
T_e (s)	6975	0.50	3.48	0.07	0.23	3.24	0.84
ϵ_0 (-)	6975	0.04	-5.81	0.12	-0.02	-6.34	0.62
θ_{Jmax} (deg)	6975	-	-	-	5.73	-	0.65
d (-)	6975	0.07	7.70	0.08	0.06	7.61	0.53

Pacific Northwest National Laboratory

902 Battelle Boulevard
P.O. Box 999
Richland, WA 99354
1-888-375-PNNL (7665)

www.pnnl.gov